UNIVERSITIES OF GLASGOW AND STRATHCLYDE
DEPARTMENT OF NAVAL ARCHITECTURE AND MARINE ENGINEERING

LOW CYCLE FATIGUE IN FLOATING PRODUCTION STORAGE AND OFFLOADING UNITS

By

Hauwa Raji

A THESIS SUBMITTED IN PARTIAL FULFILMENT OF THE REQUIREMENTS FOR THE DEGREE OF DOCTOR OF PHILOSOPHY

GLASGOW, UK
SEPTEMBER 2010

This thesis is the result of the author's original research. It has been composed by the author and has not been previously submitted for examination which has led to the award of a degree.

Signed: Date:

ABSTRACT

The purpose of this study was to investigate low cycle fatigue damage, from loading and unloading of cargo and ballast, of structural details on a Floating Production Storage Offloading (FPSO) unit. There has been an increased interest in low cycle fatigue in the offshore industry as fatigue cracks have been observed within five years of service delivery. Also FPSOs operate at constantly changing drafts. The draft variation between fully loaded and ballast drafts for some new FPSO designs may be as large as greater than 10 metres. This large draft variation result in additional low cycle fatigue which needs to be taken into account. A detailed finite element analysis was performed to check the low cycle fatigue strength of highly stressed locations and to provide an insight into the mechanism of loading and offloading. The hotspot stress approach and Dirliks rainflow counting method is employed for calculating fatigue damage. Several classification society rules are compared. It was discovered that loading and unloading generate extremely high stresses. A stress value of 1400 MPa was obtained for a critical location in the bottom stiffener detail which is about four times the yield stress of the material. This clearly shows that some critical details are governed by low cycle fatigue and not high cycle fatigue. The analysis has highlighted the fact that it is necessary to take low cycle fatigue into consideration during design.

ACKNOWLDEGEMENTS

This research work started at the University of Newcastle and was completed at the University of Strathclyde from 2006 – 2010. During this time, I have been privileged to receive support from many people.

Foremost, I would like to express my sincere gratitude to my supervisor, Professor Atilla Incecik, for his patience, encouragement, motivation and support. His guidance throughout the research process has been immeasurable. I am very much indebted to him. I am also grateful to my second supervisor, Professor Nigel Barltrop, for his detailed and constructive comments into this research and also providing his insight and experience in the field of fatigue. I would also like to thank my thesis committee, Professor P.K Das and Doctor Fei Cheng for their suggestions and comments which has improved the thesis.

Without the funding and support of the Schlumberger Foundation, I would not have been able to obtain this degree, and for this I will be eternally grateful. My thanks also go to Lloyd's Register EMEA for giving me an internship opportunity enabling me to develop a deeper understanding of my area of research.

Where would I be without my family? My parents, Talib and Rekiat Raji deserve a special mention for their tireless encouragement and support and for believing in me. Mustapha, Halima, Shehu, Bashir, Hadiza and Bahaja, thanks for being supporting and caring siblings. This work is especially dedicated to my late sister, Hannatu; you are forever in my thoughts.

Lastly, I offer my regards to my friends and colleagues who have made the stay in both Newcastle and Glasgow a memorable one and have provided support in all respect during the course of my study.

TABLE OF CONTENTS

Abstract		i
Acknowledgements		ii
Table of Contents		iii
List of Figures		vii
List of Tables		xii
Chapter One: Introduction		
1.1	Research Motivation	1
1.2	High Cycle and Low Cycle Fatigue	7
1.3	Low Cycle Fatigue in FPSOs	8
1.4	Fatigue Life Estimation Methods	10
1.4.1	Stress –Life Approach	12
1.4.2	Strain – Life Approach	17
1.4.3	Fracture Mechanics Approach	22
1.4.4	Summary of Approaches	24
1.5	Objectives and Scope of Research	25
References		30
Chapter Two: Background Material and Literature Review		
2.1	Introduction	34
2.2	Background Material	34
2.2.1	FPSOs in the Offshore Industry	34
2.2.2	Reference Vessel	36
2.2.3	Loading Sources on FPSOs	39
2.2.4	Loading and Unloading Load Cases	41
2.3	Literature Review	44
2.3.1	Fatigue: Milestones in History	44
2.3.2	Low Cycle Fatigue	47
2.3.2.1	Cyclic Properties of Ship Steel	49
2.3.2.2	Stresses and Strains at Notches	51
2.3.2.3	Plasticity Correction Factors	53

2.3.2.4 Neuber's Rule 54
2.3.3 Low Cycle Fatigue in Ship Structures 57
2.3.3.1 Ship Structures Committee (SSC) 57
2.3.3.2 The Welding Institute (TWI) 65
2.3.3.3 Other Relevant Works 69
2.4 Classification Society Rules for LCF Assessment in FPSOs 72
2.4.1 Typical LCF Assessment Procedure in Ship Structures 72
2.4.2 Lloyds Register (LR) 73
2.4.3 Det Norske Veritas (DNV) 74
2.4.4 American Bureau of Shipping (ABS) 75
2.4.5 Discussion 76
2.5 Conclusion 77
References 78

Chapter Three: Finite Element Modelling
3.1 Introduction 86
3.2 Structural Modelling 86
3.2.1 Global Structural Model 87
3.2.2 Local Structural Models 88
3.3 Local Modelling Techniques 91
3.3.1 Stress Concentration Factors (SCF) 92
3.3.2 Submodeling 92
3.3.3 Sub-Structuring 95
3.3.4 Direct Mesh Refinement 96
3.3.5 Summary of Techniques 97
3.4 Conclusion 102
References 103

Chapter Four: Hotspot Stress Approach
4.1 Introduction 106
4.2 State of the Art 107
4.3 Hot Spot Stress S – N Curve 119
4.4 Comparison of Extrapolation Procedures 120
4.4.1 Fatigue Crack Definition 120

4.5 Predicted Stresses 125
4.5.1 Bottom Plating and Stiffener Detail 125
4.5.1.1 Predicted Stresses at Bottom Detail 126
4.5.2 Side Plating - Inner Plating Stiffener Detail 130
4.5.2.1 Predicted Stresses at Side Detail 131
4.5.2.2 Predicted Stresses at Inner Detail 135
4.6 Discussion 138
References 140

Chapter Five: Fatigue Damage
5.1 Introduction 143
5.2 Rainflow Counting and Fatigue Damage 145
5.2.1 Rainflow Counting 145
5.2.2 Linear Damage Accumulation Law 145
5.2.3 Rainflow Damage in Time Domain 148
5.3 Rainflow Damage in Frequency Domain 148
5.3.1 Response Statistics 148
5.3.2 Fatigue Damage 149
5.4 Combined Fatigue Damage 153
5.4.1 Simple Linear Summation 153
5.4.2 Combined Spectrum Method 154
5.4.3 Analytical Methods 156
5.5 Classification Society Rules for Combined Fatigue Damage 158
5.6 Summary 161
References 163

Chapter Six: Analysis Results
6.1 Low Cycle Fatigue Analysis 167
6.1.1 Sequence of Loading and Unloading 167
6.1.2 Hotspot Stress Cycles 167
6.1.3 Low Cycle Fatigue Damage 177
6.1.4 Low Cycle Fatigue S-N Curve 181
6.2 Wave Fatigue Analysis 183
6.2.1 Hydrodynamic Analysis 190

6.2.2 Hydrodynamic Analysis Results 191
6.2.3 Structural Analysis 193
6.2.4 Wave (High Cycle) Fatigue Damage 196
6.3 Combined Fatigue Damage 198
6.4 Discussion 202
References 204

Chapter Seven: Conclusions and Recommendations
7.1 Summary 205
7.2 Conclusions 207
7.3 Recommendations 209

Appendix A: Cycle Counting Methods 212
Appendix B: Low Cycle and High Cycle Stress Cycles 217
Appendix C: High Cycle (Wave) Fatigue Damage 224
Appendix D: Combined Fatigue Damage 243
Appendix E: MathCAD Wave Analysis 250

LIST OF FIGURES

Figure 1.1: Forecast: Capital Expenditure on FPS Units by Year of Installation 2
Figure 1.2: Typical Cracks found in Ship Structural Details 5
Figure 1.3: Variations of Still Water Bedding Moment due to Loading and Offloading Conditions 6
Figure 1.4: High Cycle and Low Cycle Fatigue 8
Figure 1.5: Stress-Strain Hysteresis Loop 10
Figure 1.6: Fatigue Assessment Procedures of Welded Components 11
Figure 1.7: Typical S – N Curve 13
Figure 1.8: Definition of Stresses 13
Figure 1.9: Nominal Stress in a Beam-Like Component 14
Figure 1.10: Non-Linear Stress Distribution at Weld Toe 16
Figure 1.11: Comparison Specimen for Crack Initiation Behaviour at a Notch 18
Figure 1.12: Stress and Strain Ranges in a Hysteresis Loop 19
Figure 1.13: Strain-life plot (AISI, 2002) 21

Figure 2.1: General Tank Arrangement 37
Figure 2.2: Mid-ship Section 38
Figure 2.3: Global Stresses due to Combined Vertical and Lateral Bending and Torsion 39
Figure 2.4: Typical Load Cases for Low Cycle Fatigue Checks 42
Figure 2.5: The S-N Curve as described by Wohler 45
Figure 2.6: Micrographs showing how Surface Fatigue Cracks grow as the Material is Further Cycled 46
Figure 2.7: Hysteresis Loops and Cyclic Stress-Strain Curves 49
Figure 2.8: Cyclic and Monotonic Stress-Strain Curve 50
Figure 2.9: Cyclic Stress Strain Curves for Different Ship Steels 50
Figure 2.10: Definition of Stresses 52
Figure 2.11: k_e as a Function of Elastic Stress Range 54
Figure 2.12: Strain Ranges vs. Life on a Log-Log Plot 59
Figure 2.13: Typical Low Cycle S-N Curve 62
Figure 2.14: Geometry and Dimensions of Test Piece (Park and Lawrence) 65

Figure 2.15: Details of Specimen Tested by Lieurade 67
Figure 2.16: Transverse Non-Load Carrying Fillet Welds, Axial Loading 67
Figure 2.17: Test Specimen 70
Figure 2.18: S-N Curve based on Above Specimen 70
Figure 2.19: Strain-Life Curve for Welded Cruciform Joints 71

Figure 3.1: Global Structural Model 88
Figure 3.2: Intermediate Model: Cargo Oil Tank 89
Figure 3.3: Intermediate Model: Transverse Bulkhead 90
Figure 3.4: Local Model: Side-Inner Side Plating Stiffener Connection 90
Figure 3.5: Local Model: Bottom Plating with Longitudinal Stiffener 91
Figure 3.6: Methods for Local Strength Analysis 91
Figure 3.7a: Global Structural Model (ABAQUS) 93
Figure 3.7b: Magnified Submodel 93
Figure 3.8: Plate with Central Hole 98
Figure 3.9a, b and c: Stress Contours for Local Modelling Methods 98
Figure 3.10: Location of Local Models with Respect to Global Model 99
Figure 3.11: Displacement Contour Plot of Intermediate Model 100
Figure 3.12: Displacement from Intermediate Model Mapped on Global Model 100
Figure 3.13: Displacement Contour Plot of Local Model 101
Figure 3.11: Displacement from Local Model Mapped on Intermediate Model 101

Figure 4.1: Types of Hotspots 107
Figure 4.2: Shell and Solid Element Modelling 108
Figure 4.3: Finite Element Mesh of Buckling Stiffener to Flange of T-shaped Longitudinal 110
Figure 4.4: Stress Results for Detail in Figure 5.3 110
Figure 4.5: Structural Details of the T-shaped Longitudinal / Bulkhead Penetration and Typical Finite Element 113
Figure 4.6: Ship Detail Test Specimen 115
Figure 4.7: Finite Element Mesh of Ship Detail 115
Figure 4.8: Comparison of Fatigue Tests for the Ship Detail with Published Hotspot Stress Data and Stress Obtained from Surface Extrapolation 116
Figure 4.9: Dong's Stress Method Showing Mesh Insensitivity 118

Figure 4.10: Detail Studied and Definition of Crack 121
Figure 4.11: Finite Element Model showing Different Mesh Sizes 122
Figure 4.12: Predicted Stresses from Different Extrapolation Methods 124
Figure 4.13: Stress Concentration Factors 124
Figure 4.14a: Location of Hotspots in Bottom Detail 125
Figure 4.14b: Location of Hotspot in Bottom Detail 126
Figure 4.15: Predicted Stress at 60 mm from Weld Toe at BHS1 127
Figure 4.16: Predicted Stress at 60 mm from Weld Toe at BHS2 127
Figure 4.17: Predicted Stress at 60 mm from Weld Toe at BHS3 128
Figure 4.18: Predicted Stress at 60 mm from Weld Toe at BHS4 128
Figure 4.19: Predicted Stress at 60 mm from Weld Toe at BHS5 129
Figure 4.20: Predicted Stress at 60 mm from Weld Toe at BHS6 129
Figure 4.21a: Location of Hotspots 130
Figure 4.21b: Location of Hotspots 131
Figure 4.21c: Location of Hotspots 131
Figure 4.22 Predicted Stress at SHS1 132
Figure 4.23 Predicted Stress at SHS2 132
Figure 4.24 Predicted Stress at SHS3 133
Figure 4.25 Predicted Stress at SHS4 133
Figure 4.26 Predicted Stress at SHS5 134
Figure 4.27 Predicted Stress at SHS6 134
Figure 4.28: Predicted Stress at a Distance from the Weld Toe at IHS1 135
Figure 45.29: Predicted Stress at a Distance from the Weld Toe at IHS2 135
Figure 4.30: Predicted Stress at a Distance from the Weld Toe at IHS3 136
Figure 4.31: Predicted Stress at a Distance from the Weld Toe at IHS4 136
Figure 4.32: Predicted Stress at a Distance from the Weld Toe at IHS6 137
Figure 4.33: Predicted Stress at a Distance from the Weld Toe at IHS8 137

Figure 5.1: Time Domain Fatigue Damage 144
Figure 5.2: Frequency Domain Fatigue Damage 145
Figure 5.3: Constant Amplitude S-N Curve 146
Figure 5.4: Halfpenny shows Conservatism of Narrow Band Method 151
Figure 5.5: Comparison of Total Damage Calculation Methods 157
Figure 5.6: Combined Fatigue Damages 160

Figure 5.7: Combined Damage 161

Figure 6.1: Hotspot Stress Cycles at BHS5 168
Figure 6.2: Hotspot Stress Cycles at BHS6 169
Figure 6.3: Stress Contours for Loading Sequence, SEQ1 at BHS1 169
Figure 6.4: Stress Contours for Loading Sequence, SEQ1 at BHS3 and BHS4 170
Figure 6.5: Hotspot Stress Cycles at SHS1 172
Figure 6.6: Hotspot Stress Cycles at SHS5 172
Figure 6.7: Stress Contours at SHS3 and SHS5 for SEQ1 173
Figure 6.8: Stress Contours at SHS1 and SHS2 for SEQ2 174
Figure 6.9: Hotspot Stress Cycles at IHS2 175
Figure 6.10: Hotspot Stress Cycles at IHS3 176
Figure 6.11: Stress Contours at IHS1 SEQ5 176
Figure 6.12: Maximum Low Cycle Stresses for Each Detail 177
Figure 6.13: Typical Loading/unloading Cycle based on FE Data 178
Figure 6.14: Low Cycle Fatigue Damage at BHS6 179
Figure 6.15: Low Cycle Fatigue Damage at SHS1 179
Figure 6.16: Low Cycle Fatigue Damage at IHS2 180
Figure 6.17: Annual Low Cycle Fatigue Damage at Bottom Detail 181
Figure 6.18: Annual Low Cycle Fatigue Damage at Side Detail 181
Figure 6.19: Low Cycle Fatigue S-N Curve 182
Figure 6.20: Low Cycle Fatigue S-N Curve 183
Figure 6.21: Low Cycle Fatigue S-N Curve 183
Figure 6.22: Hydrodynamic/Structural Analysis of FPSO 186
Figure 6.23: JONSWAP and Pierson-Moskowitz Wave Spectra 188
Figure 6.24: Wave Pressure Contour; Direction = 0°, Freq = 0.7radians/sec 191
Figure 6.25: Wave Pressure Contour; Direction = 90°, Freq = 0.7radians/sec 191
Figure 6.26: Shear Force along the Length of the Ship 192
Figure 6.27: Bending Moment along the Length of the Ship 192
Figure 6.28: Heave RAO for Ballast Loading Condition 193
Figure 6.29: Pitch RAO for Ballast Loading Condition 193
Figure 6.30: Sway RAO for Full Loading Condition 193
Figure 6.31: Yaw RAO for Full Loading Condition 193
Figure 6.32: Mapped Pressure for Structural Model 194

Figure 6.33: Mass Distribution in Fully Loaded Condition 195
Figure 6.34: Ballast Stress transfer functions (Heading 0º to 90º) 195
Figure 6.35: Full Stress transfer functions (Heading 0º to 90º) 195
Figure 6.36: Wave Fatigue Damage vs. Wave Period for BHS3 197
Figure 6.37: Annual Wave Fatigue damage at BHS1 197
Figure 6.38: Annual Wave Fatigue damage at SHS1 198
Figure 6.39: Combined Fatigue Damage based on ABS 200
Figure 6.40: Combined Fatigue Damage based on LR 200
Figure 6.41: Combined Fatigue Damage based on DNV 201
Figure 6.42: Comparison of CS rules for Cumulative Fatigue Damage 201

LIST OF TABLES

Table 1.1: Comparison of Fatigue Assessment Procedures 26

Table 2.1: Operational Particulars 37
Table 2.2: Mid-ship Properties 37
Table 2.3: Minimum Number of Cycles for Loading/Unloading Operation 42
Table 2.4: Load Cases for Loading/Unloading Operation 43
Table 2.5: Parameters for Cyclic Stress-Strain Curve 51
Table 2.6: Values of k_m 54
Table 2.7: Fatigue Properties for the above Detail 65
Table 2.8: LR Hotspot Stress Reference S-N Curve Parameters 73
Table 2.9: DNV Proposed S-N Curve 75

Table 3.1: Comparison of Local Modelling Techniques 98

Table 4.1: IIW Recommended Meshing and Extrapolation Procedure 109
Table 4.2: Modelling Details and Analysis Results for Detail in Figure 5.5 114
Table 4.3: Geometry of Stiffener 121
Table 4.4: Hotspot Stresses for Low Cycle Load Cases 139

Table 6.1: Low Cycle Stresses 178
Table 6.2: Wave Headings and Periods 186
Table 6.3: Load Conditions 186
Table 6.4: Annual Wave Scatter Diagram for West Africa 188
Table 6.5: 100 year wave Scatter Diagram for North Atlantic 188
Table 6.6: Hotspot Stress S-N Curve Parameters 196
Table 6.7: Wave damage and low cycle damage for different sea scatter diagrams 199
Table 6.8: Combined Fatigue Damage for North Sea and West Africa 203

CHAPTER 1 INTRODUCTION

1.1 Introduction

For over two decades, ship shaped offshore units have been employed as a reliable and cost effective solution for the development of offshore fields located in deep waters and at distant locations worldwide. These include Floating Production Storage and Offloading units (FPSOs) and Floating Storage units (FSUs) operating in harsh environments and in water depths of more than 1500m. Thirty years on from their first appearance, FPSO systems still dominate the offshore market. Innovative technologies, coupled with developments of existing ones, have played a big part in maintaining this standing for so long – not least by enabling new possibilities for future projects to be considered.

According to a recent report by industry analyst Douglas-Westwood (2008 and 2009), in the period leading to 2013, more than $45.8 billion is expected to be spent on 121 floating production systems (FPS), with about 94 FPSOs – accounting for 80% of this capital expenditure - along with 12 tension leg platforms (TLPSs), 11 FPSSs and four spars are to be installed around the globe (Figure 1.1). This represents significantly greater prospects for the sector than the preceding equivalent period, which saw a total of 85 FPS units installed. Of this overall market value, the world's three major deepwater regions – Africa, North America and Latin America – account for 59% of forecast global capital expenditure.

FPSOs are typically offshore for 100 % of their design life as compared with trading tankers which operate only 70 % of the time in open seas. As such, the fatigue failure characteristics of FPSOs differ from trading tankers. Trading tankers are loaded and unloaded at still water conditions in harbour while FPSOs are subjected to more frequent loading and unloading cycles in open seas. Due to production, storage, ballast and offloading, the storage condition of the tanks in the FPSO change continuously and this brings about continuous change in loading condition.

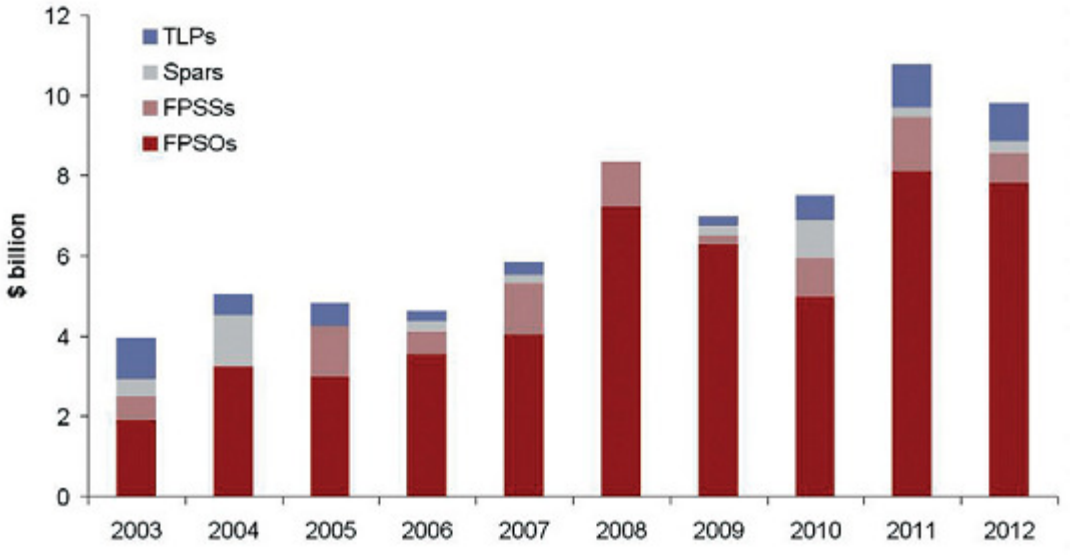

Figure 1.1: Forecast: Capital Expenditure on FPS Units by Year of Installation (Douglas-Westwood, 2009)

Along with loading and unloading cycles, the FPSO is also subjected to other forms of cyclic loading. Sources of cyclic loads include fluctuating loads, acceleration forces in floating structures, temperature fluctuations, mechanical vibration and environmental loading: wave, wind and currents. The occurrence of these loads, their magnitude, frequency and region all vary with time. These forces introduce overall fatigue loads (sagging and hogging) as well as local hull loads. Large still water forces and moments can be generated because of pressure changes from loading and offloading which causes a large variation in draft. Both low cycle large amplitude loads and high cycle low amplitude loads will contribute to fatigue damage in such structures.

Traditionally, ships were designed without explicit requirements with respect to fatigue failure. The Classification Societies demonstrated that the ships were implicitly safe against fatigue failure if the stresses are lower than the allowable stresses associated with ultimate limit state. With a growing variety of ships, their operational condition and application of new materials, it became more difficult to keep fatigue requirements implicit (Kaminski, 2007). In recent years, fatigue cracks have developed in FPSOs within few years of delivery. Significant yielding was observed for static loads and the linear elastic stress range observed was sometimes greater than three times the yield stress of the material. It has become necessary to

check the low cycle fatigue strength of highly stressed locations under repeated cyclic load mainly due to loading and unloading of cargo and ballast as these loads may cause cracks even though dynamic stresses are kept low.

Fatigue is considered to be one of the most important failure modes in mechanical and structural design. Wirsching (1998) noted that fatigue accounts for more than 80 % of all observed service failures in mechanical and structural systems. Fatigue limit state governs many parts of an offshore structure: at structural connections in the hull, especially where weld details are poor, at deckhouse endings, at hatch corners in ship decks and also at tank boundaries due to sloshing of liquids (Skjong, 1995). The fatigue control of FPSOs is directly dependent on site specific environment. Fatigue requirements in FPSOs are mandatory because they are subjected to continuously to sea actions without possibility of dry-docking for inspection and repair. Industry records show that many FPSOs suffer from fatigue damage (Fricke et al, 1997) thus, fatigue requirements in FPSOs have become a necessity.

The physics of fatigue has been well known for over 100 years but the application of this knowledge still poses a challenge. Fatigue of metals is a complex process that is still not fully understood and as such has been the subject of much active research. The fatigue of welded components is even a more complicated process. A great amount of research effort has gone into testing of welded joints, determining their fatigue characteristics as well as developing and evaluating new and existing approaches for fatigue analysis.

Fatigue cracks are initiated under the action of repeated loading on the structure. Initial defects may also be formed by fabrication procedure and remain undetected over time. Cracks initiate from such defects and propagate over a period of time. In addition to propagation, under repeated cyclic loading, cracks may also grow in an unstable way under extreme loads that can lead to catastrophic failure of the structure. The damage caused by fatigue loading can be grouped into the following three stages: crack initiation, crack propagation and final fracture. The crack initiation stage deals with the microscopic behaviour of materials. The crack propagation phase is better understood than the crack initiation process, and there exist different theories that exist to model crack growth e.g. Paris law. This process is dependent on the stress

range, the initial crack size and the geometry of the detail. In welded structures, cracks almost always start at a weld defect. The propagation period of a crack in a structural component accounts for more than 90 % of the fatigue life of that component (Mansour and Ertekin, 2003). Final fracture occurs when the crack size propagates to a critical size. The final fracture depends on the stress level, the crack size, material toughness and general environmental conditions.

Ship designers have known fatigue cracks and fatigue damages for several decades. Initially the obvious remedy was to improve the design of the structural detail. With the introduction of higher tensile steels (HTS-steels) in hull structures, at first in the deck and bottom to increase hull girder strength, and later in local structures, the fatigue problem became more imminent. The fatigue strength does not increase according to the yield strength of the steel. In fact, fatigue strength is found to be independent of the yield strength. The higher stress levels in modern hull structures have therefore led to a growing number of fatigue crack problems. To ensure that the structure will fulfil its intended function fatigue assessment, supported where appropriate by a detailed fatigue analysis, should be carried out for each individual type of structural detail. Every welded joint and attachment or other form of stress concentration is potentially a source of fatigue cracking and should be individually considered.

FPSOs consist of a large number of complicated welded components and it is known that cracks are inherent in any welded structure. Cyclic wave induced stresses causes cracks to grow, a majority of which start in local area of high stresses due to welds connecting structural elements. Figure 1.2 illustrates different types of cracks around cut outs and openings in typical ship structural details. Some of these cracks may stop growing if it moves into areas of low stresses while others may continue under cyclic stresses.

Degradation due to fatigue crack growth is a gradual phenomenon. If however fatigue life is insufficient, a catastrophic failure can occur. An early example of out of control cracks occurred in the failures of Liberty Ships built between 1941 and 1945, where cracks initiated from stress concentrations and propagated along weld lines. Almost 2751 of the ships were built over a period of 4 years, 19 of those broke into half

without warning and there were about 2000 instances of brittle fracture reported. The dramatic and catastrophic failure of the Alexander Kielland in 1981 was reported to be as a result of fatigue and poor workmanship (Incecik, 1982). Notable failures of ship shaped structures such as the MV Castor, Prestige, Erica and Petrojarl 1 are examples of the serious consequences of fatigue cracks. There is the risk of loss of life as well as environmental pollution associated with cracks in these types of structures. These failures triggered the interest of researchers into fatigue and fracture mechanics for different types of welded structures including ships. Despite all these efforts, fatigue cracking problems are still occurring in structures.

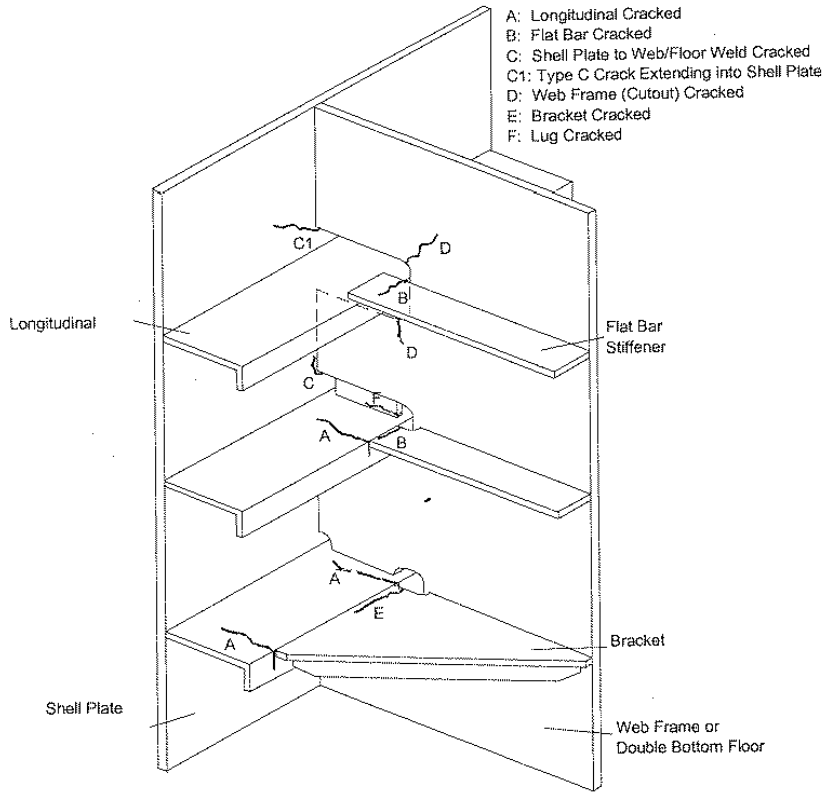

Figure 1.2: Typical cracks found in ship structural details (Bai, 2003)

The interest in low cycle fatigue in FPSOs has increased over the years because cracks have been observed within 5 years of service delivery of the structure. There are also relatively large numbers of loading/offloading cycles associated with FPSOs than other type of ship structures (Urm et al 2004). The frequency of loading and

unloading cycles can result in significant variations of resulting hull girder loading as illustrated in Figure 1.3.

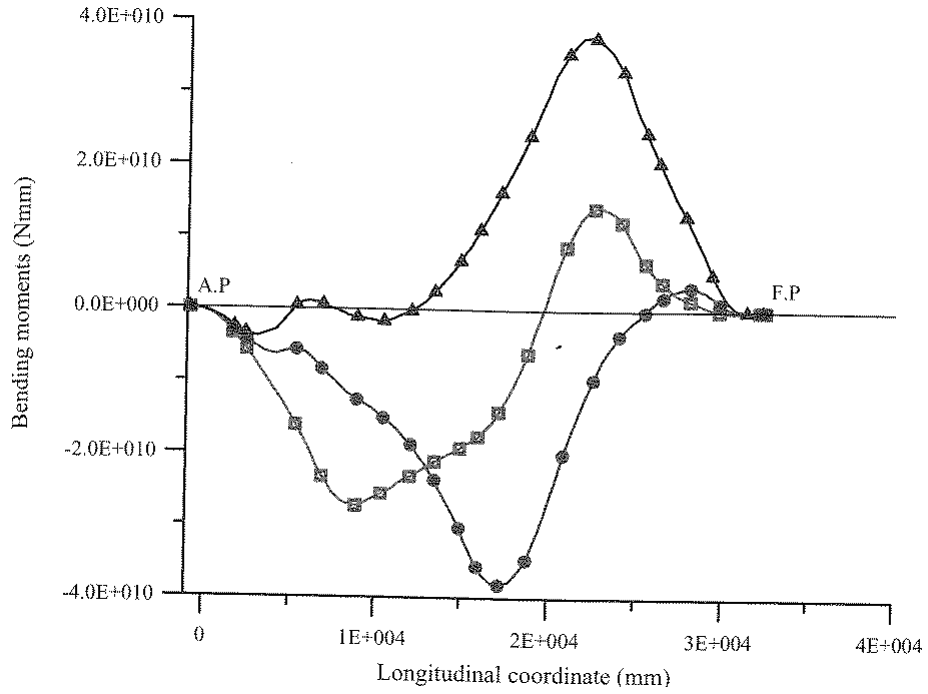

Figure 1.3: Variations in still water bending moment along vessel length due to loading and offloading conditions (Paik and Thaymballi 2007)

Low cycle fatigue is also very important in aged FPSOs especially those that have been converted from tankers, where due to accumulated fatigue damage over it's past service life; there is the loss of structural integrity in the FPSO hull. Newport et al (2004) discuss the survey and repair work of cracks found in the Kuito FPSO. The FPSO is a converted tanker deployed in offshore Angola which was previously used as a trading tanker at the Trans-Alaskan Pipeline System (TAPS) trade route and worldwide trading. Over 470 defects were found in the bottom brackets, weld cracks in the centreline girder, connections between the longitudinal stiffeners and oil tight bulkheads. These cracks were attributed to fatigue resulting from a combination of trading history, poorly designed connections and high stress ranges experienced during the loading and offloading cycle of the FPSO during service.

As stated earlier, low cycle fatigue in FPSOs is mainly associated with continuous production and periodic offloading. It is now the subject of researches by some

classification societies because of increased interest from ship owners and operators. Though some believe that the effect is moderate in some parts of the structure (Urm et al, 2004 and Lloyd's Register, 2008), it is found to significantly contribute to fatigue life in other areas of the structure. Some design codes have provided provisional procedures to assess fatigue strength under high stress and low cycles.

1.2 High Cycle and Low Cycle Fatigue

Fatigue can be divided into low cycle fatigue which is associated with low frequency and high stress and high cycle fatigue which is associated with high frequency and low stress levels. High cycle fatigue uses elastic stress amplitude as the governing load parameter. High cycle fatigue occurs at relatively high number of load cycles, where stresses and strains are largely confined to the elastic region. High cycle fatigue data is usually presented as a plot of stress, S, versus the number of cycles to failure, N. High cycle fatigue assessment is carried out using stress-life methods.

The fatigue life of a component is the number of cycles to failure at a specified stress level while the fatigue strength or endurance limit of a component is the stress below which failure does not occur and this tends to increase with an increase in static tensile strength. For example, high strength steels have much higher fatigue strength than aluminium alloys and also have a fatigue limit, meaning that below a certain stress level, steels will never fail due to cyclic loading alone. Aluminium, on the other hand, does not have a fatigue limit as it will always fail if tested to a sufficient number of cycles. This does not mean that it is wise to use a very high strength steel to maximise fatigue life because as tensile strength increases, the steel becomes more sensitive to surface conditions, residual stress state and the presence of inclusions which act as stress concentrations.

Low cycle fatigue is characterised by repeated plastic strains during cyclic loading where fatigue failure occurs at a low number of load cycles. The analytical procedure used to address strain-controlled fatigue is commonly referred to as the Strain-Life, Crack-Initiation, or Critical Location approach. This design approach is normally used where high stress concentration exists and the local material response is plastic

deformation. Low-cycle fatigue is typically associated with fatigue life between 10 to 100,000 cycles; high-cycle fatigue is associated with life greater than 100,000 cycles.

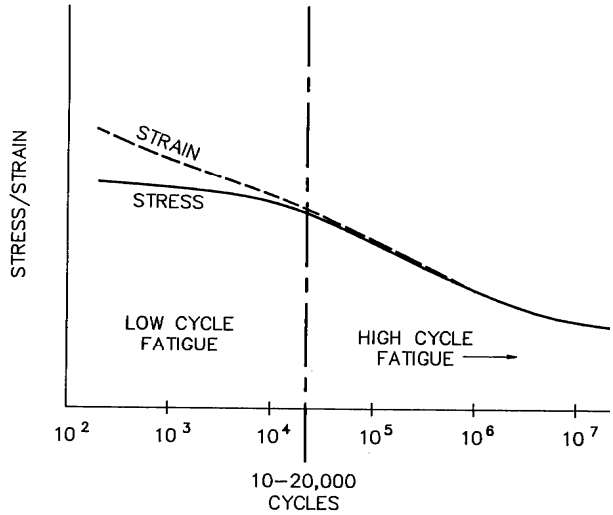

Figure 1.4: High Cycle and Low cycle Fatigue

The S-N fatigue assessment approach is favoured by most classification societies for both high cycle and low cycle fatigue problems. Lloyd's Register (2008) recently published guidance on the strength and fatigue assessment of structures for floating offshore installations. The fatigue assessment covers topics from high and low cycle fatigue assessment to cumulative damage procedures. Det Norske Veritas (2005) developed a methodology in Recommended Practice DNV-RP-C206 for fatigue design of FPSOs. This document is reviewed by Lotsberg et al (2005) and it deals with issues of hot spot stress extrapolation methods, low cycle fatigue from loading and unloading of cargo and ballast and selection of appropriate S-N curves for low cycle fatigue assessment.

1.3 Low Cycle Fatigue in FPSOs

The integrity of ships in service is generally evaluated considering the ultimate strength as one failure criterion and fatigue strength as the other. Fatigue in this context is primarily high cycle fatigue. Low cycle fatigue is normally defined as fatigue failure below 10^5 cycles. The stresses associated with low cycle fatigue are usually high enough to cause considerable amount of plastic deformation in the region of the stress concentration. Fatigue life in low cycle regime is normally expressed in

terms of total strain range, because in high stress levels, critical fatigue zones are more likely subjected to strain controlled condition rather than load or stress controlled condition. Low cycle fatigue is associated with macro plastic deformation in each cycle where significant plastic straining occurs. As such, strain is often the preferred parameter to account for the non linear response under low cycle loads.

Low cycle fatigue has received much attention since the early work of Coffin (1972) and Manson et al (1964) in the 50s and 60s. The offshore industry has developed an interest in the last 4 years especially in FPSOs because cracks were observed within 5 years of service delivery. Some of these cracks were attributed to poor fatigue resistant design and fabrication while others were due to high stresses generated by loading and unloading cycles (Wang et al, 2006).

Low cycle fatigue is important in structures that are subjected to small numbers of load cycles in their economic life. If it is required to keep all stress levels below fatigue limit, then the structure will be very heavy without this being necessary. The stress associated with low cycle fatigue is usually high enough to cause considerable amount of plastic deformation in the region of the stress concentration and has sometimes being found to be greater than three times the yield strength of the material (Heo et al, 2004). In low cycle fatigue, the relationship between stress and strain is no longer linear. This relationship between stress and strain is often characterized by a hysteresis loop, which may change from cycle to cycle. The hysteresis loop defines a single fatigue cycle in the strain life method. Stress and strain amplitudes are one half the total stress and strain ranges. The hysteresis loop is defined using values $\Delta\sigma, \Delta\varepsilon$ that are relative to some point (σ, ε) in stress – strain space.

The effect of loading and unloading of cargo and ballast has been found to give contribution to fatigue in some areas of an FPSO. The number of loading and offloading cycles in an FPSO can be up to 1000 cycles for a 20 year operational life, which is higher than that for a trading tanker. Kamiski (2007) shows that low cycle fatigue is important in FPSOs because the pressure variations on bulkheads between

the ballast tanks and cargo tanks at the bottom are high, resulting in plastic deformation.

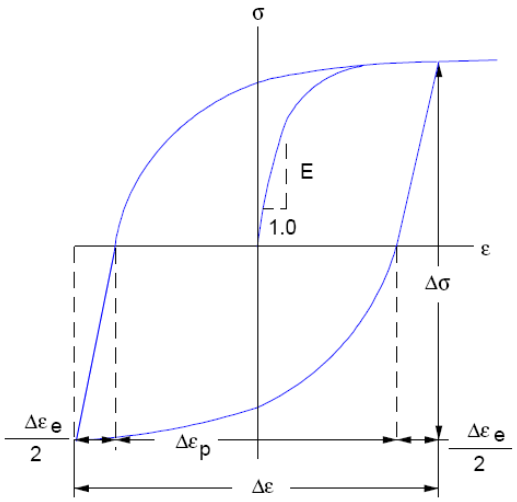

Figure1.5: Stress-strain hysteresis loop

As mentioned earlier, low cycle fatigue is receiving some attention from the offshore industry and has been subject of research (Wang et al, 2006, Heo et al, 2004 and Mravak, 2007). However, industry records show that many FPSOs still suffer from fatigue damage. Some design codes provide provisional procedures to assess fatigue strength under high stress and low cycles. Many classification societies are addressing this issue and have published several guidance documents to this effect. DNV has published documents that incorporate guidelines for low cycle fatigue assessment. ABS and Lloyd's Register also give guidance for low cycle fatigue assessment. The low cycle fatigue assessment methods in these guidelines are chosen based on several factors, the most important being the design philosophy of the Society. It is well worth mentioning that these guidelines are all different variations of the stress based fatigue assessment procedure.

1.4 Fatigue Life Estimation Methods

'Fatigue failure is by no means a rigorous science and the idealization and approximations inherent in it prevents the calculation of absolute fatigue life for even the simplest structure'

UK HSE (2001)

The prediction of fatigue lives is essential for the safe management of an offshore installation. According to the UK HSE (2001), the industry standard approach must address four specific issues:

- The operational environment of a structure and the relationship between the environment and the imposed forces in a structure.
- The initial stresses at a critical point in a structure induced by external forces acting on the structure.
- The time to failure due to accumulated stress history at a critical point.
- The definition of failure used in design.

The procedure available for fatigue life estimation of welded components is currently based on different conceptual approaches with specific applications, validity ranges and modelling requirements. According to Figure 1.6, assessment is by either the stress or strain based approaches or by crack propagation approach. Fricke (2002) provides an overview on the state of the art development in the fatigue analysis of welded joints. Comprehensive information on procedures for fatigue assessment for offshore structures is contained in (Almar-Naess, 1999). Radaj and Sonsino (2006) also give analysis procedures and application examples on the fatigue assessment of welded joints using local approaches.

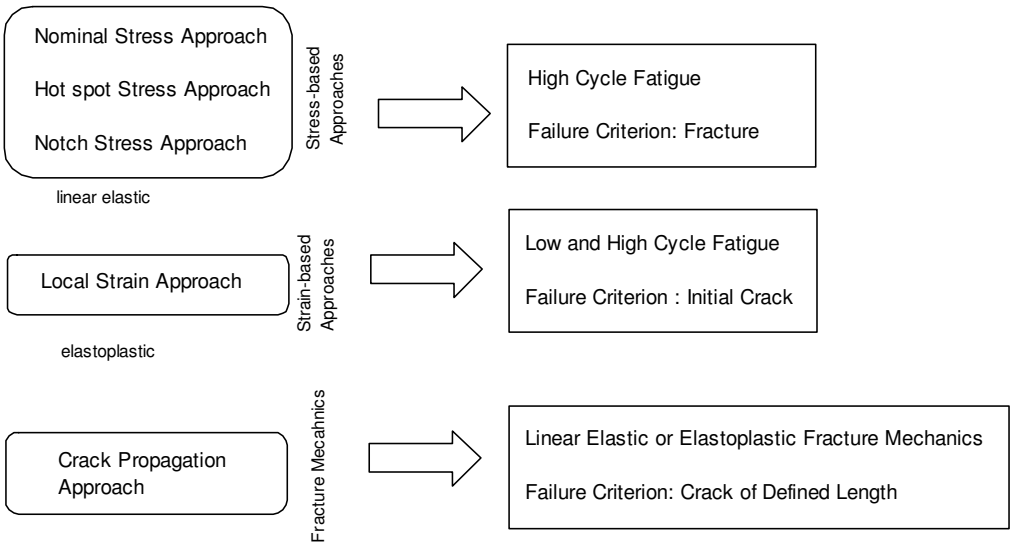

Figure 1.6: Fatigue assessment procedures of welded components

1.4.1 Stress-Life Approach

Also referred to as the S – N method, this is one of the earliest fatigue design approaches to be developed and is still a very popular tool for engineering fatigue analysis. The primary feature of the S-N approach is their range of validity presuming dominant elastic behaviour of the material and the structure. Its success is based on the fact that, for predominantly elastic loading, the state of stress in a component can often be characterized quite accurately. As long as the state of fluctuating stress can be accurately estimated, this method can do a good job of predicting fatigue (Collins, 1993).

The S-N approach is often categorised as high cycle fatigue methodology and is widely used in design applications where the applied stress is within the elastic range of the material and the resulting fatigue lives are long. The basis for this method is the S – N diagram displaying curves of stress amplitude (S) against cycles to failure (N), see Figure 1.7. The S – N curve is the quantitative relationship between the fatigue strength and the number of cycles corresponding to a specific probability of failure for a structural detail.

The use of S – N curves assumes a low but finite probability of failure at the calculated life. Information from the S-N curve, together with possible correction factors for mean stress and thickness is used to estimate the number of cycles to failure. As failure is defined generically, the constant amplitude S – N diagram can be used to relate stress to either the crack initiation period or total fatigue life. Fatigue failure occurs if the stress range exceeds the strength as defined by the S – N curve at the service life of the component under consideration or if the service life exceeds the life defined by the S – N curve at a given stress level.

The equation of a basic S – N curve may be expressed as:

$$N = A(\Delta\sigma)^{-m} \qquad 1.1$$

Where N is the number of cycles to failure, A is a material constant and m is slope parameter for the S – N curve. $\Delta\sigma$ denotes stress range.

The stress – based approach forms the basis of most rules and recommendation for fatigue design and analysis of components and structures (DNV 2003, DNV 2006 and Lloyd's Register 2004). When applying this method to structural details, one has to choose between several types of stress analysis and corresponding S-N curve. The three main approaches are the nominal stress approach, the hot-spot stress approach and the notch stress approach, see Figure 1.8.

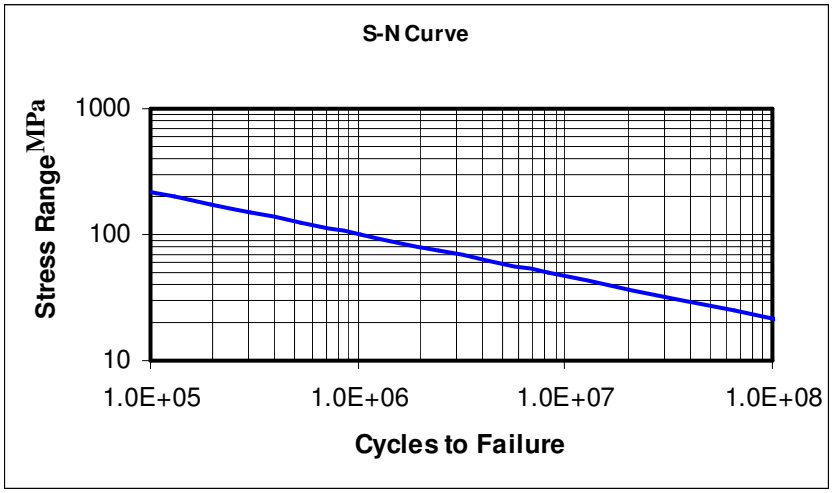

Figure 1.7: Typical S – N curve

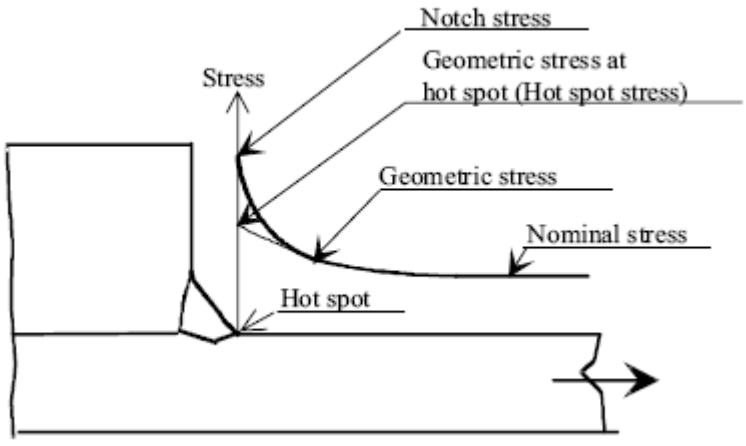

Figure 1.8: Definition of stresses

Nominal Stress Approach

Historically, fatigue assessment of welded structures is based on the nominal stress approach with categorised details and appropriate stress-life (S – N) curves. The nominal stress is determined from the sectional properties of the structure based on simple linear elastic theory. A nominal stress range versus fatigue life curve is obtained from fatigue tests of the weld detail of interest. These stresses use the nominal stress field calculated remote from the localised stress concentration together with the S – N curves of nominal stress amplitudes to determine fatigue life. The nominal stress S – N curve comprises the influence of material, geometry and surface effects but the effect of the weld is ignored. Figure 1.9 shows the variation of the nominal stress in a beam-like component.

The design S – N curve is usually some statistical bound to published experimental data, typically mean minus 2 standard deviation of log N. As the nominal S – N curve refers to a particular detail, it is not necessary to quantify the local stress concentration effect of the detail itself. Hence, the effects of increase in stresses from structural discontinuities, local notches and predeformations are ignored.

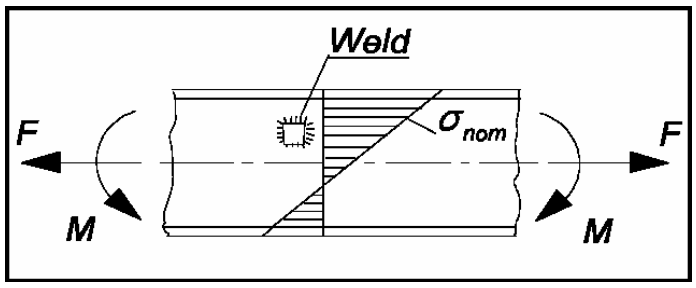

Figure 1.9: Nominal stress in a beam-like component

While the nominal stress approach is the most widely used in fatigue design, it is difficult to define nominal stress values for complex structures such as ships (Bai, 2003) as it does not evaluate geometric and stress concentration effects. This issue may be overcome by the use of either the hotspot stress or notch stress. Even with this limitation, the nominal stress approach is quite reliable given that the nature of the welded joint under consideration correlates closely to the given class of joint for

which the curve is established. The method requires little computational effort especially for simple geometries. Nominal stress approach is the basis for fatigue assessment in many areas of mechanical and structural design. This method is basic to design guidelines and codes like the British Standards, ASME boiler codes (BS 5500), IIW recommendations, European standards and also design guidelines for classification societies in the marine industry.

Hotspot/Structural Stress Approach

The hotspot stress (HSS) approach is an extension of the nominal stress method. The structural/hotspot stress is applied when nominal stress cannot be defined due to complicated geometry effects. The hotspot stress is the local stress at a hotspot (critical point) where a crack may be initiated. It includes all the stress raising effects of the structural detail excluding the stress concentration due to the weld itself. The hotspot stress is computed as the sum of the membrane stress and the local bending stress excluding the non-linear peak stress due to the weld notch (Figure 1.10).

$$\sigma_{hotspot} = \sigma_{membrane} + \sigma_{bending} \qquad 1.2$$

The assessment of fatigue strength and service life is carried out by a comparison of the HSS amplitude or range in a component with a base hotspot S-N curve for the welded connection. The local stress concentration due to the weld notch is excluded but this is assumed to be implicitly included in the S-N curve.

The hotspot method has the advantage that once the S-N curves are established for typical welds, an infinite number of details can be investigated. The method is also compatible with the finite element method and there exist different approaches for finite element modelling of welds. This in a way makes the method more complex than the nominal stress approach. For most details, a fine mesh finite element model is required to obtain an accurate stress distribution because of higher stress gradients at the location of the hotspot. An extrapolation procedure is generally used to define the hotspot stress. Extrapolation methods are sensitive to element sizes, element types and modelling techniques. Many authors have investigated extrapolation procedures and

classification societies have developed guidelines for this type of analysis. The main drawback of the HSS method is that it is only applicable to evaluation of failure by toe cracking. However, this is not a severe drawback since structures with a possibility of toe cracking is associated with bad design practices. Chapter Five (5) covers a more detailed description and application of this method.

Notch Stress Approach

Notch stress is the total stress which includes geometric stress and stress due to the presence of the weld itself assuming a linear elastic material behaviour (Figure 1.10). The notch stress is said to be the product of the hotspot stress and a weld concentration factor. The weld concentration factor can be estimated from parametric formulae, from diagrams or calculated from finite element or boundary element models.

This approach is restricted to the assessment of failure from the weld toe or weld root. It is not applicable where considerable stress components parallel to the weld or parallel to the root gap exist. For structural steels and aluminium an effective notch root radius of r = 1 mm has been verified to give consistent results. For fatigue assessment, the effective notch stress is compared with a common fatigue resistance curve. The method is limited to plate thicknesses t >= 5 mm. For smaller wall thicknesses, the method has not yet been verified (Maddox, 2001).

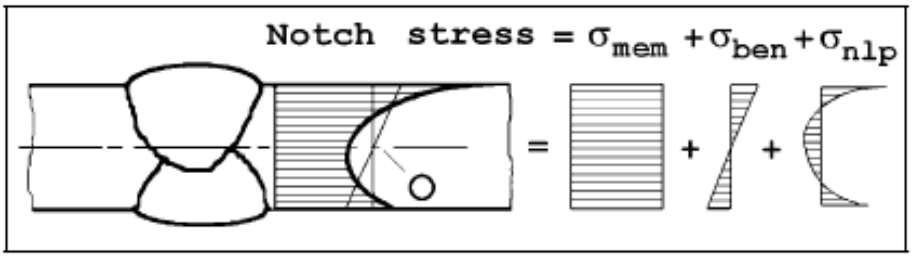

Figure 1.10: Nonlinear stress distribution at weld toe

The limitation of this approach is the local geometry of the toe or root of a weld is variable and not known at the design stage, thus the weld detail is normally idealised as having a particular shape and weld toe or root radius. Local stress may then be

determined parametrically by equations or numerically using finite elements. Some researchers (HSE, 1999) recommend this method only for comparative studies of fatigue performance of different welded joints. Until recently, the notch stress approach did not appear in fatigue design specifications. DNV and BV have proposed the use of this approach for fatigue assessment of some ship details.

All the stress based methods rely on empirical data, a stress measure and Basquin's relation. The nominal stress method utilizes experimental reference materials and a very coarse and limited stress measure. In the practical design of ship structural details it can be difficult to define the nominal stress level to be applied together with the geometry specific S-N curves. Also, the use of a limited number of established S-N curves in fatigue design may complicate the utilisation of improved local detail design and workmanship in the fatigue life assessment (IACS, 2006). The hotspot stress incorporates a more complete stress measure procedure as opposed to the nominal stress approach. The hotspot stress has to be determined by extrapolation of stresses outside the notch region. The finite element mesh has to be fine enough to represent the geometric stress in this region. Strict consistency in FE modelling is required. Practice for extrapolation has varied as its basis is founded on experience from test measurements and numerical analysis of stress distributions at the hot spot region (IACS, 2006)**.** The notch stress method relies on very concise empirical foundation and a very detailed stress measure. The notch stress approach in its simple form has been successfully applied to non-welded machine parts with an expected infinite life (Radaj, 1990). Radaj et al (2006) state that the notch stress approach for welded joints should be applied in cases where the nominal or structural stress approach is deficient or impossible. It can be used for an absolute assessment of fatigue strength but should then be combined with evidence from test results. The approach is especially well suited for relative design evaluations based on parametric studies. In the finite life range, the notch stress approach should be combined with the notch strain and crack propagation approaches.

1.4.2 Strain-Life Approach

The strain-life method is based on the assumption that in many components, the response of the material in critical locations, such as notches, is strain or deformation

dependent. The main idea behind this method is that the mechanical behaviour of a material at the notch root with respect to local deformation, local damage and crack initiation is similar to that of a miniature axially loaded unnotched specimen with respect to global deformations, global damage and complete fracture, Figure 1.11.

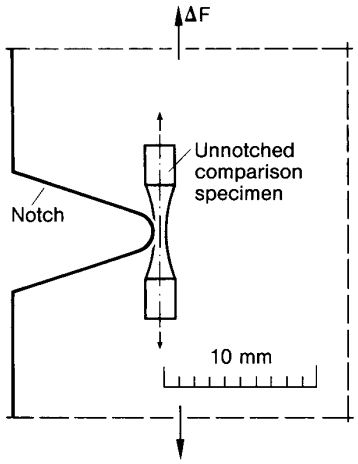

Figure 1.11: Comparison specimen for crack initiation behaviour at a notch

Fatigue assessment in the strain-life approach involves determining the stresses and strains at the notch root in the elastic-plastic condition and comparing them with the strain-life curve of the material in the miniature specimen up to complete fracture. The calculation of notch stresses and strains is based on a stabilised cyclic stress-strain curve. The expected fatigue life is determined using the strain-time history at the notch root and smooth strain-life fatigue properties of the material. These properties are combined with a method for determining local notch stress and strain that considers plastic deformation. Elasto-plastic finite element method, Neuber's rule and Glinka's strain energy density method are the most common methods for determining local stresses and strains.

Crack growth is not explicitly accounted for in the strain – life method and for this reason, strain life methods are considered crack initiation life estimates. According to Bai (2003) the failure criteria for the strain life approach may be one of the following:

- The life to a small detectable crack
- The life to a certain % decrease in load amplitude

- The life to a certain decrease in the ratio of loading to unloading moduli
- The life to fracture

The strain-life fatigue approach assumes that steady state hysteresis loops can be reduced to elastic and plastic strain ranges to give total strain ranges as illustrated in the hysteresis loop given in Figure 1.12.

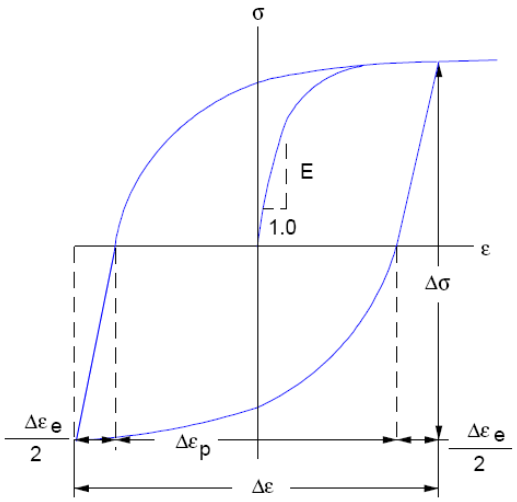

Figure 1.12: Stress and strain ranges in a hysteresis loop

The total strain amplitude $\frac{\Delta\varepsilon_T}{2} = \frac{\Delta\varepsilon_e}{2} + \frac{\Delta\varepsilon_p}{2}$

Basquin (1910) observed that the stress – life plot could be linearized with full log coordinates thereby establishing the exponential law of fatigue. Basquin's equation can be expressed in terms of true elastic strain amplitude as:

$$\varepsilon_e = \frac{\Delta\varepsilon_e}{2} = \frac{\sigma_f'}{E}(2N_f)^b \qquad 1.3$$

The parameters σ'_f and b are fatigue properties of the metal. The fatigue strength coefficient, σ'_f, is approximately equal to σ_f for many metals. The fatigue strength exponent, b, varies between approximately -0.05 and -0.12.

Coffin (1971) and Manson (1965) both working independently on a thermal-fatigue problem, established that plastic strain-life data could also be linearized with log-log coordinates. As with the true stress-life data the plastic strain-life data can be related by the power-law function:

$$\varepsilon_p = \frac{\Delta\varepsilon_p}{2} = \varepsilon_f^{'}\left(2N_f\right) \qquad 1.4$$

where ε_p = plastic-strain amplitude; ε'_f = fatigue ductility coefficient; and *c* = fatigue ductility exponent. The parameters ε'_f and c are also fatigue properties where ε'_f is approximately equal to ε_f for many metals, and c varies between approximately -0.5 and -0.7. The total strain for a fully reversed testing is expressed as the sum of the elastic and plastic strains:

$$\frac{\Delta\varepsilon_T}{2} = \frac{\Delta\varepsilon_e}{2} + \frac{\Delta\varepsilon_p}{2} = \frac{\sigma_f^{'}}{E}\left(2N_f\right)^b + \varepsilon_f^{'}\left(2N_f\right)^c \qquad 1.5$$

Where

N_f	=	cycles to failure
ε	=	strain amplitude
ε_e	=	elastic strain amplitude
ε_p	=	plastic strain amplitude
E	=	modulus of elasticity
b	=	fatigue strength exponent
c	=	fatigue ductility exponent
$\sigma_f^{'}$	=	fatigue strength coefficient
$\varepsilon_f^{'}$	=	fatigue ductility coefficient

This equation is the foundation for the strain-based approach to fatigue and is called the strain-life relationship. The equation is represented graphically in Figure 1.13; the two straight lines represent the elastic strain and the plastic strain. At large strains or short lives, plastic strain component is predominant and at small strains or long lives, elastic strain component is dominant.

The parameters of the strain life curve may be obtained from the following three methods (Wang, 2006):

- Direct measurement from testing though there is very little data available in literature
- Using published fatigue parameters of steels having similar monotonic properties. There is a catalogue of fatigue parameters for a wide variety of steels.
- Empirical relationships for parameters based on monotonic tests. Extensive fatigue testing of steels has led to empirical forms in which the parameters can be established from such monotonic properties.

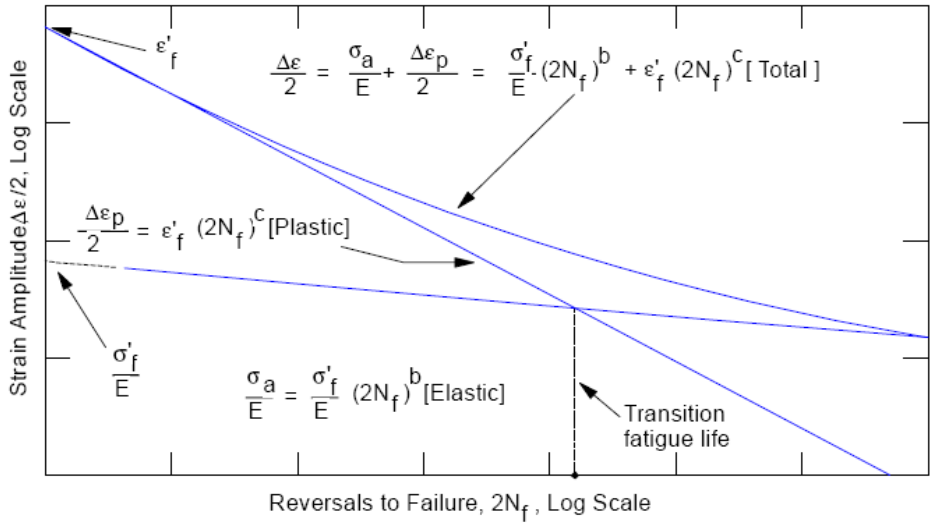

Figure 1.13: Strain-Life Plot (AISI, 2002)

The strain-life approach involves the techniques for converting the loading history, geometry and materials properties (monotonic and cyclic) into a fatigue life prediction. The procedure involved in the prediction process must be performed sequentially. Firstly, the stress and strain at the critical region is estimated and then a cycle counting method is used to reduce the load-time history. The next step is to use the finite element method to convert the reduced load-time history into a strain-time history and also to calculate the stress and strain in the highly stressed area. When a local stress-strain history has been calculated, a valid cycle-counting method must be used to identify ranges of strain that are being applied. When strain cycles have been

counted, experimental data from tests carried out under constant-strain conditions will be needed for the life estimation (not S-N data from conventional constant-load tests). Crack initiation methods are employed to predict the fatigue life. Palmgren and Miner linear rule may be used to accumulate the fatigue damage. Finally, the damage values for all cycles are summed until a critical damage sum (failure criteria) is reached.

The strain life method gives a reasonably accurate picture of the crack initiation stage and accounts for cumulative damage due to variation in cyclic load. It is a comprehensive approach that can be applied to both high cycle and low cycle fatigue problems. For high cycle application, the plastic strain term becomes negligible and the total strain life is reduced to elastic effects. The method also accounts for plastic strain, residual stresses and variable amplitude loading and is easily extrapolated to other cases: notch geometry, materials load cases and multi-axial loading. The main limitation of this method is that more complicated to apply than the stress-based approach. The lack of adequate and appropriate material data and experience with the method also limit the use of the strain-life method.

1.4.3 Fracture Mechanics

Fracture mechanics is employed in the fatigue assessment of structures or components subjected to high cycle fatigue condition, in situations where the normal fatigue strength assessment method may be unreliable or wholly inappropriate. Fracture mechanics approach determines the fatigue strength and service life of a structural component with an existing crack. The life of the structure is obtained by integrating a relevant crack growth laws. The most popular crack growth law was proposed by Paris and Erdogan and it assumes that the real flaws can be idealised as sharp tipped cracks, which propagate at a rate that is a function of the range of the cyclic stress intensity factor, ΔK.

Rate of crack propagation $\frac{da}{dN}$ (in mm per cycle) = $A(\Delta K)^m$

A, m are constants which depend on the material and the applied conditions, including environment and cyclic frequency. ΔK is the range of stress intensity factor

corresponding to the applied stress cycle and the instantaneous fatigue crack dimension. Cyclic crack propagation occurs when the threshold value of K is exceeded and ends when the critical value of K is reached or the load carrying capacity of the remaining cross-section is reached with a larger crack length.

For a crack in an elastic body subject to a load, the elastic energy stored in the body is a function of two independent variables: the displacement of the load, and the area of the crack. The energy release rate is defined by the partial derivative of the elastic energy of the body with respect to the area of the crack. This definition of the energy release rate assumes that the body is elastic, but invokes no field theory. Indeed, the energy release rate can be determined experimentally by measuring the load-displacement curves of identically loaded bodies with different areas of the cracks. No field need be measured. Many materials, however, can be modelled with a field theory of elasticity. When a material is modelled by such a field theory, the energy release rate can be represented in terms of field variables by an integral, the J integral. The J integral can be developed for both linear and nonlinear elastic theories and is mainly used to describe crack propagation in the case of higher stresses and strains with accompanying plastic deformation at the crack tip.

Typically, the crack initiation life using the local approaches and the crack propagation life using fracture mechanics is added up to give the total life of a specimen. Some argue that small cracks or flaws caused by fabrication processes or preloading are inherent in welded components so the fatigue life of such components should be based simply on crack propagation. Generally, an initial crack size is introduced into fatigue calculations for this purpose. In principle, this argument is correct but the behaviour of very short cracks cannot be described correctly on the basis of the usual fracture mechanic approach. The fracture mechanic approach only gives acceptable results for the behaviour of larger cracks in welded connections joints.

1.4.4 Summary of Approaches

A summary of the fatigue life estimation methods is shown in Table 1.1. The nominal stress approach is considered the most classic and robust. The effectiveness of the approach is based on the condition that the structural component and the test specimen correspond in all respect of all influence parameters. Fatigue rules were based on the use of nominal stress approach till the early nineties (Lotsberg and Landet, 2005). The use of more refined FEA resulted in the need for an assessment procedure more refined than the nominal stress approach hence the development of the hotspot stress approach and also the fact that the nominal stress cannot be readily calculated in regions of non uniform stress (e.g. due to loading or geometric stress concentration from structural arrangement).

The use of the hotspot stress method avoids the drawbacks of the nominal stress method. The hotspot stress has the widest application and is agreed to be a better approach for fatigue analysis of ship structural elements (Lotsberg, 2006) and (Bergan and Lotsberg, 2006). While the notch stress evaluation has the advantage of referring directly to the notch at which the crack initiation is expected, the procedure is known to be numerically intensive because a very fine mesh is required to capture the exact stress peaks at the notch.

Classification societies find the S-N approach more attractive than the other approaches mainly because it is convenient to use the existing stress concentration factors available in the design codes to compute local stresses and the fatigue damage from low cycle and high cycle fatigue is easily combined. A comparative study of different classification society rules based on the nominal stress, hotspot stress and notch stress approaches was carried out on a pad detail of a Panamax container vessel by Fricke et al (2002). Large differences in predicted lives, ranging from 1.8 to 20.7 years are found mainly because the stresses varied significantly between each approach coupled with uncertainties regarding S-N curves. The S-N method for fatigue assessment is still far from perfect.

S-N approaches are tailor made for high cycle fatigue problems. However, when load levels increase (low cycle regime), the S-N method breaks down which is when the

local strain based approach becomes very useful. The application of the local strain method to low cycle fatigue problems has increased in popularity recently and is most widely favoured because it accounts for the plasticity in the structure. The method has been successfully applied to LCF problems but its application to HCF problems introduce a level of uncertainty due to the relatively limited number of points available in the HC region of the LCF damage curves.

Fracture mechanics is not suitable for defining precise fatigue strengths or lives since the result will be dependent, to a very large extent, on the assumptions made regarding the values of the constants in the crack growth equations, size of initial flaw, shape of resulting fatigue crack etc. Thus if the objective is to define a particular fatigue strength or life, care should be taken to make the most pessimistic assumptions.

1.5 Motivation and Scope of Research

The present work was motivated by the occurrence of fatigue cracks in ship structures within a few years of delivery, even though high cycle fatigue strength had been checked at the design stage and the lack of tools to predict the occurrence of such cracks. Significant yielding has also been observed for static loads, where the linear elastic range was much greater than the material yield stress. All these problems are thought to be caused by low cycle fatigue but this is yet to be proven and the problems are causing a lot of concern in the offshore industry. Until recently, existing fatigue design codes did not cover low cycle fatigue problems. Several classification societies have issued preliminary guidance notes on tackling low cycle fatigue problems in FPSOs but these design notes and guidance have not been fully tested. Some studies have also been carried out on low cycle fatigue problems in ship structures and it has been suggested that further research work be carried out to make guidance on the fatigue life estimation of ship structure considering low cycle fatigue.

Table 1.1: Comparison of Fatigue Assessment Procedures

	Stress Life	Strain life	LEFM
Assumptions	Most life is consumed by nucleating crack. Accounts for Elastic deformation only. Nominal stresses and material strength control fatigue. Accurate determination of notch concentration factor for each geometry and material is important	Plasticity around stress concentration. Local stresses and strains control fatigue behaviour. Accurate determination of notch concentration factor for each geometry and material is important.	Nominal stress and crack size control fatigue. Accurate determination of initial crack size
Advantages	Changes in material and geometry can be easily evaluated. Large empirical database for steel and standard notch shapes	Takes plasticity effect into account Mean stress effects are accounted for.	It is the only method that deals directly with cracks
Limitations	Does not account for notch root plasticity. Mean stress effects are often in error. Requires empirical Kf for good results.	Requires accurate and empirical Kf Other factors like surface finish and processing variables have to be taken into consideration.	Complex sequence effects Requires accurate determination of initial crack size
FATIGUE LIFE ESTIMATE			
Material Data	S-N curve	Cyclic stress-strain curve, strain -life curve	Crack width life curve
Component geometry	Stress concentration factors	Stress concentration factors	Stress intensity factor
Loading	$\Delta\sigma, \sigma_m$	$\Delta\sigma, \sigma_m$	$\Delta\sigma, \sigma_m$

The scope of this work is to calculate the low cycle fatigue damage and the accumulated fatigue damage from the combined effect of high cycle and low cycle fatigue damages in several critical structural details of an FPSO. As noted earlier, preliminary guidelines have been issued by classification societies on low cycle

fatigue assessment and how to combine low cycle damage to damage from high cycle fatigue to obtain the total fatigue life of a welded component. These methods are largely based on the S-N approach.

This research will attempt to compare these methods and propose an improved assessment procedure. In order to clarify the above mentioned scope, the procedure outlined in the following paragraphs will be employed.

1. Review and benchmark existing methods for predicting low cycle fatigue in metals used in the shipping industry and a review of low cycle fatigue damage.

2. Carry out a global finite element analysis on a FPSO to determine its responses to loading and unloading of cargo and ballast.

In FPSOs, the quasi static loading due to loading and unloading of cargo and ballast is the single most significant load case causing low cycle fatigue. The loading and unloading time of an FPSO is typically around 10 days but has been found to be a little as 3 days in some cases. Unloading is generally carried out within the last twenty four hours of the loading/unloading cycle. For the purpose of this study, several operational scenarios will be taken into account. A global finite element model will be developed and analysed under these scenarios. From the global analysis, areas prone to high stresses will be noted and subjected to further study.

3. Determine the actual stresses and stress gradients in the local models.

Local finite element models of the areas prone to low cycle fatigue damage will be developed. These local details will be selected based on the global analysis and experience of fatigue failure of typical structural details available in literature. Local modelling techniques are applied and a review of local modelling techniques will be carried out. The most appropriate local modelling method will be selected for the analysis.

The actual stresses at the areas of stress concentration will be determined using the hot spot stress approach. The hotspot stress approach is generally accepted and widely used method by classification societies for fatigue crack problems. The International Institute of Welding (IIW) gives explicit guidelines on meshing techniques and methods of stress extrapolation from finite element analysis. Different extrapolation methods will be studied with the aim of selecting the method most suitable to this problem. The stresses obtained from extrapolation procedures will be verified with parametric formulae.

4. Determine and compare low fatigue damage using formulations proposed by various classification societies (CS).

Low cycle fatigue damage will be obtained using the hotspot stresses calculated above with plasticity corrections. The classification societies have proposed preliminary guidelines for determining low cycle fatigue damage. These guidelines are based on the S-N approach with a majority of the CS using the high cycle S-N curves for fatigue in the low cycle region.

5. Determine high cycle fatigue stresses and damage.

The damage from high cycle fatigue is required to compute the cumulative fatigue damage on the structure. This involves evaluation the FPSOs response to wave-induced loading using spectral analysis. A hydrodynamic analysis will be carried out to evaluate the wave pressure on the hull of the FPSO. A range of wave periods and headings will be accounted for. The long-term distribution of load responses for high cycle fatigue analyses will be estimated using the wave climate, represented by scatter diagrams. The sea environments of the North Atlantic and the West Coast of Africa will be employed. The aim here is to compare the effect of low cycle fatigue damage on the total fatigue damage between these two very different seas. The North Sea is characterized by relatively high wave heights as compared to the West Coast of Africa. The former will generate more high cycle fatigue damage than the latter, which in turn may affect the effect of the magnitude of the low cycle fatigue damage on the structure.

6. Develop an improved procedure for combining fatigue damage due to high cycle and low cycle fatigue on an FPSO unit.

There are several methods for determining the cumulative fatigue damage from two different processes. Linear summation, combined spectrum, empirical formulations and time domain method are the most common. This section will compare all these methods with the aim of developing a more improved cumulative damage procedure.

The presented calculation procedures will give a better understanding of low cycle fatigue failure and cumulative fatigue damage procedure. Low cycle fatigue analysis can be incorporated into design to optimise inspection schemes. Low cycle fatigue analysis can also improve failure prediction which will in turn improve operations on the FPSO.

REFERENCE

1. ABS (2003). 'Guide for the Fatigue Assessment of Offshore Structures'. American Bureau of Shipping. USA
2. AISI (2002) 'Design Manual: Automotive Steel Design Manual'. American Iron and Steel Institite.
3. Almar-Naess A. (1999) 'Fatigue Handbook – Offshore Steel Structures'. Third Edition, Tapir Publishers Norway.
4. Bai Y (2003). 'Marine Structural Design' Elsevier, London.
5. Basquin O.H (1910). 'The exponential law of endurance tests, American Society for Testing and Materials Proc 10, pp. 625–630.
6. Coffin L.F (1971) 'A Note on Low Cycle Fatigue Laws'. Journal of Materials, Volume 6, No. 2.
7. Bergan P.G and Lotsberg I. (2006). 'Fatigue Capacity of FPSO Structures'. Journal of Offshore Mechanics and Arctic Engineering. Transactions of the ASME. Vol. 128, pp 156 – 161
8. Coffin L.F (1972) 'The Effect of High Vacuum on the Low Cycle Fatigue Law'. Metall. Trans., Volume. 3A, No. 7
9. Collins J.A (1993) 'Failure of Materials in Mechanical Design: Analysis, Prediction and Prevention'. 2nd Edition. John Wiley and Son
10. DNV (2006). 'Classifitaion Notes No 30.7: Fatigue Assessment of Ship Structures'. Guidance Notes. Det Norske Veritas. Norway.
11. DNV-RP-C203. (2005). 'Fatigue Design of Offshore Steel Structures'. Recommended Practice. Det Norske Veritas. Norway.
12. DNV-RP-C206. (2005). 'Fatigue Methodology for Offshore Ships'. Recommended Practice. Det Norske Veritas. Norway
13. Douglas-Westwood (2008); 'The World's Floating Production Market Report 2008 – 2012.
14. Fricke W. (2002) 'Fatigue Analysis of Welded Joints: State of Development' Journal of Marine Structures' Volume 16 pp 185-200.
15. Fricke W., Cui W., Kierkegaard H., Kihl D., Koval M. Mikkola T., Parmentier G., Toyosada M. and Yoon J.H. (2002) 'Comparative Strength Assessment of a Structural Detail in a Containership using Various Approaches of Classification Societies'. Journal of Marine Structures, Volume 15 pp 1-13.

16. Fricke W., Petershagen H. and Paetzold H. (1997) 'Fatigue Strength of Ship Structure, Part 1: Basic Principles'. Germanischer Lloyd. Hamburg Germany.
17. Health and Safety Executive (1999). 'Background to New Fatigue Guidance for Steel Joints and Connections in Offshore structures'. Failure Control Limited, Surrey.
18. Heo J.H., Kang J., Kim Y., Yoo I., Kim K. and Urm H. (2004). 'A Study on the Design Guidance for Low Cycle Fatigue in Ship Structures'
19. http://www.offshore-technology.com/features/feature40937/
20. IACS (2006) 'Background Document: Design Verification Fatigue Strength, Common Structural Rules for Double Hull Oil Tankers'. IACS, London.
21. Incecik A. (1982).'Design Aspects of the Hydrodynamic and Structural Loading on a Floating Offshore Platform under Wave Excitation'. PhD Thesis. Department of Naval Architecture and Ocean Engineering, Glasgow University.
22. Kaminski M.L (2007).'Sensing and Understanding Fatigue Lifetime of New and Converted FPSOs'. Offshore Technology Conference, Houston, Texas.
23. Lloyd's Register (2004). 'Ship Right Fatigue Design Assessment: Level 3 Procedure'. Guidance on Direct Calculation. Lloyd's Register EMEA.
24. Lloyd's Register (2008). 'Ship Right FOI - Design, Construction and Installation- Floating Offshore Installation of Structures Design Guidance'. Lloyd's Register EMEA.
25. Lotsberg I. (2005). 'Background for Revision of DNV-RP-C203 Fatigue Analysis of Offshore Steel Structure'. Proceedings of ASME 24th International Conference on Offshore Mechanics and Arctic Engineering. OMAE 2005-67549.
26. Lotsberg I. (2006). 'Fatigue Design of Plated Structures using Finite Element Analysis'. SAOS 2006 Vol. 1 No. 1 pp 45 – 54. Woodshead Publishing Ltd
27. Lotsberg I. and Landet E. (2005). 'Fatigue Capacity of Side Longitudinals in Floating Structures'. Journal of Marine Structures. Vol. 18 pp 25 – 42. Science Direct.
28. Maddox S.J. (2001). 'Recommended Hot-Spot Stress Design S-N Curve for Fatigue Assessment of FPSOs'. The 11th International Offshore and Polar Engineering Conference, Norway. The International Society of Offshore and Polar Engineers (ISOPE) Proceedings.

29. Manson S.S. and Hirschberg M.H. (1964) 'Fatigue Behaviour in Strain Cycling in the Low and Intermediate Cycle Range. Fatigue: An Interdisciplinary Approach'. Proceedings of the 10th Sagamore Army Materials Research Conference.
30. Manson S.S. (1965) 'Fatigue: A Complex Subject-Some Simple Approximations'. Experimental Mechanics. Journal for the Society of Experimental Stress Analysis, Volume 5pp. 193–226.
31. Mansour A.E. and Ertekin R.C. (2003). 'Fatigue and Fracture'. Proceedings of the 15th International Ships and Offshore Congress. ISSC. Volume 1 pp 329-392.
32. Mravak Z. (2007). 'Low Cycle Fatigue'. Bureau Veritas.
33. Newport A., Basu R. and Peden A. (2004). 'Structural Modifications to the FPSO Kuito Cargo Tanks'. OMAE Specialty Symposium on FPSO Integrity. Houston.
34. Paik J.K and Thayamballi A.K (2007). 'Ship-Shaped Offshore Installations: Design, Building and Operation'. Cambridge University Press, New York.
35. Radaj D. (1990). 'Design and Analysis of Fatigue Resistant Structures'. Abington Publishing Limited, Cambridge.
36. Radaj D., Sonsino C.M. and Fricke W. (2006). 'Fatigue Assessment of Welded Joints by Local Approaches'. Woodhead Publishing Limited, Cambridge.
37. Skjong R. (1995) 'Applications in Offshore Structures'. Probabilistic Structural Engineering Handbook: Theory and Industrial Applications. Chapman and Hall. USA.
38. UK HSE (2001) 'The Effects of Local Joint Flexibility on the Reliability of Fatigue Life Estimates and Inspection Planning'. Offshore Technology Report 2001/056. UK Health and Safety Executive
39. Urm H.S., Yoo I.S., Heo J.H., Kim S.C. and Lotsberg I. (2004)."Low Cycle Fatigue Strength Assessment for Ship Structures". 9th Symposium on practical design of Ships and Other Floating Structures, Germany.
40. Wang X., Kang J.K., Kim Y. and Wirsching P. (2006)'Low Cycle Fatigue of Marine Structures'. Proceedings of OMAE 2006
41. Wikipedia contributors, 'Alexander Kielland (platform)', Wikipedia, The Free Encyclopedia, 18 June 2007, 17:06 UTC,

<http://en.wikipedia.org/w/index.php?title=Alexander_Kielland_%28platform%29&oldid=139013008

42. Wirsching P.H. (1995) 'Probabilistic Fatigue Analysis'. Probabilistic Structural Engineering Handbook: Theory and Industrial Applications. Chapman and Hall. USA
43. Wirsching P.H. (1998).'Fatigue Reliability'. Structural Safety and Reliability. Construction Research Communications Limited. ISSN 1365-0556

CHAPTER 2: BACKGROUND MATERIAL AND LITERATURE REVIEW

2.1 Introduction

There has been an enormous amount of research work presented and published on the subject of fatigue assessment in ship structures. Research in this area is still ongoing because the fatigue assessment of welded details is a very challenging process. There has been an increased interest in the fatigue behaviour of ship structures at high stress levels and low number of cycles of loading, referred to as low cycle fatigue. Generally, fatigue strength of most structural members in the cargo area of a vessel or ship is checked for high cycle fatigue due to dynamic load, however cracks have been reported within few years after delivery of ship (Urm et al, 2004 and Wang et al 2006), which is suspected to be low cycle cracks.

The purpose of this chapter is to present background material and techniques that will support the research in the remainder of the study and a review of the history of fatigue with an in-depth review of low cycle fatigue in the shipping industry. General information on the growing use of FPSOs in the offshore industry will be discussed and the reference vessel used in the rest of this thesis will be presented. The sources of loading on FPSOs will be discussed with special focus on low cycle fatigue loading. A typical low cycle fatigue assessment procedure is presented and a review available method for determining stresses and strains at notches as well as cyclic properties of steel is summarised.

2.2 Background Material

2.2.1 FPSOs in the Offshore Industry

The first purpose built FPSO hull was constructed in 1987. By the early 1990s there were about 30 vessels in operation but only a handful of these were purpose built. This trend changed towards the end of the 90s due to increases in the cost of conversion, the lowering cost of new construction and an aging tanker fleet. There are currently over 190 FPSO systems in service worldwide and more than 20 under

construction, accounting for 63% of all floating installations (Shimamura, 2002). They are found all over the world, with the exception of the Gulf of Mexico, with the largest presence in the North Sea and the West Coast of Africa. Though a majority of FPSOs are operating in relatively calm and benign waters, its uses in marginal waters and harsh environment as the North Sea is not without its challenges.

FPSOs are effective in remote and deep water locations where sea bed pipelines are not cost effective. They eliminate the need to lay expensive long distance pipelines from the oil well to an onshore terminal. FPSOs are also an economical option in smaller oil fields which can be exhausted in a few years and do not justify the expense of installing a fixed oil platform. The FPSO can be moved to another location once the field is depleted.

The hull forms used for FPSOs and trading tankers look quite similar and operate in a somewhat similar manner. They are subjected to the same extreme fatigue loading and will both have similar design life. That being said, because of their different applications, they will have different design requirements and therefore different designs. Trading tankers spend most of their lives moving cargo from one location to another, in either of two draft conditions- ballast or full. FPSOs on the other hand are stationary, have zero forward speed with continuously changing draft. Paik and Thayamballi (2007) listed the major differences between FPSOs and trading tankers as follows:

- The units are fixed in a specific site, generating specific loads as opposed to a trading tanker which has the option of weather routing in case of bad weather.
- FPSOs are permanently moored which means it is offshore 100 % of the time i.e. operation is continuous without dry docking. Tankers are in the open seas only about 70 % of the time.
- Tankers operate at defined drafts: fully loaded and ballast whereas FPSOs operate at constantly changing drafts due to varying states of loading and unloading. The large draft variation between fully loaded and ballast drafts for some new FPSO designs may be as large as 10 metres.

- Tankers are typically loaded and unloaded in still water conditions while in harbour while FPSOs have more frequent loading and offloading cycles with significant environmental effects present. This is important because large still water forces and moments can occur due to different loading patterns which may be very different from that of trading tankers.

Adequate prediction of fatigue crack propagation is important in FPSOs as compared with other ships because of their higher cost of off-hire and more severe consequences of failure (Paik and Thayamballi, 2007). Uncertainties exist in assessing both the stresses resulting from applied loads and the response of a particular structure which together control fatigue performance. The basis of fatigue analysis is to estimate these stresses, noting the uncertainties involved with S – N curve derived from experimental data.

2.2.2 Reference FPSO

The FPSO employed here is a double skin, single bottom tanker assumed to be operating in the central North Sea and the West Coast of Africa. The ship hull has a length of 234.2m, a breadth of 44.8m and a depth of 23.8m. The structure consists of seven cargo tanks, capable of storing 850,000 barrels of crude oil based at 98 % full capacity, and two slop tanks surrounded by ballast tanks. The tanks are formed by longitudinal and transverse bulkheads, including a longitudinal centreline wash bulkhead. Figure 2.1 shows the general tank arrangement and Figure 2.2 illustrates the mid ship section of the FPSO. Table 2.1 and Table 2.2 show the operational parameters and structural data of the FPSO.

The FPSO structure is supported by twelve caternary mooring lines which are anchored to the seabed by piles in six pairs. Pumping is carried out by hydraulically-driven, 1,400m³/h cargo pumps, powered by high-voltage motors. When offloading, four pumps are used simultaneously. The turret and swivel anchor the facility to the seabed, acting as the entry point for the well fluids and the exit points for gas exports and water injection. The FPSO is designed to accommodate 14 risers for production, water injection and gas export, as well as control umbilicals.

The vessel has a fatigue design life of 20 years with a safety factor of three. The entire structure is made from Grade DH high tensile steel with the exception of the areas around the neutral axis and the longitudinal stiffening.

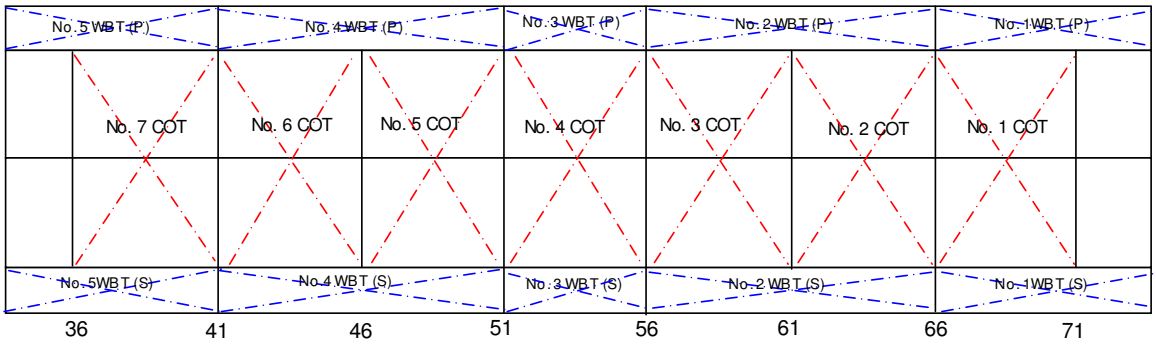

Figure 2.1: General Tank Arrangement

Table 2.1 Operational Particulars

Tonnage	129 550 Tonnes
Capacity	850 500 Bbls
Production per day	85 000 Bopd
Production cycle	10 days
Offloading time	9 days

Table 2.2 Structural mid-ship properties

Length between perpendiculars	L_{pp}	225.8 m
Length of scantlings	L_{scant}	219.026 m
Breadth at mid-ship	B	44.8 m
Depth at mid-ship	D	23.8 m
Design draft	T_{design}	16.65 m
Scantling draft	T_{draft}	16.8 m
Block coefficient	C_b	0.9617
Structural area	A	6.2955×10^6 mm^2
Mid-ship neutral axis	z	11.617 m
Mid-ship vertical moment of inertia	Izz	1.5474×10^9 mm^4
Mid-ship horizontal moment of inertia	Iyy	5.6532×10^8 mm^4

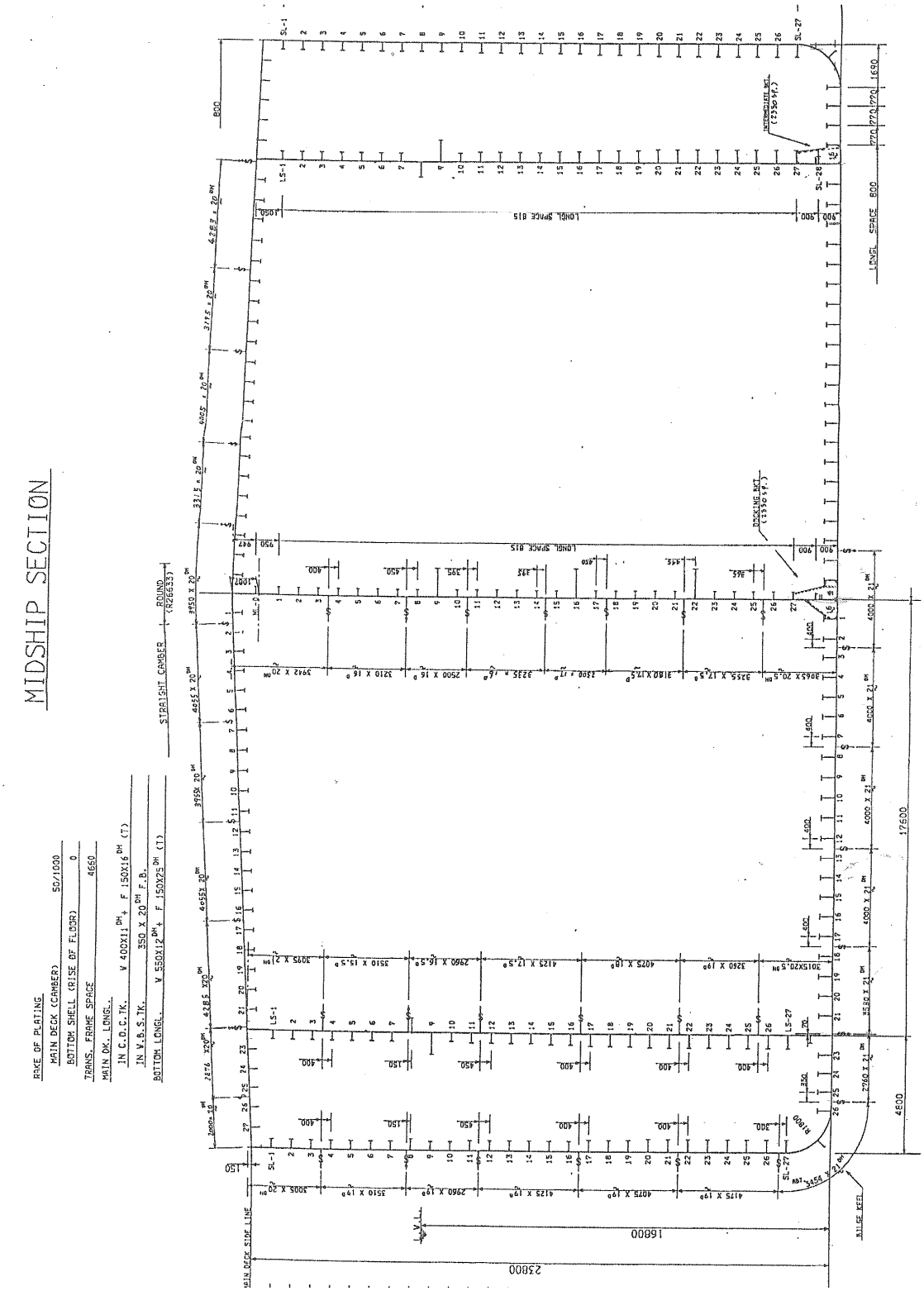

Figure 2.2: Mid-ship section

2.2.3 Loading Sources

In a ship structure, the stress or strain cycles are generally caused by the seaway and by changing still water bending moments. These loads produce bending stress and shear stress in the ship's hull girder, see Figure 2.3. The global stresses: vertical bending, lateral bending and torsional bending stresses combine in the primary structural members of the ship structure (Stambaugh and Van Mater, 1990). Superimposed on the hull girder loads are local stresses caused by changes in hydrostatic pressure and local loading from ships cargo or ballast. These stresses are plane stresses within a thin walled plate structural member. In a transverse plane, bending and shear stresses are caused by differences in hydrostatic pressure and internal cargo loads or ballast. These stress patterns are transmitted to structural details.

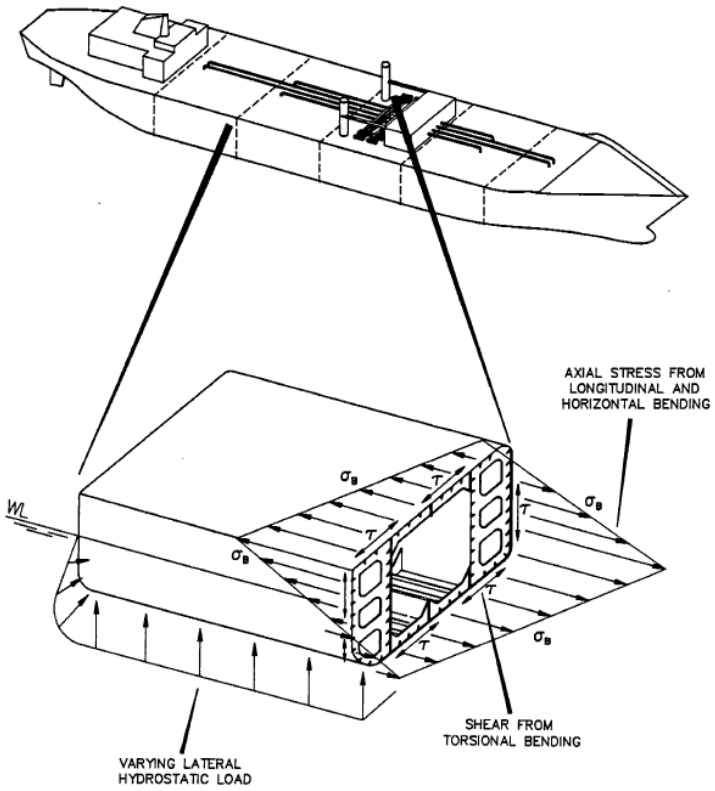

Figure 2.3: Global stresses due to combined vertical and lateral bending and torsion

FPSOs in service are permanently moored but their loads and responses are not stationary. In such structures, both low cycle high amplitude loads and high cycle low

amplitude loads contribute to fatigue damage. Many studies have been carried out on fatigue loading of offshore structures characterising sea environment, structural response and statistical description of the loads (Munse et al, 1983), (Mansour et al, 1993). Wave – induced actions are the primary source of fatigue loading on offshore structures but other loadings are of important significance to fatigue assessment. Munse et al (1983) identified the following cyclic fatigue load sources in ship structures:

- Low frequency wave induced loads (quasi-static): These loads are caused by the wave forces on the hull and the ship motions induced by these forces. These cyclic stresses occur at the frequency of encounter of the ship with the wave system. The level of stress experienced is directly related to (although not directly proportional to) the significant wave height of the encountered seaway. Low frequency loads are usually about 10^7 - 10^8 cycles during the design life of the ship structure.
- High frequency wave induced loads (dynamic): This occurs about 10^6 cycles during ship's design life. These stresses are induced by dynamic wave loads which act on the ship's structure. The most common sources are bottom slamming, green water, and flare impact. Dynamic loads produce whipping and springing elastic motions of the hull, typically at higher frequencies than the frequency of wave encounter.
- Still water loading: 300-500 cycles
- Thermal loads: These stresses are about 7000 cycles and arise from the thermal expansion of the topside in the day and contraction during the night. The thermal stresses are also affected by the amount and location of sun exposure occurring during daylight hours.

The hull girder bending and local pressure fluctuation contribute the highest to total fatigue damage (Bai, 2003). Cargo loading and unloading can cause significant yielding which in turn can cause cracks at hotspots even when dynamic stresses are low (Urm et al , 2004). The web stiffeners on the bottom and inner bottom longitudinals, heel and end connections of horizontal stringers in transverse bulkheads to longitudinal

bulkheads and lower stool connections to inner bottom are some of the most vulnerable spots in view of loading and unloading stresses.

2.2.4 Loading and Unloading Load Cases

Dynamic loads due to waves are the most significant loads for high cycle fatigue assessment while quasi-static loads from loading and unloading of cargo and ballast are the most significant for low cycle fatigue assessment. In high cycle fatigue assessment, the design cycle is usually taken as 6.3×10^8 seconds for a 20 year design life. For low cycle fatigue calculations, the design cycle may depend on trading routes and operational conditions and new building specifications. The minimum number of design cycles is shown in Table 2.3 as recommended by Urm et al for FPSOs. This refers to the number of loading and unloading cycles in a 20 years design life, e.g. 500 for normal tankers. Due to the uncertainty associated with the number of actual design cycles at the design stage, a safety factor of 2 is normally employed for actual designs.

Loading and unloading is the single most significant load case causing low cycle fatigue (Wang et al, 2006). The most critical load case generating the maximum stress range is used in LCF assessment. Depending on the location to be checked, the load condition applied may be different. The difficulty in hydrostatic predictions lies in the fact that at the way the FPSO will be operated i.e. what tank and when will be filled is unknown at the design stage. The sequence and timing of loading and offloading cargo depends entirely on the operator of the FPSO. In the case of the FPSO employed here, it is assumed that the loading and unloading time is 10 days. Urm et al (2004) suggested the load cases illustrated in Figure 2.4 to check typical locations for low cycle fatigue assessment for tankers with one centre-line bulkhead.

Table 2.4 shows the loading and unloading load cases that will be employed to obtain stresses at potential crack locations. The FPSO has seven tanks (numbered 1 to 7) separated by a central bulkhead. Fourteen loading conditions are considered depending on which tank is loaded and which tank is empty. For example, load condition 5a (LC 5a) implies that the odd numbered tanks are half filled (i.e. to 50 % capacity). Based on the loading and unloading load cases, five loading scenarios are

created. Sequence 1 (SEQ1) implied that the tanks are loaded in the following fashion: ballast – middle tank is half filled – all the tanks are half filled - fully loaded state. This applies to the other loading sequences.

Table 2.3: Minimum number of design cycles for low cycle fatigue (Urm et al, 2004)

Ship Type	Minimum Design Cycle
Oil Tankers	500
Chemical Tankers	750
Panamax Bulk Carriers	1000
Capesize Bulk Carriers	750
Shuttle Tankers	1500

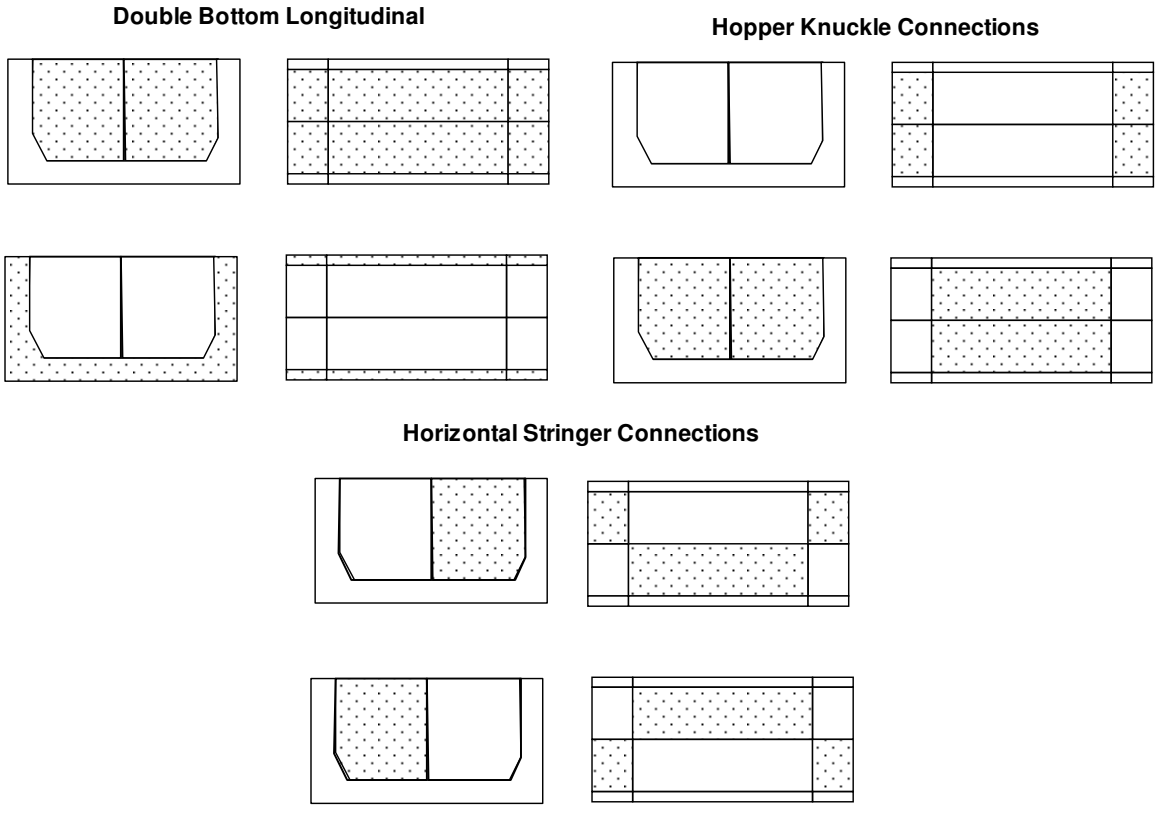

Figure 2.4: Typical load cases for low cycle fatigue checks (Urm et al, 2004)

Table 2.4: Static load cases for loading and unloading operations

Load Cases	Description
LC 1	Ballast
LC 2	4 COT 50 % capacity
LC 3	All tanks at 50 % capacity
LC 4	All tanks full
LC 5a	Odd numbered tanks (1,3,5 and 7) at 50 % capacity
LC 5b	Odd numbered tanks (1,3,5 and 7) full
LC 5c	COT 1, 3, 5 and 7 full capacity + COT 2, 4 and 6 at 50 % capacity
LC 6a	Even numbered tanks (2, 4 and 6) at 50 % capacity
LC 6b	Even numbered tanks at 100 % capacity
LC 6c	COT 2, 4 and 6 full capacity + COT 1, 3, 5 and 7 at 50 % capacity
LC 7a	COT 1P, 2SB, 3P, 4SB, 5P, 6SB, 7P at 50 % capacity
LC 7b	COT 1P, 2SB, 3P, 4SB, 5P, 6SB, 7P full
LC 8a	COT 1SB, 2P, 3SB, 4P, 5SB, 6P, 7SB at 50 % capacity
LC 8b	COT 1SB, 2P, 3SB, 4P, 5SB, 6P, 7SB full
Loading/Unloading Operation	
No.	Loading Sequence
SEQ1	1 – 2 – 3 – 4 – 1
SEQ2	1 – 5a – 5b – 5c – 4 – 1
SEQ3	1 – 6a – 6b – 6c – 4 – 1
SEQ4	1 – 7a – 7b – 4 – 1
SEQ5	1 – 8a – 8b – 4 – 1
COT = Cargo oil tank SB = Starboard P = Port	

2.3 Literature Review

2.3.1 Fatigue: Milestones in History

Fatigue is defined by ASTM (1996) as:

The process of progressive localized permanent structural change occurring in a material subjected to conditions which produce fluctuating stresses and strains at some point or points and which may culminate in cracks or complete fracture after a sufficient number of fluctuations.

The first article on fatigue was published by W.A.J Albert in 1837. He was a German mining engineer who established the relationship between applied load and durability by devising a test machine for iron chains. When the railway industry began to develop in the mid 19th century, fatigue failure of railway axles became prevalent and that drew serious attention to the effect of cyclic loads (Schutz, 1996). This resulted in the first systematic fatigue investigation by August Wohler between 1852 and 1870 (Wohler, 1860). He conducted tests on full scale rail axles under axial, bending and torsion loads. He presented his test results in an S – N diagram (stress vs. number of cycles to failure) which is still the way fatigue data is presented today. Each curve on such a diagram is still referred to as a Wohler line (Figure 2.5). Wohler initiated the development of design strategies for fatigue, identified the importance of cyclic and mean stress and also showed that the effect of the cyclic stress range was more important than the maximum stress. He also discovered that there is a limiting stress range which may be applied indefinitely without failure - now known as the 'fatigue limit'.

The next important step in fatigue was by Bauschinger (1881) when he made a breakthrough in low cycle fatigue and wrote the first paper on cyclic stress – strain hysteresis behaviour of materials. His work is the first indication that one single reversal of inelastic strain could change the stress – strain behaviour of metals. By 1900, over 80 papers had been published on the subject of fatigue. Fatigue failure was being reported not only in railway axels but also in chains, marine equipment and power generating machines (Toth and Yarema, 2006), (Vervoot and Wurmann, 2006).

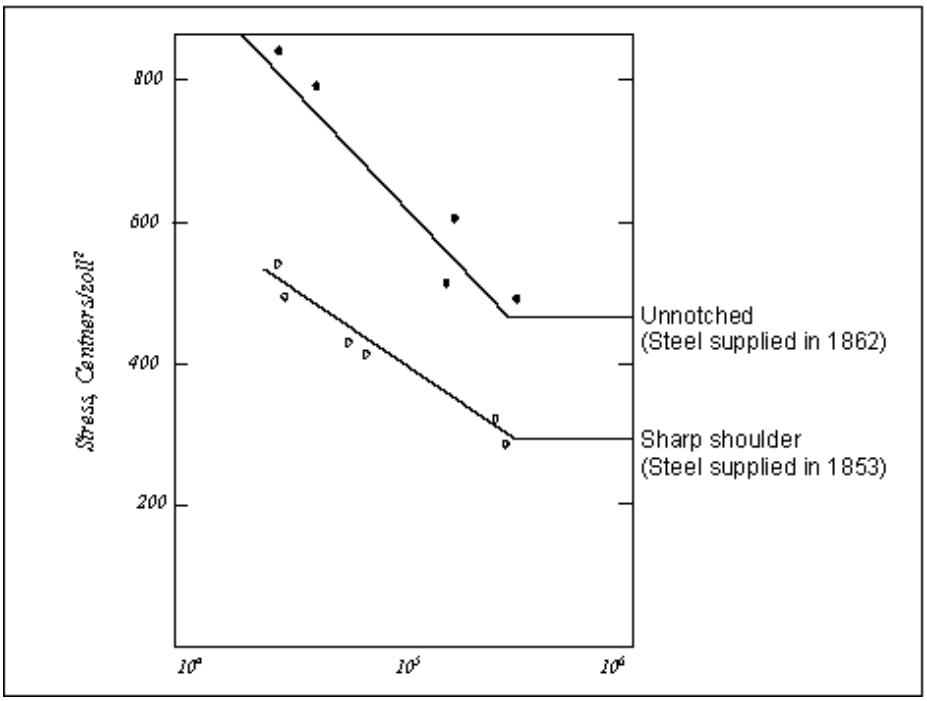

Figure 2.5: The S – N curve as described by Wohler (1 Centners per Zoll^2 = 0.75MPa)

In 1903, Alfred Ewing and Humphrey (Ohnami, 1992) published a paper titled 'The Fracture of Metals under Repeated Alternations of Stress' in which they studied the effect of localised slip lines and slip bands on the formation of micro cracks (Figure 2.6).

Basquin (1910) observed that stress range vs. fatigue life could be modelled using a power relationship resulting in a straight line when plotted on a log – log scale. This behaviour corresponded to elastic material behaviour.

At the beginning of the 20th century A.A Griffith (1921) published the results of his experiments on the brittle fracture of glass. His work describes the relationship between applied nominal stress and crack length at fracture. He found that the strength of the glass was dependent on the size of microscopic cracks. This showed the fatigue failure was not restricted to iron and steel structures. His pioneering experiments developed the basis for fracture mechanics. G.R Irwin (1957) further applied Griffith's theory to metals with small plastic deformations at the crack tip and used stress intensity factor, K, to quantify crack tip force.

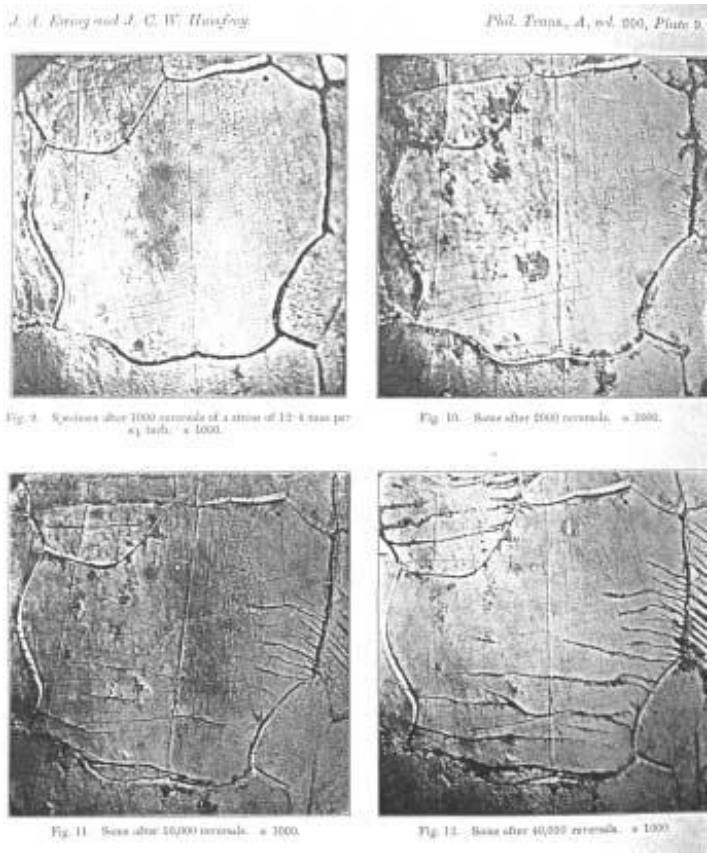

Figure 2.6: Micrographs showing how surface fatigue cracks grow as material is further cycled (no higher resolution available)

Palmgren (1924) and Miner (1945) came up with the first practical design tool for fatigue analysis. They put forward a simple linear cumulative damage model for irregular repeated loads. The linear damage law is recognised as the Palmgren – Miner law. This law proved to be very popular in the engineering field because of its simplicity. Several modifications relating to damage ratio and endurance limits have been proposed over the years but the Palmgren – Miner law still remains the most accepted method for fatigue damage calculation.

Between 1950 and 1960, Coffin (1971, 1972) and Manson (1964, 1966) independently worked on low cycle strain controlled fatigue behaviour. They found that plastic strains were responsible for fatigue damage and proposed an empirical relationship between strain and fatigue life.

Paris (1963) proposed methods for predicting the rate of growth in individual cracks. He showed that fatigue crack growth rate could be best defined using the stress

intensity factor range. This was the first systematic method for handling crack propagation using fracture mechanics.

Another milestone was set in fatigue methods in 1969 by Tatsuo Endo and M. Matsuiski when they devised a rainflow counting algorithm for the reliable application of Palmgren-Miner's rule to random loads (Matsuiki and Endo, 1969). In the mid 1970's Elber studied the mechanism and importance of crack closure in slowing the growth of a fatigue crack due to wedging effect of plastic deformation left behind at the crack tip.

The efforts spent on fatigue investigations in the 20th century are huge. Mann (1990) published books on developments in fatigue and his work arrived at about 100 000 (one hundred thousand) references in the 20th century compared to less than 100 in the 19th century. Schijve (2003) raised the obvious question –Is the problem of fatigue so difficult and complex, or are we not clever enough to eliminate fatigue from our industrial products?

In more recent years, many changes in aspects of fatigue assessment and design have been prominent due to the advent of computer technology. Finite element analysis paved the way for the local strain approach and fatigue crack growth modelling techniques. Software for different fatigue life models has been developed and the ability to simulate real loadings with components, specimens and even full scale structural testing is carried out with relative ease. Over the years, there have been conferences on fatigue with world leading experts and more are planned in the future. If fatigue problems still exist in the over this long period of time, then something needs to be explained.

2.3.2 Low Cycle Fatigue

Low cycle fatigue is associated with macro plastic deformation in each cycle where significant plastic straining occurs. Under low cycle fatigue, failure can occur in a small no of cycles, say 1000 or less. The stress associated with low cycle fatigue is usually high enough to cause considerable amount of plastic deformation in the region of the stress concentration where periods of visible cracks are hardly present. Fatigue

in the low cycle regime is normally expressed in terms of total strain rather than stress range because the local fatigue sensitive zone is more likely to be subject to strain controlled conditions rather than stress controlled conditions.

The plastic behaviour of the fatigue life of a highly stressed region is more accurately described as a function of cyclic strain amplitude. Stress-strain behaviour is thus characterised by a stress-strain hysteresis loop. A hysteresis loop illustrated in Figure 2.7 defines a single fatigue cycle in the strain life method. The area within the hysteresis loop is the energy per unit volume dissipated during a cycle. The hysteresis loop is defined using values of stress amplitude, $\Delta\sigma$ and strain amplitude, $\Delta\varepsilon$ which are relative to some point (σ,ε) in stress – strain space. A cyclic stress-strain curve is defined by a family of stabilized hysteresis loops at different strain amplitudes. Material hardening (increased resistance to deformation) or softening (decreased resistance to deformation) can be observed from a cyclic curve, see Figure 2.7. The cyclic stress strain response of a material is fitted to the Ramberg-Osgood form:

$$\varepsilon^T = \varepsilon^e + \varepsilon^p = \frac{\sigma}{E} + \left(\frac{\sigma}{K'}\right)^{1/n'} \qquad 2.1$$

Masing's hypothesis (1926) states that the cyclic stress-strain response can be expressed in terms of stress and strain amplitudes, which in turn can be expressed in terms of ranges.

$$\frac{\Delta\varepsilon}{2} = \frac{\Delta\varepsilon^e}{2} + \frac{\Delta\varepsilon^p}{2} = \frac{\Delta\sigma}{2E} + \left(\frac{\Delta\sigma}{K'}\right)^{1/n} \qquad 2.2$$

K' = cyclic strength coefficient and n' = cyclic strain hardening exponent. They are obtained from the intercept and slope of a log-log plot of cyclic stress amplitude against cyclic plastic strain amplitude. This equation is then used together with Neuber's rule or elastic-plastic finite element method to compute local stress and strains at the area of interest.

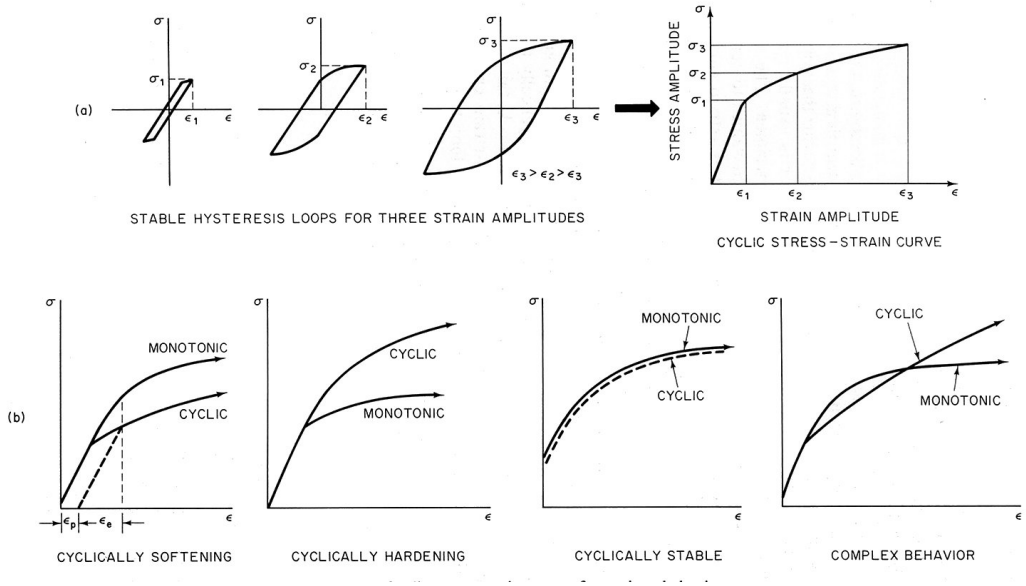

Figure 2.7: Hysteresis loops and cyclic stress-strain curves

2.3.2.1 Cyclic Properties of Ship Steel

The stress-strain response of cyclically loaded material can be quite different from the one when it is loaded monotonically. During loading, material may exhibit strain hardening, strain softening, its response can be stable and in some cases it can even behave differently in various loading phases. The well accepted and widely used method of describing stress-strain response of most cyclically loaded metal materials is stabilized or mid-life true stress - true strain curve. It can be determined from strain-controlled cyclic experiments performed on a number of standard material specimens.

A set of representative hysteresis curves, resulting cyclic stress-strain curve and monotonic stress-strain curve are shown in Figure 2.8. General methodology and exact procedure for determination of material stress-strain response to completely reversed, cyclic, uni-axial, tensile-compressive loading are given in ASTM Standard E606 (2005).

The cyclic stress-strain curves of most metals can be successfully represented with the Ramberg-Osgood relationship given in Equation 2.1. Heo et al (2004) carried out incremental step tests on different base metals and weld metals to obtain cyclic stress

strain relations. Four different steels used in the ship building industry were tested. Figure 2.9 shows cyclic stress strain curves for different material type and Table 2.5 presents the cyclic stress strain parameters. Kim et al (2006) and Kim et al (2006) tested Grade A steel and weld metal used in the shipping industry. The cyclic stress-strain parameters of the base and weld metal obtained corresponded with results of test results in Heo et al.

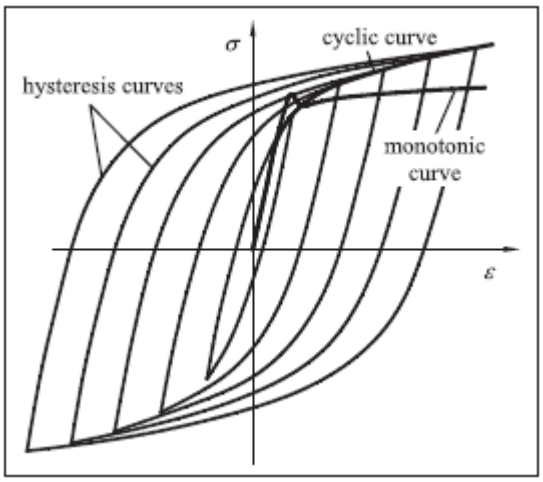

Figure 2.8: Cyclic and monotonic stress-strain curves

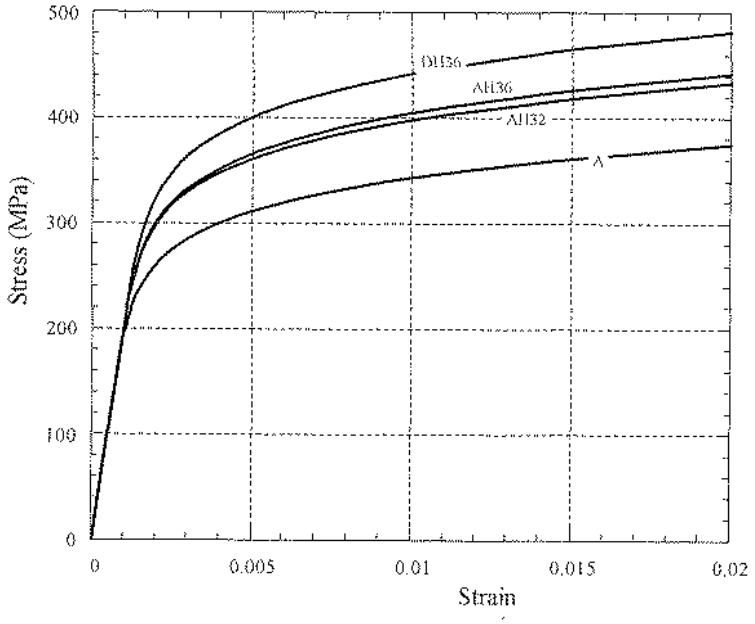

Figure 2.9: Cyclic stress strain curve for different steel grades (Heo et al)

Table 2.5: Parameters of cyclic stress-strain curve

Material	A	AH32	AH36	DH36
K' (MPa)	592	669	694	739
n'	0.114	0.108	0.112	0.106

2.3.2.2 Stresses and Strains at Notches

Elastic-plastic finite element method is an important tool in the local strain approach. It is capable of providing full field stress-strain distribution within a structure and is considered a more accurate method of determining local stress and strain at notches (Wanlin, 1998). Although the finite element method is an efficient tool, there exist empirical approaches which facilitate a rapid fatigue damage analysis and save costs and time associated with performing detailed elastic-plastic finite element analysis. Empirical methods such as the use of plasticity correction factors available in BS5500 (2009), Neuber's rule (Neuber, 1961), Glinka's equivalent strain energy density method (Glinka, 1985), Seeger and Heuler's method (Seeger and Heuler, 1980) and their modifications (Topper et al, 1969) and (Yee et al, 2004) are frequently used to estimate the elastic-plastic response at a hotspot based on elastic solutions.

Alternative methods for determining stress-strain distributions at hotspot locations include the whole field optical techniques like the electronic speckle-pattern interferometry-ESPI (Labbe, 2006), (Vial-Edwards et al , 2001) and (Yang et al, 2003), as well as techniques based on the Moiré effect (Martinez at al, 2003, Post et al, 1994, and Han et al, 2001). In general, these techniques cannot be used to measure efficiently the relatively large deformations that a sample undergoes during plastic deformation. Because of their high-sensitivity, the optical techniques are used to measure very small changes in the strains. Hence they are more suitable as a comparative tool. A significant amount of research has been carried out using these techniques but the details are beyond the scope of this thesis.

Although the strain-life approach is preferred for predicting fatigue life, approximate methods based on pseudo elastic stress is widely used in low cycle fatigue analysis. This is due to the fact that most structural design codes uses stress ranges as a primary

design parameter, not strain ranges and it is also convenient to use existing stress concentration factors in the design codes. The pseudo stress range is obtained by transforming the elastic stress range by a plasticity factor to account for the plastic deformation in the material at the location of the hotspot. The most popular methods of achieving this are:

- Plasticity correction factors have been published in British standard: BS5500 – Specification for Unfired Fusion Welded pressure Vessels. The pseudo stress is obtained by multiplying the plasticity correction factor with the elastic stress range from the finite element analysis.
- Define a cyclic stress strain curve and employ Neuber's rule which relates the actual stress and strain in both elastic and plastic states, to the nominal elastic stress state to obtain the local stress and strain. The pseudo stress is then the strain range multiplied by Young's modulus. Figure 2.10 shows the definition of stress and strain components. In the diagram, the elastic stress is obtained from finite element analysis. The aim is to find a point on the cyclic stress – strain curve that gives the same product. Numerical iteration using Neuber's rules is used to find that point.

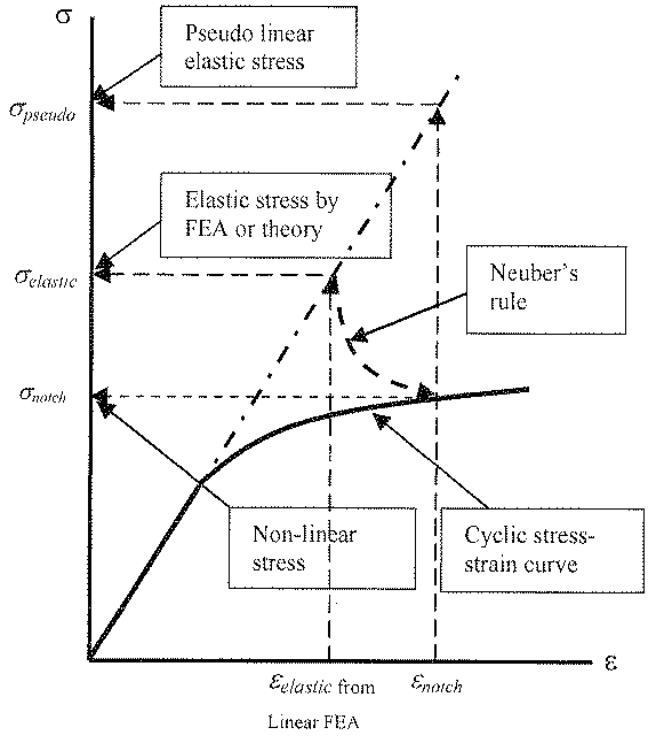

Figure 2.10: Definition of stress and strain components (Wang et al, 2006)

2.3.2.3 Plasticity Correction Factors

Low cycle fatigue assessment should be carried out based on total strain range rather than the total stress range due to the significant plasticity that may occur at the notched area from high stress under cyclic loading. However most rules in the shipping industry use an approach based on pseudo elastic stress range instead of the total strain approach because most ship designers are familiar with the use of stress range for fatigue strength evaluation.

The concept of plasticity correction is convenient because it is easier to use existing stress concentration factors in available design codes than determining strain concentration factors which is a time consuming and expensive process. Another advantage in using stress range instead of strain range is the convenience of combining low cycle fatigue damage with damage from high cycle fatigue.

Pseudo elastic stress range is obtained using the concept of the plasticity correction factor. If the cyclic properties of the steel us unknown, then the concept of plasticity correction factor given in BS5500 is usually adopted. This plasticity correction factor, k_e, is expressed as follows:

$$k_e = 1 \qquad \frac{\Delta\sigma_{fem}}{\sigma_y} < 2.0$$

$$k_e = 0.443\left[\left(\frac{\Delta\sigma_{fem}}{2\sigma_y}\right) - 1\right]^{0.5} + 1 \qquad 2.0 \le \frac{\Delta\sigma_{fem}}{\sigma_y} \le 3.0 \qquad 2.3$$

$$k_e = 0.823 + 0.164\left(\frac{\Delta\sigma_{fem}}{\sigma_y}\right) \qquad \frac{\Delta\sigma_{fem}}{\sigma_y} > 3.0$$

σ_y is the yield stress of the material.

Wang (2008), for the American Bureau of Shipping (ABS), established an approximate relationship between the plasticity correction factor, k_e, and the elastic stress range for four steels used in the shipping industry and this is illustrated in Figure 2.11. The relationship is expressed as:

$$k_e = 0.5 + k_m \Delta\sigma_e \geq 1. \qquad 2.4$$

The values of k_m are given in the table below:

Table 2.6: Values of k_m (ABS, 2008)

Material	Mild	HT32	HT36	HT40
k_m	11.2 x 10^{-4}	9.6 x 10^{-4}	9.4 x 10^{-4}	8.56 x 10^{-4}

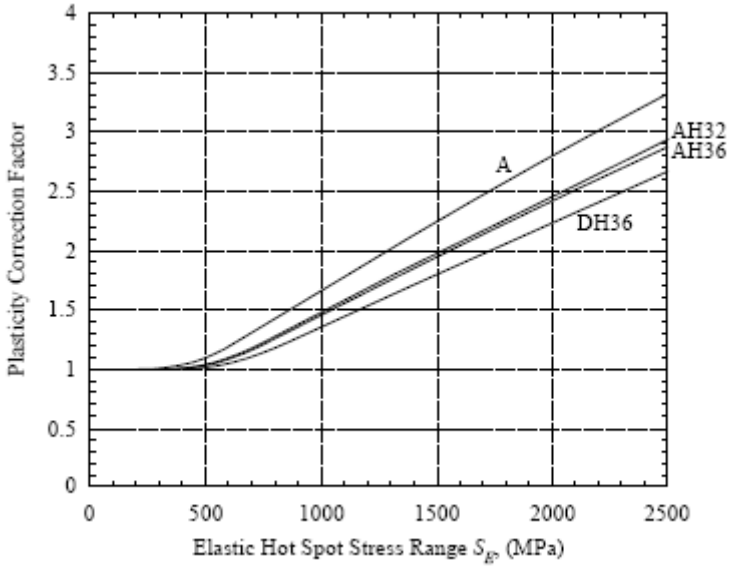

Figure 2.11: k_e as a function of elastic stress range (Wang, 2008)

2.3.2.4 Neuber's Rule

Neuber's rule and Glinka's equivalent strain density rules are the most general, simple empirical methods used to obtain notch strain. Neuber's rule or Glinka's rule are employed for calculating plasticity correction factor, if the cyclic stress-strain properties of the material are known.

Neuber proposed a simple approximation to estimate elastic-plastic notch stress state. Neuber's rule states that the maximum stress and strain at the notch root under elastic-plastic deformation are related through the following equation:

$$K_T^2 = K_\sigma \cdot K_\varepsilon \qquad 2.5$$

$$K_\sigma = \frac{\sigma}{S}; K_\varepsilon = \frac{\varepsilon}{e}$$

where K_σ and K_ε are the stress concentration factor and the strain concentration factor respectively and K_T is the theoretical stress concentration factor.

The rule is applied when local stresses and strains are within proportional limit i.e. $K_T = K_\sigma = K_\varepsilon$. Wundt (1972) has shown that beyond this limit, with increasing nominal stress, the elastic stress concentration factor decreases while the strain concentration factor increases. It has also been reported that the use of theoretical stress concentration factor in Neuber's rule overestimates the true solution especially when predicted life was based on component failure. Despite this, Neuber's approximation is still popular in estimating the cyclic fatigue life of notched specimens.

Manson and Hirschberg (1965) and Topper et al (1969) applied Neuber's rule to predict crack initiation life. Their results showed that good predictions could be obtained if the theoretical stress concentration factor was replaced by a fatigue strength reduction factor. Neuber's rule was then modified using a fatigue strength factor, K_F, for component based failure.

$$\frac{(K_F S)^2}{E} = \sigma\varepsilon \qquad 2.6$$

Neuber's rule associated with the cyclic stress-strain relation, leads to equation (2.12) representing the notch stress state:

$$\frac{(K_F S)^2}{E} = \sigma \cdot \left[\frac{\sigma}{E} + \left(\frac{\sigma}{K'} \right)^{1/n'} \right] \qquad 2.7$$

Seeger et al (1980) suggested that when there is significant plasticity in the nominal region, general yielding will occur and Neuber's rule may give non-conservative results and modified Neuber's rule to account for this effect. Neuber's rule is only valid for mild plasticity. Large plastic yielding will cause the Neuber's rule to under predict the actual pseudo elastic stresses and this can result in non conservative designs when the measured stresses are applied in analysis. Molski and Glinka (1981) stated that Neuber's rule gave non-conservative results and proposed an alternative relationship based on an energy density criterion. This method is referred to as Glinka's equivalent strain energy density method (ESED). The strain energy density is used to form the fatigue parameter which is related to fatigue life. A historical description of the energy based method is described in detail in Fatemi and Yang (1998).

ESED is based on the assumption that the strain energy density at the notch root is approximately the same for linear-elastic and elastic-plastic notch behaviour. For elastic-plastic behaviour at the notch root, the strain energy density is given by:

$$\frac{(K_T S)^2}{E} = \sigma\left[\frac{\sigma}{E} + \frac{1}{n+1}\left(\frac{\sigma}{K'}\right)^{1/n'}\right] \qquad 2.8$$

Comparing the Neuber's and Glinka's methods, it is noted that in the elastic range, local stress and strains calculated by Neuber's rule and ESED are equal, while in the plastic range, Neuber's rule always yields higher stresses and strains. It is well recognised by a great number of experimental results that in most cases Neuber's rule overestimates the notch-tip stresses and strains in low cycle fatigue, while ESED method tends to underestimate the notch stress and strain (Fatemi, 2003) and (Murakami and Kusumoto, 1973). Furthermore, the accuracy of these methods depends strongly on the level of the nominal stress relative to the material's yield stress, the material's constitutive law, the stress concentration factor as well as the nature of the stress state. It is still agreed that conventional Neuber's approximation gives the most conservative result in estimating elastic-plastic stress strain state.

2.3.3 Low Cycle Fatigue (LCF) in Ship Structures

Between 1940 and 1960, a huge amount of research data on fatigue of metals was published (Vedeler, 1961). During this time, a distinction was made between low cycle fatigue and high cycle fatigue based on the number of load applications to failure, and the importance of high-stress low cycle fatigue was highlighted as a potential failure criteria. But a majority of the investigations into fatigue failure was focused on relatively low nominal stress leading to failure at a high number of cycles i.e. high cycle fatigue. Some structures like ships structures and aircrafts may be subjected to unusually high stresses resulting in failure at a small number of load cycles. Structural experience with ship-shaped structures indicated as early as that the 1960s that LCF was an important structural problem.

A literature search was carried out at the beginning of this study to obtain information on the state of the art in low cycle fatigue in the offshore industry. It was found that there is little literature available in this area and a large number of the papers and reports found were not relevant to this work. The Ship Structures Committee (SSC) carried out some extensive testing on the low cycle fatigue properties of ship steel between 1960 and 1970. The Welding Institute (TWI) has surveyed literature on low cycle fatigue research relevant to the offshore industry and more recently classification societies and several authors have published guidelines on low cycle fatigue of welded sections. The pool of resources is quite small. This section will review the above-mentioned literature, some of which are quite old.

2.3.3.1 Ship Structures Committee

In 1961, Vedeler (1961) presented a paper titled ‘A Naval Architect’s Reflections on Some Research Problems with Ship Steel’, in an SSC report. He reported a catalogue of cracks, based on a four year investigation, found in the shell and decks of ships structures with respect to their number, size and position. Over two hundred oil tanks with length of over four hundred feet were studied; sixty-five had cracks at points of stress concentration in the shell or deck areas attributed to fatigue. One hundred and forty four dry cargo ships were also part of the study. Fifty-three are found to have fatigue related cracks. He drew a conclusion that ‘for ordinary ships in ordinary

waters, the problem for 95 % of cracks appearing in open waters seemed to be due to high-tension low-cycle fatigue'. The challenges associated with the use of high tensile steel versus ordinary steels are also highlighted. He noted that in welded structures like ships, there are residual stresses as high as or even higher than the yield point of the steel. The use of high tensile steel automatically leads to higher residual stresses and this will definitely impact fatigue behaviour. He stresses the importance of further research into the effect of low cycle fatigue on ships structures.

Later that year, the SSC commissioned a project to study the behaviour of ship steels under LCF conditions. The project was divided into four phases: a literature review on the state of the art, studies of small coupon-type specimens, studies of notched plate specimens and studies on welded specimens. The results of the investigations were presented in the following reports.

- SSC 137: Low-Cycle Fatigue of Metals – Literature Review (Yao and Munse, 1961)
- SSC 151: Low-Cycle Fatigue Behaviour of Axially Loaded Specimens of Mild Steel (Yao and Munse, 1965)
- SSC 143: Crack Propagation in Low-Cycle Fatigue of Mild Steel Rolfe and Munse, 1963)

The following sections will attempt to summarise the salient points:

It was found very early in low cycle fatigue investigations (Kommers, 1912) that the magnitude of cyclic deformation is an important factor. As such, most simulations of material behaviour in regions of high stress concentration was carried out under strain/deformation conditions.

Evan's (1957) conducted tests on mild steel specimens with the aim of determining the elongation of the specimen to failure. He also showed that there existed a linear relationship between cyclic strain and the number of cycles to fracture when plotted in a log-log form.

Low (1955, 1956) and Johansson (1956) carried out tests on various metals and both investigations found a linear relationship between strains and corresponding lives on a log-log plot. Orowan (1952) suggested that the linear relationship between plastic strain and corresponding life be expressed in terms of a plastic strain parameter:

$$\varepsilon_p * N = \mathrm{C} \qquad 2.9$$

where ε_p is the plastic strain and C is a constant. Orowan's theory explains the fatigue behaviour of an idealized material at points where stress concentrations exist. Manson (1953), as well as Gross and Stout (1955) suggested that the relationship be empirically modified for cases where strains representing gross deformations are used. A new variable m is introduced to take the form:

$$\varepsilon_p * N^m = \text{Constant} \qquad 2.10$$

m is the slope of the log ε_p vs. log N diagram, see Figure 2.12

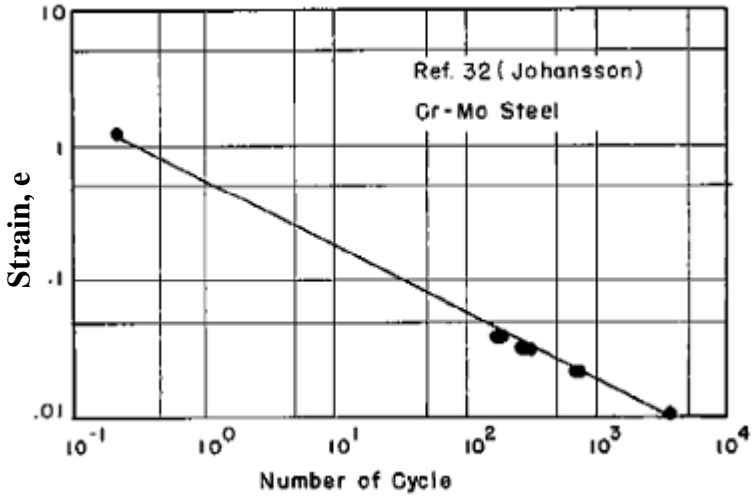

Figure 2.12: Strain Range vs. Life on Log-Log Plot. (Yao and Munse, 1961)

Coffin and his associates (1954a, 1954b, 1954c, 1957, 1959a, 1959b and 1960) conducted extensive LCF tests on 347 stainless steel specimens under thermal and mechanical strain cycling. They found that for a wide range of materials, a constant

slope of m = 0.5 was the best fit. Furthermore, by assuming N = ¼ cycles, the plastic strain was found to be in good agreement with true strain at fracture (ε_f) measured in a static test. Thus, Coffin's relationship can be expressed as:

$$\varepsilon_p * N^{1/2} = \frac{\varepsilon_f}{2} \qquad 2.11$$

Gurney (1968) presented an exhaustive summary of SSC 137 in his book 'Fatigue of Welded Structures'. He argued that N = ¼ cycles was not representative of static tensile tests even though the equation does give reasonable if not conservative solutions, at least for lives up to 5000 cycles. This relationship shows that at least, in un-welded specimens, material strength is irrelevant in defining LCF behaviour and that material ductility is a more significant parameter. This agrees with a conclusion in (Rolf and Munse, 1963) that a material with good high cycle fatigue strength may not necessarily behave well in low cycle fatigue.

Dubuc (1961) and Major (1959) found that the value of *m* is not constant but greatly dependent on the material and test conditions like temperature, loading method and strain ratio. For steels used in pressure vessels, fatigue life is largely dependent on total strain range than on plastic strain range. At fatigue life of 10000 cycles, all steels tested gave the same total strain range – 0.8 %, but the slope of the $\varepsilon - N$ curve varied. For example, the carbon steels gave an average slope of -0.42 while complex alloy steels gave a slope of -0.21. This means that at shorter lives, the carbon steel with lower strength and higher ductility performs better in low cycle fatigue than the complex alloy steels. Gross (1963) experiment on several materials found values of m ranging from 0.42 to 4.2.

Martin (1961) obtained an energy based expression for the relationship between strain and specimen lives as:

$$\varepsilon_p * N^{1/2} = \frac{\varepsilon_f}{\sqrt{2}} \qquad 2.12$$

Yao and Munse (1965) studied the LCF behaviour of mild steel small coupon specimens with the aim of developing a general low cycle fatigue hypothesis for metals. They studied 240 ship steel specimens under varying load conditions. They reported that for mild steel tested under various strain ratios, the value of m is best expressed as:

$\frac{1}{m} = 1 - 0.86r$, r is the strain ratio. 2.13

A general hypothesis is developed to describe the cumulative effect of plastic strain/deformation on LCF behaviour of metals. This hypothesis takes into account the compressive plastic strain, the tensile plastic strain and the number of cycles to failure. The hypothesis is based on the assumption that LCF fractures occur in tension only and that fracture is produced by an accumulation of plastic deformation experienced by the material. The investigators verified the proposal with test data.

$$\sum_{i=1}^{n}\left[\left(\frac{\Delta\varepsilon_t}{\Delta\varepsilon_{t1}}\right)^{1/m}\right]_i = 1.0 \qquad 2.14$$

i = number of applications of tensile load, $\Delta\varepsilon_t$ is the cyclic tensile change in plastic true strain, $\Delta\varepsilon_{t1}$ is the cyclic tensile change in plastic true strain at n = 1, n is the number of applications of tensile loads prior to fracture and *m* is a variable dependent on the amount of cyclic compressive strain or relative strain ratio (r).

Pian and D'Amato (1958) noted from experimental results that the shape of a typical S-N curve for low cycle tests can be described but it is difficult to make any precise analysis of the test results at lower number of cycles. The curves noted to be entirely flat in the low cycle region particularly for plain specimens, become concave downwards and finally joins up to the high cycle fatigue curve. Figure 2.13 shows the initial portion of a low cycle S-N curve as flat. Hartmann and Strickley (1942) tested 6 aluminium alloys in the low cycle range and presented their results in S-N form. The results showed that at very low cycles – ½ to 10^4 – the curve was flat.

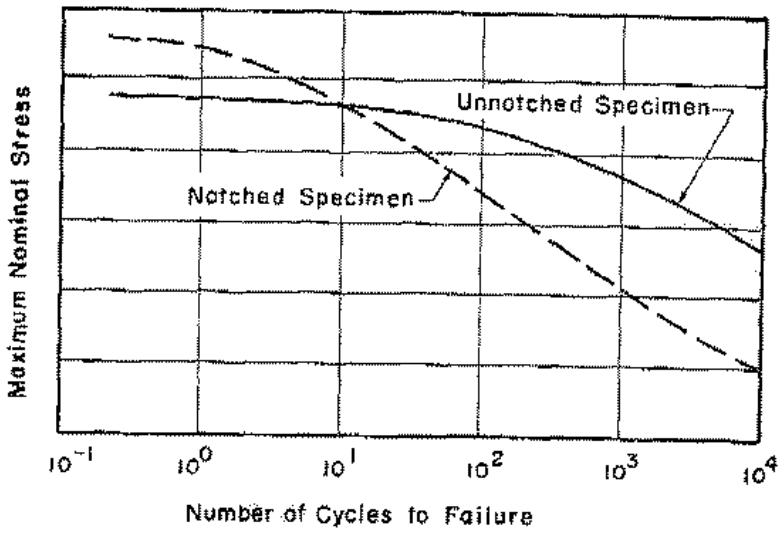

Figure 2.13: Typical low cycle S-N curve (Yao and Munse, 1965)

Hardrath et al (1953) observed the phenomenon of 'minimum life at high stress levels' in their research. They noted that if a specimen has survived the first load cycle, it would not fail until a certain 'minimum life' was exceeded. Illg et al (1955) test results agreed with Hadrath's findings.

Yao and Mosborg (1959) investigated the LCF behaviour of ABS –Class C normalised steel and showed that for lives less than 1000 cycles, strain was more sensitive measurement of life than the nominal stress. This goes to show that stress is not a good indicator of fatigue life in the low cycle region and the strain is a more indicative parameter.

Rolf and Munse (1963) studied parameters affecting crack growth at high stress levels in mild steel. Type of loading cycles, aging effect, temperature and geometry are some of the parameters studied while investigating the rate of crack growth on flat plate specimens with central notches. A hypothesis relating to the rate of crack growth and stress is presented to describe the behaviour during crack propagation. The test results obtained in the study are verified with existing crack propagation theories. The occurrence of a visual crack is used to establish the beginning of crack propagation.

Fatigue crack propagation behaviour of mild steel is divided into the three stages: initial, linear and final stage. The initial stage is a very short period in the total life of

the specimen and is dependent on the stress levels, number of cycles to crack initiation, initial geometry and the changing stress field around the crack tip. The rate of crack growth and the strain field ahead of the crack tip increases with crack length. At this stage, crack growth is proportional to the crack length. At the linear stage, a linear rate of crack propagation occurs and crack propagation rate remains constant. The strain field ahead of the crack tip also remains constant. And at the final stage, the crack nears the edge of the specimen and this behaviour is governed by eccentricity in the specimen and edge effects.

There have been several investigations into the low cycle behaviour of welded joints. Most of the investigations relate to butt welds which are encountered more frequently in the pressure vessel industry. Investigations have shown that butt welds do not reduce LCF behaviour of the parent material (Bowman and Dolan, 1953) and (Bat, 1957). However, welded attachments and notches can reduce the LCF behaviour mainly because of the strain concentration they produce (Bowman, 1955). Information on simple fillet welded and butt welded joints in the as-welded condition was largely unavailable until investigations carried out by The Welding Institute (Rosenberg et al, 1991) led to compilation of test results for welded joints. This report will be reviewed later on in the literature.

Pellini et al (1965) suggested that for welded structures under LCF conditions, the most important characteristic is the crack propagation rate especially for materials with high yield stress. Materials that demonstrate high crack growth rate are critically dependent on the initiation period for providing satisfactory LCF life. The crack initiation stage is influenced by the conditions near the point of origin while the crack propagation stage is affected by the conditions throughout the entire cross section that the crack traverses. He also showed that for several materials, the crack propagation rate can be expressed in terms of the total strain as:

$$\frac{dl}{dN} = C\varepsilon_T^4 \qquad 2.15$$

Where l is the length of the crack, C is a constant, N and ε_T are as previously defined. For some steels, the rate of crack growth is independent of the static strength but if

materials are compared in terms of proportional strain range then crack growth rate increases with increase in yield stress. He concluded that although using a high strength material can achieve a reduction in size and weight of the structure, the high strength materials work with larger strains than materials of lower strength. As such, the LCF crack propagation rate would be higher and there would be less material to resist crack growth. A high strength material loaded in proportion to its yield strength would exhibit inferior LCF characteristics. The advantage of a high strength material is their ability to carry higher loads in the low – strain elastic region so Gurney (1968) argued that for better LCF performance, high strength material should be used at a design stress similar to a lower grade material so that the high strength material can work in the elastic range where the low strength material would be plastic.

In most complex structures, defects are usual especially near high strain regions. Thus, the initiation stage is completely eliminated as a defect is the same as an initiated crack. In such cases, the fatigue life of the structure is the crack propagation period with failure occurring when a 'critical' crack size is reached. Also in may of these structures, information of crack growth rate may be used to establish inspection procedures.

In more recent years, Park and Lawrence (1988) reporting in SSC-346 provided low cycle fatigue test results for heat affected zones (HAZ) and for weld material of details commonly encountered in ship construction. All the specimens are tested using shielded metal arc welding process and each weld had four possible weld toe and two incomplete joint penetration sites for fatigue crack initiation.

One of the details tested is shown in Figure 2.14. It consists of a centre plate with two loading plates welded to the centre plate by all round fillet welds. ASTM A-36 steel grade is used as a base metal for the specimen. The estimated fatigue properties for the specimen are listed in Table 2.7. A series of cruciform welded joints was also tested. The base metal was ASTM 441 grade 50 steel which is comparable to ASTM AH-36 steel grade.

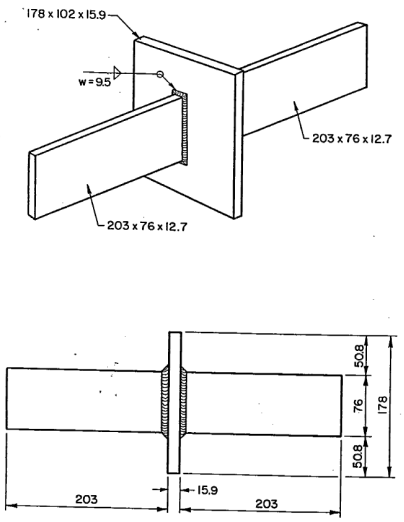

Figure 2.14: Geometry and dimension of test piece (Park and Lawrence, 1988)

Table 2.7: Fatigue properties for the above detail (Park and Lawrence, 1988)

Material Property	Weld Metal	Heat Affected Zone (HAZ)
Ultimate strength	782 (MPa)	849 (MPa)
Yield strength	475 (MPa)	516 (MPa)
Fatigue strength exponent, b	-0.0858	-0.084
Fatigue ductility exponent, c	-0.6	-0.6
Cyclic hardening exponent, n’	0.143	0.14
Cyclic strength coefficient, K’	1207 (MPa)	1312 (MPa)
Fatigue strength coefficient	1119 (MPa)	1184 (MPa)
Residual stress	310 (MPa)	310 (MPa)

2.3.3.2 The Welding Institute (TWI)

In 1991, Rosenberg et al conducted a survey of literature for TWI on LCF behaviour of welded joints in the offshore industry and a good number of papers are highlighted. A large portion of the literature obtained was considered inappropriate because they related entirely to the low cycle fatigue tests on butt welds or cylindrical specimens which are not relevant to FPSOs. Others dealt with LCF behaviour on a microscopic material level with emphasis on chemical composition of the metal. The review highlighted the lack of information on the low cycle fatigue behaviour of welded joints.

In the review only 10 published papers was found to have useful data relevant to the offshore industry. The test data is presented in the form of S-N curves and for comparative purpose, the mean and design S-N curves for corresponding joint classes based on Department of Energy Guidance notes (1984) are plotted with the test data. The weld types represented on the survey were transverse butt welds, longitudinal non-load-carrying fillet welds, transverse non-load-carrying fillet welds, transverse load-carrying fillet welds and tubular joints. The following paragraphs will review these papers.

Dunn and Anderson (1984) tested transverse load carrying fillet welded specimens under constant displacement cantilever bending in which failure is identified as the loss of load carrying capacity. They showed that low cycle fatigue life of the fillet welded test pieces are underestimated when using ASME III procedures.

Harrison (1969) published fatigue test result for high strength steel and as-welded non-load-carrying fillet welded specimens. The tests were carried out under load and strain control. The stress ranges obtained from the test are approximately half the number of cycles required to initiate a macro-crack.

Lieurade (1978) carried out low cycle fatigue tests on welded cruciform joints. Two geometries: transverse load carrying and transverse non-load-carrying geometries are considered Figure 2.16 shows the S-N curve for the specimen in Figure 2.15 tested by the author under axial loading.

Lieurade and Maillard-Salin (1978) presented low cycle fatigue test results carried out on transverse butt welds and cruciform joints. The fatigue lives obtained correspond to the appearance of a crack of area not greater than 5 % of the area of the nominal section.

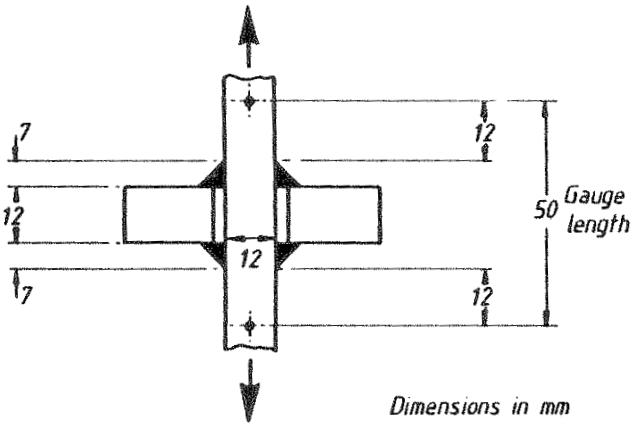

Figure 2.15 Details of specimen tested by Lieurade (1978)

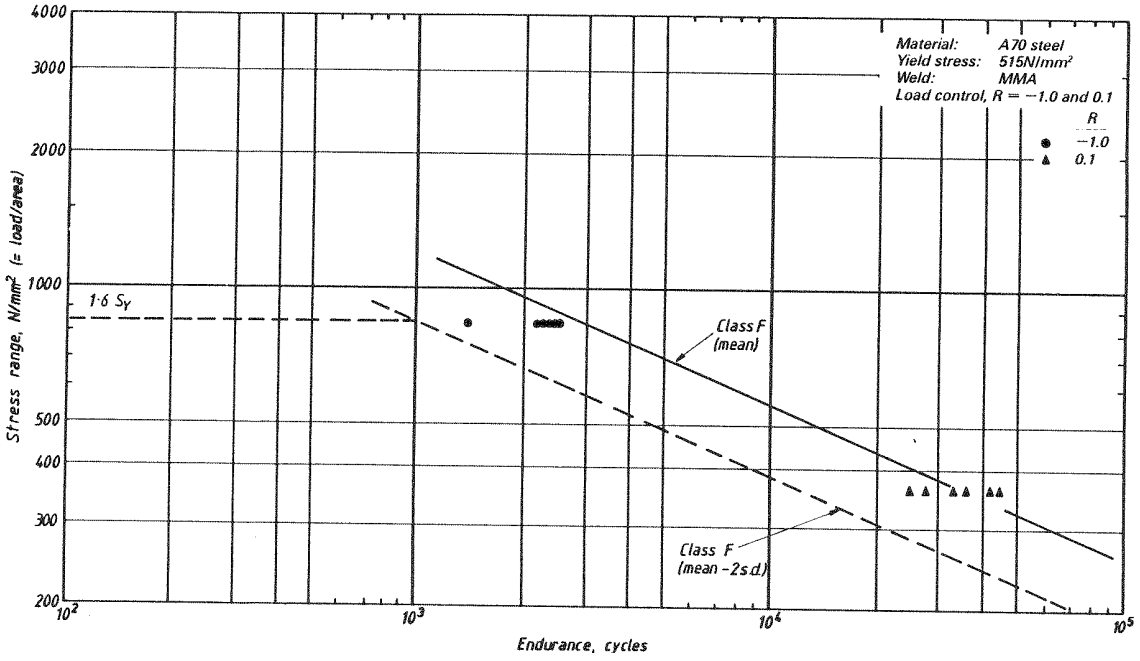

Figure 2.16: Transverse non-load-carrying fillet weld, axial loading

Nihei (1981) studied the influence of fluctuating mean stress on the low cycle fatigue behaviour of transverse butt welds. Radziminski and Lawrence (1970) investigated the fatigue resistance of three high yield steels under uniaxial loading. They found that the cyclic behaviour of the three materials can be reasonably described with the same S-N curve for a range of lives of approximately 10^4 to 10^6 cycles. The same behaviour was observed for full penetration butt welds in which fatigue failures initiated at the toe of the weld reinforcement.

Trufyakov and Yakubovskii (1981) investigated the low cycle fatigue strengths of four different types of welded joints. The effect of joint type and strength of the parent material on fatigue performance are considered on the basis of quasi-static loading and fatigue failure in the low cycle region.

TWI (2004) published a follow up report to review the current status in design and evaluate more recent experimental data with the aim of evaluating the treatment of high stress ranges. This report was published thirteen years after the first and there was still very limited information on LCF behaviour of welded joints. The same literature as the previous report is reviewed.

It is reported that the majority of the welded joints in the first report are safe based on comparison with Department of Energy (DOE, 1984) S-N curves. The report concludes that the limits on stress range and allowable stress for static loading is satisfactory and there is no need to extrapolate the design curves to higher stress ranges based on the available data. In a report on low cycle fatigue resistance, it is argued that the high stress levels in low cycle fatigue are possible but only in theoretical problems rather than in practical conditions and that these stress levels were unlikely to occur in actual offshore installations meaning that strength checks can in fact design can prevent low cycle fatigue failure. Recent experiences with fatigue failures in newly built FPSOs disprove this statement.

The Department of Energy Guidance notes (1984) suggest the use of constant amplitude high cycle S-N curves in the treatment of low cycle fatigue. The high cycle S-N curves are extrapolated back linearly on a log-log basis to a limiting stress range. This limiting stress range for welded joints in regions of simple tensile stress is restricted to twice the allowable axial stress which is 0.8 of the yield stress in extreme conditions and 0.6 of yield stress in normal operating conditions. There are restrictions in the application of these rules because the loading mode is generally and it is only applicable to mild steel and 50D specification steel.

2.3.3.3 Other Relevant Work

The American Society for Testing and Materials (ASTM) has published several technical series on low cycle fatigue and life prediction. STP 490 (Wundt (1972): 'Effects of Notches on Low Cycle Fatigue' is an extensive literature review on the effects of notches and discontinuities on life in low cycle fatigue regime. The review covers papers published over a period of 14 years. The areas of interest include cyclic stress strain curves, Neuber's rule in low cycle fatigue, fatigue strength reduction factors and low cycle fatigue tests in bending. STP 942 (Solomon et al, 1985): 'Low Cycle Fatigue', and STP 770 (Amzallag et al, 1980): 'Low Cycle Fatigue and Life Prediction' contains a wide range of research topics including cyclic deformation, damage, micro-structural effects of LCF, notches and thermal LCF and are presented in over 80 papers.

Only two of the papers were found to be applicable to the present study. The work of Lieurade and Maillard-Salin on cruciform joints which has been reviewed earlier and research carried out by Truchon (1982).

Truchon (1982) carried out low cycle fatigue tests on notched specimens for a wide variety of steels and derived an elastic plastic fatigue strength reduction factor to account for local plasticity effects in the low cycle fatigue region. Low cycle fatigue data with unnotched specimens is used to analyse fatigue crack initiation data using Neuber's rule.

Similarly, Murakami and Kusumoto (1973) developed a low cycle fatigue strength prediction method where the number of cycles to initiate a crack is estimated for a notched specimen from the characteristics of the hysteresis loops of an unnotched specimen. Good prediction is obtained for annealed carbon steel notched specimens under completely reversed loads and the authors are confident that the method can be applied to other materials.

More recently, Heo (2004) et al for Daewoo Shipbuilding and Marine Engineering (DSME) carried out low cycle fatigue tests on base metal and welded joints for a wide range of ship steels. The base metal ranged from mild steel to high tensile steel and

the weld metal was made using conventional welding procedure. Non-load-carrying partially penetrated cruciform fillet welded joints was used as a test specimen as illustrated in Figure 2.17. The test was carried out under strain control condition and the strain ratio was set to zero meaning that the strain value fluctuated between zero and a specified maximum value. Wang (2008) compared the test results of Heo et al with data from the test carried out by Rosenberg et al on longitudinal non-load carrying fillet welds. The results are plotted in terms of pseudo hot spot stress and the number of cycles to failure. The ABS D class S – N curve for plated details is plotted as reference and Figure 2.18 shows that in the low cycle fatigue region, using the D curve, as a design S-N curve will yield conservative results.

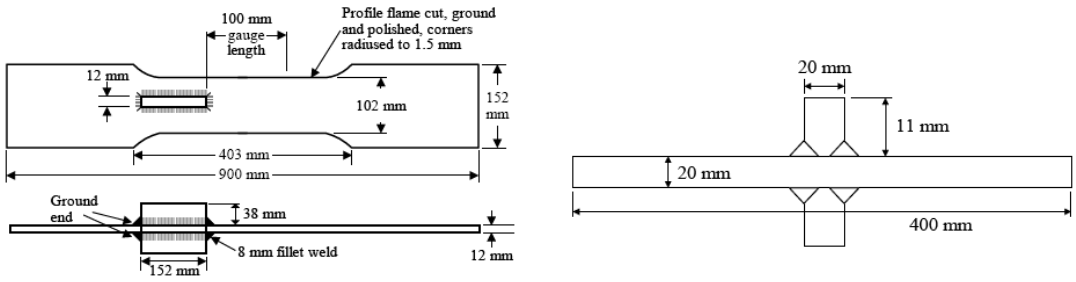

Figure 2.17: Test specimen

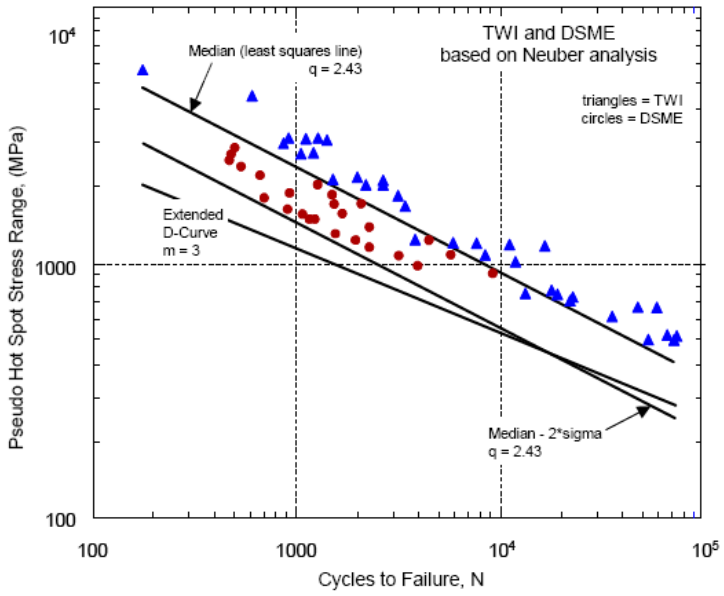

Figure 2.18: S-N curve based on the above specimen

Kim et al (2005) report monotonic and cyclic tests carried out to obtain stress strain curves for base metal and weld metal of ship structures. LCF tests for mild steel 'A' grade and a welded cruciform joint is reported in the form of a strain-life curve. The strain life curve (Figure 2.19) together with the cyclic stress strain curve can be used as the basis for fatigue design for welded ship structures. Kim et al (2006) also published results obtained using electronic speckle pattern interferometry (ESPI) to determine full field strain of a welded cruciform joint and comparing the resulting fatigue lives with lives determined using Neuber's rule and established codes. Low cycle fatigue life corresponding to the pseudo elastic stress calculated from maximum strain measured by ESPI system shows better agreement with the DNV I S - N curve for plated details than the results from the theoretical method using Neuber's rule.

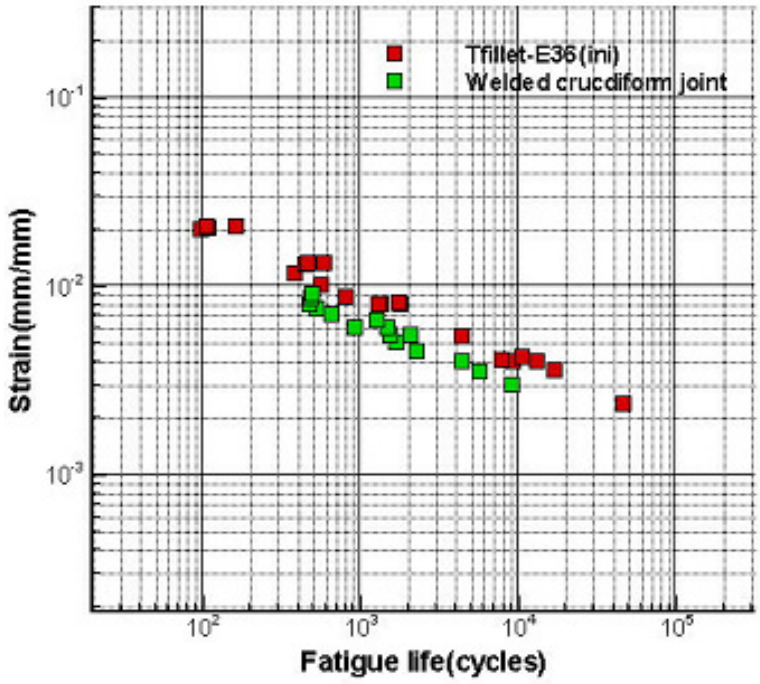

Figure 2.19: Strain life curve for welded cruciform joints

Tateishi et al (2007) discuss a local strain based approach to predict the fatigue strength of welded joints in extremely low-cycle fatigue region. Low-cycle fatigue tests were conducted on T-shaped welded joints in order to locate crack initiation sites and to obtain the fatigue life. The local strain field around the welded toe was analyzed by elasto-plastic FE analysis, and the local strain amplitude at the cracking point was quantified. Extensive research on low cycle fatigue has revealed that the

strain amplitude at the cracked point, the so called local strain, dominates the low-cycle fatigue life.

Wang et al (2006) proposed a fatigue damage prediction method for welded joints in the low-cycle fatigue regime in ship structures. In the paper, a literature review of material behaviour under low-cycle large stress range investigated, and the possible approaches to obtain the strain-life curve are discussed. In the outlined procedure, the hot-spot stress is used and the pseudo hot-spot stress range is derived based on elastic hot-spot stress range and material stress-strain curve with the application of Neuber's hypothesis. A suitable design S-N curve has been derived from tests carried out on non-load-carrying fillet joints under strain control condition.

2.4 Classification Society Rules for Low Cycle Fatigue Assessment

Classification societies are addressing the issue of low cycle fatigue and several draft guidance documents have been issued. DNV has published documents on low cycle fatigue assessment: Fatigue Methodology for Offshore Ships (DNV-RP–C206, 2006) Guidelines for Building and Classing Floating Production Installations' by ABS (2009) and Lloyds Register's Ship Right Floating Offshore Installation (2008) also specify provisional guidance for low cycle fatigue assessment.

These methods chosen by each classification society is based on several factors, the most important being the owners design philosophy. These methods are all variations of the stress-based fatigue assessment procedure. The guidance notes are all quite similar: the use of rain flow counting algorithm, the use of plasticity correction factor based on BS5500, the use of high cycle fatigue S – N curve and also the use of linear damage law to determine fatigue damage.

2.4.1 Typical Low Cycle Fatigue Assessment Procedure for FPSOs

A simplified low cycle fatigue assessment based on the stress based approach involves the following steps:

i. Select the structural details to be analysed

ii. Define load configuration that is characteristic of a typical loading and unloading cycle experienced by the FPSO

iii. Calculate the still water stresses for each loading condition

iv. Define a stress sequence in a complete loading and unloading cycle and evaluate the stress ranges and cycles using counting methods.

v. Evaluate the pseudo elastic stress ranges using a plasticity correction method in order to employ the S – N curve. Note that Neuber's or Glinka's rule can be used if the cyclic stress- strain curve is known, if this is not known, then the BS5500 formulation may be used.

vi. Calculate fatigue damage per cycle based on S – N curve and then the cumulative fatigue damage for the design life based on the number of loading and unloading cycles using Miner's rule.

2.4.2 Lloyds Register (LR)

The stress range for low cycle fatigue is based on hot-spot stress. Low cycle pseudo stress range is obtained using elastic hot spot stress, $\Delta\sigma_{fem}$ obtained from linear finite element analysis and a plasticity correction factor, k_e, based on BS5500.

$$\Delta\sigma_{LCi} = k_e * \Delta\sigma_{fem} \qquad 2.16$$

The fatigue damage from the quasi –static still water stress cycles (low cycle fatigue damage) is determined from the following:

$$D_{LCF} = \sum_{i=1}^{n} \frac{\left[k_e\left(\sigma_{LCi} + 0.5\left(\sigma_{HCTi} + \sigma_{HCBi}\right)\right)\right]^m}{c} \qquad 2.17$$

n = no of quasi static 'still water' stress cycles

σ_{LCi} = ith highest stress range from quasi static 'still water' stress cycles

σ_{HCTi} = highest wave induced stress range over the duration of the peak of the ith highest quasi static 'still water' stress cycle

σ_{HCBi} = highest wave induced stress range over the duration of the trough of the ith highest quasi static 'still water' stress cycle

m = Slope of the SN curve at around 1000 cycles

c = Intercept of SN curve at around 1000 cycles

The S-N curve for LCF assessment is the hot spot stress S-N curve specified in LR FDA rules. The parameters are given in Table 2.8.

Table 2.8: Hotspot stress reference S-N curve parameters

	Log A		m	m
	Mean Curve	Design Curve	$N \leq 10^7$	$N>10^7$
Fillet Weld	12.636	12.200	3.0	5.0
Free Edge	14.033	13.625	3.5	5.5

2.4.3 Det Norske Veritas (DNV)

In 2000, DNV proposed a methodology based on allowable notch stress range to avoid LCF induced cracks in ships structures. Further studies were carried out by Heo et al (2004) and a design methodology for LCF was proposed. Through test programs, cyclic stress strain curves for mild and high strength steels of different material grades and the strain life curves of welded and base metal is obtained. Strain values from nonlinear finite element analysis are compared with base metal and welded component test results. Neuber's rule is noted to be most conservative in estimating stress strain state at the local hot spot. Urm et al (2004) developed a simplified LCF assessment procedure and a process for combining LCF damage and HCF damage based on earlier work carried out by Heo et al. A minimum design cycle of 500 is recommended for tankers though the actual design cycle may be higher.

A section on low cycle fatigue in combination with high cycle fatigue is included in the commentary section of the most current release of DNV-RP-C203: Fatigue Design of Offshore Steel Structures. To determine low cycle fatigue damage it is recommended to calculate a stress range from the wave action corresponding to the largest expected stress range during a loading/unloading process. This stress range

from the wave action is added to the low cycle stress range to obtain an effective stress range which is used for low cycle fatigue damage calculation.

$$D_{LCF} = \frac{n_{LCF}(\Delta\sigma_e)}{A}$$

$$\Delta\sigma_e = \Delta\sigma_{LCF} + \Delta\sigma_{HCF}$$

$$\Delta\sigma_{HCF} = \Delta\sigma_0\left(1 - \frac{\log n_{lcf}}{\log n_0}\right)^{1/h} \qquad 2.18$$

$\Delta\sigma_e$ = Effective stress range

$\Delta\sigma_0$ = Largest stress range corresponding to n_0 cycles from waves

n_{lcf} = Number of loading/unloading cycles during lifetime

h = Weibull shape parameter

The S-N curve adopted for LCF assessment is the extension of the existing DNV design curve I for HCF above 10000 cycles- parameters are given in Table 2.9.

Table 2.9: DNV Proposed LCF S-N curve

S-N Curve	Material	$10^2 \leq N < 10^4$	
		Log A	M
I	Welded Joints	12.76	3.0
III	Base Metal	13.0	3.0

2.4.4 American Bureau of Shipping (ABS)

The ABS philosophy towards low cycle fatigue is that the fatigue strength of welded joints and details in subjected to low cycle fatigue loads is to be based upon at least 20 years of operation of the ship. The number of cycles for the loading and unloading operation for the structure should not be less than 1200. The stress employed is the elastic hotspot stress at the toe of a weld in question. The elastic hotspot stress is obtained from finite element analysis and transformed to a pseudo elastic stress using a plasticity correction factor which has been derived for different ship steels. It should be noted that in the elastic high cycle range a pseudo hot spot stress will be the same as an elastic hot spot stress. They will differ in the low cycle range. The design S-N

curve in the low cycle region is taken as a modified D curve. It is assumed that the LCF design S-N curve is applicable to static induced stresses. Miner's rule is applied to produces the expression of low cycle (static stress) damage.

ABS Guide to Fatigue Strength Assessment of Ship-Type Installations includes a comprehensive guidance on low cycle fatigue damage from loading and unloading. Wang et al (2006), for ABS, investigated typical material behaviour under low cycle stress range and recommended characteristic material properties based on experimental data. The pseudo hot spot stress range is calculated from the elastic hot pot stress range and material stress-strain curve with the application of Neuber's rule. The total stress range associated with low cycle quasi static process is obtained, as the method proposed by LR, adding the static stress range to the median of the largest stress range for the wave induced load. For the modified D curve, the low cycle fatigue S-N curve is given as:

$NS^m = A$ For 100 < N < 10000

where m is 2.4 and A is 3.51 x 10^{10} (MPa). Basic Miner's rule is applied to obtain fatigue damage.

$D_{lcf} = \frac{n_{lcf}}{N_{lcf}} = \frac{n_{lcf} S^m}{A}$, n_{lcf} which is the total loading and unloading cycles should not be less than 1200 for a ship installation to be operated for 20 years.

2.4.5 Discussion

The methodologies proposed by the classification societies are all based on the assumption that Miner's linear damage rule applies and that rainflow analysis is used to identify the stress cycles. These S-N approaches are based on the hotspot stress method. This will be discussed in the following chapter where several extrapolation procedures will be tested to select the best suited to the research. The main differences lie in the S-N curve and also the method of accounting for plasticity effects in the calculated stresses. It will be interesting to see how these two factors affect low cycle fatigue damage. Cumulative damage is not discussed in this chapter. The process of

combining low cycle fatigue damage and high cycle fatigue damage is in the author's opinion challenging and is dealt with exhaustively in Chapter 6.

2.5 Conclusion

This chapter has presented background information which will not be further researched in the thesis and will be used as supporting data in the rest of the thesis. The importance of FPSOs in the offshore industry is discussed and structural details of the reference vessel that will be use in the remainder of the study are presented. General fatigue loads on FPSOs are discussed as well as low cycle fatigue loading in FPSOs. The quasi-static load cases and loading and unloading sequences that will be used in finite element analysis are presented. Cyclic properties of ship steels are discussed and a summary of empirical formulations for transforming the elastic stress obtained from finite element analysis to pseudo elastic stress is presented. The techniques, formulations and data presented in this chapter will be referred to in subsequent chapters to support low cycle fatigue assessment.

A brief summary of the milestones of fatigue through history has been presented. A literature review of low cycle fatigue of metals and welded components was outlined. Investigations by the Ship Structures Committee, The Welding Institute and other researchers are reviewed and it is quite obvious from the extent of the available literature that there is a lack of general information and test data on the low cycle fatigue of welded steel structures. A typical low cycle fatigue assessment procedure as applied to FPSOs is presented. Classification society rules for low cycle fatigue assessment from loading and unloading of FPSOs is outlined and their similarities highlighted. This information will be used later on in the course of the thesis for comparative purposes i.e. the different approaches by the CS will be compared.

REFERENCES

1. ABS (2009) 'Guidelines for Building and Classing Floating Production Installations' American Bureau of Shipping. ABS Plaza, Texas.
2. Amzallag C., Leis B.N. and Rabbe P. (1980) 'Low Cycle Fatigue and Life Prediction' STP 770, American Society for Testing and Materials ASTM
3. ASTM (1996) 'Metal Handbook, Volume 19 Fatigue and Fracture' American Society for Testing and Materials ASTM
4. Atzonline:http://www.atzonline.com/index.php;do=show/site=a4e/sid=4489942194b44d11b38617370101052/alloc=38/id=61/special=Special+Simulation
5. B. Han, D. Post and P. Ifju, (2001). 'Moiré Interferometry for Engineering Mechanics: Current Practices and Future Developments, Journal of Strain Analysis 36, Volume 10, pp. 1–17
6. Bai Y (2003). 'Marine Structural Design' Elsevier, London
7. Barltrop N. (2004) 'Marine Materials and Structures'. Course notes, Department of Naval Architecture and Marine Engineering. University of. Glasgow
8. Basquin O.H (1910). 'The Exponential Law of Endurance Tests' American Society for Testing and Materials Proc 10, pp. 625–630.
9. Bat A.A. (1957) 'Study of Fatigue Strength of Welded Joints in Steel' NL2 No. 6
10. Bauschinger J. (1881), 'Ueber die Veranderung der Elasticitatsgrenze und Elastcitatsmodul Verschiedener', Metal Civiling N.F., 27, 289-348
11. Bowman C.E. and Dolan T.J.(1953) 'Biaxial Fatigue Properties of Pressure Vessel Steels' Welding Research Supplement, Volume 8 No 11 pp 529-537
12. Bowman C.E. and Dolan T.J.(1955) 'A Study of Biaxial Fatigue Properties of Pressure Vessel Steels' Welding Research Supplement, Volume 20 No 1 pp 51-59
13. BS 5500(2009) 'Specification for Unfired Fusion Welded Pressure Vessels'. British Standards Institution.
14. Coffin L. F. Jr. (1954a). 'A Study of the Effects of Cyclic Thermal Stresses on a Ductile Metal'. Trans. ASME, 76:6,
15. Coffin L. F. Jr. (1960). 'An Investigation of Thermal-Stress Fatigue as Related to High-Temperature Piping Flexibility'. Trans. ASME, vol. 79 pp. 1637-1651

16. Coffin L. F. Jr. and Read J. H. (1957). 'A Study of the Strain Cycling and Fatigue Behaviour of a Cold Worked Metal'. International Conference on Fatigue, p. 415, 1957.
17. Coffin L. F. Jr. and Tavernelli J.F. (1959a). 'The Cyclic Straining and Fatigue of Metals'. Trans. Metallurgical Society of AIME, vol. 215, p. 794
18. Coffin L. F. Jr. and Wesley R. P. (1954b).'An Apparatus for the Study of Effects of Cyclic Thermal Stresses on Ductile Metals'. Trans. ASME, 76:6
19. Coffin L.F (1971) 'A Note on Low Cycle Fatigue Laws'. Journal of Materials, Volume 6, No. 2.
20. Coffin L.F (1972) 'The Effect of High Vacuum on the Low Cycle Fatigue Law'. Metall. Trans., Volume. 3A, no. 7,
21. Coffin L.F. Jr. (1954c). 'The Problem of Thermal Stress Fatigue in Austenitic Steels at Elevated Temperatures'. ASTM Special No. 165, Symposium on Effect of Cyclic Heating and Stressing on Metals at Elevated Temperatures
22. Coffin L.F. Jr. (1959b). 'Design for Low-Cycle Fatigue'. SESA Design Clinics
23. Department of Energy (1984). 'Background to New Fatigue Guidance for Steel Welded Joints in Offshore Structures'. HMSO
24. DNV-RP-C206. (2005). 'Fatigue Methodology for Offshore Ships'. Recommended Practice. Det Norske Veritas. Norway.
25. Dubuc J. (1961). 'Plastic Fatigue under Cyclic Stress and Cyclic Strain with a Study of the Bauschinger Effect'. Ph. D. Thesis submitted to Ecole Polytechnique, University de Montreal, Canada.
26. Dunn J.W. and Anderson J. (1984) 'An Assessment of the Over-Conservatism of the ASME III Low Cycle Fatigue Predictions for Fillet Welds'. 2nd International Conference on Fatigue and Fatigue Thresholds, Volume III pp1753-1761.
27. ESDEP Course Notes. WG12: Fatigue
28. Evans E. W. (1957). 'Effect of Interrupted Loading on Mechanical Properties of Metals'. The Engineer (London), 203.5274, Part 1
29. Fatemi A. (2003). 'Cyclic Deformation and Strain-Life Approach'. University of Toledo

30. Fatemi A. and Yang L. (1998) 'Cumulative Fatigue Damage and Life Prediction Theories: a Survey of the State of the Art for Homogenous Material'. International Journal of Fatigue. Volume 20 No. 1. pp 9-34
31. Glinka G. (1985) 'Energy Density Approach to Calculation of Inelastic Strain–Stress near Notches and Cracks. Engineering Fracture Mechanics 22(3):485–508.
32. Griffith A. A. (1921), 'The Phenomena of Rupture and Flow in Solids', Philosophical Transactions of the Royal Society of London, A 221: 163–198
33. Gross J.H and Stout R.D. (1955). 'Plastic Fatigue Properties of High Strength Pressure-Vessel Steels'. The Welding Journal 34.4 Research Supplement.
34. Gross J.H. (1963). 'Low Cycle Fatigue of Materials of Submarine Construction'. Naval Engineering Journal Volume 75 No. 4 pp 783-795
35. Gurney T.R (1968). 'Fatigue of Welded Structures'. British Welding Research Association. Cambridge University Press.
36. Hardrath. H. F, Landers B. G. and Utley E. C. (1953). 'Axial Load Fatigue Tests on Notched and Unnotched Sheet Specimens of 61S-T6 Aluminium Alloy, Annealed 347 Steel and Heat Treated 403 Stainless Steel'. NACA TN 3017
37. Harrison J.D (1969) 'Further Low Cycle Fatigue Tests on Butt and Fillet Welded High Strength Steel'. Weld Institute Report No. C215/11/69.
38. Hartmann E. C. and Strickley G. W. (1942). 'The Direct Stress Fatigue Strength of 17s-T Aluminium, A11oy through the Range of ½ to 5 x 10^9 Cycles of Stress NACA TN 86.
39. Heo J.H., Kang J., Kim Y., Yoo I., Kim K. and Urm H. (2004). 'A Study on the Design Guidance for Low Cycle Fatigue in Ship Structures'. PRADS 2004
40. Hoffman M. and Seeger T. (1985).'A Generalised Method for Estimating Multiaxial Elastic-Plastic Notch Stresses and Strains-Part 1 and Part 2, ASME J. Engineering Material Technology., Vol.107,250-260.
41. Illg W. and Hardrath H.F. (1955). 'Some Observations on Loss of Static Strength due to Fatigue Cracks'. NACA RM L55D15a
42. Irwin G (1957) 'Analysis of Stresses and Strains near the end of a Crack Traversing a Plate'. Journal of Applied Mechanics 24, 361–364.
43. Johansson A. (1956). 'Fatigue of Steels at Constant Strain Amplitude and Elevated Temperatures'. Stockholm Colloquium on Fatigue IUTAM.

44. Kaminski M.L (2007).'Sensing and Understanding Fatigue Lifetime of New and Converted FPSOs'. Offshore Technology Conference, Houston, Texas.
45. Kim K., Kim B., Kim Y., Lee C. and Lee S. (2006). 'A Study on Low Cycle Fatigue Behaviour of the Steel for Ship Building Industry'. Key Engineering Materials, Volume 297 – 300, pp 10-15.
46. Kim K., Kim K., Lee K., Kwon J., Park S. and Lee N. (2006). 'Effect of Local Strain on Low Cycle Fatigue Measured by ESPI System'. Key Engineering Materials, Volume 321 – 323, pp 678-683.
47. Kim K.S., Kim B.O., Kim Y.K., Lee C.H., and Lee S.W. (2005). 'A Study on Low Cycle Fatigue Behaviour of the Steel for Shipbuilding Industry'. Key Engineering Materials. Volume 321-323 pp 678-683.
48. Kommers T. B. (1912). 'Repeated Stress Testing'. New York International Association for Testing Materials.
49. Labbe F. (2006).'Strain-Rate Measurements by Electronic Speckle-Pattern Interferometry (ESPI)'. Optics and Lasers in Engineering. Elsevier Limited.
50. Lieurade H.P. (1978) 'Low Cycle Fatigue Behaviour of Cruciform Welded Joints in High Yield Stress Steels'. Soudages et Techniques Connexes, Volume 32 Nos. 11/12 pp 405-418.
51. Lieurade H.P. and Maillard-Salin (1978) 'Low Cycle Fatigue Behaviour of Welded Joints in High Strength Steel'. ASTM STP 770 pp311-336.
52. Lloyd's Register (2008). 'Ship Right FOI - Design, Construction and Installation- Floating Offshore Installation of Structures Design Guidance'. Lloyd's Register EMEA.
53. Low A. C. (1956). 'Short Endurance Fatigue'. International Conference on Fatigue of Metals.
54. Low A.C. (1955) 'The Bending Fatigue Strength of Aluminium Alloy MG5 Between 10 and 10 Million Cycles'. Journal of Royal Aeronautical Society Vol. 59.
55. Maddox S.J. (1991) 'Fatigue Strength of Welded Structures' Second Edition, Abington Publishing, England
56. Major H. (1959) 'Thermal and Mechanical Fatigue of Nickel and Titanium' Transactions of ASM Volume 51 pp 421.437
57. Mann J.Y (1990) 'Bibliography on the Fatigue of Materials, Components and Structures'. Volume 1-4, covering 1838-1996. Pergamon Press.

58. Manson S.S (1953) ‘Behaviour of Materials under Conditions of Thermal Stress’. NACA Technical Note 2933
59. Manson S.S. (1966). ‘Thermal Stress and Low Cycle Fatigue’. McGraw Hill, New York
60. Manson S.S. and Hirschberg M.H. (1964) ‘Fatigue Behaviour in Strain Cycling in the Low and Intermediate Cycle Range. Fatigue: An Interdisciplinary Approach’. Proceedings of the 10th Sagamore Army Materials Research Conference,
61. Mansour A.E., Lin M., Hovem L. and Thayambaili A. (1993) ‘Probability-Based Ship Design Procedures: A Demonstration. Report to Ship Structures Committee, SSC-368.
62. Martinez A., Rodriguez-Vera R., Rayas J. and Puga H. (2003). ‘Fracture Detection by Grating Moiré and In-plane ESPI Techniques’. Optical Laser Engineering 39, pp. 525–536.
63. Martins D.E. (1961) ‘An Energy Criterion for Low Cycle Fatigue’. Journal of Basic Engineering, Transactions of ASME
64. Matsuiski M. and Endo T. (1969) ‘Fatigue of Metals Subjected to Varying Stress’. Japan Society of Mechanical Engineering.
65. Miner M.A (1945). ‘Cumulative Damage in Fatigue’. Journal of Applied Mechanics 12 , pp. A159–A164
66. Molski K. and Glinka G. (1981).’A Method of Elastic-Plastic Stress and Strain Calculation at Notch Root’. Material Science and Engineering, Vol. 50, pp 93-100.
67. Mravak Z. (2007). ‘Low Cycle Fatigue’. Bureau Veritas
68. Munse W.H., Wilbur T.W., Tellalian M.L., Nicoll K. and Wilson K. (1983) ‘Fatigue Characterization of Fabricated Ship Detail for Design’. SSC-318, Ship Structures Committee Washington DC
69. Murakami Y. and Kusumoto S. (1973) ‘Notch Effect in Low Cycle Fatigue’. The Japan Society of Mechanical Engineers. Volume 16 No 101 pp1637-1647.
70. Neuber H. (1961). ‘Theory of Stress Concentrations for Shear Strained Prismatic Bodies with Arbitrary Non-linear Stress Strain Law’. Transactions of ASME. Journal of Applied Mechanics.
71. Nihei M et al (1981) ‘Effect of Programmed Mean Stress on fatigue Strength of Welded Joints for SM58 Steel’. Trans NRIM, Volume 23 No. 3 pp 33-44.

72. Ohnami M. (1992). 'Fracture and Society'. Ohmsha Limited, Tokyo Japan.
73. Orowan E. (1952). 'Stress Concentrations in Steel under Cyclic Loading'. Weld. Res. Suppl. Volume 31 No 6.
74. Paik J.K and Thayamballi A.K (2007). 'Ship – shaped Offshore Installations: Design, Building and Operation'. Cambridge University Press, New York.
75. Palmgren A.Z. (1924). Die Lebensdauer von Kugellagern, Z. des Verein Deutscher Ingenieure 68 pp. 339–341.
76. Paris P. and Erdogan F. (1963). 'A Critical Analysis of Crack Propagation Laws'. Journal of Basic Engineering, Transactions of the American Society of Mechanical Engineers
77. Park S.K. and Lawrence F.V (1988) 'Fatigue Characterization of Fabricated Ship Details for Design –Phase II', Ship Structures Committee. SSC-346.
78. Pellini W.S, Goode R.J., Puzak P.P., Lange E.A and Huber R.W (1965) 'Review of Concepts and Status of Procedure for Fracture Safe Design of Complex welded Structures involving Metals of Low to Ultra High Strength Vessels. NRL Rep 6300
79. Pian T. H. H. and D'Amato R. (1958). 'Low-Cycle Fatigue of Notched and Unnotched Specimens of 202.4 Aluminium Alloy under Axial Loading'. WADCTN 58-27.
80. Post D., Han B. and Ifju P. (1994). 'High Sensitivity Moiré: Experimental Analysis for Mechanics and Materials'. Springer, New York
81. Radziminski J.B and Lawrence F.V. (1970) 'Fatigue of High Strength Steel Weldments'. Welding Journal Research Supplement, Volume 49, pp365-374.
82. Rolfe S.T. and Munse W.H. (1963). 'Crack Propagation in Low-Cycle Fatigue of Mild Steel'. Ship Structure Committee. SSC-143.
83. Rosenberg T.D., Andrews R.M. and Gurney T.R. (1991) 'A Compilation of Fatigue Test Results for Welded Joints Subjected to High Stress/Low Cycle Condition – Stage 1'. Prepare by the Welding Institute for the Department of Energy: Report OTI 91 552
84. Schijve J. (2003). 'Fatigue of Structures and Materials in the 20th Century and State of the Art'. International Journal of Fatigue, Volume 25 pp679-702
85. Schutz W. (1996) 'A History of Fatigue'. Engineering Fracture Mechanics' Volume 54, pp. 263–300

86. Seeger T. and Heuler P. (1980) 'Generalised Application of Neuber's Rule' Journal of Testing and Evaluation 8, pp. 199-204
87. Shimamura Y. (2002) 'FPSO/FSO: State of the Art'. Journal of Marine Science and Technology. Pp 59 – 70.
88. Solomon H.D., Halford G.R. Kaisand L.R. and Leis B.N (1985) 'Low Cycle Fatigue'. STP 942, American Society for Testing and Materials ASTM
89. Stambaugh K.A and Van Mater P.R. (1990) 'Fatigue Performance under Multi-axial Loading'. SSC-356, Ship Structures Committee Washington DC
90. STM Standard E606-04 (2005). 'Standard Practice for Strain-Controlled Fatigue Testing'. ASTM International
91. Tateishi K., Hanji T. and Chen T. (2007) 'Low Cycle fatigue Assessment of Welded Joints based on Local Strain Approach'. International Institute of Welding IIW, Doc. XIII-2160-07.
92. Topper T.H., Wetzel R.M., Morrow J. (1969) 'Neuber's Rule Applied to Fatigue Notched Specimens,' Journal of Materials, Vol. 4, No. 1, pp. 200-209.
93. Toth L. and Yarema S. (2006). 'Formation of the Science of Fatigue of Metals. Part 1. 1825-1870'. Material Science, Volume 42, No.5
94. Truchon M. (1982). 'Application of Low Cycle Fatigue Test Results to Crack Initiation from Notches'. Low Cycle Fatigue and Life Prediction, ASTM STP 770. pp 254-268
95. Trufyakov V.I. and Yakubovskii V.V. (1981) 'Low Cycle Fatigue of Welded Joints under Zero Tension Loadings'. Automatic Welding, Volume 34 No 10
96. UK HSE (1999).'Background to New Fatigue Guidance for Steel Joints and Connections in Offshore Structures'. OTH 92 390, Failure Control Limited, Surrey.
97. UK HSE (2004). 'Review of Low Cycle Fatigue Resistance'. Failure Control Limited, Surrey.
98. Urm H.S., Yoo I.S., Heo J.H., Kim S.C. and Lotsberg I. (2004)."Low Cycle Fatigue Strength Assessment for Ship Structures". 9th Symposium on practical design of Ships and Other Floating Structures, Germany.
99. Vedeler G. (1961). 'A Naval Architects Reflections on Some Research Problems with Ship Steel'. Ship Structure Committee. SSC-140.
100. Vervoot S. and Wurmann W. (2006) 'History of Fatigue'. nCode International

101. Vial-Edwards C., Lira I., Martinez A. and Miinzenrnayer M. (2001). 'Electronic Speckle Pattern Interferometry Analysis of Tensile Tests of Semi-hard Copper Sheets'. Exp Mech 41 (2001), pp. 58–62.

102. Wang X. (2008) 'Structural Integrity of FPSO Conversions'. Deep Water Offshore Technology Symposium. China

103. Wang X., Kang J.K., Kim Y. and Wirsching P. (2006)'Low Cycle Fatigue of Marine Structures'. Proceedings of 25th International Conference of Offshore Mechanics and Arctic Engineering. OMAE 2006-92268

104. Wanlin G., Wang C.H and Rose L.R.F. (1998).' Elasto-plastic Analysis of Notch-Tip Fields in Strain Hardening Materials'. Department of Defence, DSTO Aeronautical and Marine Research Laboratory, Australia.

105. Wikipedia Authors: http://en.wikipedia.org/wiki/Fatigue_ (material)

106. Wöhler A. (1860). ' Versuche über die festiykeit eisenbahnwagenuchsen, Z Bauwesen 10

107. Wundt B.M. (1972).'Effect of Notches on Low-Cycle Fatigue, a Literature Survey'. STP 490, American Society for Testing and Materials ASTM.

108. Yang S.Y., Lim J.Y and Lee S. (2003) 'Evaluation of Notch Tip Strains using Whole Optical Measurement Techniques'. ATEM 2003, JSME-MMD

109. Yao J. T. P. and Mosborg R.J. (1959). 'Unpublished Progress Report'

110. Yao J.T.P and Munse W.H. (1961). 'Low – Cycle Fatigue of Metals – A Literature Review'. Ship Structure Committee. SSC-137.

111. Yao J.T.P. and Munse W.H. (1965). 'Low-Cycle Fatigue Behaviour of Axially Loaded Specimens of Mild Steel'. Ship Structure Committee SSC 151.

112. Yee D., Matsuoka S., Suzuki N and Maeda Y. (2004).' Further Investigation of Neuber's Rule and the Equivalent Strain Energy Density (ESED) Method'. International Journal of Fatigue 26, pp 447-455

CHAPTER 3 FINITE ELEMENT MODELLING

3.1 Introduction

Finite element (FE) analysis is one of the most popular numerical methods in the study of crack problems (1-12). Cracks are generally initiated in local areas so for an accurate description of the stress distribution due to geometric irregularities and the presence of notches, a local assessment is important. It is an enormous task to model large structures like ships because of the sheer scale of the number of local details. A fine global model will take a lot of time and computer resources, so a less time consuming but accurate method is a necessity to obtain relevant stresses. When modelling complex structures, like ships, there are sometimes several millions of degrees of freedom in the initial structure. A global model that is based on a simplified geometric model will have small details such as cut-outs or joints removed. These details do not affect the overall behaviour of the structure, but may have a bearing on fatigue and safety. Such details are studied through a series of local analysis.

In this research, the FE modelling and analysis is carried out using FEMAP, ANSYS and ABAQUS Standard software respectively. ABAQUS Standard is part of the ABAQUS Suite which is a commercial all purpose FEA tool.

3.2 Structural Modelling

Three levels of finite element modelling are carried out for the fatigue analysis of the FPSO: global, intermediate and local. A coarsely meshed 3D finite element model of the whole ship is developed using shell and beam elements. The coarse global model is used to obtain the stress results suitable for determining deformations and forces and also for locating areas of high stress. The deformations or forces are then applied as boundary conditions to the intermediate and/or local model with the purpose of obtaining a more accurate description of the stress distribution in the detail.

3.2.1 Global Structural Model

Global models are generally used to identify critical areas that have high stresses. Figure 3.1 shows a cross-section of the global FE model of the FPSO developed using a combination of shell and beam elements. For visual clarity, the image does not include the transverse web frames. The combined stiffener technique is sometimes employed to reduce the time required to develop and analyse the highly detailed finite element model. In the combined stiffeners method, multiple stiffeners are combined to give a resultant stiffened plate or beam that yield a similar dynamic response with the original plate. A lower mesh density can be adopted to develop a coarser FE model, thereby shortening the computational time. Sectional properties of the combined stiffeners may be expressed with the following relationships:

$$N = \frac{N_s}{N_{comb}} \qquad 4.1$$

$$A_{comb} = NA_s \qquad 4.2$$

$$I_{comb} = NI_s \qquad 4.3$$

$$J_{comb} = NJ_s \qquad 4.4$$

N = Ratio of the number of original stiffeners vs. combined stiffeners

A = Cross sectional area

I = Moment of Inertia

J = Polar moment of Inertia

Subscript ‘s’ and ‘comb’ refers to the stiffeners and the combined stiffeners.

Che (2000) adopts this procedure in the assessment of ship structural details employing simplifying techniques. Zhang (2003) et al compared the combined stiffness method with an equivalent orthotropic method in the modelling of a stiffened structure subjected to underwater explosion. In the equivalent orthotropic method, the density and stiffness of the secondary stiffeners are smeared and combined with the joining plate. The results showed that the combined stiffener method provided better correlation with the actual discretised model.

The global model is represented by one element between the combined stiffeners and 4 elements between frames. The shell elements are modelled using 4-node quadrilateral stress/displacement elements with large strain formation and reduced integration. This is denoted S4R in ABAQUS and is suited for a wide range of applications. The beam elements are represented using 3-node quadratic beams.

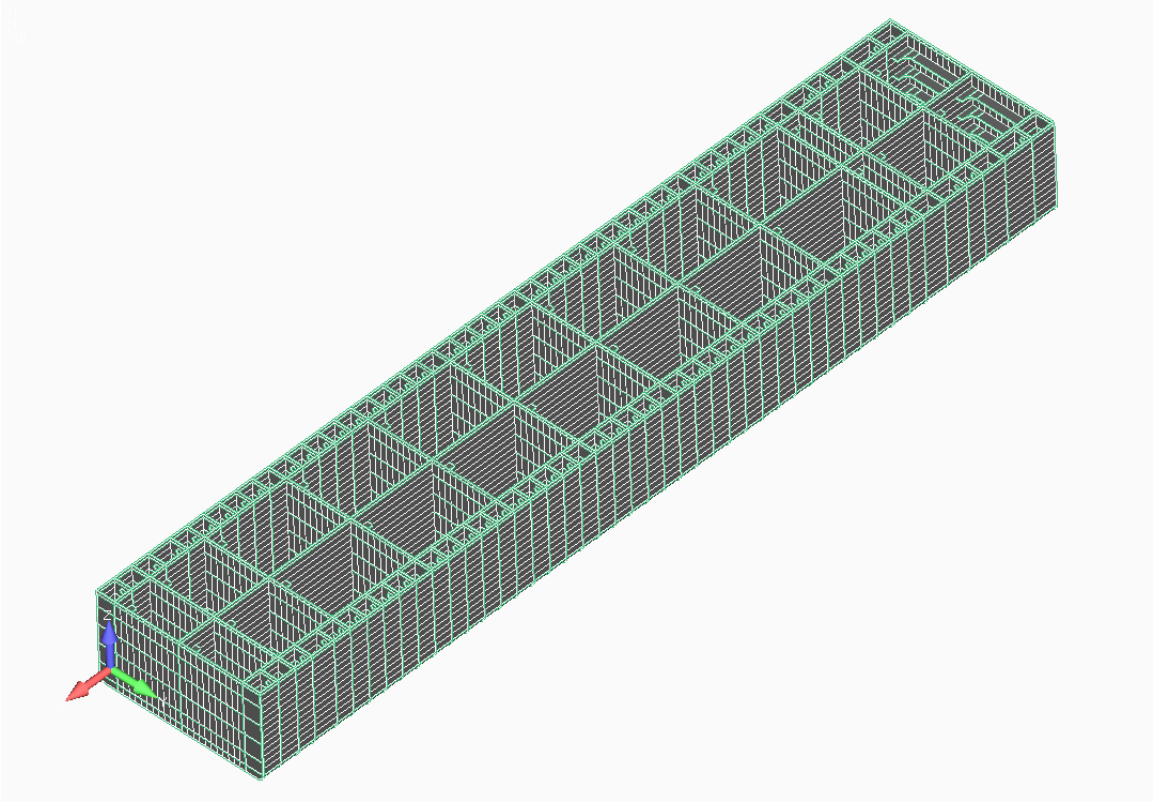

Figure 3.1: Global structural model

3.2.2 Local Structural Models

To obtain an accurate description of the stress-strain distribution in the highly stressed areas identified from the global model, local models are developed. The local models are usually referred to as sub-models. Stresses in these models are derived by transfer of boundary deformations or boundary forces from the coarse global model. Such transfer of data between models requires that the various mesh models be compatible i.e. meshes in the coarse model produce deformations and/or forces applicable as boundary conditions for the finer mesh models. Two intermediate models and two fine mesh models are used to obtain a reasonable stress distribution.

- The first intermediate model illustrated in Figure 3.2 is located at frame 51 in the global FE model (see Figure 2.1) and includes the transverse bulkhead, side shell plating, bottom shell plating and the deck.
- The second intermediate model is taken from frame 53 to 54 in the longitudinal direction of the global FE model (see Figure 2.1). This includes oil tight transverse bulkhead, vertical stiffeners and girders. This is shown in Figure 3.3.
- There are two sub-models. The first detail consists of the welded connections between the side shell and the inner side shell longitudinal stiffener connection to water tight bulkheads and typical web frames. The second sub-model is located at the bottom shell and consists of the bottom shell stiffener connection to the transverse web frame (Figure 3.4 and Figure 3.5). The fine mesh is generated using 2nd order beam and shell elements. In all the details, the welds are not modelled.

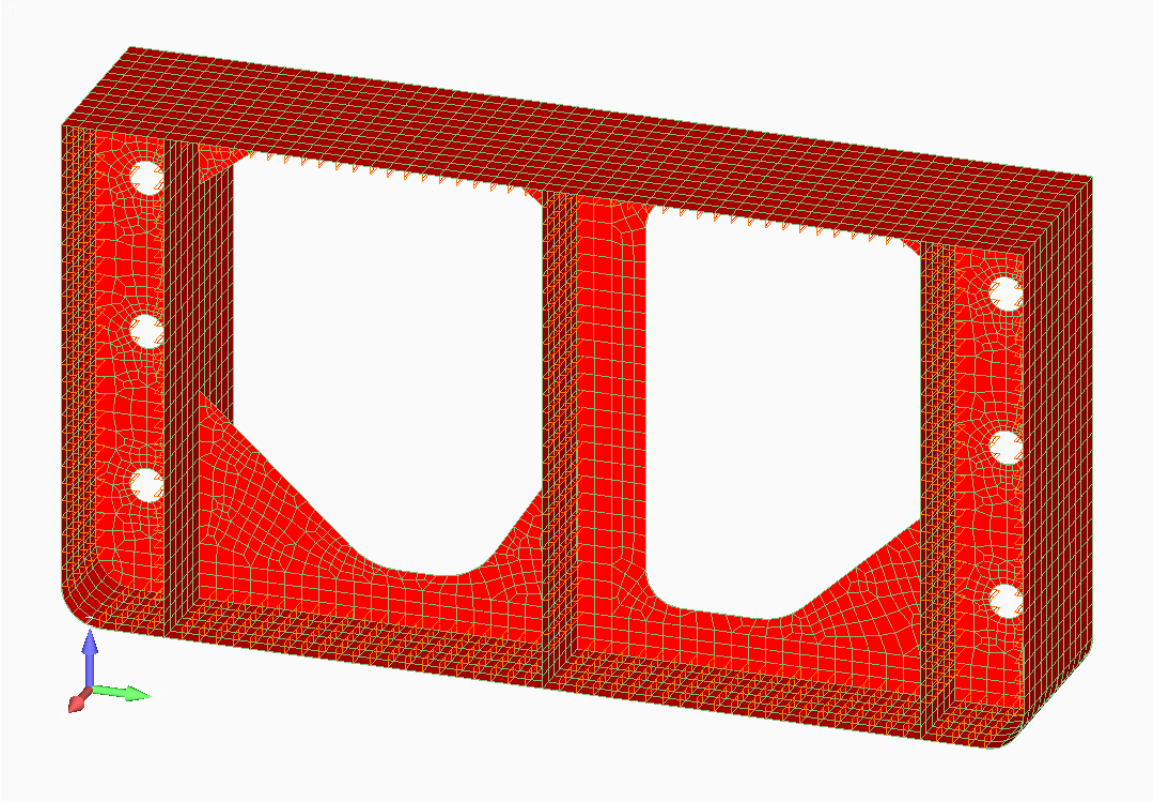

Figure 3.2: Intermediate model: Cargo Oil Tank

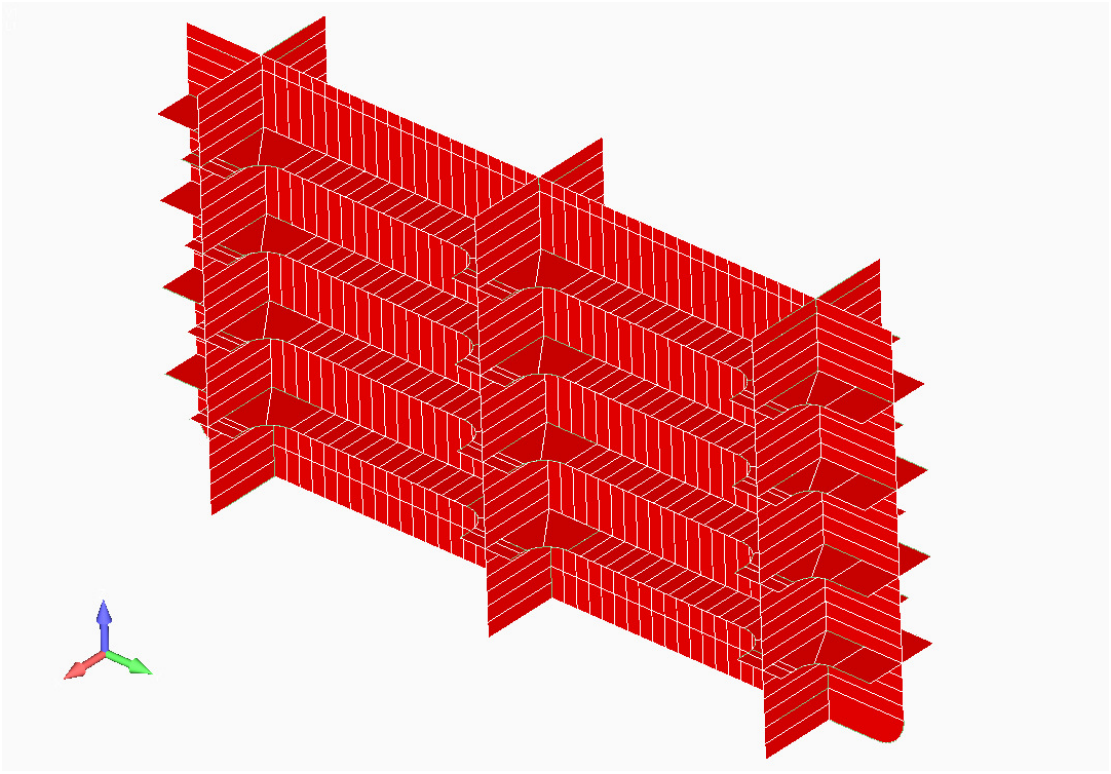

Figure 3.3: Intermediate model: Transverse bulkhead

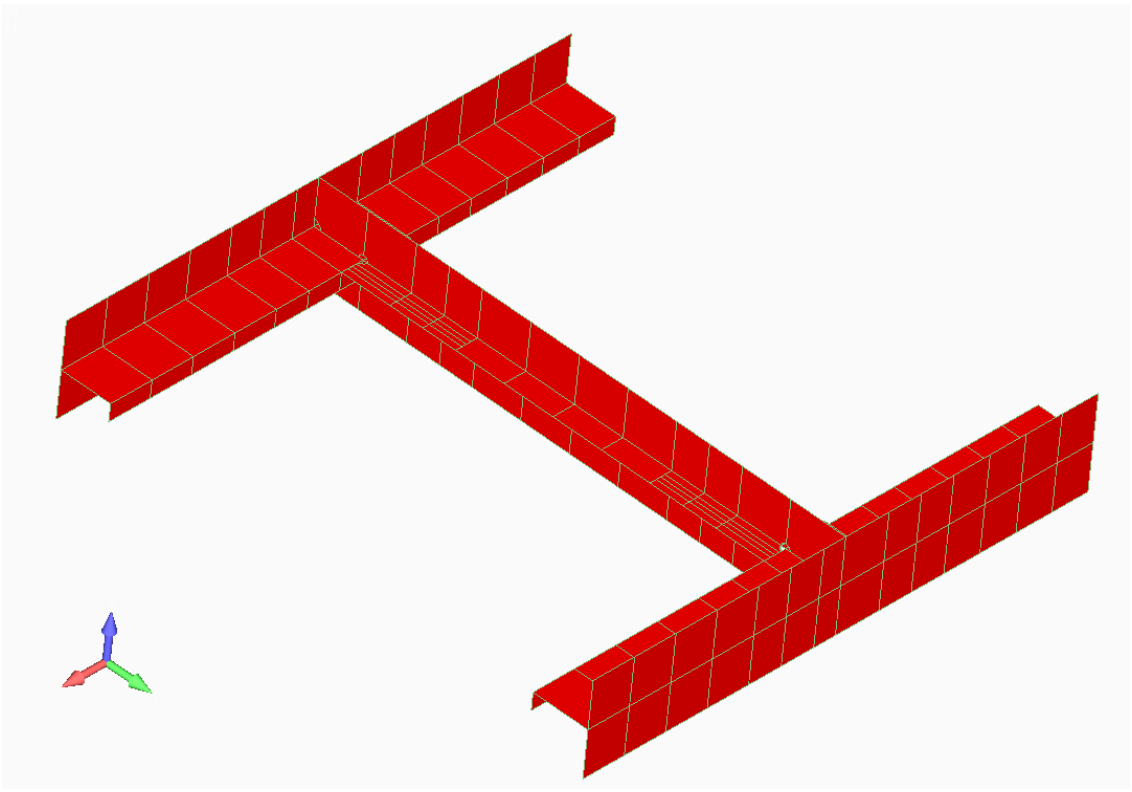

Figure 3.4: Local model: Side-inner side plating stiffener connection

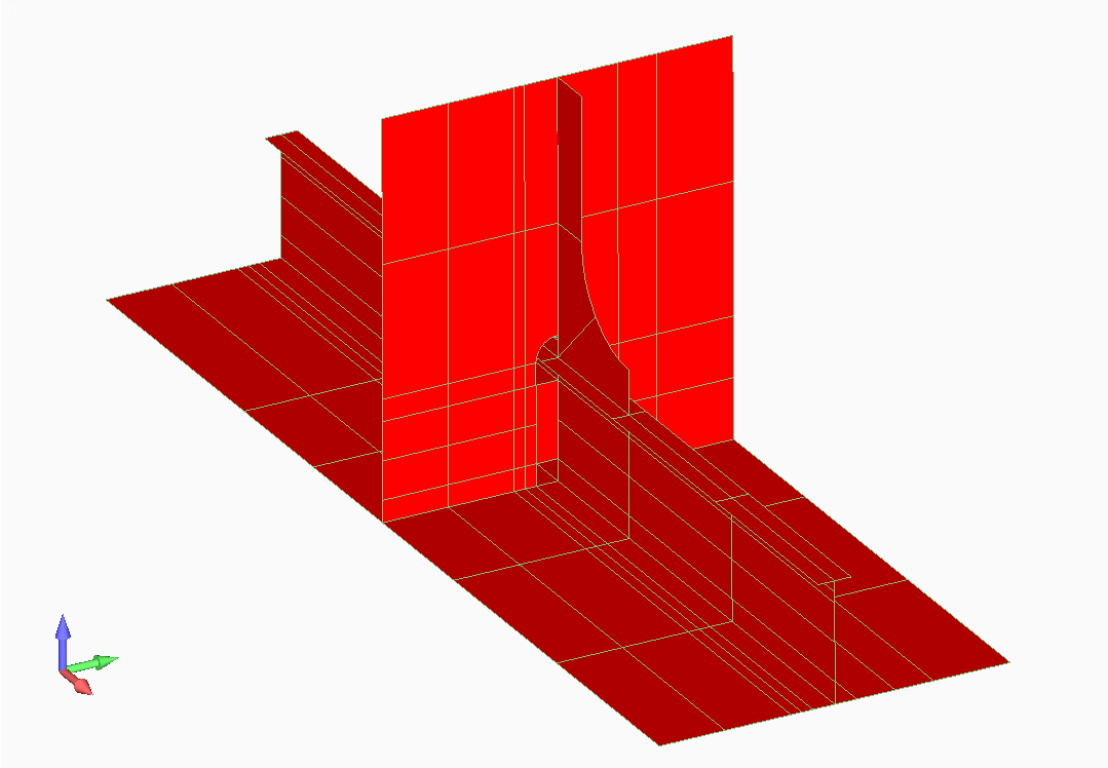

Figure 3.5: Local model: Bottom plating with longitudinal stiffener

3.3 Local Modelling Techniques

In the FE analysis of complex and large structures, the global FE mesh is usually too coarse to produce satisfactory results in the region of interest, such as a stress concentration area. The results away from this region, however, may be adequate. To obtain more accurate results in such a region, one can either re-analyze the entire model with greater mesh refinement, or generate an independent, more finely meshed model of only the region of interest and analyze it.

In ship-shaped structures it is necessary to determine the global response of a vessel under different loading conditions and transfer these global outputs to a local model to determine the response in critical areas. For example, the actual stresses at notches at the intersection of a stiffener and a web attached to the bottom shell plating of an FPSO can only be obtained through accurate representation of the geometry, yet the response is dependent on global and local load effects. A typical FPSO may be

hundreds of meters long but detailed stresses are required in local areas with element sizes typically down to 10 mm. There are several local modelling techniques available and the most common methods are: using stress concentration factors, submodeling, sub-structuring and a direct mesh refinement of the global model. These methods are illustrated in Figure 4.6.

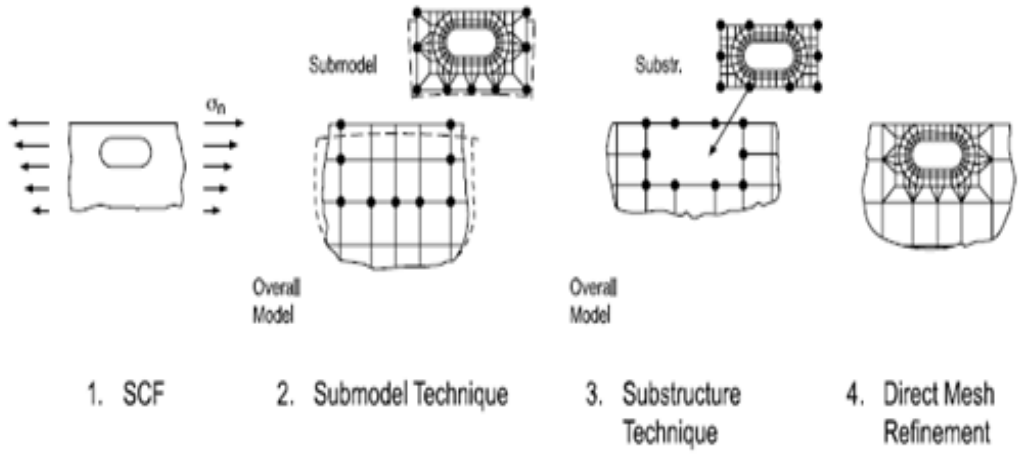

Figure 3.6: Methods for local strength analysis (Von Selle, 2009)

3.3.1 Stress Concentration Factors (SCF)

The use of stress concentration factors is one of the oldest methods for determining stresses at a notch. SCF's can be obtained either analytically or experimentally. They are generally published in charts and are widely available in various textbooks and handbooks (Peterson, 1974) and (Young, 2007). It is a very fast and effective method but works only if SCF data is available and if the nominal stress state of the structure can be correctly determined.

3.3.2 Submodeling

Submodeling is a finite element technique that can be used to obtain more accurate results in a particular region of a model. A finite element mesh may be too coarse to produce satisfactory results in a given region of interest. The results away from this region, however, may be satisfactory. Reanalyzing the entire model using a greater mesh refinement in order to obtain more accurate results in one particular region is time-consuming and costly (ANSYS, 2006). Instead, submodeling can be used to

generate an independent, more finely meshed model of only the region of interest and then analyze it. It is most useful when it is necessary to obtain an accurate, detailed solution in a local region and the detailed modelling of that local region has negligible effect on the overall solution. Submodeling is also known as cut-boundary displacement method or specified boundary displacement method. This approach involves solving a coarse global model and identifying the areas of interest. Then a suitable local model is cut out containing the area of interest (See Figure 3.7a and 3.7b). The cut out plane of the local model is critical to the accuracy of this method. The plane should be selected a locations where the stress level is approaching zero or where there is a constant stress distribution. The local model is meshed finely and solved with solutions from the global model driving the boundaries.

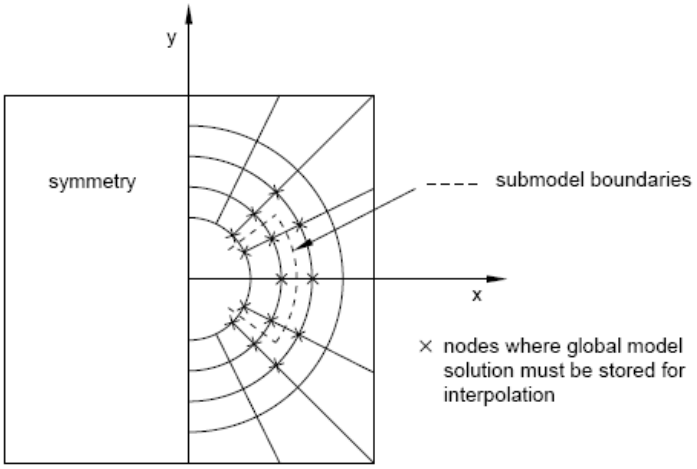

Figure 3.7a: Global structural model (ABAQUS, 2006)

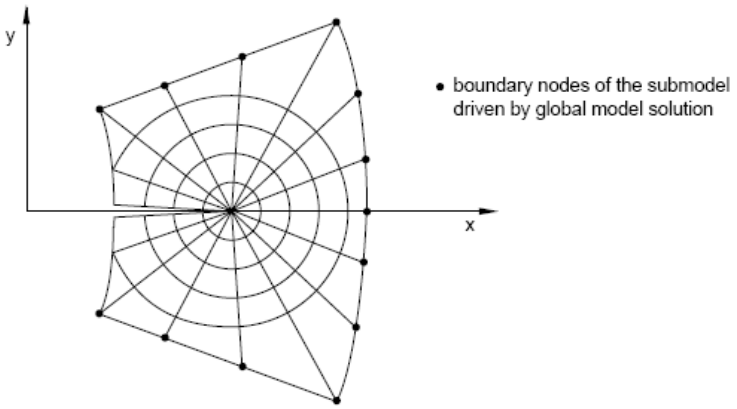

Figure 3.7b: Magnified sub model from Figure 3.7a

A submodeling analysis is carried out using the following process:

- Running a global analysis and saving the results in the vicinity of the submodel boundary;
- Defining the total set of driven nodes in the submodel;
- Defining the time variation of the driven variables in the submodel analysis by specifying the actual nodes and degrees of freedom to be driven
- Running the submodel analysis using the "driven variables" to drive the solution

The submodel is completely independent of the global analysis. The only link between the submodel and the global model is the transfer of the time-dependent values of variables saved in the global analysis to the relevant boundary nodes of the submodel. Since the submodel is a separate analysis, submodeling can be used to any number of levels; a submodel can be used as the global model for a subsequent submodel. The actual driven variables are defined as a submodel boundary condition. The boundary conditions are "driven variables" obtained from the results of the global analysis. The degrees of freedom on the driven nodes of the submodel must exist at the forcing nodes of the global model.

The global model in a submodeling analysis must define the submodel boundary response with sufficient accuracy. In general, the solution at the boundary of the submodel must not be altered significantly by the different local modelling. It is important is to verify that the cut boundaries of the submodel are far enough away from the concentration. The accuracy can be checked by comparing contour plots of important variables near the boundaries of the submodeled region. Using this technique saves solution-time on large finite element models. It reduces, or even eliminates, the need for complicated transition regions in solid finite element models. It also promotes experimentation with different designs for the region of interest.

There are several ways of applying the submodeling technique. The most popular is the specified boundary condition in which state variables are transferred from a global solution to determine the boundary response of the sub-model for representing the

effect of the rest of the structure (Geiro at al, 1998). The specified boundary condition is classified into: the stress boundary or internal force method and the displacement boundary or enforced displacement method. The internal force method involves applying cut boundary forces at all the cut boundaries of the sub-model, constraining the model such that it is statically determinate. In the displacement boundary method, all cut boundary displacements are applied to the cut boundaries. In most cases, no further constraints are required. The latter is often used in practice and is key in the study of Cormier et al (1999) and Srinivasan et al (1999). The displacement boundary method is preferred because it is easier to implement and in some cases, displacements are generally more accurate than stresses in FE solutions (Beishem and Sinclair, 2002).

Geiro et al (1998) applied the submodeling technique to identify critical response areas in a bulk carrier and quantify stress ranges for fatigue life estimation. Kitamura et al (2002) compared the boundary displacement method to a modified stress displacement method in their research. Classification societies (26-31) also suggest the submodeling technique as a preferred method for analysing local details.

3.3.3 Substructuring

Substructuring was invented by aerospace engineers in the early 1960s to carry out a first-level breakdown of complex systems such as a complete airplane (Unknown, 2009). The concept was then picked up and developed extensively by the offshore and shipbuilding industries. Substructures are collections of elements from which the internal degrees of freedom have been eliminated. Retained nodes and degrees of freedom are those that will be recognized externally at the usage level (when the substructure is used in an analysis), and they are defined during generation of the substructure. Substructuring reduces computer time and allows solution of very large problems with limited computer resources. In a structure with repeated patterns (such as the four legs of a table), you can generate one substructure to represent the pattern and simply make copies of it at different locations, thereby saving a significant amount of computer time.

Sub-structuring allows a large FE model to be analysed as a collection of components (substructures). A finite element model of each substructure is created and solved for the degree of freedom nodes shared with other substructures in terms of internal degree of freedom. The global model is then assembled with only the shared nodes and solved. Finally, the solutions of the shared degrees of freedom are used to solve for the internal degree of freedom. Each substructure is a super element for the global model. This approach is useful when there is not sufficient computer power to handle large models. It is also useful in design companies where different departments may be working on different parts of the structure

In ANSYS, substructuring involves 3 main steps called 'passes': the generation pass, the use pass and the expansion pass. In the generation pass, a group or finite elements are condensed into a single substructure. This is done by identifying a set of master degrees of freedom, used mainly to define the interface between the substructure and other elements. In the use pass, the substructure is made part of the model. The entire model may be a substructure or the substructure may be connected to other normal finite elements. The solution from the use pass consists only of the reduced solution for the substructure (that is, the degree of freedom solution only at the master DOF) and complete solution for the other normal finite elements. In the expansion pass the results at all degrees of freedom in the substructure is calculated. If multiple substructures are used in the use pass, a separate expansion pass will be required for each substructure. The displacement boundary conditions are automatically applied internally at the master degrees of freedom during the expansion pass solution and are not deleted when the solution completes.

3.3.4 Direct Mesh Refinement

A global model may be refined locally to obtain local stresses. For FPSOs where there are a lot of local details, this can result in a very large finite element system and corresponding computer time. If the mesh transition between the locally refined areas and the rest of the global model is not properly modelled, errors in calculation may occur. An extension of this method is the adaptive meshing process which automatically remeshes a surface during analysis to improve its integrity. There are two levels of refinement: The H-refinement changes the size and shape of the element

while the P-refinement changes the order of the element shape function. This concept and fundamentals of this method is dealt with extensively in (Plewa et al, 2003) and sample applications discussed in (Berger and Colella, 1989).

In the earlier stages of this study, the direct mesh refinement method was employed. It was observed that because of the extent of the model, a smooth transition from the fine mesh of the local detail to the global model is very difficult to achieve. The only way of obtaining a moderately accurate mesh is by reducing the mesh size of the global model. This makes the finite element model very large and may introduce some instability in the model.

3.3.5 Summary of Techniques

Local modelling techniques are available in most commercial finite element codes e.g. ABAQUS, ANSYS and NASTRAN. The limitations of all the methods were studied extensively by Makinen (2005). He noted that the sub-structuring technique required node to node correspondence and a previous knowledge of how the structure is likely to behave. It also requires a recalculation of the global model. The submodeling technique provides modelling flexibility and the critical location need not be known in advance. Several local models can be studied using the same global model and it is not necessary to recalculate the global model. It also allows the generation of the global model as well as defining the local details in parallel.

The direct mesh refinement and the submodeling technique were applied to a simple plate with a central hole. Due to symmetry, only a quarter sector of the plate is modelled, see Figure 3.8. The section was analysed with a coarse mesh which represented the global model, then a submodel was cut around the area of the hole. A mesh refinement of the area around the hole was done to check the mesh refinement technique. The stress contours are shown in Figure 3.9 and Table 3.1 shows the stresses as compared with simple theoretical formulations for the plate. The submodel technique seems to have performed better.

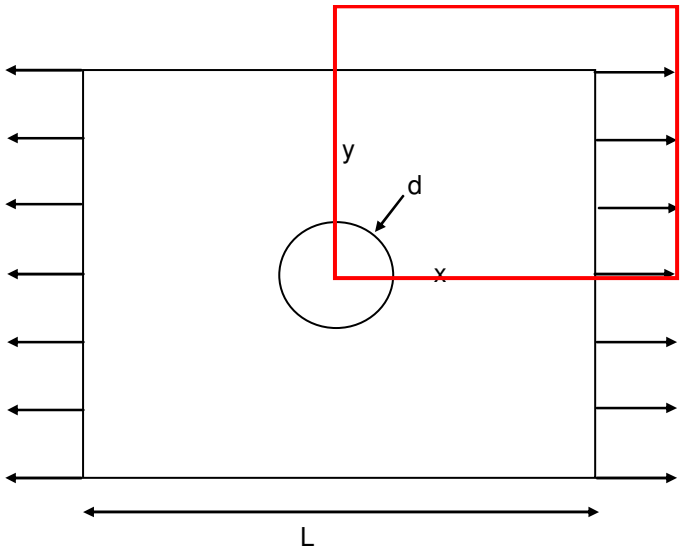

Figure 3.8: Plate with a central hole

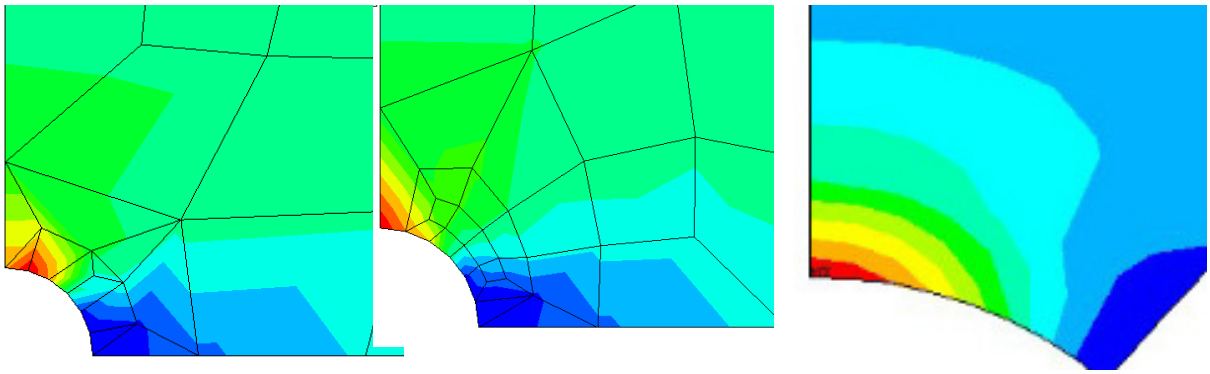

(a) Global model (b) Mesh refinement c) Submodel

Figure 3.9a, b and c: Stress contours for the local modelling methods

Table 3.1: Comparison of local modelling results

Results Comparison (Stress in the x direction)			
	Target	FE Analysis	Ratio
Coarse Model	2613	1550.46	0.6
Mesh Refined Model	2613	1993.41	0.76
Submodel	2613	2010.2	0.96

The submodeling technique is further tested for loading condition 2 (Table 2.4). The location and extent of the intermediate model and the sub-model is illustrated in Figure 3.10. At an appropriate distance from the "hot-spot" of interest a "cut" is performed in the coarse model. The nodal displacements of the coarse model are the automatically transferred to the sub-model as boundary conditions. The method is verified by mapping the range of displacements results obtained from the local model onto the global model.

Figure 3.11 shows the displacement contours plot of the intermediate model. The result from the global model in Figure 3.12 is used to drive the boundaries of the intermediate model. The range of the displacement values from the intermediate model is mapped onto the global model and it is immediately clear that the submodeling technique provides reasonably accurate boundary results. The intermediate model is used to drive the local bottom longitudinal connection as shown in Figure 3.13 and Figure 3.14. The submodeling technique works in this case also.

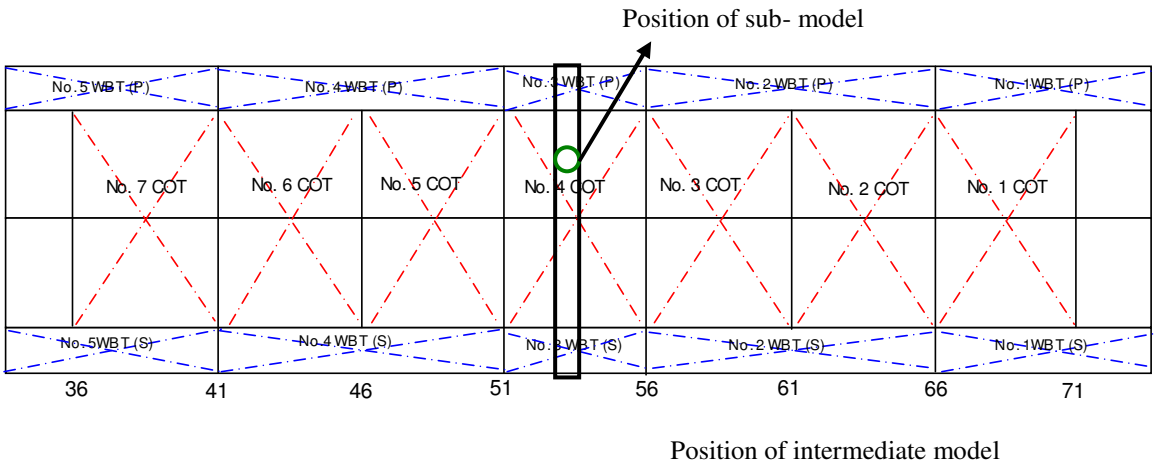

Figure 3.10: Location of local models with respect to global model

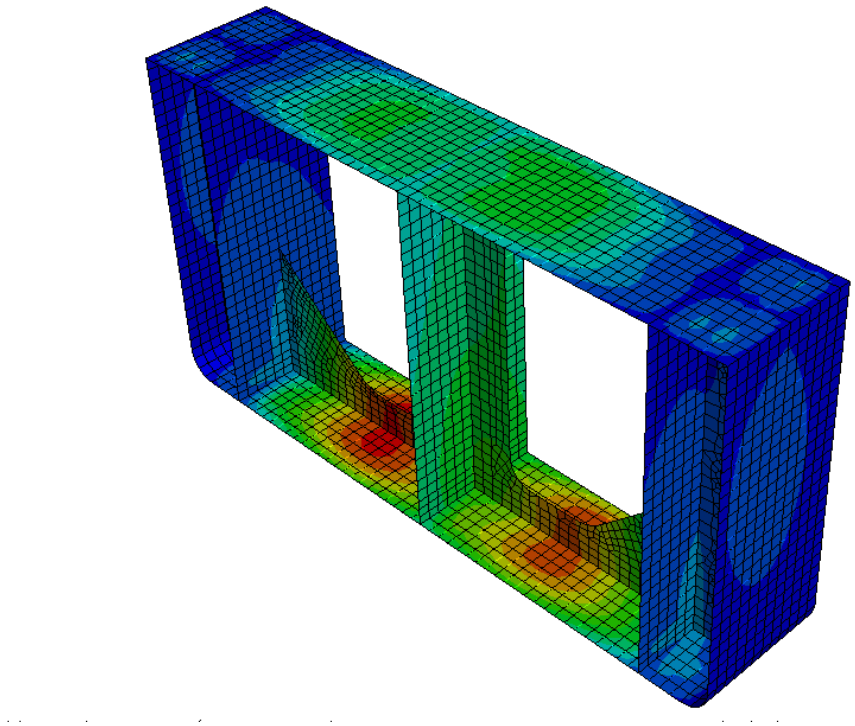

Figure 3.11: Displacement contour plot for intermediate model

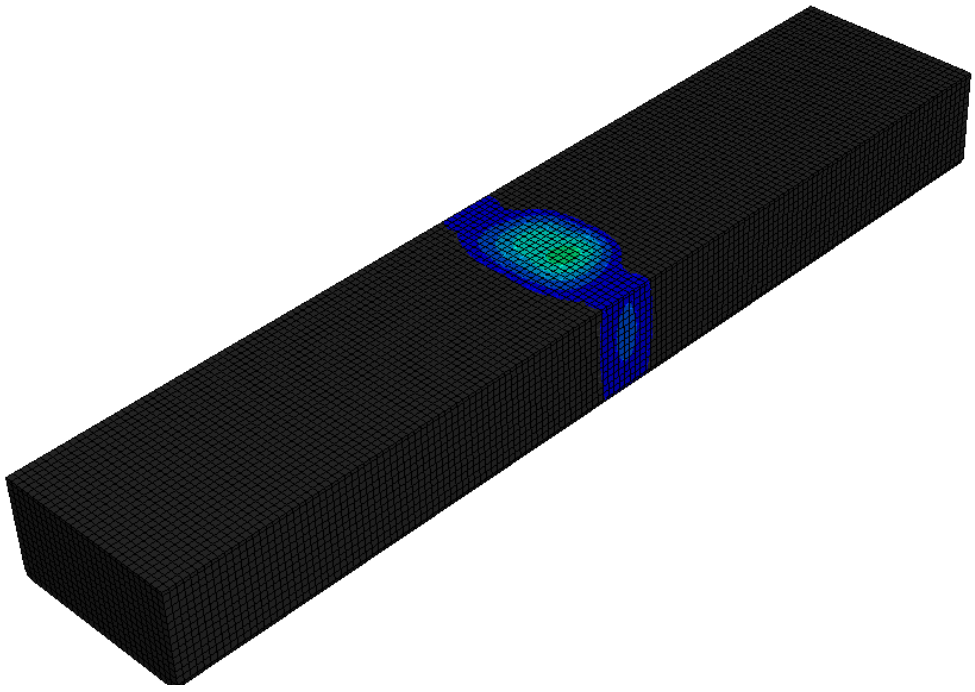

Figure 3.12: Displacement from intermediate model mapped on global model

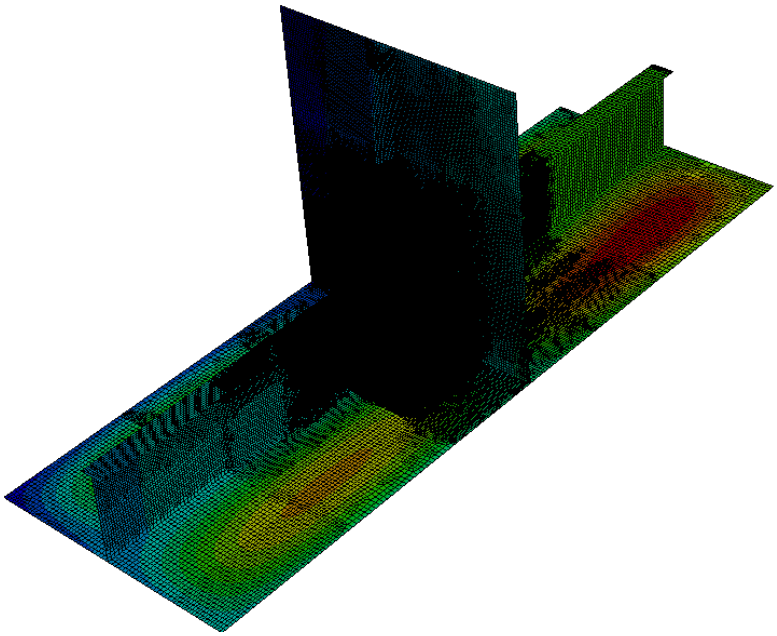

Figure 3.13: Displacement contour plot for local model

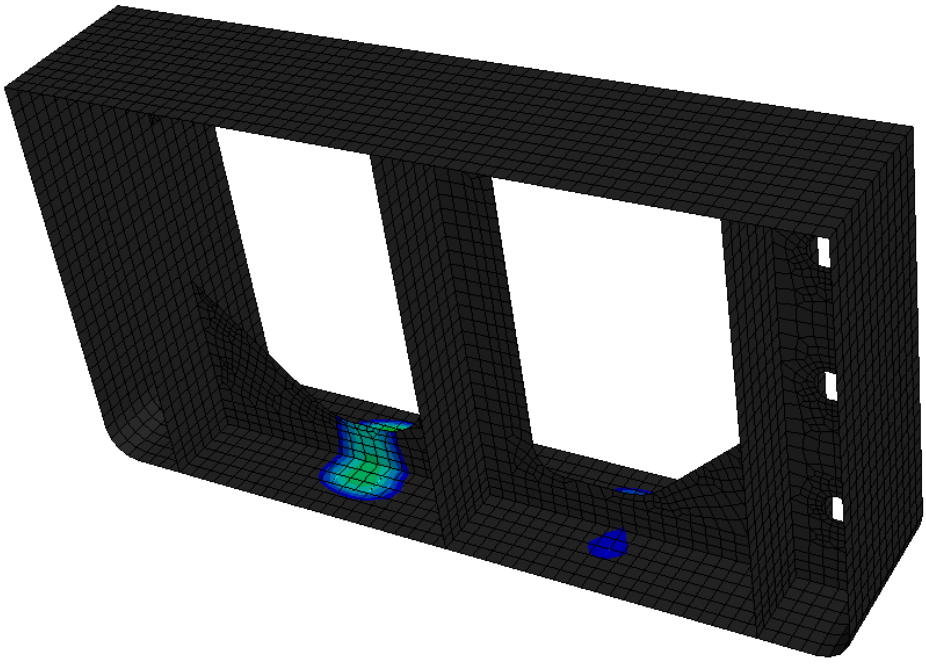

Figure 3.14: Displacement from local model mapped on intermediate model

3.4 Conclusion

This chapter has provided a summary of local modelling techniques available in finite element method. Stress concentration factors, direct refinement, substructure method and submodeling method are the most common local modelling techniques. Stress concentration factors are convenient to use but for complicated structures like an FPSO, the nominal stress state is difficult to obtain. A direct refinement of the global model was unacceptable because of the sheer scale of the global model. The FPSO of interest is over 200 meters and local areas can be as small as 0.1 x 0.1 m. Sub structuring method requires a recalculation of the global model, doubling the analysis time when compare with the sub-modelling method. The submodeling method has been tested and the results show that it is adequate for the accurate determination of stresses in the local details of interest. Hence, the submodeling technique with displacement boundary solution is tested for a selected load case. The submodeling technique will be used in the rest of the thesis to determine the local stresses at the areas of interest.

REFERENCES

1. Niemi E. (1993) 'Stress Determination for Fatigue analysis of Welded Components' IIW doc.XIII-1221-93.
2. Niemi E. (2000) 'Recommendations of Modelling, Stress Evaluation and Design' IIW Document XIII WG3-06-00
3. Fricke W. (2001) 'Recommended Hot-Spot Analysis Procedure for Structural Details of FPSOs and Ships Based on Round-Robin FE Analysis'. ISOPE Proceedings, Stavanger, Norway,
4. Healy B.E. (2004) 'A Case Study Comparison of Surface Extrapolation and Battelle Structural Stress Methodologies' Proceedings of the 23rd International conference on Offshore Mechanics and Arctic Engineering.
5. Poutiainen L., Niemi E., (2000). 'The determination of Hot Spot Stress in Gusset Structures using a Coarse Element Mesh'. IIW doc. XIII-1820-00.
6. Yamada K., Xiao Z., (2004) 'A New Method of Evaluating Fatigue Strength of Welded Toe Failures'. IIW doc. XIII-2022-04.
7. Dong P., Kyuba H. (1993). 'Equilibrium-Equivalent Structural Stress Approach to Fatigue Analysis of a Tubular Joint'. IIW doc. XIII-1993-03.
8. Poutiainen I., Marquis G. (2004). 'A Single-Point Structural Stress Assessment Procedure for Load-carrying Fillet Welds'. IIW doc. XIII-2012-04- Fatigue Assessment of Complex Welded Steel Structures 19
9. Nihei K. et al. (1993) 'Study on Unified Fatigue Strength Estimation Method for Fillet Welded Plate Structures (1st Report) Simplified Calculating Method of Hot Spot Stress'. Journal of Kansai Society of Naval Architects Japan.
10. Petershagen H. (1991). 'A Comparison of Two Different Approaches to the Fatigue Strength Assessment of Cruciform Joints'. IIW doc. XIII-1410-91.
11. Niemi E. (1995), Introduction of Structural Stress Approach to fatigue Analysis of Plate Structures'.
12. Von Selle H., Doerk O., and Scharrer M. (2009). 'Global Strength Analysis of Ships with Special Focus on Fatigue of Hatch Corners'. Analysis and Design of Marine Structures, Taylor and Francis Group.

13. Zhang Z.J., Ho C.C. and Chan Y.W. (2003) 'FE Modelling of a Stiffened Structure subjected to Underwater Explosion'. DSO National Laboratories, Singapore.
14. Che X., Lee F.K., and Libby D.H. (2000) 'Simplified Stress Analysis of Ship Structures'. American Bureau of Shipping New York.
15. Peterson R.E (1974). Peterson's Stress Concentration Factors'. John Wiley and Sons.
16. Young W.C. and Budynas R.G (2007). 'Roark's Formulas for Stress and Strain'. McGraw-Hill.
17. Adaptive Mesh Refinement – Theory and Applications. Proceedings of the Chicago Workshop on Adaptive Mesh Refinement Methods, 2003. Springer link.
18. Berger M.J. and Colella P. (1989). 'Local Adaptive Mesh Refinement for Shock hydrodynamics'. Journal of Computational Physics, Volume 82.
19. Unknown (2009)' Super elements and Global-Local Analysis'
20. ANSYS Personnel (2007). 'ANSYS User's Manual, Revision 11.0, Vol. 1'. ANSYS Inc: Canonsburg, Pennsylvania, 1995.
21. Geiro A., Grundy P., Cannon S. and Nguyen V. (1998). 'Advanced Finite Element Techniques for Hull Structural Analysis'. 8th ISOPE Proceedings Canada.
22. Cormier N.G., Smallwood B.S., Sinclair G.B. and Meda G. (1999). 'Aggressive Submodeling of Stress Concentrations'. International Journal for Numerical Methods in Engineering, Volume 46.
23. Srinivasan S., Biggers Jr. S.B., Latour Jr. R.A., (1999). 'Identifying Global/Local Interface Boundaries using an Objective Search Method'. International Journal for Numerical Methods in Engineering, Volume 39.
24. Beishem J.R and Sinclair G.B. (2002). 'Three-dimensional Submodeling of Stress Concentrations'. ANSYS Proceedings.
25. Kitamura M., Ohtsubo H., Akiyama A. and Bandho H. (2002). 'Submodeling Analysis of Ship Structure with Super convergent Patch Recovery Method'. 12th ISOPE Proceedings Japan.
26. DNV-RP-C203. (2005). 'Fatigue Design of Offshore Steel Structures'. Recommended Practice. Det Norske Veritas. Norway.

27. DNV-RP-C206. (2006). 'Fatigue Methodology of Offshore Ships'. Recommended Practice. Det Norske Veritas. Norway.
28. DNV (2006). 'Classification Notes No 30.7: Fatigue Assessment of Ship Structures'. Guidance Notes. Det Norske Veritas. Norway.
29. Lloyds Register (2008). 'Ship Right FOI - Design, Construction and Installation- Floating Offshore Installation of Structures Design Guidance'. Lloyds Register EMEA.
30. Lloyds Register (2004). 'Ship Right Fatigue Design Assessment: Level 3 Procedure'. Guidance on Direct Calculation. Lloyds Register EMEA.
31. ABS (2003). 'Guide for the fatigue Assessment of Offshore Structures'. American Bureau of Shipping. USA
32. Makinen H (2005) 'Global and Local FE Models in the Fatigue Analysis of Ships'. Masters Thesis, VTT Technical Research Centre of Finland.

CHAPTER 4 HOT SPOT STRESS APPROACH

4.1 Introduction

The hotspot stress (HSS) method was first proposed 30 years ago by the combined effort of classification societies, offshore operators and research institutes for the fatigue assessment and design of tubular joints (Urm et al, 2004). The basis and development of the HSS approach to the fatigue assessment of welded joints has been researched extensively by Almar-Naes (1999), Fricke (2003), Marshall (2005), Huther and Lieurade (1997) and Niemi (1995) to name a few. The hotspot stress method is generally applied to welded joints when there is clearly no defined nominal stress due to complicated geometric effects and also where structural discontinuity is not comparable to any classified structural detail.

Recent developments and increasing demand has seen the HSS approach being extended to non tubular sections like plated components found in ship structures. The European Standard (Eurocode 3, 1993) for the design of steel structures was the first general design rule to include HSS approach for plated structures. The International Institute of Welding (Hobbacher, ed. 2005) developed guidelines for HSS determination and published a designer's guide in 2001. Subsequently fatigue design rules based on this method was published by several classification societies -BV, DNV and API.

HSS is determined by finite element analysis or test measurements. The nonlinearity during calculation is eliminated by extrapolation of the stresses at the surface to the weld toe or by linearization of the stress through the plate thickness. The HSS approach in plated structures is often criticised mainly because of the challenges in defining appropriate reference point for stress extrapolation. As stated earlier, offshore codes have published HSS procedures and these procedures all differ from one another. Uncertainties about the suitability of the HSS approach have been raised because of the large scatter and difference between analysis result and measured stress and also the choice of appropriate S-N curves (Wang et al 2006). Despite all the uncertainties associated with it, the HSS approach is still an active area of research

because it is considered a practical method and offers a better alternative to fatigue assessment of complex ship details than the nominal stress approach.

4.2 State of the Art

There is a tremendous amount of literature available on the hotspot stress approach and it is impossible to review them all. This section will aim at reviewing landmark papers that deal with the application of hotspot stress method in ship structural details particularly those commonly found in FPSOs.

The International Institute of Welding (IIW) created an active working group for the development of guidelines for the determination of hot spot stresses. This resulted in the publication of a comprehensive guidance on the HSS approach. The guidelines include procedures for FE mesh techniques, element property selection and extrapolation procedure. The IIW identified two types of hotspots based on the location of crack on the plate and on the orientation of the crack with respect to the weld toe. This is shown in Figure 4.1. In type (a) the hot spot stress is transverse to the weld toe on the plate surface and in type (b) the hot spot stress is transverse to the weld toe at plate edge. Stress extrapolation points and element mesh sizes are recommended based on this description.

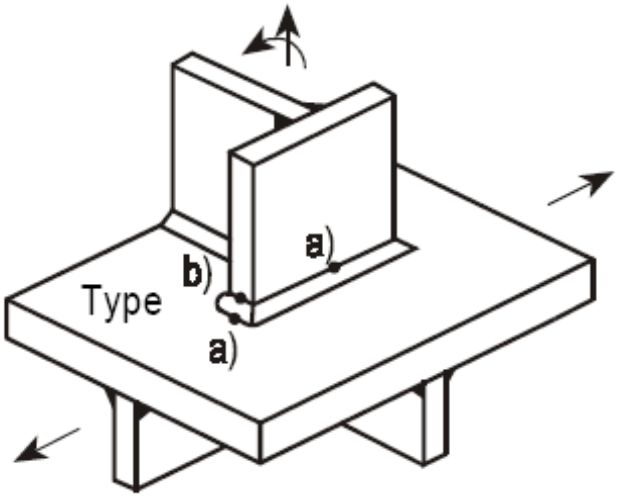

Figure 4.1: Types of hotspots (IIW)

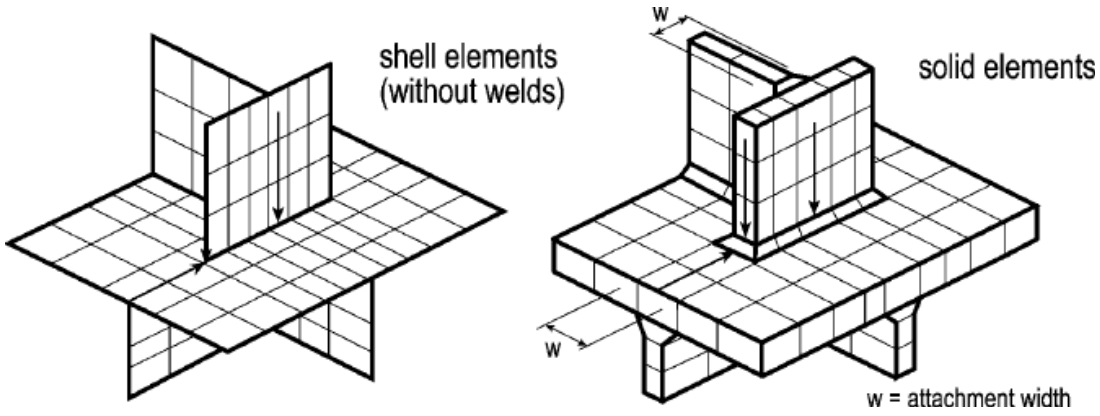

Figure 4.2: Shell and solid element modelling

In general, hotspot stresses cannot be obtained through analytical methods and parametric formulae are rarely available. As such the finite element method is almost always preferred. The finite element modelling technique for HSS can be divided into two groups: using plate or shell elements without weld representation (in some cases the weld may be included in a simplified way) and using solid models as illustrated in Figure 4.2. The hot spot stress components are evaluated at the plate surface or edge by extrapolation techniques. The surface extrapolation method is the most popular extrapolation procedure and has been adopted by many class societies and regulatory bodies. It relies on the predicted sampling of stress at a discrete distance away from the weld toe and the extrapolation of that stress to the weld toe. The extrapolation points are chosen far enough from the weld so that the surface values represent the structural stresses at those locations.

There are several recommendations on stress evaluation and extrapolation procedure for hot spot stress and several parametric formulas for determining HSS concentration factors. Radaj (1990) showed that for plated or shell structures the hot-spot stress is the sum of the membrane and bending stresses which can be determined by linearization of the stress through the plate thickness or by extrapolation of the stress at the surface of the weld toe.

Niemi (1995, 2001) published a background document presenting the HSS approach for plate-type welded structures with detailed FE methods for its determination. Maddox (2001) employed the IIW recommendations for stress extrapolation to

validate related design S-N curves. The IIW recommendations for calculating the hotspot stress is obtained from stresses from FEA or the strains from strain gauges located at specified distances from the weld toe. The stress or the strains are then extrapolated to the weld toe using a two or three point formula, see Table 4.1.

Table 4.1: IIW Recommended Meshing and Extrapolation Procedure

Type of model and weld toe		Relatively Coarse Model		Relatively Fine model	
		Type a	Type b	Type a	Type b
Element Size	Shells	t x t	10 x 10 mm	0.4 t x t	≤4 x 4 mm
	Solids	t x t	10 x 10 mm	0.4 t x t	≤4 x 4 mm
Extrapolation points	Shell	0.5t and 1.5t, Mid-side nodes	5 & 15 mm Mid-side nodes	0.4t and 1.0t, Nodal points	4, 8, 12 mm Nodal points
	Solid	0.5t and 1.5t, Surface Centre	5 & 15 mm Surface Centre	0.4t and 1.0t, Nodal points	4, 8, 12 mm Nodal points

In 2001, several papers on fatigue assessment of FPSO details were presented at the International Society of Offshore and Polar Engineers (ISOPE) conference. Fricke (2001) spearheaded a joint industry project to investigate finite element modelling and analysis of typical structural details in FPSOs with the aim of developing recommendations on appropriate hotspot stress method and S-N data for fatigue design. Five details were studied for which stress measurements and fatigue tests results already existed in open literature. Among the selected details is the connection of a buckling stiffener to a flange of a T-shaped longitudinal, see Figure 4.3. This detail is common in FPSO and tanker structures and had previously been experimentally tested by a Japanese research project. Three extrapolation procedures are investigated. Linear extrapolation over reference points 0.5 and 1.5 x plate thickness t away from the hotspot, linear extrapolation over reference points 0.4 and 1.0 x plate thickness t away from the hot spot and no extrapolation, but considering the stress value at 0.5 x plate thickness t as the relevant hot spot stress. Different element types are also investigated. Fricke compared the hotspot stress and estimated

fatigue lives against the design curves published by IIW. It was concluded that solid elements overestimate hotspot stress while the shell elements underestimate the hotspot stress, see Figure 4.4. He also noted that the IIW hotspot stress design S-N curves is acceptable for fatigue strength prediction when the linear extrapolation method is employed but when the stress is read out from a single point (0.5t or 5 mm from the weld toe), the selected design curve should be reduced by one class.

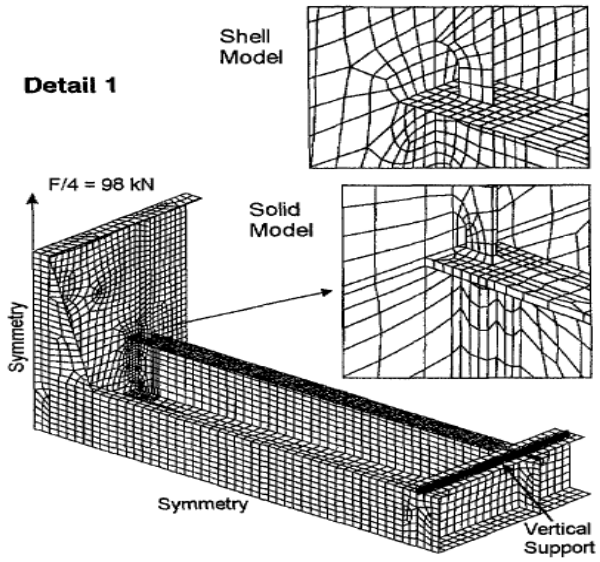

Figure 4.3: Finite element mesh of buckling stiffener to flange of T-shaped longitudinal (Fricke, 2001)

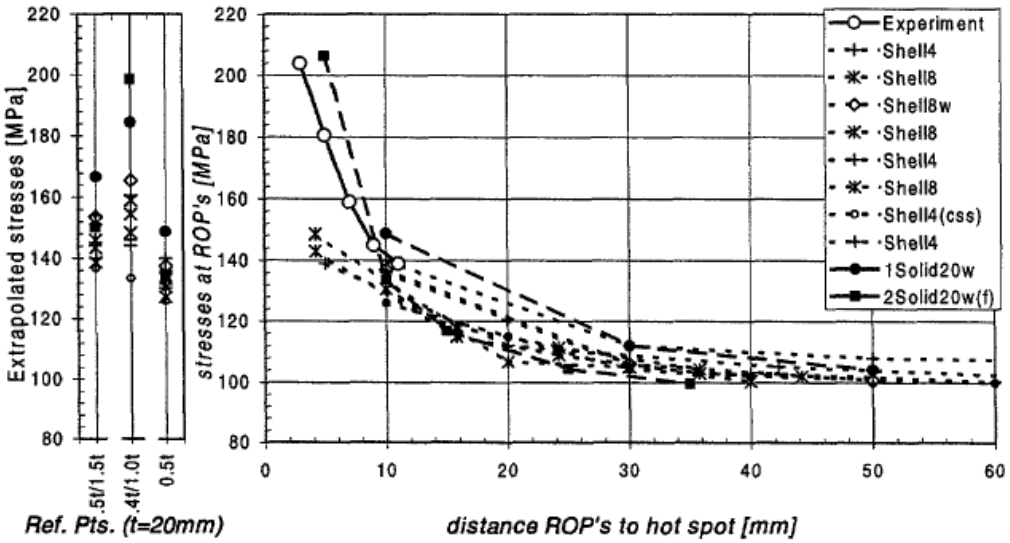

Figure 4.4: Stress results for detail in Figure 4.3

Rucho et al (2001) verified Fricke's conclusion in their work on side longitudinals. A comparison of fatigue measurements and finite element analysis is carried out. Full scale fatigue testing of five test specimens of side longitudinals of an FPSO was carried out at the structural laboratories of DNV. The geometry of the full scale test specimens correspond to those commonly found in FPSOs. Based on the 0.5t/1.5t extrapolation procedure, there is a general acceptable agreement between the measured stress and the calculated hot spot stresses.

Norman and Lotsberg (2001) studied the fatigue life improvement of scallops. Scallops also referred to as cut-outs or mouse holes are used in welded structures and plate intersections for efficient construction and drainage. The weld and stress concentration at a scallop represents a potential source for fatigue cracking. Three extrapolation methods used by classification societies (DNV, LR and ABS) and Niemi's method are investigated for five different types of scallop geometries. The scallop geometries are modelled with solid elements. The extrapolation methods are noted to follow the same stress variations but gave different stress values.

Maddox evaluated fatigue data for typical details found in FPSOs on the basis of the hotspot stress design S-N curve and extrapolation methods. Depending on the detail being analysed, the 0.5t/1.5t linear extrapolation procedure resulted in stresses up to 12 % higher than the 0.4t/1.0t method. For simple details, both methods are acceptable if fatigue class 90 is used. But for complex details with higher stress gradients, fatigue class 80 is recommended. The single point stress method (0.5t) gives a large scatter and lower stresses. Stress at 0.3t is found to be a better stress estimate than at 0.5t.

In 2004, the American Society of Mechanical Engineers (ASME) organised a specialty symposium on the integrity of FPSOs. Sixty two papers providing design recommendations and solutions for arresting fatigue and loading problems were presented. Bergan and Lotsberg (2004) provide an exhaustive review of DNV's effort to tackle hull fatigue problems. The hotspot stress approach is linked to corresponding S-N curve to match fatigue test results. Extrapolation procedures are investigated for different structural details. The stresses obtained from the FE analysis and experiment showed good agreement with the measured stresses. The calculated stress is used with

fatigue class 90 which corresponds to DNV class D S-N curve. For FE modelling, a t x t mesh with linear extrapolation at 0.5t and 1.5t from the weld toe is recommended.

Lotsberg (2004) assessed the HSS concept for plated structures and outlined steps for fatigue analysis of marine structures. FE modelling techniques for different element types as well as extrapolations procedures are studied. He concluded that the stresses obtained by linear extrapolation (0.5t/1.5t) can be used with FAT90 S-N curve and a stress calculated from a single point is linked with FAT80 curve. This agreed with earlier conclusions reached by Maddox.

Lotsberg and Sigurdsson (2004) calibrated a HSS S-N curve to be used with FE analysis of plated structures. Target stress concentration factors are set for five typical ship details based on Fricke's work. A recommended hotspot stress S-N curve is arrived at that is linked to FE modelling and derivation of hotspot stress.

Lotsberg and Landet (2004) studied the fatigue behaviour of the connections between side longitudinals and transverse frames. Stresses are measured at different hotspot areas for calibration of finite element analysis and link to S-N curve. The measured stresses at the hot spot regions were found to be in good agreement stresses derived by FE analysis.

In normal practice, when using shell elements the hotspot stress is obtained by extrapolating predicted stresses to the element intersection line. Extrapolation to the weld toe is done if the weld has been included in the finite element model. ABS proposed to extrapolate the stress to the weld toe even though the weld had not been included in the model. Tvieten et al (2007) report large differences in calculated HSS based on different extrapolation procedures. The single point method showed the smallest variability and the IIW linear extrapolation method gave the highest stress values.

Fricke et al (2007) within the MASTRUCT project conducted a round robin analysis where three different structural details were assessed by calculating the structural hot spot stresses and effective notch stresses. The details studied include a thickness step at a butt joint between plates, a penetration of a T-shaped longitudinal through a

bulkhead with four hotspots at different locations , see Figure 5.5, and a fillet-welded end joint of a rectangular hollow section where the root of the one-sided weld is prone to fatigue and is assessed with effective notch stress. Different modelling techniques and evaluation procedures are tested. The computed stresses exhibit some scatter which is highest in the T-shaped longitudinal detail especially when shell elements are used for the model. The resulting stress concentration factors are given in Table 4.2 along with element type, weld modelling and stress extrapolation method. This scatter is attributed to differences in finite element type and property, the mesh density and the type of stress extrapolation used to determine the stress. From the fatigue tests, target stress concentration factors are derived based on the difference between the hotspot Fatigue Class 100 and the nominal fatigue class obtained from tests. This yields smaller stress concentration factors ranging from 1.24 for hotspots 2 and 3 to 1.44 for hotspots 1 and 4. Compared to these values, the computed values are conservative.

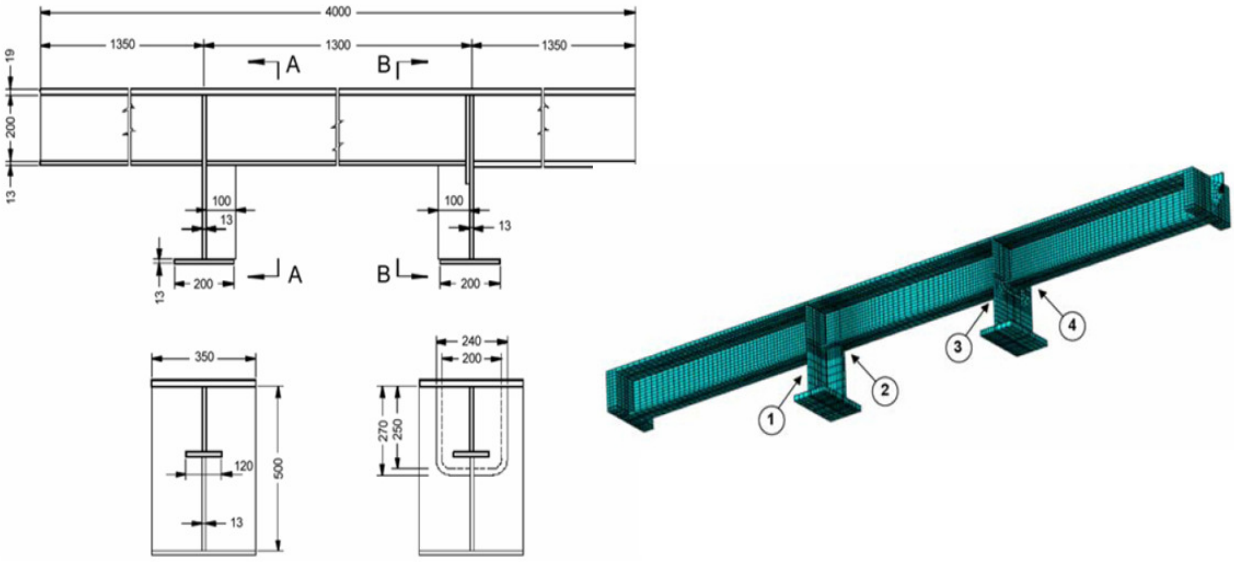

Figure 4.5: Structural details of the T-shaped longitudinal / bulkhead penetration and typical finite element (Fricke et al, 2007)

Table 4.2: Modelling details and analysis results for detail in Figure 5.5

Parti-cipant	Soft-ware	Elem.type, weld mod., stress extrap.	SCF 1	SCF 2	SCF 3	SCF 4
A	Ideas/ Permas	solid, weld not modelled	-	1.93	1.83	-
B	Ansys	solid, weld modelled	1.62	1.67	1.61	1.61
C	Patran Nastran	Shell Quad4, with shape function	1.76	1.50	1.48	1.67
C	Patran Nastran	Shell Quad8, with shape function	1.66	1.37	1.36	1.53
D	Ansys	p-meth., no weld, global convergence	1.81	1.60	1.54	1.79
E	Abaqus	Shell, weld not modelled	1.67	1.69	-	-
E	Abaqus	Solid, weld 1+4, IIW 0.4t / 1.0t	1.61	1.68	-	-
E	Abaqus	Solid, weld 1+4, linearis. over t	1.74	1.63	-	-
F	Nisa	8 nodes shell IIW 0.5t / 1.5t	1.90	1.43	1.37	1.89
Mean value			1.72	1.61	1.53	1.70
Coefficient of variation			5.8%	10.3%	11.4%	8.4%

Smith et al (2008) for The Welding Institute (TWI) recently carried out a comprehensive study on finite element analysis for fatigue analysis for welded joints. Three fatigue test specimens representing welded structural details are studied. They include a longitudinal gusset in a ship structural detail shown in Figure 4.6, a cover plate beam and a tubular T-joint. Element type, size and order, extrapolation procedures and the effect of weld overfill are investigated based on three different extrapolation procedures: surface stress extrapolation, through thickness integration and nodal force method. The through thickness integration method uses predicted stress distribution in the plate below the weld toe. The stresses are integrated to obtain a nodal force and a moment which are then used to calculate the structural stress at the weld toe. The nodal force method also uses calculated forces and moments at the weld toe, but the nodal forces are determined using displacements which makes the solution more accurate. The ship detail is modelled using linear quadratic shell elements and brick elements. Element size varies from 2t to 0.25t; t is the thickness of the longitudinal stiffeners. The models are developed with and without the fillet weld included (Figure 4.7). Available fatigue data is then compared with the calculated stresses as a basis for a hotspot stress design S-N curve.

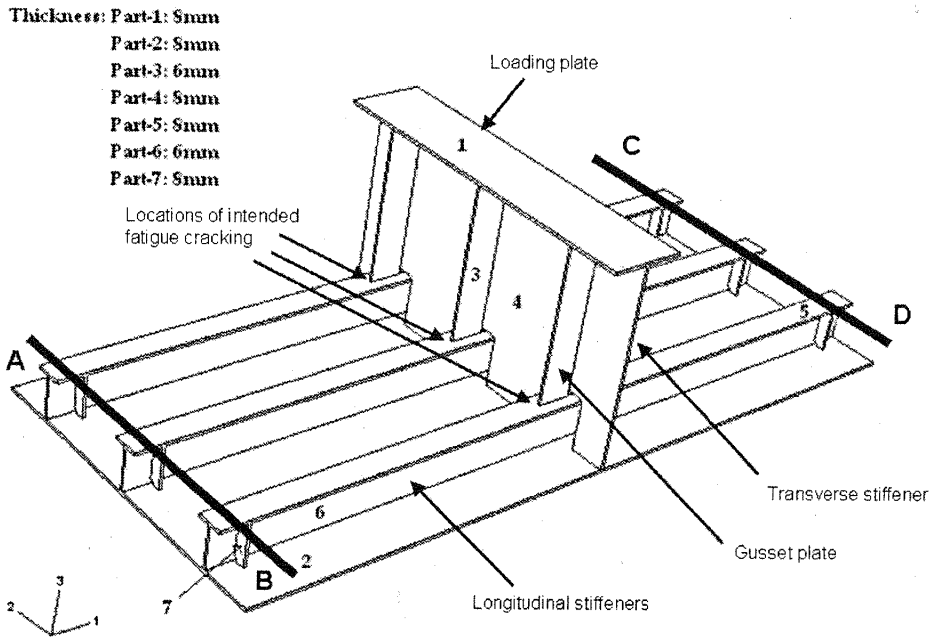

Figure 4.6: Ship detail test specimen

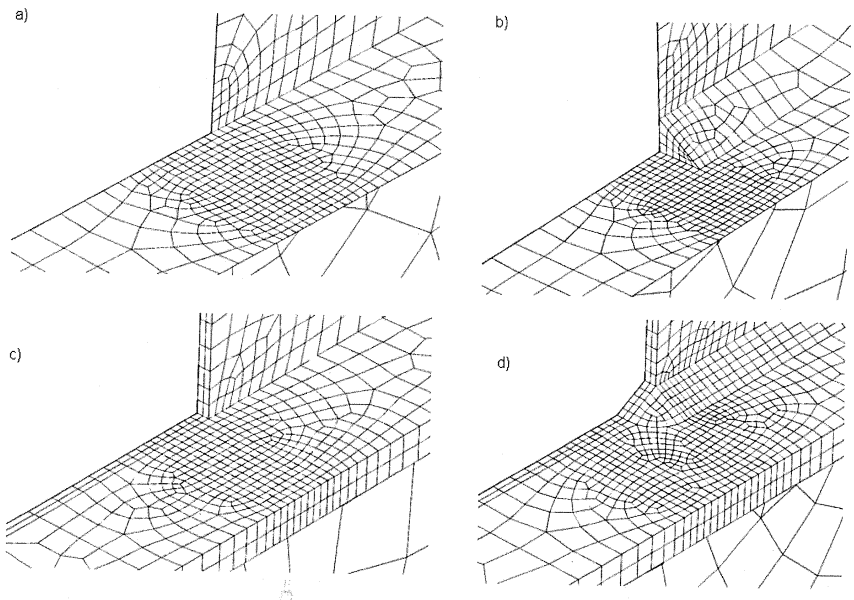

Figure 6 Models of the ship detail showing the intersection between the gusset plate and the stiffener flange:
a) Shell model without weld;
b) Shell model with weld;
c) Brick model without weld;
d) Brick model with weld.

Figure 4.7: Finite element mesh of ship detail

It is reported that the surface stress extrapolation method is the best method for calculating hotspot stress because it gives good results for a wide range of modelling options. The method however, tends to underestimate the hot spot stress value compared with the through thickness integration and the nodal force methods particularly when elements are modelled using quadratic bricks. The IIW FAT90 S-N curve which is essentially the same as the BS 7608 Class D S-N curve is proposed for use with the calculated stress. Full details of fatigue tests performed on behalf of LR for the ship detail is reported. The fatigue test results are compared with existing hotspot stress data obtained from structural components incorporating fillet weld stiffeners. This is presented in Figure 4.8 together with Class D mean and design S-N curves. There is good agreement between the fatigue test results and published data based on calculated stresses. The database also supports Class D S-N curve as a hotspot stress based design curve.

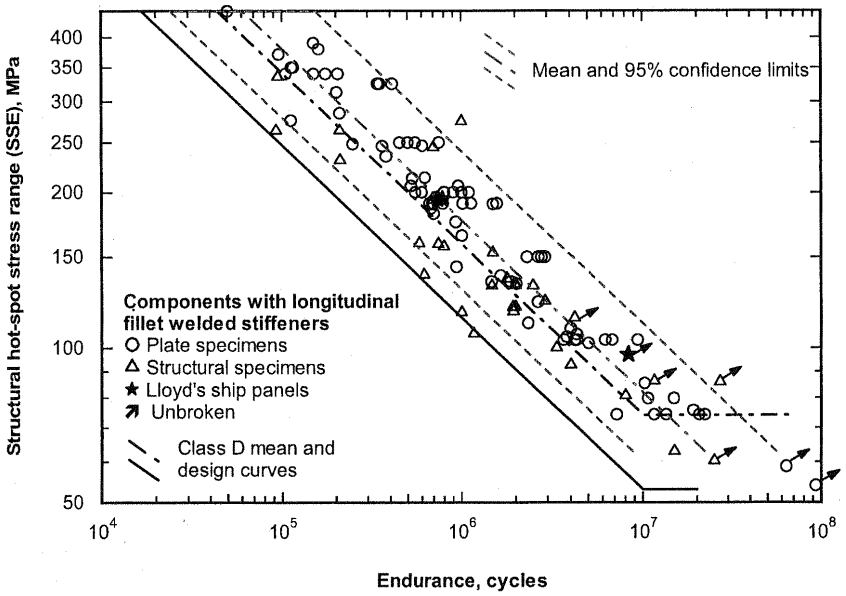

Figure 4.8: Comparison of fatigue tests for the ship detail with published hotspot stress data and stress obtained from surface extrapolation (Smith et al, 2008)

Concurrent with the IIW recommendations, Dong and his associates (2001, 2003a, 2003b) published alternative hot spot stress computation methods that combine features of through thickness and surface extrapolation procedures. Dong's hotspot stress approach is not used in this work but it is the author's opinion that it is worth a mention. The method is briefly described for shell elements.

The hotspot stress is the sum of the linear membrane and shell bending stress due to equilibrium tractions at the weld boundary rather than being extrapolated from element surface stresses. It can also be evaluated using the element nodal forces in the weld toe section, from which the line forces and moments are calculated on the basis of appropriate shape functions (resulting in the membrane and bending stresses). A linear system of equation is solved to obtain the line forces and moments for all nodal points connected by the weld toe line. It is recommended that the fillet weld be modelled by inclined shell elements generating a continuous weld line for stress evaluation with inclusion of areas at the ends of attachments.

Nodal forces and moments in the weld line are determined using finite element software like ABAQUS and then the global coordinate system is converted to the local to orient with the weld. Line forces and moments with linear distribution between the nodal points are then derived from the nodal forces and moments. Finally the line forces, f_x, (vector normal to the weld line) and line moments m_z (vector in the weld line) are converted to (membrane and bending) structural stresses with respect to shell thickness t:

$$\sigma_s = \sigma_m + \sigma_b = \frac{f_x}{t} + \frac{6m_z}{t^2} \qquad 4.1$$

According to the author, this method has the advantage over other methods by being mesh insensitive. This means that, as long as the mesh is fine enough to describe the geometry changes along the weld, the element type and size do not matter. Figure 4.9 illustrates the mesh insensitivity of the procedure as obtained for a single lap joint modelled with eight-node plane strain elements. Dong has also validated the method for ship structural details.

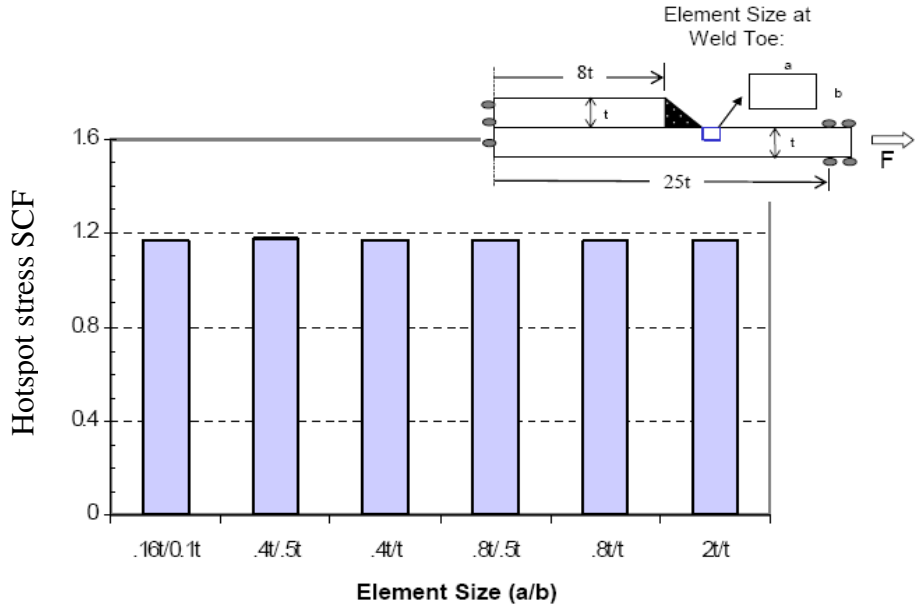

Figure 4.9: Dong's stress method showing mesh insensitivity (Dong, 2005)

There are several uncertainties relating to Dong's method. Lotsberg and Landet (2004) note that the structural stress approaches may improve the methodology for hot spot stress calculations but they are highly laborious and complicated to use especially when it comes to post processing and result derivation.

Fricke and Kahl (2005) carried out a comparative study of the hot spot stress approach, Dong's structural stress approach and a structural stress method proposed by Xiao and Yamada (2004). In spite of the difference in the stress definitions, the fatigue lives predicted with the three approaches are not too distant from each other.

Poutiainen et al (2004) investigated Dong's structural stress approach and compared it with the linear extrapolation procedure (0.4t/1.0t) and through thickness (at the weld toe) method. The conclusion was reached that for 2D details with one element thickness in all directions; all the methods work quite well. For 3D details though, the structural stress approach is mesh sensitive and requires more care.

Healy (2004) presents the fatigue life assessment of a side shell detail of an FPSO where he compares the hotspot stress approach with the structural stress approach. The connection was analysed with varying mesh sizes (0.125t to 2t), three surface extrapolation methods and the structural stress method. Each method converged to a

different S-N curve and the structural stress method gives very unpredictable damage result.

Kim et al (2009) and Kim and Kang (2008) also carried out a study on the fatigue life of ship structural details based on the comparison of the hotspot stress approach and the structural stress approach. The two methods were found to produce consistent results of life estimation with a 10 % difference.

Xu and Barltrop (2007) have proposed a new approach of analysing stress singularities to allow for the classification of details to a limited number of weld classes. According to elastic stress analysis, structural sharp corners are singularities and may be classified by type and strength. It is shown that once a correspondence between these characteristics and the structure under consideration has been ascertained, this provides guidance on the mesh size needed to analyse a structure, on the size-dependent stress concentration factors and an additional crack size for more accurate crack growth calculations.

4.3 Hotspot Stress S – N Curve

The hotspot stress S-N curves can be presented using stress or strain ranges but are generally based on strains measured from various test specimens near the point of crack initiation. The strain ranges are measured with strain gauges at several sections along the weld toe and extrapolated to the weld toe from two or three strain measurement points.

The IIW hotspot stress design S-N curve is expressed in terms of fatigue class. Fatigue class identifies the allowable characteristic strength in MPa of a structural detail corresponding to a fatigue life of two million cycles with a 95 % probability of survival, assuming a slope of m = 3. IIW recommendations define different hot spot curves for butt welds, fillet welds and cruciform joints. Fatigue class of FAT 100 is used for non load carrying fillet welds while FAT90 is used for load carrying fillet welds. Butt welds and cruciform joints are assessed according to their nominal fatigue classes.

Partenen and Niemi (1996) published a butt weld design curve determined using hot spot stress approach. This is based on fatigue test results of more than 180 welded steel specimens in various configurations carried out at Lappeenranta University of Technology between 1980 and 1993. A mean fatigue strength of FAT 148 and characteristic fatigue strength of FAT 107 were obtained by considering all the specimens in one series. For toe failure of welded joints with plate thickness up to 10 mm, it is recommended that the fatigue class FAT 100 can be used as the design curve.

In Eurocode 3, the fatigue life estimation can be based on hot spot stress ranges. The hot spot stress is defined to be the maximum principal stress in the parent material adjacent to the weld toe. For full penetration butt welds two different hot spot curves are presented. FAT 90 is used, if weld profile and permitted weld defects acceptance criteria are satisfied and FAT 71 when only permitted weld defects acceptance criteria are satisfied.

4.4 Extrapolation Procedures

4.4.1 Fatigue Crack Definition

To select the most suitable extrapolation procedure for this study, different hotspot stress surface extrapolation procedures are tested. The detail selected for the study is in the vicinity of the bottom shell longitudinal and web stiffener of the FPSO. Figure 4.10 shows the concerned section of the bottom shell longitudinal with a possible crack location along the hotspot. Before extrapolation, the distribution of stresses along the line of extrapolation is computed at the nodes defining the line of extrapolation. The nodal stresses are then determined by averaging contributions from all the elements around the hotspot under consideration. The stress is now linearly extrapolated along a line perpendicular to the weld toe of interest.

Table 4.3: Geometry of stiffener

Item	Meters (m)
Stiffener spacing	0.8
Height of stiffener	0.55
Thickness of web	0.012
Width of flange	0.15
Thickness of flange	0.016
Thickness of transverse web	0.021
Thickness of bottom shell	0.021

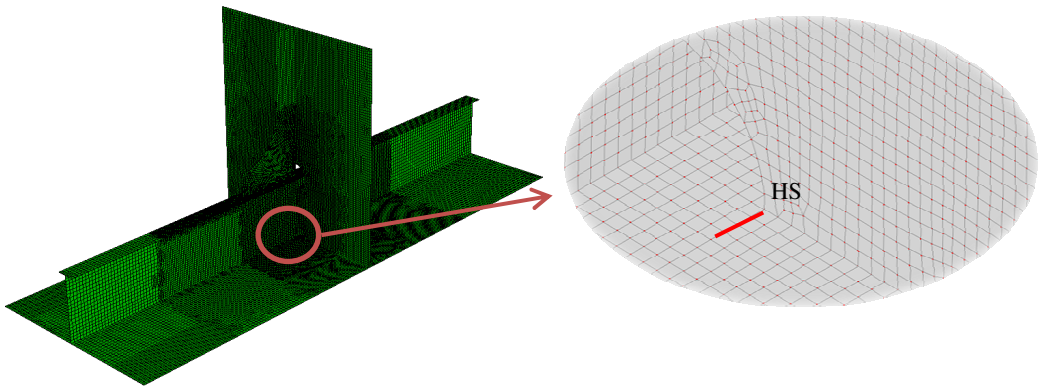

Figure 4.10: Detail studied and definition of crack

The aim of this section is to select the most appropriate surface extrapolation procedure for this study. Three stress extrapolation procedures are studied illustrated in Figure 4.11:

1. The quadratic extrapolation method recommended by IIW. The nodal stresses at three reference points 4 mm, 8 mm and 12 mm from the weld toe are evaluated. A fine mesh finite element model is developed using a 4-node shell quadratic element. The element size around the weld toe of interest is set at 4 mm.
2. The linear extrapolation procedure using reference points at 0.5t and 1.5t from the weld toe (t is the plate thickness) is tested. Two different finite element models with different mesh sizes are explored. The first is the t x t mesh which is favoured by most classification societies. Four node quadratic shell elements are used. The finite element model is developed with a mesh size of 10 mm x 10 mm using 8-node shell quadratic elements for the second model.

The stresses are extrapolated 5 mm and 15 mm away from the weld toe. The nodal stresses used to determine the hotspot stress are read out from the mid-side nodes of the elements around the area of interest.

3. The stress at a single read out point, 0.5t is also tested. A mesh size of 10mm by 10mm is used to develop the finite element model.

The extrapolated hot spot stresses are derived directly from the averaged nodal surface stresses at the reference points using extrapolation equations given as:

- Quadratic extrapolation, using points at 4, 8 and 12mm : $\sigma_{hs} = 3\sigma_{4mm} - 3\sigma_{8mm} + \sigma_{12mm}$
- Linear extrapolation, using points at 0.5t or 5mm and 1.5t or 15mm: $\sigma_{hs} = 1.5\sigma_{0.5t} - 0.5\sigma_{1.5t}$
- Single point stress, $\sigma_{hs} = \sigma_{0.5t}$

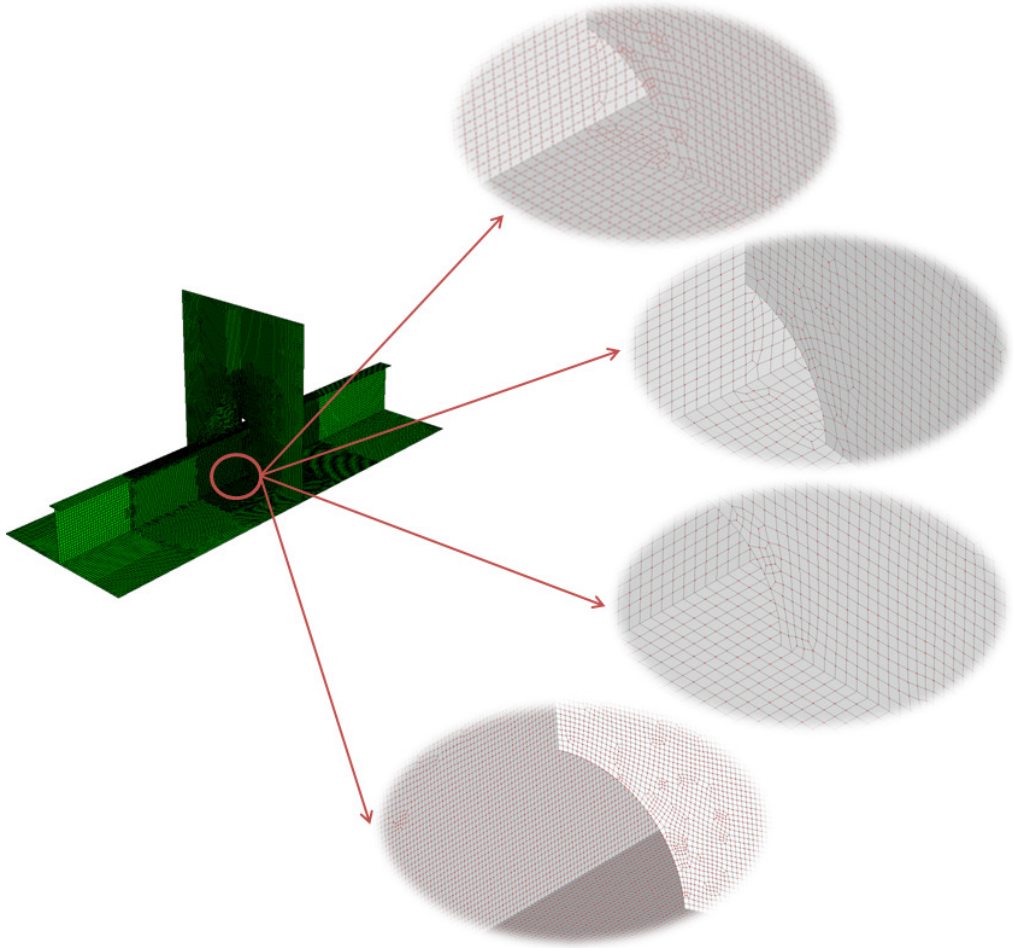

Figure 4.11: Finite element model showing different mesh size

The predicted stresses at 100 mm from the weld toe in Figure 4.12. The nominal stress is assumed to be stresses at enough distance away from the hotspot where the effect of the stress concentration is minimal. Based on this assumption, the hotspot stress concentration factor for all the models is calculated using the extrapolated stresses and compared with the stress concentration factor from simple beam theory. This is illustrated in Figure 4.13.

Storsul et al (2004) presented calculated and measured stresses at welded connections between side longitudinals and transverse frames in ship structures. Several meshing techniques and extrapolation procedures are tested and compared with measured data. They show that using eight node shell elements for the finite element model predicts too high stresses. This conclusion is confirmed in this test as it is also noted that the model with the eight-node shell elements predicts the highest stresses at the hot spot.

The stresses obtained by quadratic extrapolation shows good agreement with the calculated theoretical stress concentration factor and the linear extrapolation procedure clearly underestimate the stresses at the hotspot.

The quadratic extrapolation method is preferred over linear extrapolation in cases where principal stress increases non-linearly in front of the weld toe. It is assumed that non-linear portion of the stress disappears at a distance, 0.4t, from the weld toe. In case of thicker plates non-linear portion of the stress may extend further than 0.4t from the weld toe. In such cases, linear extrapolation might underestimate actual hot-spot stress, thus quadratic extrapolation could be used (Healy, 2004). Other global geometry can also influence the extent of non-linear portion of the stress at the vicinity of the weld toe. Cover plates on beams is one example, where quadratic extrapolation is found to yield better fatigue life estimates over linear extrapolation. Based on these results, the quadratic extrapolation procedure will be used in the rest of the thesis to obtain the stresses at the selected hotspot.

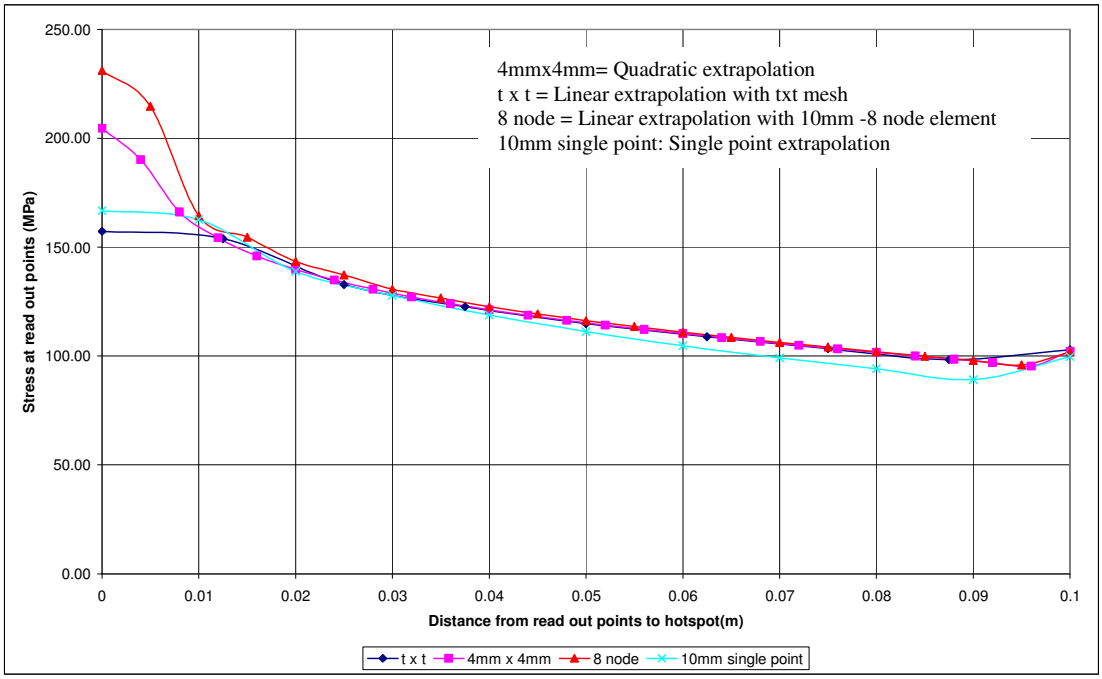

Figure 4.12: Predicted stresses from different extrapolation methods

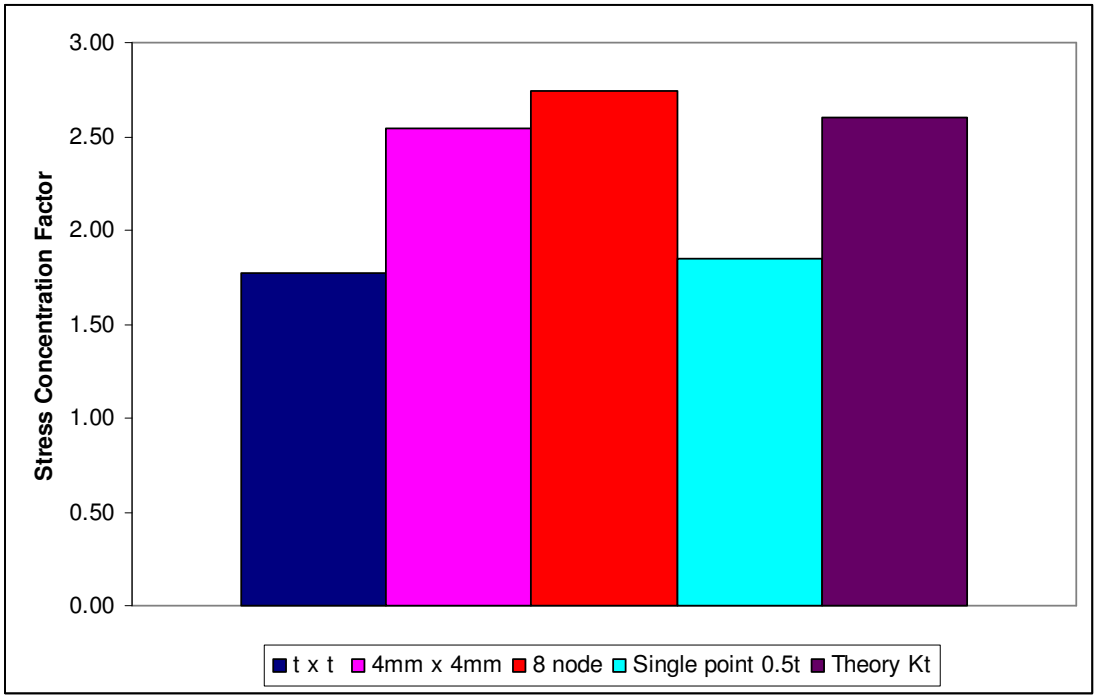

Figure 4.13: Stress concentration factors

4.5 Predicted Stresses

4.5.1 Bottom Plating and Stiffener Detail

This detail represents the connection between a transverse web, bottom shell plating and longitudinal stiffeners of the FPSO (Figure 4.14). The loading applied is representative of loading and unloading operation as given in Table 2.4. Figure 4.14a and Figure 4.14b shows six different hotspot locations where potential fatigue cracking might occur. These locations are located at sharp corners or cut-outs. The predicted stresses from the finite element analysis of the detail is determined for all potential crack initiation sites and for all the low cycle quasi static load cases listed in Table 2.4.

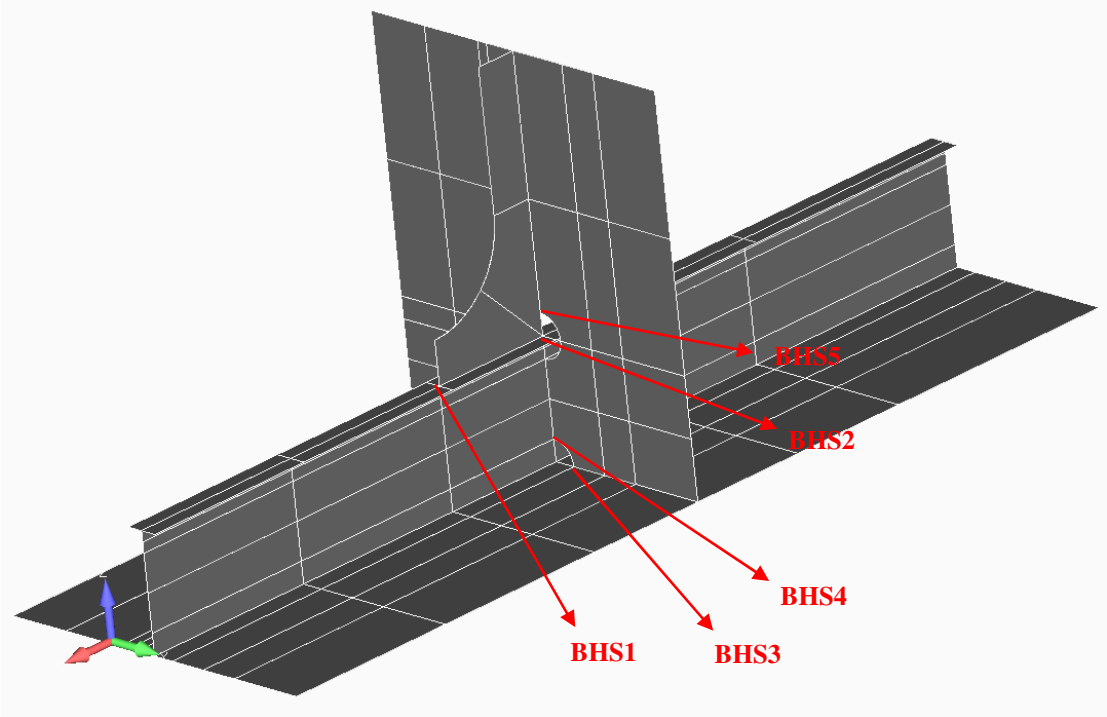

Figure 4.14a: Location of hotspots in bottom detail

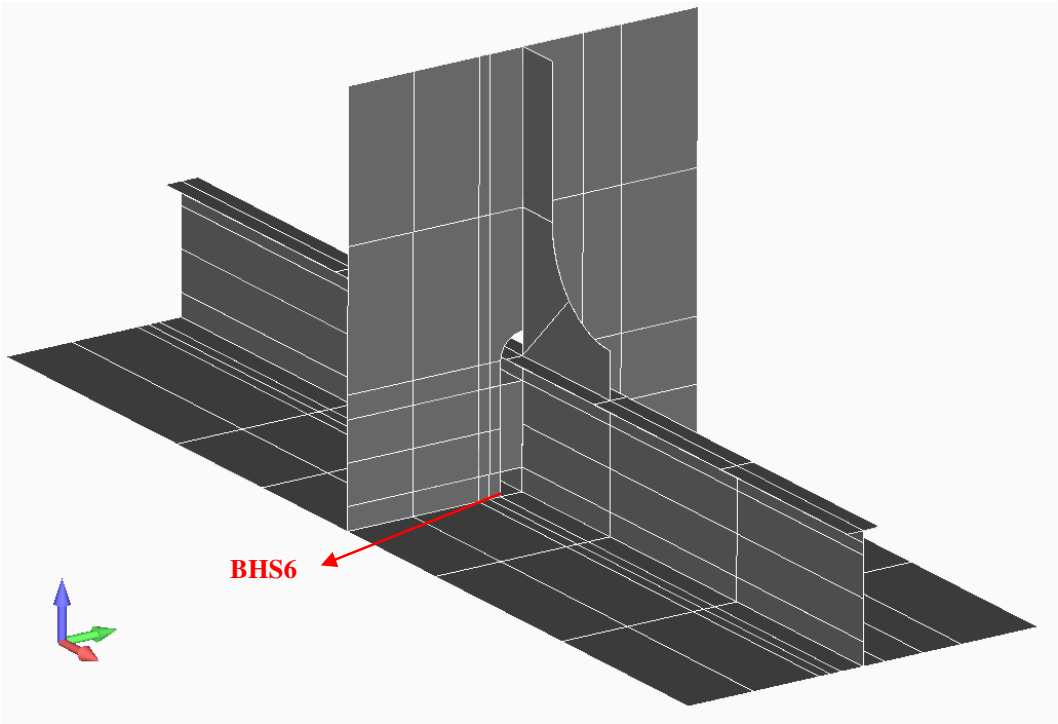

Figure 4.14b: Location of hotspot in bottom detail

4.5.1.1 Predicted Stresses at the Bottom Detail

The predicted stresses for the selected hotspots for the range of loading conditions are presented in Figure 4.15 to Figure 4.20. The stresses are plotted 60 mm away from the weld location. These are elastic stresses obtained from linear finite element analysis of the submodel based on the loading conditions given in Table 2.4. As stated earlier, the boundary of the submodel is driven by the displacements obtained from the global analysis results. The stresses are read out along the potential crack location which is the weld toe in the cases considered. In Figure 4.15, legend 4 refers to the stresses at the considered hotspot for the fully loaded loading condition and 6a shows the stresses when the even numbered tanks are loaded to half their capacity (refer to legend at the footer of the page). Figures 4.15 through to 4.33 all represent the stresses at the weld toes for all the potential hotspots selected.

A further study show that in Figure 4.15 through 4.17, the most critical loading condition is when the cargo oil tanks of the FPSO are fully loaded. Figure 4.18 through 4.20 shows that loading condition 8b generates the highest stresses.

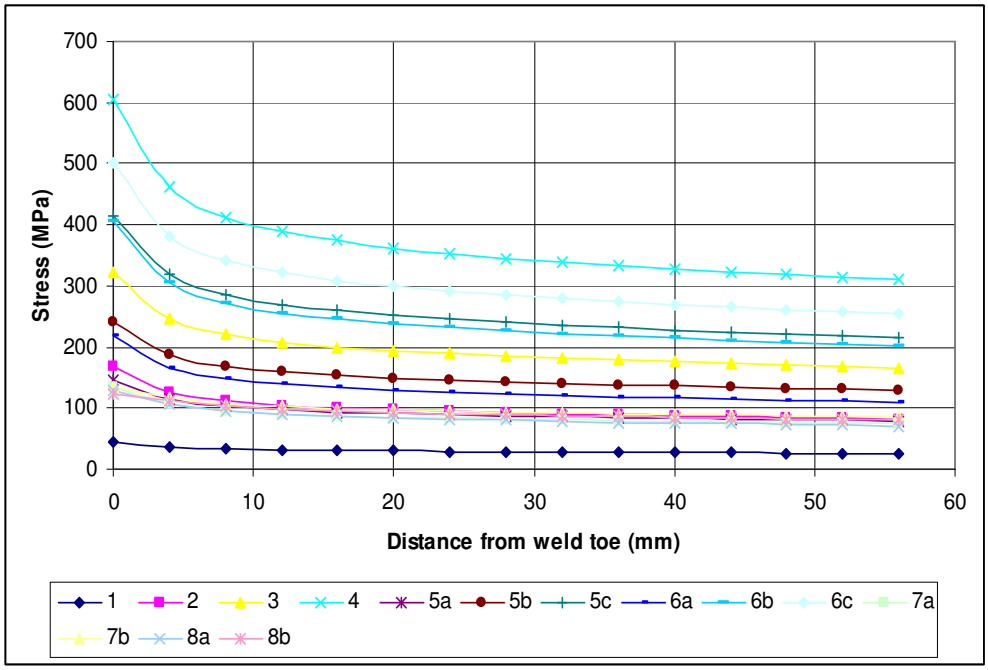

Figure 4.15: Predicted stress at 60 mm from weld toe at BHS1

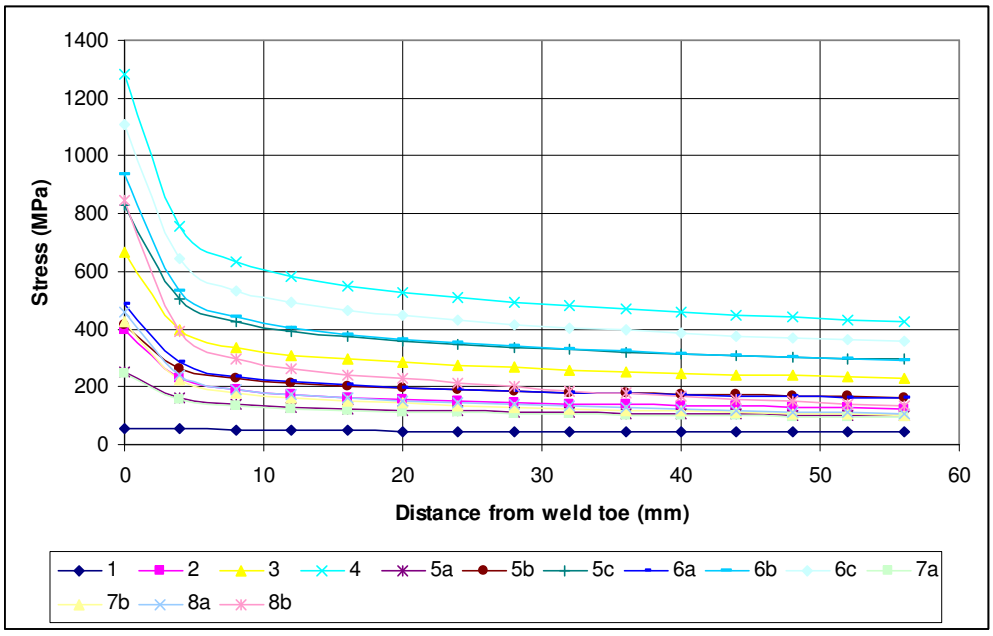

Figure 4.16: Predicted stress at 60 mm from weld toe at BHS2

1 = Ballast
2 = 4COT half
3 = All COT half
4 = All COT full
5a = Odd COT half
5b = Odd Tanks full
5c = Odd COT full + Even COT half
COT = Cargo Oil Tank
6a = Even COT half
6b = Even COT full
6c = Even COT full + Odd COT half
7a = Alternate odd tanks half
7b = Alternate odd tanks full
8a = Alternate even tanks half
8b = Alternate even tanks full

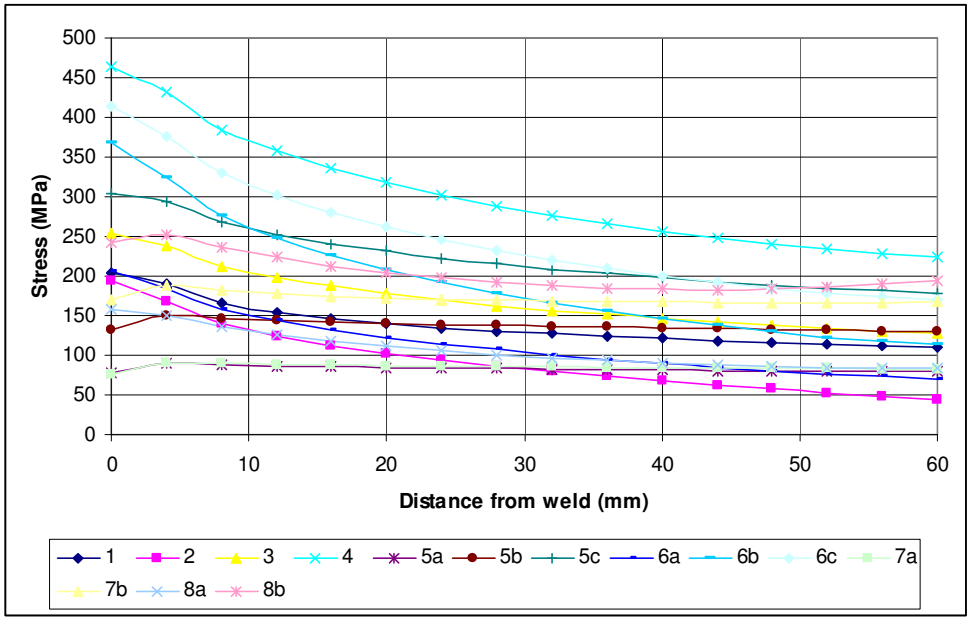

Figure 4.17: Predicted stress at 60 mm from weld toe at BHS3

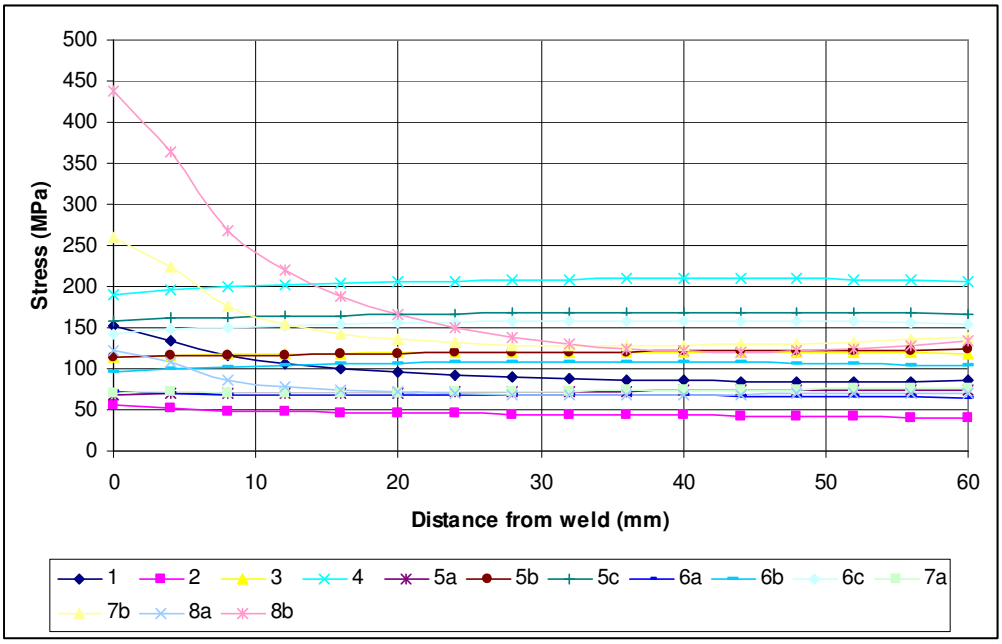

Figure 4.18: Predicted stress at 60 mm from weld toe at BHS4

1 = Ballast
2 = 4COT half
3 = All COT half
4 = All COT full
5a = Odd COT half
5b = Odd Tanks full
5c = Odd COT full + Even COT half
COT = Cargo Oil Tank
6a = Even COT half
6b = Even COT full
6c = Even COT full + Odd COT half
7a = Alternate odd tanks half
7b = Alternate odd tanks full
8a = Alternate even tanks half
8b = Alternate even tanks full

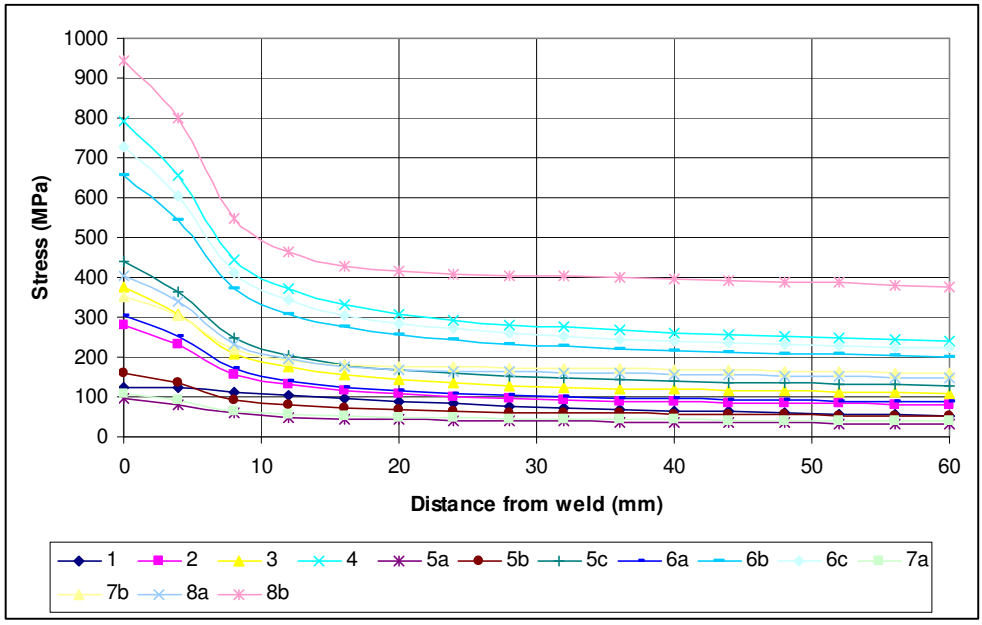

Figure 4.19: Predicted stress at 60 mm from weld toe at BHS5

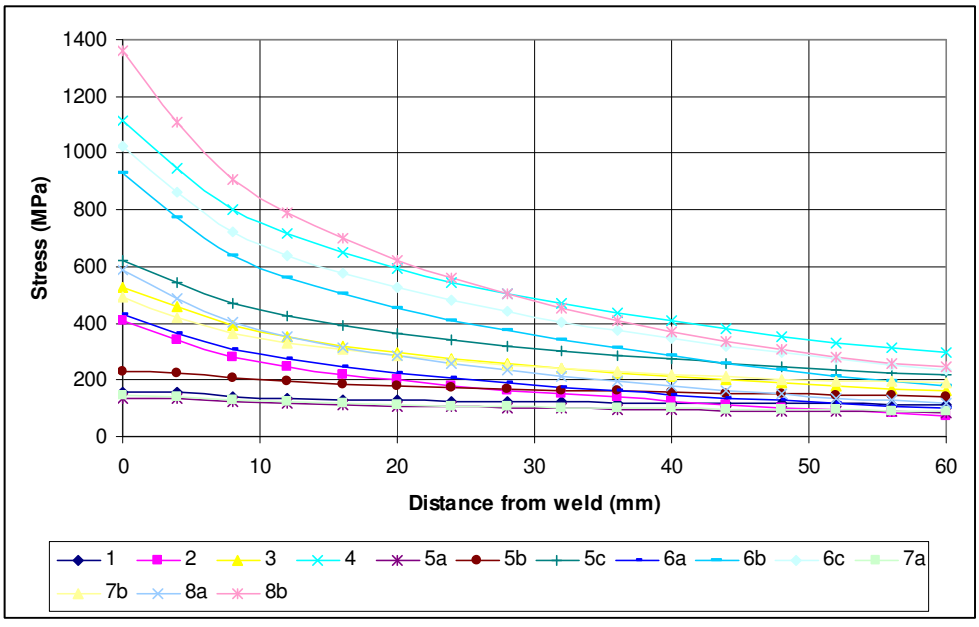

Figure 4.20: Predicted stress at 60 mm from weld toe at BHS6

The ballast loading state is the least critical i.e. this load case generates the least amount of stress at least for BHS1 and BHS2 while the least critical loading varies for the remaining potential crack locations. This shows that the loading states critical to one hotspot may not be critical for another. The maximum predicted stress obtained is just under 1400 MPa at location BHS6 for loading condition 8b (see Figure 4.20); this

value is almost four times the yield stress of the material. The single bottom plating in this FPSO may have contributed to this very high stress.

4.5.2 Side Plating - Inner Side Plating and Stiffener Connection

This detail represents the connection between a side shell longitudinal, a transverse web frame of the ballast tank and an inner side shell longitudinal. There is a web stiffener running from the flange of the side longitudinal to the flange of the inner side longitudinal. Figure 4.4 in Chapter 4 shows the full detail of this connection. The overall dimension of the detail is presented in Table 4.4. Figure 4.21a, 4.21b and 4.21c show the hot spot locations where possible fatigue cracking might occur. The predicted stresses from the finite element analysis of the detail are determined for each hotspot and for each low cycle load case.

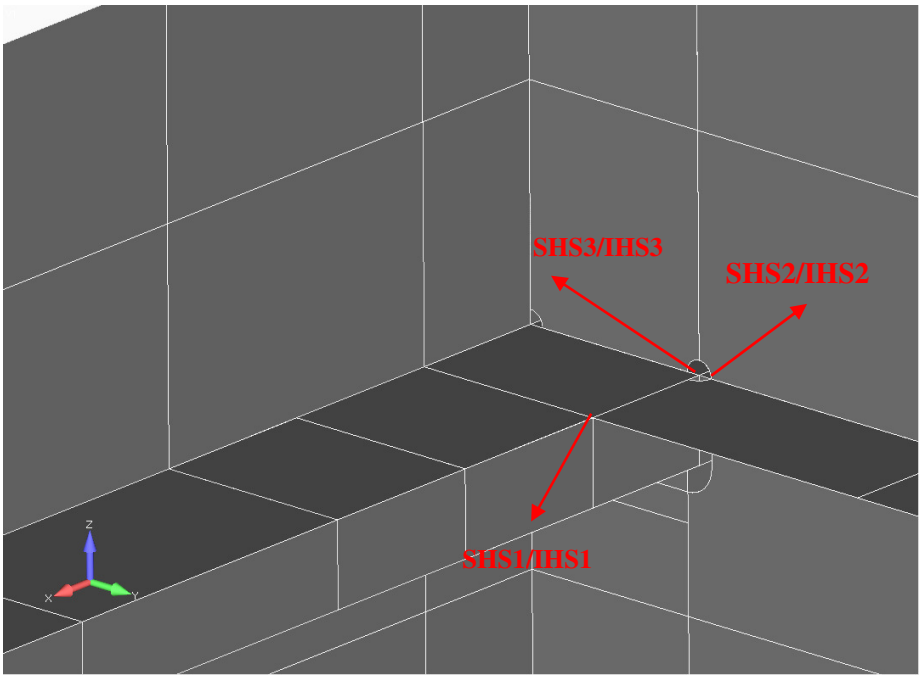

Figure 4.21a: Location of hotspots

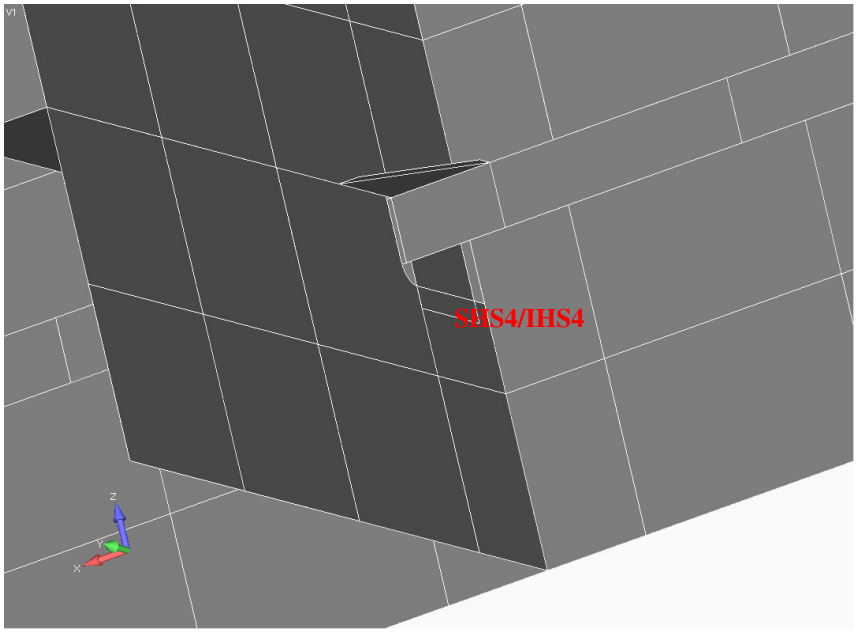

Figure 4.21b: Location of hotspots

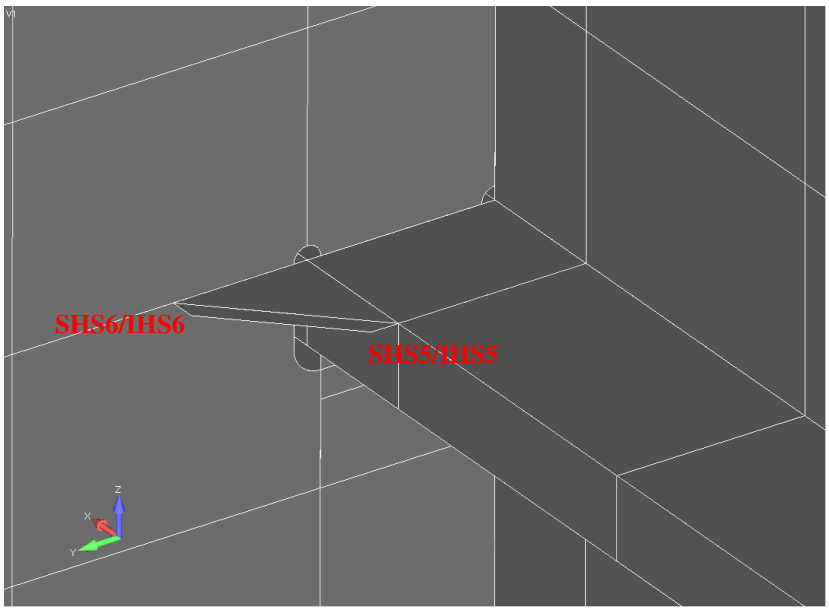

Figure 4.21c: Location of hotspots

4.5.2.1 Predicted Stresses at the Side Detail

The predicted stress for the potential crack locations is presented in Figure 4.22 to Figure 4.27. The most critical load case for all the locations with the exception of SHS4 (Figure 4.25) is the ballast loading condition, generating a maximum stress of 650 MPa at hotspot SHS1. For SHS4 the fully loaded state creates the same amount of stress as the ballast state.

The most critical stress from the low cycle quasi-static load cases for the side longitudinal connection is about 50 % of the value of the most critical stress at the bottom longitudinal connection. One can deduce that the bottom detail is more susceptible to cracks based low cycle load cases selected.

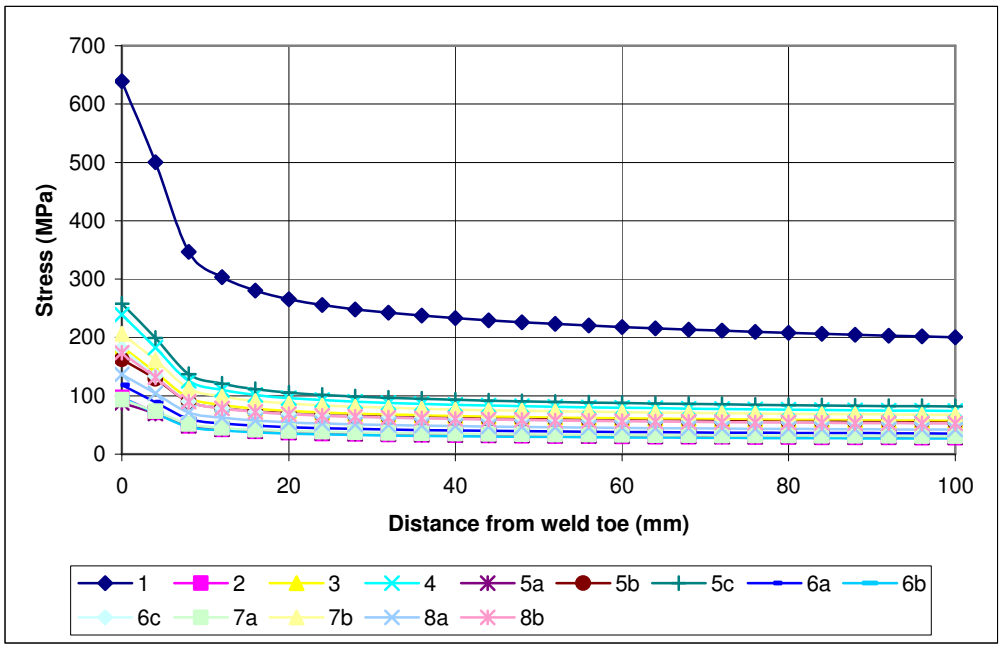

Figure 4.22: Predicted stress at SHS1

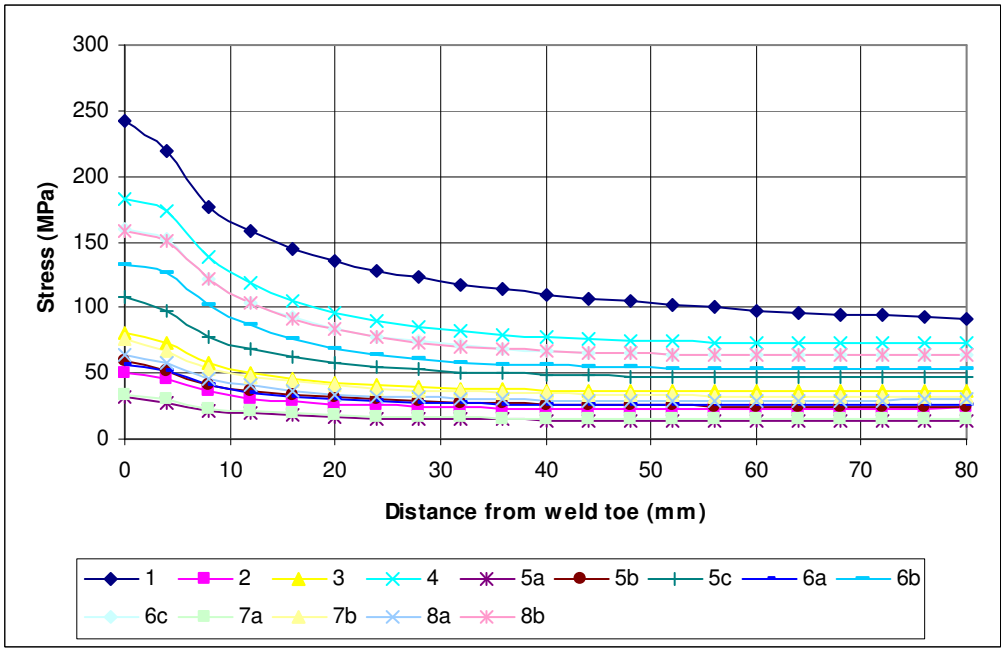

Figure 4.23: Predicted stress at SHS2

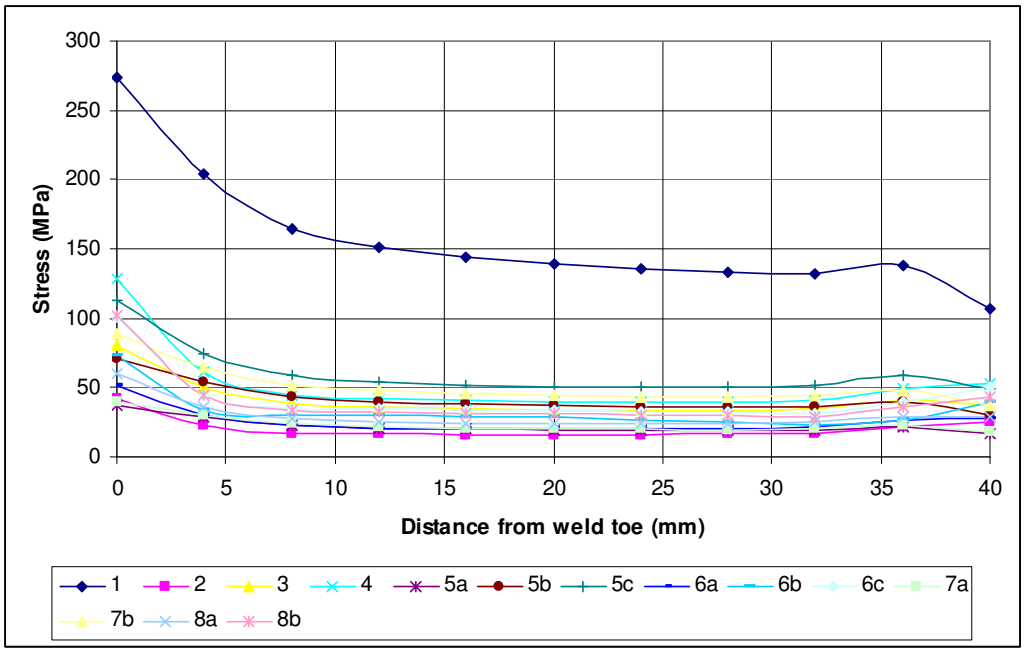

Figure 4.24: Predicted stress at SHS3

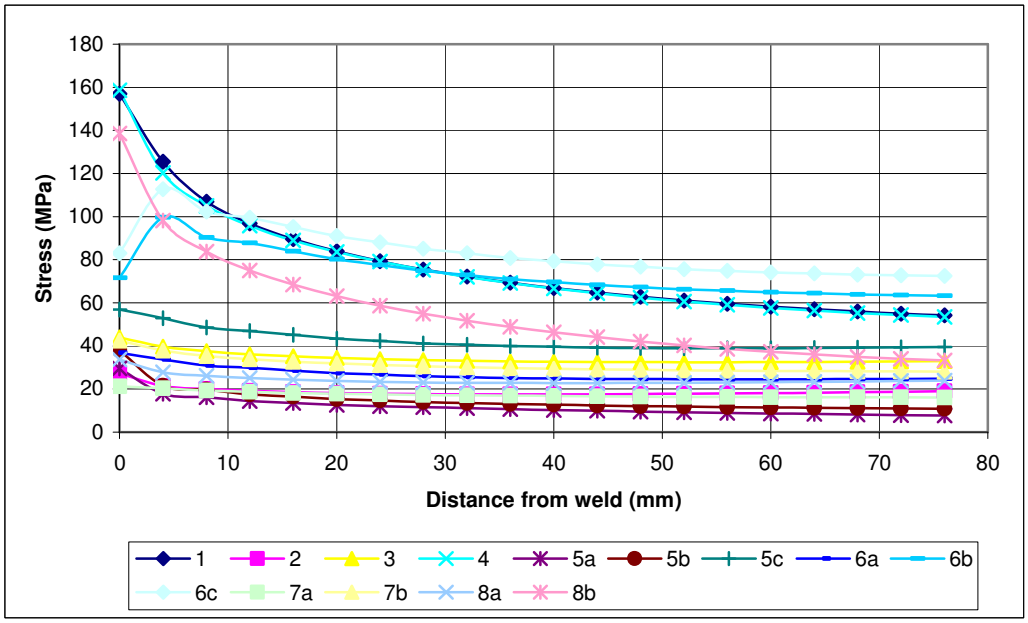

Figure 4.25: Predicted stress at SHS4

1 = Ballast
2 = 4COT half
3 = All COT half
4 = All COT full
5a = Odd COT half
5b = Odd Tanks full
5c = Odd COT full + Even COT half
COT = Cargo Oil Tank
6a = Even COT half
6b = Even COT full
6c = Even COT full + Odd COT half
7a = Alternate odd tanks half
7b = Alternate odd tanks full
8a = Alternate even tanks half
8b = Alternate even tanks full

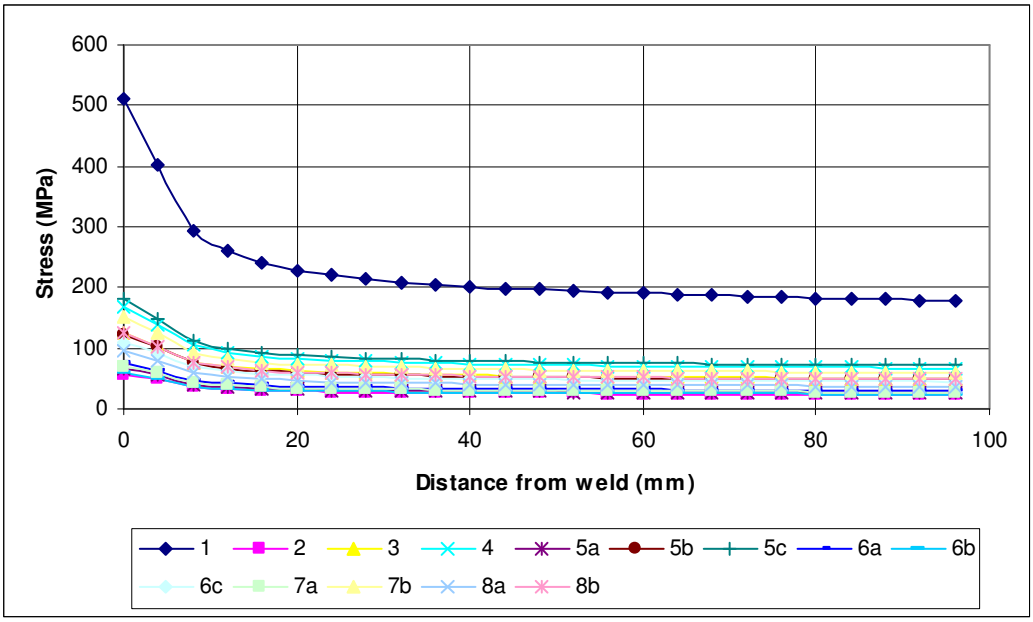

Figure 4.26: Predicted stress at SHS5

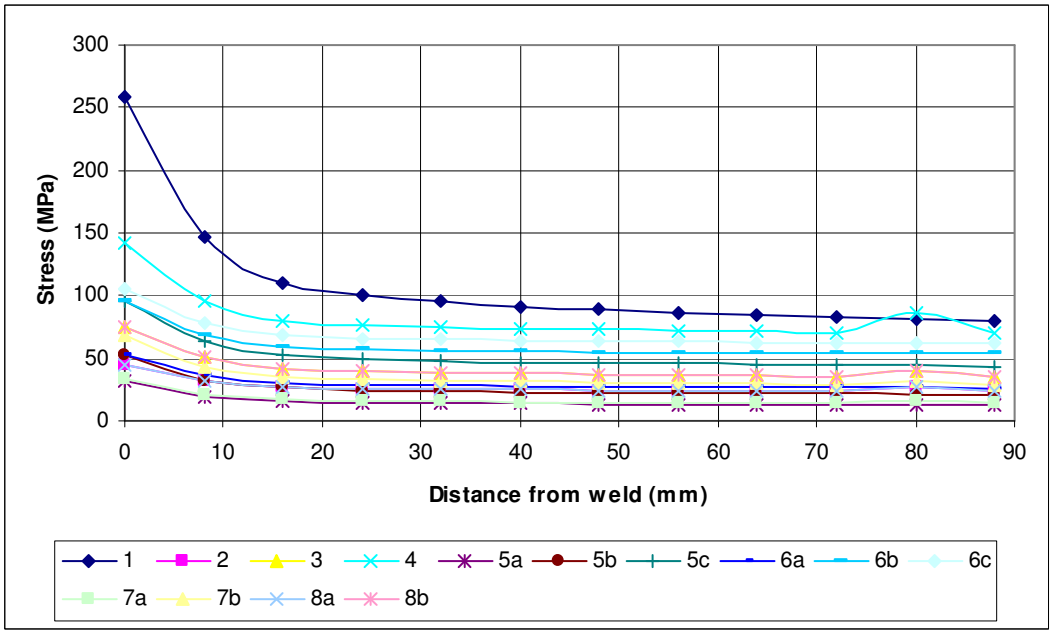

Figure 4.27: Predicted stress at SHS6

1 = Ballast
2 = 4COT half
3 = All COT half
4 = All COT full
5a = Odd COT half
5b = Odd Tanks full
5c = Odd COT full + Even COT half
COT = Cargo Oil Tank
6a = Even COT half
6b = Even COT full
6c = Even COT full + Odd COT half
7a = Alternate odd tanks half
7b = Alternate odd tanks full
8a = Alternate even tanks half
8b = Alternate even tanks full

4.5.2.2 Predicted Stresses at Inner Side Detail

The predicted stress for the selected hotpots is presented in Figure 4.28 to Figure 4.33. It is interesting to note that the stresses generated by the low cycle loads are not as significant for the inner side longitudinal detail as it is for the side longitudinal connection. The maximum predicted stress is about 300MPa for IHS1.

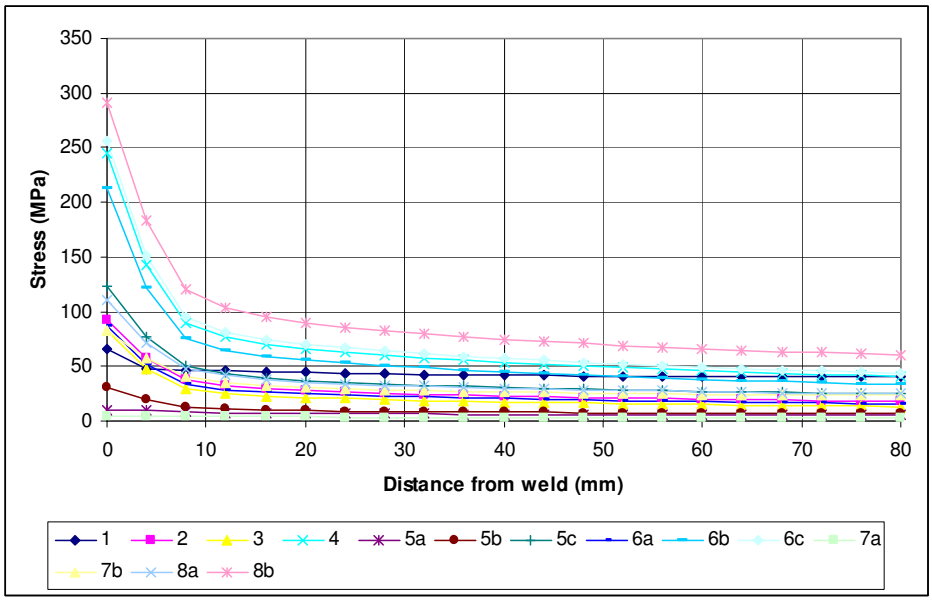

Figure 4.28: Predicted stress at a distance from the weld toe at IHS1

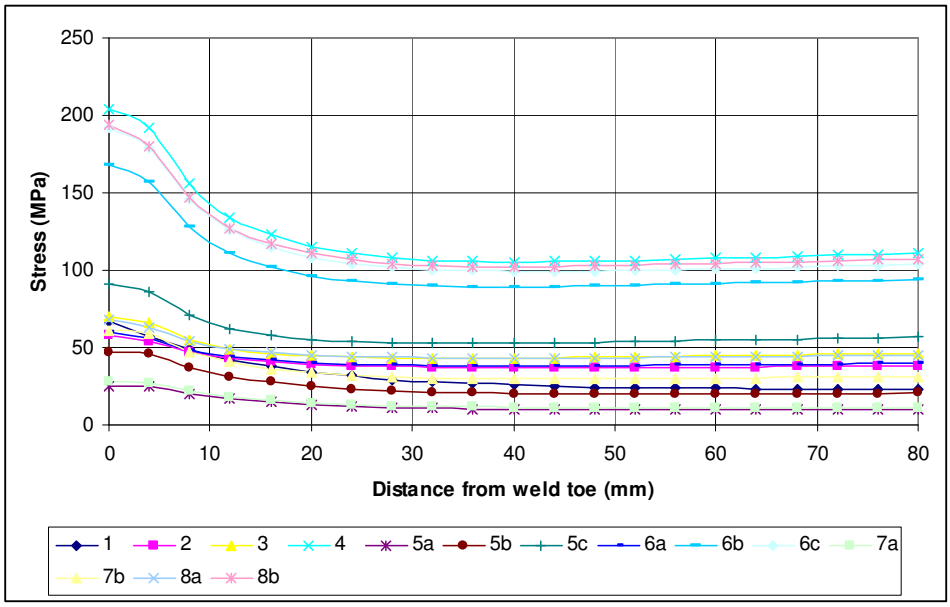

Figure 4.29: Predicted stress at a distance from the weld toe at IHS2

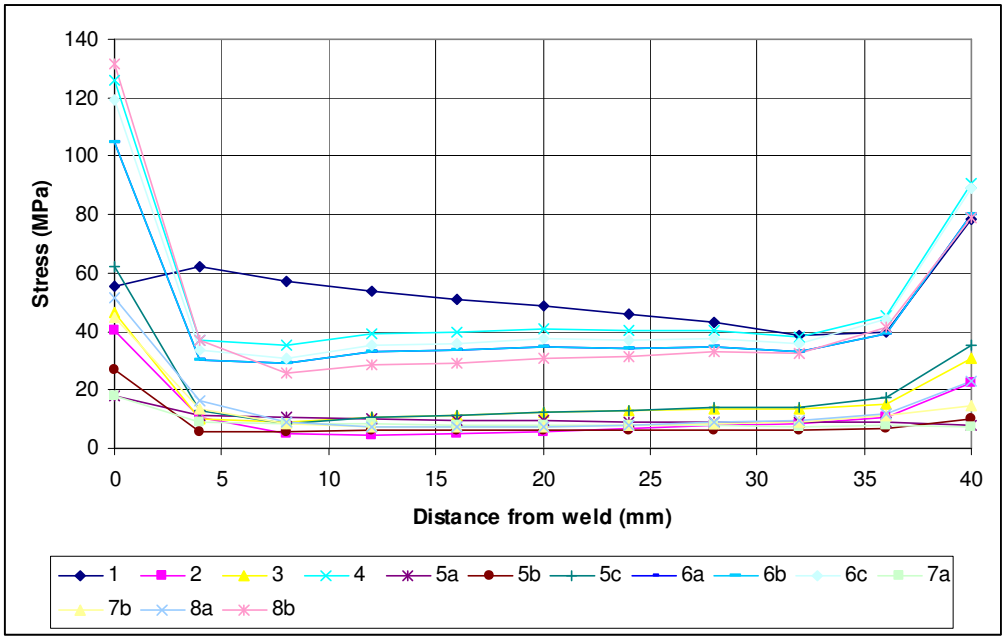

Figure 4.30: Predicted stress at a distance from the weld toe at IHS3

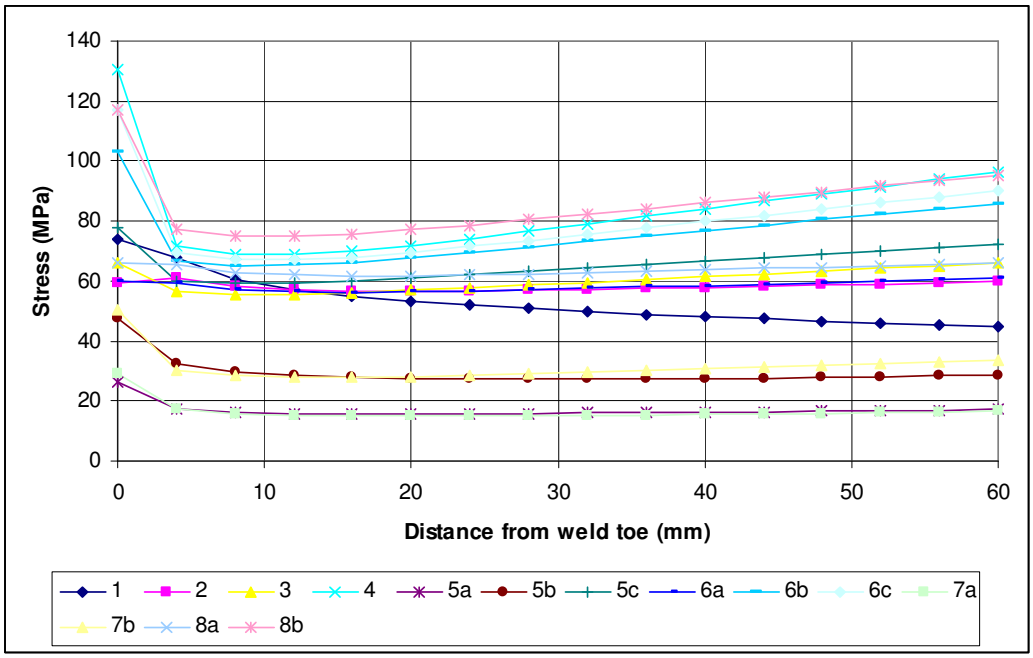

Figure 4.31: Predicted stress at a distance from the weld toe at IHS4

1 = Ballast
2 = 4COT half
3 = All COT half
4 = All COT full
5a = Odd COT half
5b = Odd Tanks full
5c = Odd COT full + Even COT half
COT = Cargo Oil Tank

6a = Even COT half
6b = Even COT full
6c = Even CO full + Odd COT half
7a = Alternate odd tanks half
7b = Alternate odd tanks full
8a = Alternate even tanks half
8b = Alternate even tanks full

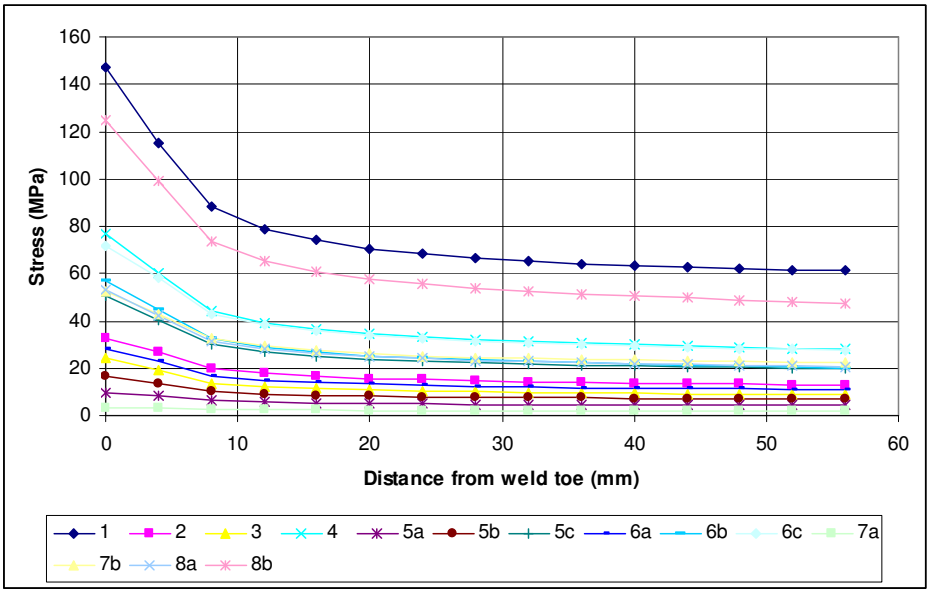

Figure 4.32: Predicted stress at a distance from the weld toe at IHS5

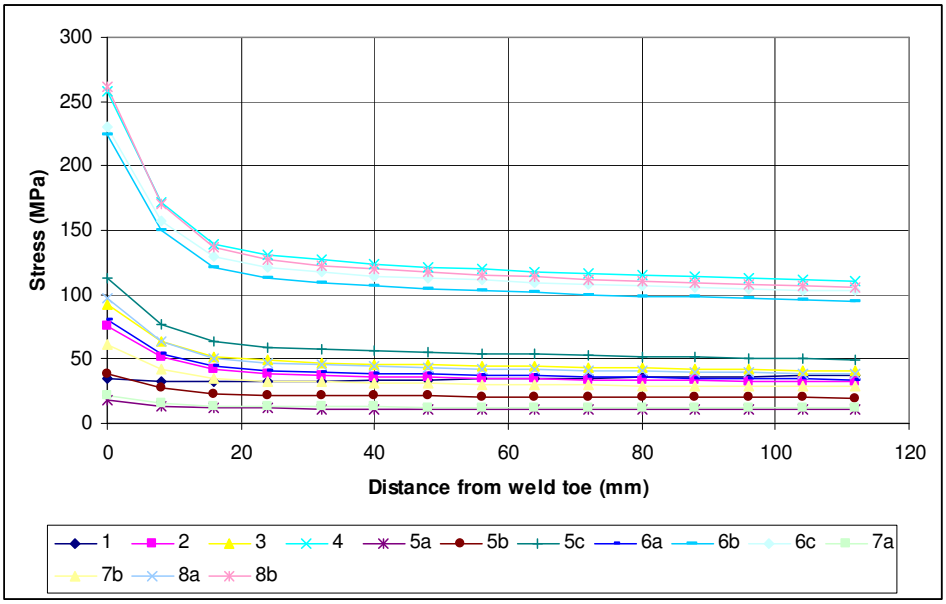

Figure 4.33: Predicted stress at a distance from the weld toe at IHS6

1 = Ballast
2 = 4COT half
3 = All COT half
4 = All COT full
5a = Odd COT half
5b = Odd Tanks full
5c = Odd COT full + Even COT half
COT = Cargo Oil Tank

6a = Even COT half
6b = Even COT full
6c = Even COT full + Odd COT half
7a = Alternate odd tanks half
7b = Alternate odd tanks full
8a = Alternate even tanks half
8b = Alternate even tanks full

4.6 Discussion

A literature review of the hotspot stress approach was presented at the beginning of the chapter. Finite element meshing techniques and extrapolation procedures are discussed. Several extrapolation methods are tested for the bottom longitudinal connection and the quadratic extrapolation method is selected as the most applicable to this research.

A critical finite element analysis of 18 possible crack locations at the bottom longitudinal, side longitudinal and inner side longitudinal connection is carried out. These locations are subjected to the selected low cycle load cases. These critical locations were selected based on industry experience and the global analysis of the whole structure. Industry experience has shown that the side shell details of FPSOs are highly susceptible to fatigue damage and a finite element analysis of the global model revealed that the bottom plating and its connections experienced high stresses. The predicted stresses at a selected distance from the weld toe are presented. From the finite element analysis, it is noted that the bottom detail of the FPSO undergoes very high bending stresses which generate local stresses in the connection. This is due to the structural configuration of the FPSO: single bottom and double sided.

Using the quadratic extrapolation method, the hotspot stresses at the selected potential crack locations are obtained. This is presented in Table 4.4. These stresses are obtained by reading the stresses at 4 mm, 8 mm and 12 mm from the weld toe and employing the quadratic extrapolation formula - $\sigma_{hs} = 3\sigma_{4mm} - 3\sigma_{8mm} + \sigma_{12mm}$. These hotspot stress values will determine the loading/ unloading stress cycles which is obtained from the loading and unloading sequences in Table 2.4 and will be used to calculate low cycle fatigue life. For BHS1 , for example, under loading sequence 1 will undergo a loading cycle from 41MPa to 145.79 MPa to 285.17 MPa and finally to 533.16 MPa.

Table 4.4: Hotspot Stresses for Low Cycle Load Cases (MPa)

			Hotspot Stress for Low Cycle Load Cases (MPa)													
Detail		Hotspots							Load Cases							
			1	2	3	4	5a	5b	5c	6a	6b	6c	7a	7b	8a	8b
		BHS1	41.79	145.79	285.17	533.16	130.70	214.55	367.97	192.06	354.92	441.89	121.37	129.67	119.86	125.05
		BHS2	58.54	291.30	500.30	948.85	197.82	323.74	624.46	359.46	680.74	813.91	191.27	295.33	318.03	546.61
Bottom Detail		BHS3	226.80	207.27	272.22	496.48	91.64	153.33	328.84	219.90	390.27	441.60	92.30	198.51	169.55	270.48
		BHS4	158.39	57.75	115.19	194.53	69.74	116.44	159.45	72.07	97.47	145.75	74.74	300.76	141.07	507.03
		BHS5	133.21	355.86	473.36	1007.59	117.95	200.30	554.94	385.14	836.79	928.97	134.05	448.07	520.38	1228.37
		BHS6	176.04	422.73	550.42	1154.36	145.17	247.26	648.46	449.37	957.80	1061.94	154.11	498.85	605.00	1385.37
		SHS1	764.06	111.95	216.79	281.64	105.56	138.20	111.11	209.05	111.83	246.04	111.83	246.04	160.50	203.69
		SHS2	353.55	73.26	119.07	250.89	49.08	90.47	160.01	83.85	176.42	218.53	53.02	114.60	93.91	215.34
Side Detail		SHS3	268.39	33.73	70.99	91.99	38.58	70.93	102.49	43.09	40.45	64.03	40.39	86.46	52.01	65.58
		SHS4	152.61	23.26	42.41	141.75	18.97	22.85	59.58	37.93	115.68	130.77	21.94	41.39	30.01	118.51
		SHS5	586.37	112.16	147.90	200.50	78.77	145.00	213.22	88.76	72.05	129.75	83.05	178.98	112.16	147.90
		SHS6	295.44	48.33	84.10	36.11	59.55	106.92	213.22	57.14	105.63	113.46	38.69	76.71	48.33	84.10
		IHS1	48.00	91.24	78.93	234.74	12.95	30.81	122.93	84.57	201.45	246.71	4.42	87.88	112.48	291.59
		IHS2	96.64	75.61	94.12	277.21	32.04	60.92	123.49	79.80	228.71	263.78	35.66	81.52	90.69	268.41
Inner Detail		IHS3	68.94	20.62	14.11	44.35	12.25	6.11	23.92	16.89	36.58	43.27	9.21	22.54	28.78	62.49
		IHS4	79.00	65.90	58.56	76.42	19.48	36.57	61.48	63.43	69.63	73.25	20.31	33.03	70.24	81.50
		IHS5	160.57	38.19	27.78	87.76	10.98	18.63	57.90	32.94	65.62	83.61	4.17	59.50	60.77	141.88
		IHS6	36.06	83.72	101.78	284.65	19.14	41.88	124.49	87.82	247.98	252.82	22.73	66.85	107.95	289.83

REFERENCE:

1. ABS (2010) 'Guide for Building and Classing Floating Production Installation'. American Bureau of Shipping, ABS Plaza Texas.
2. Almar- Naess A. (1999) 'Fatigue Handbook-Offshore Steel Structures'. Tapir forlag, Trondheim Norway.
3. Bergan P.G. and Lotsberg I. (2004) 'Advancement in Fatigue Assessment of FPSOs'. OMAE-FPSO
4. Dong P. (2001) 'A Structural Stress Definition and Numerical Implementation for Fatigue Analysis of Welded Joints'. International Journal of Fatigue. Volume 53 pp 865-876
5. Dong P. (2003) 'A Robust Structural Stress Method for Fatigue Analysis of Ship Structures'. OMAE-2003-37313
6. Dong P. and Hong J.K. (2003) 'Analysis of Hot Spot Stress and Alternative Structural Stress Methods'. OMAE-2003-37315
7. European Standard EN 1993-1-9:2005 'Eurocode 3: Design of Steel Structures – Part 1-9: Fatigue'.
8. Fricke W. (2001) 'Recommended Hot-Spot Stress Analysis for Structural Details of FPSOs and Ships based on Round-Robin FE Analyses'. Proceedings of the Eleventh International Offshore and Polar Engineering Conference.
9. Fricke W. (2003) 'Fatigue Analysis of Welded Joints: State of Development'. Journal of Marine Structures Volume 16 pp 185-200.
10. Fricke W. and Kahl K. (2005) 'Comparison of Different Structural Stress Approaches for Fatigue Assessment of Welded Ship Structures'. Journal of Marine Structures. Volume 18 pp 473-488
11. Fricke W., Bollero A., Chirica I., Garbatov Y., Jancart F., Kahl A., Remes H., Rizzo C.M., von Selle H., Urban A., Wei L. (2007) 'Round Robin Study on Structural Hot-spot and Effective Stress Analysis'. International Conference on "Advancements in Marine Structures" MARSTRUCT 2007, Glasgow, UK
12. Healy B. (2004) 'A Case Study of Surface Extrapolation and Battelle Structural Stress Methodologies'. OMAE-2004-51228
13. Heo J.H., Kang J., Kim Y., Yoo I., Kim K. and Urm H. (2004). 'A Study on the Design Guidance for Low Cycle Fatigue in Ship Structures'. PRADS 2004

14. Hobbacher A. (ed. 2005) ‘Recommendation for Fatigue Design of Welded Joints and Components’. IIW doc XIII-1965-03/XV-1127-032
15. Huther M. and Lieurade H. P. (1997) ‘Application of the Hotspot Stress Method’. Proceedings of the International Conference on Performance of Dynamically Loaded Welded Structure. New York: WRC, p. 332–8.
16. Kim M.H. and Kang S.W. (2008) ‘Testing and Analysis of Fatigue Behaviour in Edge Details: A Comparative Study Using Hot Spot Stress and Structural Stresses’. Ocean Engineering. Elsevier Limited.
17. Kim M.H., Kim M.S., Kim Y.N., Kim S.G., Lee K.E. and Kim G.R.(2009) ‘A Comparative Study for the Fatigue Assessment of Ship Structure by the use of Hot Spot Stress and Structural Stress Approaches’. Ocean Engineering. Elsevier Limited.
18. Lloyds Register (2008). ‘Ship Right FOI - Design, Construction and Installation- Floating Offshore Installation of Structures Design Guidance’. Lloyds Register EMEA.
19. Lotsberg I. (2004) ‘Recommended Methodology for Analysis of Structural Stress for Fatigue Assessment of Plated Structures’. OMAE-FPSO
20. Lotsberg I. and Landet E. (2004) ‘Fatigue Capacity of Side Longitudinals in Floating Structures’. OMAE-FPSO
21. Lotsberg I. and Sirgudsson G. (2004) ‘Hot Spot Stress S-N Curve for Fatigue Analysis of Plated Structures’. OMAE-FPSO
22. Maddox S.J (2001) ‘Recommended Hot-Spot Stress Design S-N Curves for Fatigue Assessment’. Proceedings of the Eleventh International Offshore and Polar Engineering Conference.
23. Marshall P.E and Wardenier J. (2005) ‘Tubular versus Non-Tubular Hotspot Stress Methods’. International Institute of Welding, IIW-XIII-XV-193-07
24. Niemi E. (1995) ‘Structural Stress Approach to Fatigue Analysis of Welded Components’. IIW XIII-1819-00
25. Niemi E. and Marquis G. (2001) ‘Introduction to the Structural Stress Approach to Fatigue Analysis of Plated Structures’. Proceedings of The IIW Fatigue Seminar, Tokyo Institute of Technology, 2002
26. Norman M. and Lotsberg I. (2001) ‘Fatigue Life Improvement of Scallops in Ships/FPSOs using Finite Element Analysis’. Proceedings of the Eleventh International Offshore and Polar Engineering Conference.

27. Partenen E. and Niemi E. (1996) 'Hot Spot Stress Approach to Fatigue Strength Analysis of Welded Components; Fatigue Test Data for Steel Plate Thickness up to 10mm'. Fatigue and Fracture of Engineering Materials and Structures, Volume 19 No 6, pp709-722.
28. Poutiainen I., Tanskanen P. and Marquis G. (2004) 'Finite Element Methods for Structural Hot Spot Stress Determination: a Comparison of Procedures'. International Journal of Fatigue. Volume 26 pp 1147-1157
29. Radaj D. (1990) 'Design and Analysis of Fatigue Resistant Structures'. Abington Publishing, Cambridge UK.
30. Rucho P., Maherault S., Chen W., Berstad A., and Samnoy G.E. (2001) 'Comparison of Measurements and Finite Element Analysis of Side Longitudinals'. Proceedings of the Eleventh International Offshore and Polar Engineering Conference. Pp 73-80.
31. Smith S., Maddox S., He W., Zhou D. and Saraswat R. (2008) 'Computer-Based Fatigue Analysis for Welded Joints- Third Progress Report'. TWI Report 16881/5/08
32. Storsul R., Landet E. and Lotsberg I. (2004) 'Calculated and Measured Stress at Welded Connections Between Side Longitudinals and Transverse Frames in Ship Shaped Structures'. OMAE-FPSO
33. Tveitven B.W., Wang X. and Berge S. (2007) 'Fatigue Assessment of Aluminium Ship Details by the Hot-Spot Stress Approach'. ABS Technical Papers.
34. Urm H.S., Yoo I.S., Heo J.H., Kim S.C. and Lotsberg I. (2004)."Low Cycle Fatigue Strength Assessment for Ship Structures". 9th Symposium on practical design of Ships and Other Floating Structures, Germany.
35. Wang X., Kang J.K., Kim Y. and Wirsching P. (2006)'Low cycle Fatigue of Marine Structures'. Proceedings of 25th International Conference of Offshore Mechanics and Arctic Engineering. OMAE 2006-92268
36. Xiao Z.G. and Yamada K. (2004) 'A Method of Determining Geometric Stress for Fatigue Strength Evaluation of Steel Welded Joints'. International Journal of Fatigue Volume 26:1277–93.
37. Xu L. and Barltrop N. (2007) 'Analysis of Sharp Corners in Structural Details'. International Conference on "Advancements in Marine Structures" MARSTRUCT 2007, Glasgow, UK

CHAPTER 5 FATIGUE DAMAGE

5.1 Introduction

Much of fatigue data available in literature has been generated from constant amplitude and constant frequency tests. Fatigue life prediction involves the use of a damage law, a method for cycle counting from a known stress history and a cumulative damage procedure using the fatigue properties of the material. Cycle counting methods are used to identify the constant amplitude stress ranges and the associated number of cycles present in a stress history. The damage accumulated due to these constant amplitude blocks is calculated individually and then summed using Palmgren – Miner's rule to obtain the total accumulated damage of the structure.

Most real life structures like ships rarely experience constant amplitude loading. When the stress history of the structure is known in advance, time domain analysis with a cycle counting method with an appropriate damage model is used to compute fatigue damage. A typical time domain analysis procedure is presented in Figure 5.1. Fatigue life prediction using data presented in the time domain involves calculations that can become very complicated (Barltrop and Adams, 2004). Although time domain analysis is easily applied to deterministic events, for random events as considered in offshore structures, a time domain solution represents only one realisation of the random process and cannot be taken as representative of the whole random process. Usually, many time histories are needed in order to formulate reliable statistical considerations about the distribution of rainflow cycles, the fatigue damage and the service life of the system (Benascutti and Tovo, 2006). This makes the approach, even if easy from a theoretical point of view, is very costly and time consuming. Alternatively, frequency domain approaches are applied.

Frequency domain analysis is based on spectral methods in which irregular stress response is modelled as a stochastic process. This process is described in the frequency domain in terms of its power spectral density (PSD) which gives a picture of the power distribution over frequencies, see Figure 5.2. Frequency domain methods are able to produce approximate analytical expressions by which cycle distribution

and fatigue damage under a cycle counting procedure can be obtained directly from the PSD of the stress. The analytical methods are explicit functions of some spectral bandwidth parameter which will become the main quantities controlling fatigue damage. In the frequency domain, calculations can be performed much more quickly at the acceptable cost of a slight reduction in accuracy. Another significant advantage of this is that the fatigue prediction process can be directly incorporated into control design. This approach is often the best where random signals span lengthy time series.

The main limitation of the frequency domain method is that there is no exact theoretical framework for the broadband Gaussian processes applied due to the complexity of cycle extraction rules which define the rainflow algorithm. This makes the relationship between rainflow cycle distribution and the process spectral density very complicated. Approximate methods have been developed following simple theoretical formulations. Most rely on fatigue damage and life estimation (Wirsching and Light, 1980), (Petrucci and Zuccarello, 2004) and some others address rainflow cycle distribution (Dirlik, 1985), (Zhao and Baker, 1992).

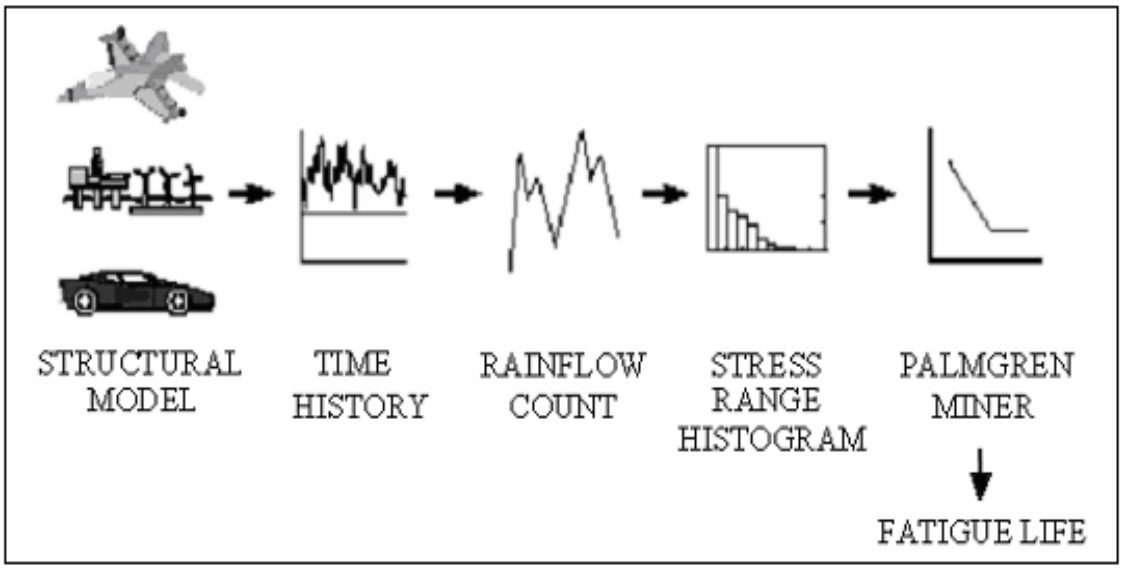

Figure 5.1: Time domain fatigue damage (Bishop and Sheratt, 2000)

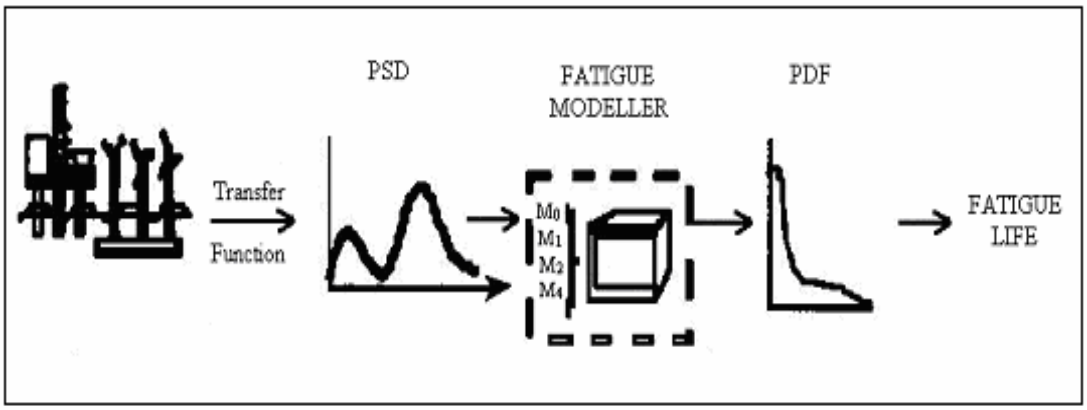

Figure 5.2: Frequency domain fatigue damage (Bishop and Sheratt, 2000)

5.2 Rainflow Counting and Fatigue Damage

5.2.1 Rainflow Counting

Counting methods was initially developed for the study of fatigue damage generated in aeronautical structures. Level crossing counting, peak counting, simple range counting, reservoir counting and rainflow counting methods are some of the commonly used counting methods available in literature and they count the either stress or deformation ranges. The rainflow counting method is the most popular cycle counting method and was developed by Prof. T. Endo (1969) and his colleagues in Japan.

The rainflow and reservoir counting methods are regarded as the most relevant to fatigue damage of welded joints (Maddox, 1991). Rainflow counting method produce a summation of stress ranges by combining positive and negative half-cycles and the reservoir technique employs a method which identifies complete cycles in terms of the stress range. The reservoir method is often convenient for hand calculations of short stress histories while rainflow counting is employed for computer application of longer and more complex stress histories (Barltrop, 2001). A detailed description of the rainflow and reservoir counting methods is presented in Appendix A.

5.2.2 Linear Damage Accumulation Law

Many cumulative damage theories have been proposed to improve fatigue life prediction. Fatemi and Yang (1998) and Collins (1993) have both published

comprehensive reviews of the available models that have been proposed to predict fatigue life of components using constant amplitude data. The most common linear damage rule was proposed by Palmgren and Miner. Palmgren first suggested the concept in 1924. The idea was further developed by Miner in 1945. Life estimates may be obtained by using the Palmgren-Miner's rule together with a cycle counting procedure. The aim is to estimate how many blocks of stress can be applied before failure occurs. This theory can be expressed using S-N plots.

From the S-N diagram below, the number of cycles of S_1 is N_1 which would cause failure if no other stresses were present. Operations at stress amplitude S_1 for a number of cycle's n_1 smaller than N_1 would produce a fraction of damage D_1. Operation over a spectrum of different stress levels result in a damage fraction D_i for each stress level S_i in the spectrum. Failure will occur if the fraction exceeds one.

$$D_1 + D_2 + ... + D_{i-1} + D_i \leq 1 \qquad 5.1$$

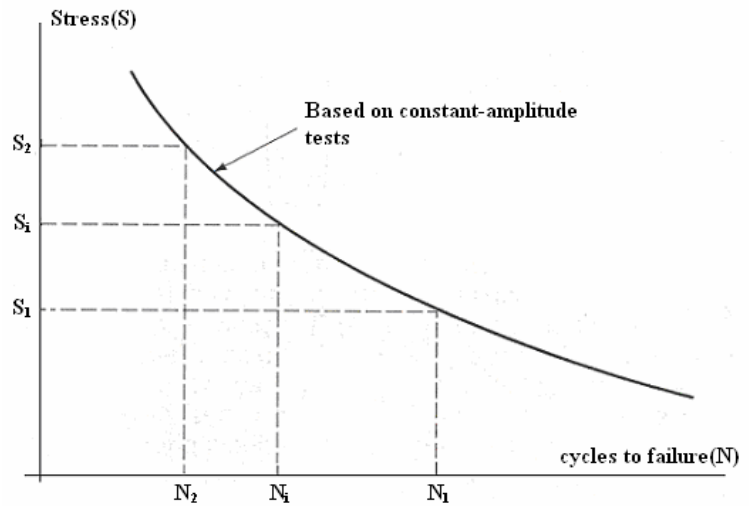

Figure 5.3: Constant Amplitude S-N curve (Collins, 1993)

According to Palmgren-Miner's rule, the damage fraction at any stress level S_i is linearly proportional to the ratio of the number of cycles of operation to the number of cycles that produces failure at that stress level. Total damage can then be defined as the sum of all the fractional damages over a total of n blocks.

$$D = \sum_{i=1}^{n} D_i \qquad 5.2$$

Where n_i is the number of load cycles applied at constant stress S_i and N_i is the fatigue life at stress S_i as obtained from the S – N curve. Miners damage criterion, D, is zero, therefore, failure occurs when D is equal to unity. Miner's rule has been accepted as a simple and effective model for predicting fatigue life under variable strain amplitude. The hypothesis was devised for use in the classical S-N fatigue analysis to allow for the problem of various stress ranges and variable numbers of associated cycles. There are however several limitations of this hypothesis:

- It does not recognise the probabilistic nature of fatigue and there is no simple way to relate predicted life by rules with the characteristic of a probabilistic distribution.
- There is sometimes an effect in the order in which the reversals occur. Sometimes, cycles of high stress followed by low stress cycle can cause more damage than would be predicted by the rule. (Load sequence effects are ignored. The theory predicts that damage caused by a stress cycle is independent of where it occurs in the load history.)
- The rate of damage accumulation is independent of the stress level. This does not usually correspond with observed behaviour. At high strain amplitude, cracks will initiate in a few cycles whereas a low strain, there is very little propagation failure.

Since the publication of Miner's work, the linear damage rule has been demonstrated to be unreliable. Wirsching et al (1995) and Lee et al (1996) show that the median damage values of test specimens under certain loading conditions range from 0.15 to 1.06. Despite these limitations, the linear damage rule is still the most applied damage calculation technique.

Several nonlinear theories have also been proposed to overcome the limitations of the linear damage rule. One of such theories was proposed by Richard and Newmark (1948) and later developed by Marco and Starkey (1954). Nonlinear theories have

been observed to have good correlation to observed material behaviour and can be used to determine damage in high temperature applications where creep is predominant.

5.2.3 Rainflow Fatigue Damage in Time Domain

Based on the distribution of rainflow cycles and the parameters of the S – N curve, the fatigue damage under Palmgren-Miner's law can be calculated from the following:

$$D_{RF} = \frac{n}{A}\int_0^\infty s^m p_{RF}(s)ds \qquad 5.3$$

where n is the number of stress cycles in total time and $p_{RF}(s)$ is the amplitude probability density function (PDF) of the rainflow cycles. From the above equation, the rainflow fatigue damage of a random process is dependent on the constant amplitude loading strength, the expected rate of occurrence and the distribution of the rainflow cycles through the marginal density.

The above definition of fatigue damage is not useful to frequency domain analysis because of the complication of the rainflow counting algorithm i.e. there is no explicit analytical solution for the distribution of rainflow cycles. The definitions of the rainflow cycles are set up in terms which are not amenable to statistical analysis, for this reason, all the methods existing in literature are approximate. The next section reviews some of the approaches relevant to the offshore industry.

5.3 Rainflow Counting in Frequency Domain

5.3.1 Response Statistics

When spectral analysis techniques are used, a Power Spectral Density (PSD) of stress is used as input from which a fatigue life estimate is required. The PSD is an alternative way of representing an equivalent time history of stress. The characteristics of the PSD function called nth moments are used to obtain the PDF of

the rainflow stress ranges. The relevant spectral moments are computed from the following function:

$$\lambda_n = \int_0^\infty f^n S(f) df \qquad 5.4$$

λ_n is the nth moment of the spectral density function and S (f) is the spectral density representing a random process. By means of spectral moments the following properties can be obtained:

Root mean square $\sigma = \sqrt{\lambda_o}$

Rate of mean upcrossings (mean upcrossings/sec) $\nu_0 = \sqrt{\lambda_2 / \lambda_0}$

Peak rates (peaks/sec) $\nu_p = \sqrt{\lambda_4 / \lambda_2}$

The spectral density can also be used to describe spectral width parameters. The most common is:

$\varepsilon = \sqrt{(1 - \alpha^2)}$ where bandwidth parameter $\alpha = \dfrac{\lambda_n}{\sqrt{\lambda_0 \lambda_{2m}}}$

Note that the index *m* can take non-integer values. The bandwidth parameters are dimensionless numbers. In a narrow band processes, they tend towards unity, while in broadband processes they approach zero (Lutes and Sarkani, 1997).

5.3.2 Fatigue Damage in Frequency Domain

The first frequency domain method for predicting fatigue damage from PSD's made use of the narrow band approach which assumes that the PDF of peaks is equal to the PDF of stress amplitudes. Bendat (1964) showed that the PDF of the peaks of a narrow banded signal could be represented by a Rayleigh distribution as the bandwidth reduced. He also assumed that all positive peaks in the time history would be followed by corresponding troughs of similar magnitude regardless of whether they formed stress cycles. For a narrow banded process, the probability density of the stress range σ is known to follow a Rayleigh distribution:

$$p(\sigma) = \frac{\sigma}{4\lambda_0} \exp\left(-\frac{\sigma^2}{8\lambda_0}\right) \qquad 5.5$$

In T seconds, the number of cycles of stress for the stress range is given by $\delta n = n * p(s)\delta s$. The fatigue damage associated with that band of stress cycles is:

$$\delta D = \frac{\delta n}{N} = \frac{\delta n}{A\sigma^{-m}} = \frac{n\left(\frac{\sigma}{4\lambda_0}\right)\exp\left(-\frac{\sigma^2}{8\lambda_0}\right)}{A\sigma^{-m}} \qquad 5.6$$

The expected fatigue damage is obtained by integrating equation 5.6 and gives

$$D_{NB} = \frac{n}{A}(8\lambda_0)^{m/2}\Gamma\left(1+\frac{m}{2}\right) \qquad 5.7$$

where A and m are properties of the S-N curve, λ_0 and σ are as described earlier.

If the process is not narrow-band as in offshore structures, the damage predicted is not exact but a narrow-band approximation of rainflow damage for a wide band process. It has been demonstrated that the narrow band solution gives conservative results when used to estimate the fatigue life of a wide band process (Rychlik, 1993). The reason lies in the assumption that peaks are matched with corresponding troughs of similar magnitude. Wide-band histories usually have smaller waves riding on a low frequency carrier. As Bendat (1964) assumes that all positive peaks are matched with corresponding values of similar magnitude, the damage is grossly exaggerated for wide-band histories as shown in Figure 5.4.

The need for a rapid fatigue analysis method based on frequency domain became apparent in the offshore industry in the eighties. Large jacket platforms were being designed and fatigue damages had to be avoided. Transient dynamic analysis proved too intensive for the time domain software available because of the large structural models and high number of load combinations. Dynamic wave and wind load was already provided in frequency domain so it was sensible to take advantage of a frequency domain analysis. The problem was now how to calculate a reasonable fatigue life using resultant PSDs from the frequency domain analysis.

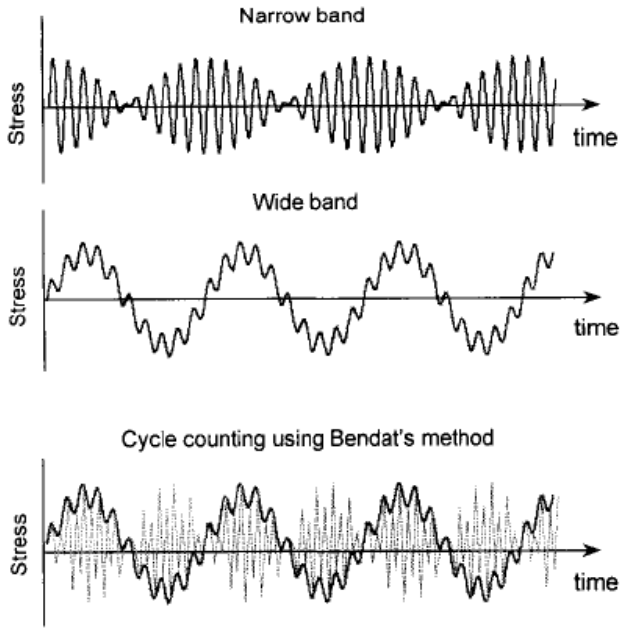

Figure 5.4: Halfpenny (1999) shows conservatism of narrow band method

Sea spectra are relatively wide-banded so several authors proposed modifications to the narrow band solution for application to offshore problems. One of the notable methods was by Wirsching and Light (1980) who proposed an empirical correction factor dependent on the slope of the S-N curve and a bandwidth parameter. This correction factor reduced the damage from the narrow band solution. This formulation was proposed for the offshore industry but has been found to be applicable to a wide range of industrial problems.

Kam and Dover (1988) and Gall and Hancock (1985) also proposed semi-empirical corrections based on the narrow band solution. The corrections are in the form of an equivalent stress parameter and experience has shown that they do not work particularly well outside offshore applications (Halfpenny, 1999).

In 1985, Dirlik proposed an approximate solution based on amplitude distribution following extensive simulations using Monte Carlo technique. This is the most famous empirical formula for the rainflow amplitude density which is approximated from the sum of an Exponential and two Rayleigh probability densities. Dirlik compared the rainflow ranges for signals to the zeroth, first, second and fourth moments of a PSD and produced an expression for the rainflow ranges.

$$p_{DK}(s) = \frac{1}{2\sqrt{\lambda_0}}\left[\frac{D_1}{Q}e^{-\frac{Z}{Q}} + \frac{D_2 Z}{R^2}e^{-\frac{Z^2}{2R^2}} + D_3 Z e^{-\frac{Z^2}{2}}\right] \qquad 5.8$$

Where $Z = \frac{\sigma}{2\sqrt{\lambda_0}}$ is a normalised amplitude and the following are the best fitting parameters:

$$x_m = \frac{\lambda_1}{\lambda_0}\left(\frac{\lambda_2}{\lambda_4}\right)^{1/2} \qquad Q = \frac{1.25(\alpha_2 - D_3 - (D_2 R))}{D_1}$$

$$D_1 = \frac{2\left(x_m - \alpha_2^2\right)}{1+\alpha_2^2} \qquad R = \frac{\alpha_2 - x_m - D_1^2}{1-\alpha_2 - D_1 + D_1^2}$$

$$D_2 = \frac{1-\alpha_2 - D_1 + D_1^2}{1-R} \qquad D_3 = 1 - D_1 - D_2$$

The approach proposes that the probability density function and damage depends on four spectral moments (i.e. $\lambda_0, \lambda_1, \lambda_2, \lambda_4$). The rainflow damage is obtained from:

$$D_{RF} = \frac{\nu_p}{A}\left(2\sqrt{\lambda_0}\right)^m \left[D_1 Q^m \Gamma(1+m) + \left(\sqrt{2}\right)^m \Gamma\left(1+\frac{m}{2}\right)\left(D_2 |R|^m + D_3\right)\right] \qquad 5.9$$

Halfpenny (1999) presented the concept of frequency domain fatigue analysis and reviewed existing methods concluding that Dirlik's method (Dirlik, 1985) is best recommended for general use. Many researchers have also pointed out the accuracy of Dirlik's formula as it constantly outperforms all other available methods. Its main limitation though, is that it is not supported by any theoretical justification. Bishop (1988) achieved this justification when a theoretical solution for predicting rainflow ranges from moments of area of the PSD was produced. Bishop's method is computationally intensive and shows little improvement form Dirlik's empirical approach.

Recently, Benascuitti and Tovo (2006) presented a comparison of spectral methods for fatigue analysis of wide band spectrum with focus on the distribution of rainflow cycles and the consequent fatigue damage calculated under the linear damage rule.

The narrow band approximation, Wirsching-Light correction formula, Dirlik's approximation, Zhao-Baker's method, Tovo-Benascuitti method and a new empirical method proposed by the authors are compared with results of time-domain calculation. This new empirical method assumes that the narrow band correction is dependent only on the $\alpha_{0.75}$ bandwidth parameter and is completely independent of the slope, m of the S-N curve. According to the authors, the most accurate methods are Dirlik's approximation, Zhao-Baker and Tovo-Benascuitti methods and the new empirical method respectively.

5.4 Combined Fatigue Damage

Ships and offshore structures are often subjected to the combined effect of high frequency and low frequency loads. If a linear structure is being considered, it is practical to determine the fatigue damage under the combined high frequency and low frequency loads by separately considering high and low frequency stress histories. It is however, non-conservative to obtain combined fatigue damage as a simple addition of the two fatigue damages because of the nonlinear relation of fatigue damage and stress. There are several methods available to calculate cumulative fatigue damage from the combined effect of high frequency and low frequency processes.

- Simple Summation
- Combined Spectrum
- Analytical Methods

5.4.1 Simple Linear Summation

In this method, damage from the low frequency process and that from the high frequency process are calculated independently and total damage of the structure is assumed to be the linear summation of the two.

$$D_T = D_1 + D_2$$

D_1 = Calculated fatigue damage from the high cycle loading

D_2 = Calculated fatigue damage from the low cycle loading

This method gives an acceptable estimate of fatigue life however; it may underestimate damages in cases where low frequency stresses are higher than high frequency stresses (API, 1995). A simple summation also does not account for the augmentation of the low-frequency stress amplitudes by the wave-frequency amplitudes. Simple summation is therefore non-conservative and should not be used (DNV, 2006). API (2005) suggests using this method as a guide for a typical fatigue calculation and employ other available methods to validate the result.

5.4.2 Combined Spectrum Method

The combined spectrum method is applied if the stresses from the high frequency and low frequency processes are both significant. Here, both the low and high frequency spectra are calculated separately and then added together to obtain a combined spectrum. The characteristics of the combined spectrum in terms of standard deviation and up-crossing rate are determined and then total damage is calculated based on these characteristics. This method is always conservative and may sometimes significantly overestimate actual fatigue damage (Andersen et al, 2008). The combined spectrum method has been used to determine damage of structures subjected to wave conditions described as a combination of swell and wind seas like in areas of West Africa. It is also employed in damage of station keeping systems for floating structures.

Andersen et al (2008) proposed a simple methodology based on the combined spectrum method to calculate the total fatigue damage in non-collinear wind generated sea and swell for an FPSO in the Norwegian seas. The method is used to calculate the fatigue damage of side shell longitudinal stiffeners at the mid-ship section. The fatigue damage was based on component-based spectral fatigue calculation and notch stress obtained from nominal stress and SCF specified in DNV CN30.7 (DNV, 2003). The relative contributions from sea and swell to the total damage are identified as well as the sea states and headings that contribute most to the total damage.

Hwang et al (2007) applied the combined spectrum method in obtaining the total damage due to swell and wind seas of the Agbami FPSO located in the west offshore of Nigeria. The combined spectrum method is also the basis for the formula for combined damage proposed by DNV.

DNV-RP-203 (2006) and Lotsberg (2005) presented a simple method for combining fatigue damage from two dynamic processes based on the combined spectrum method using rainflow counting. Constant stress amplitudes are considered as random processes and the method uses information from the mean zero up-crossing frequency and the calculated fatigue damage for each individual process.

$$D = D_1\left(1-\frac{\nu_2}{\nu_1}\right)+\nu_2\left[\left(\frac{D_1}{\nu_1}\right)^{1/m}+\left(\frac{D_2}{\nu_2}\right)^{1/m}\right]^m \qquad 5.10$$

where D_1 and D_2 are as defined earlier.

ν_1 = mean zero up crossing frequency for high cycle fatigue

ν_2 = mean zero up crossing frequency for low cycle fatigue

This formula was developed for narrow band frequencies. DNV in RP-206 (2006) modified the above formulation because it gave a high level of conservatism in fatigue damage results when applied to wide band processes. A level of conservatism in excess of 200 % is observed when the frequency ratio is larger than 10. A dual narrow-band correction factor is proposed. This factor is multiplied by the fatigue damage from the earlier formula and is recommended for use when the frequency ratio is greater than 4. It is noted that the correction factor greatly reduces the conservatism of the earlier approach. If the low frequency load is strongly dominant, this conservatism is lost (ISSC, 2009). This formulation is useful in mooring systems and risers subjected to low frequency stresses induced by vessel slow drift motions and wave frequency stresses.

ABS (2007) also uses the combined spectrum method for combined fatigue damage from a wave frequency and low frequency response. The stress spectra of the two frequency bands are combined using the same formula as DNV's method. The

combined spectra are a function of the root mean square of the stress ranges and the mean up crossing frequency.

5.4.3 Analytical Methods

Simple analytical methods have been proposed by several authors to estimate damage from the combined effect of high and low frequency process. The analytical procedure combines a damage accumulation law with a cycle counting method. For a combination of fatigue damage from two wide band processes, the analytical procedures covered in section 6.3 may be applied. The following are extensions of the narrow band method.

Jiao and Moan (1990) presented theoretical models for estimating fatigue damage under two narrow-banded -high and low frequency- Gaussian processes. The theoretical results are compared with results from extensive Monte Carlo simulations and cycle counting by rainflow method and found to be satisfactory. Gao and Moan (2006) extended this formulation to combination of non-Gaussian narrow-banded low and wave frequency mooring line tension of a semi-submersible.

Huang and Moan (2007) derived a formula for evaluating combined fatigue damage from Gaussian high and low frequency loads and extended it to a combination of non-Gaussian responses. The formula is derived by considering actual loads as stochastic processes not constant amplitude stresses as is the assumption in DNV formula. The numerical simulation showed that the predicted damage using the proposed method is very simple to use and close to rainflow prediction. The proposed method is compared with DNV formula and it was found that DNV's method may overestimate fatigue damage by 30 % up to more than 100%.

Another method for combining fatigue damages is based on the square root sum of the squares rule. This method is popular in random vibration analysis. The combination of damages is based on the assumption that the processes act at the same time but are independent of each other. Stress is proportional to the cube root of damage, the total damage is estimated from:

$$D_T = \left(D_1^{2/3} + D_2^{2/3} \right)^{3/2} \qquad 5.11$$

Barltrop (2010) compared the simple linear damage method and the square root sum of squares method for combining broad-band and deterministic fatigue damages in wind turbines. The linear procedure suggests a simple addition of the stress ranges while the quadratic method is more random. The linear method is safer than the quadratic method.

Heo et al (2007) performed experimental works to validate DNV's proposed method and the linear method for combining damages due to low cycle and high cycle loading. Fatigue tests on cruciform welded joints under various load cases were carried out. The fatigue test data was then compared with results from low cycle and high cycle fatigue tests respectively. Fatigue damage due to the combined fatigue tests were calculated and compared based on pseudo hot spot stress and nominal stress. Figure 5.5 illustrates the total damage calculated for different load cases using the different methods. The most accurate damage value was obtained from linear combination method with peak to peak range based on pseudo hotspot stress taking mean stress into account.

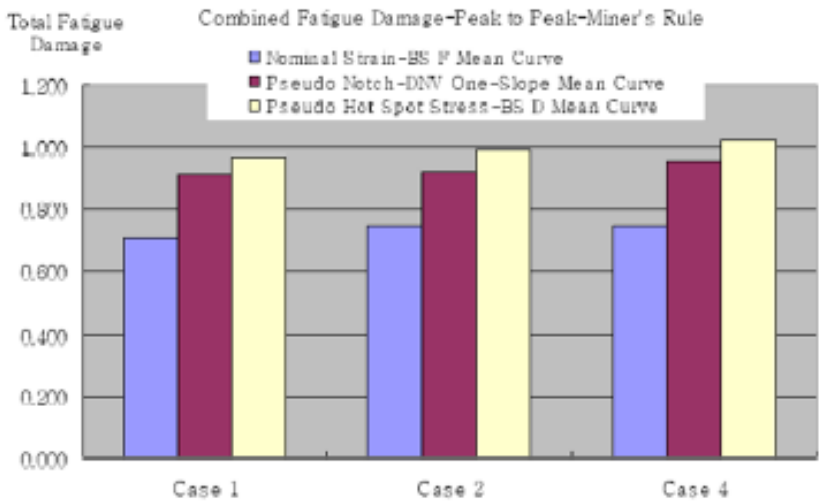

Figure 5.5: Comparison of total damage calculation methods (Heo et al, 2007)

The conclusion is that combined spectrum method gives a conservative estimate of damage when the two response spectra are independent. For dependent stress

responses like quasi-static wave response and springing response, the method is un-conservative.

5.5 Classification Society (CS) Rules for Combined Damage from Loading and Unloading and Wave Stress Cycles

Loading and unloading process produces very low frequency static loads including oscillatory still water bending moment (SWBM) and still water pressure. It is a general consensus that Palmgren-Miner's rule is the most convenient method of computing low cycle fatigue damage in welded joints. CS proposed methodologies are based on the assumption of rainflow counting technique and Miner's linear damage rule. Fatigue damage from low cycle loads can also be estimated using statistical methods. This involves expressing the low cycle fatigue loads in terms of a determining the root mean square value and the mean up-crossing frequency of the stress range based on either the loading manual or from observational data. The root mean square value of the stress is then combined with that induced by wave loads using the square root of the sum of the squares (SRSS) method to obtain a total damage value.

Lloyds Register (2008) proposes the following for the combination of damage from loading and unloading cycles and wave cycles:

$$D = D_{LCF} + D_{HCF} - D_{HCFadj} \qquad 5.12$$

D_{HCF} = High cycle fatigue damage

D_{LCF} = Low cycle fatigue damage $= \sum_{i=1}^{n} \frac{\left[k_e(\sigma_{LCi} + 0.5(\sigma_{HCTi} + \sigma_{HCBi})\right]^m}{c}$

n = number of low stress cycles

σ_{LCi} = ith highest stress range for low stress cycles

σ_{HCTi} = highest wave induced stress over the duration of the peak of σ_{LCi}

σ_{HCBi} = highest wave induced stress over the duration of the trough of σ_{LCi}

m = slope of S – N curve at 1000 cycles

c = intercept of S – N curve at 1000 cycles

D_{HCFadj} = the adjustment to account for high cycle fatigue cycles which have been included in the low cycle fatigue damage calculation.

$$= \sum_{i}^{n} \frac{1}{N[0.5(\sigma_{HCTi} + \sigma_{HCBi})]} \qquad 5.13$$

N (σ) = number of cycles obtained from reference S – N curve at stress range σ, assuming elastic strain.

$$= \frac{c}{\sigma^m}$$

Then, D_{HCFadj} may be rewritten as:

$$= \sum_{i}^{n} \frac{[0.5(\sigma_{HCTi} + \sigma_{HCBi})]^m}{c}$$

The low cycle fatigue damage is determined from an effective stress range. The effective stress range is the sum of the low cycle fatigue stress range and the wave stress range with the same return period. So that the fatigue damage for the low cycle process is increased by that effective stress range. As such, the number of loading/unloading cycles of the wave stress range becomes included in the low cycle fatigue calculation. This is subtracted in the D_{HCFadj} term so as not to include it twice.

LR state that the wave stresses may be calculated based on the combined stress history of the low stress and wave stress cycles. If the combined stress history is unknown, the highest wave stress range is assumed to occur in phase with the highest quasi-static stress peak. The second highest wave stress range should be assumed to occur in phase with the highest quasi-static stress trough and so on, i.e.

$$\sigma_{HCTi} = \sigma_{HC(2i-1)}$$
$$\sigma_{HCBi} = \sigma_{HC(2i)}$$

σ_{HCk} is the kth highest wave stress range over the design life of the FPSO.

ABS (2009) in the recent 'Guide for Fatigue Assessment of Ship-Type Installation' proposes the following:

$$D_T = \frac{D_{LCF}^2 + 2\delta D_{LCF} D_{HCF} + D_{HCF}^2}{\sqrt{D_{LCF}^2 + D_{HCF}^2}} \qquad 5.14$$

δ = 0.02

D_{LCF} = low cycle fatigue damage

D_{HCF} = high cycle fatigue damage

The low cycle fatigue damage is obtained using the equivalent stress concept as LR and Palmgren-Miner damage rule. DNV proposed the following for the combined damage due loading and unloading and wave frequency is:

$$D_T = \sqrt{D_{hcf}^2 + D_{lcf}^2} \le 1.0 \qquad \text{For } 0.25 \le D_{lcf} \le 1.0 \qquad 5.15$$

For low cycle fatigue damage less than 0.25, fatigue damage due to high cycle fatigue shall be satisfied:

$$D_{hcf} \le 1.0 \qquad \text{For } D_{lcf} < 0.25 \qquad 5.16$$

The following figure shows the requirement for combined fatigue damages based on this rule.

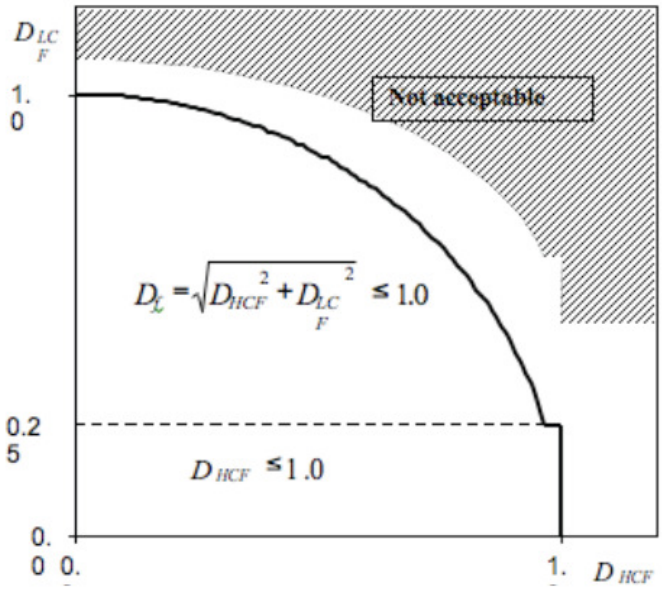

Figure 5.6: Combined Fatigue Damages (Winterstein, 2010)

5.6 Summary

Winterstein (2010) compared several proposed combination rules from damage due to low cycle loads (loading and unloading) and damage due to high cycle loads i.e. wave loading on FPSOs. Lotsberg's method, the random vibration approach which is based on adding variances of the stresses, the simple linear summation and quadratic summation method based on the square root of the sum of squares (SRSS) not variance. The combined spectrum method using the square root sum of squares stress gave the least conservative fatigue damage result as it resulted in the largest safe region as illustrated in Figure 5.7.

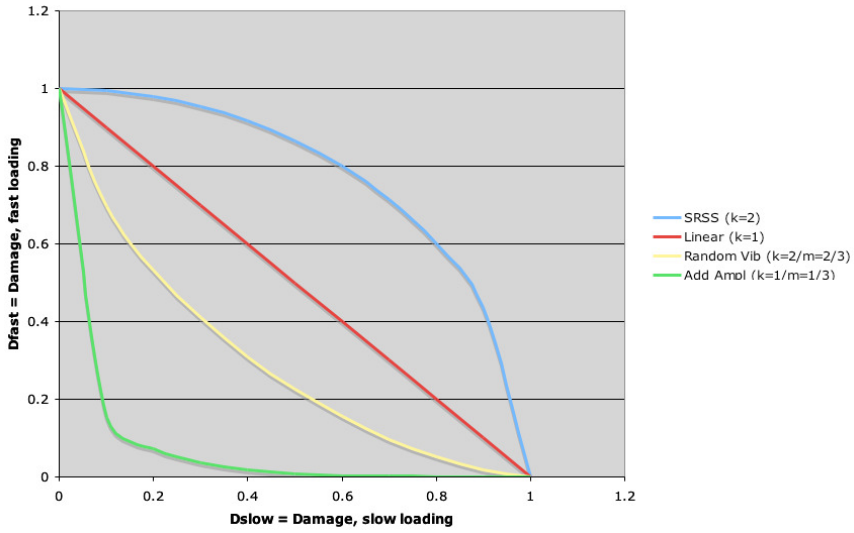

Figure 5.7: Combined Damage

The combined spectrum method for the combined fatigue damage has been developed for two dynamic processes and can be represented in a spectral form. The stresses caused by loading and unloading operations in an FPSO are usually represented by a series of still water load cases from which cyclic stresses are computed for the fatigue prone areas and cannot be represented in a spectral form.

The proposed CS rules for fatigue damage are similar in that they are all based on the assumption of rainflow counting technique and Miner's linear damage rule. The stress range from low cycle stress is enhanced by the peak stresses from the high cycle wave loading occurring at the same time as the low cycle loads. LR and DNV include an

adjustment factor to the total damage which is to account for high cycle fatigue stresses already included while counting the low cycle stress ranges. This adjustment to the total fatigue damage is considered by ABS is the form of a constant. Generally this factor is a relatively small value compared to the overall fatigue and may have a negligible effect on the total fatigue damage of the structure.

In this thesis, high cycle fatigue damage will be determined using Dirlik's rainflow approximation method. The stress cycles from the low cycle loading will be counted using the rainflow technique and Palmgren-Miner's rule will be used to calculate the damage. The CS rules for combined fatigue damage will be compared.

REFERENCE

1. ABS (2004) (updated 2007) 'Spectral-based Fatigue Analysis for Vessels'. American Bureau of Shipping, ABS Plaza Texas.
2. ABS (2009 updated 2010) 'Guide for Building and Classing Floating Production Installation'. American Bureau of Shipping, ABS Plaza Texas.
3. Andersen O.J., Haver S., Oma N., Rognebakke O., and Sado O. (2008) 'Fatigue Assessment of Side Shell Details of an FPSO based on Non-collinear Sea and Swell'. Proceedings of ASME 27th International Conference on Offshore Mechanics and Arctic Engineering. OMAE 2008-57241
4. API (1995) 'Recommended Practice for Design and Analysis of Station-keeping Systems for Floating Structures'. American Petroleum Institute, Dallas.
5. ASTM E 1049-05. (Reapproved 2005). 'Standard Practices for Cycle Counting in Fatigue Analysis'. ASTM International.
6. Barltrop N. (2010) 'Wind Turbine Broadband + Deterministic Fatigue'. University of Strathclyde.
7. Barltrop N. (2001) 'Marine Materials and Structures'. Course notes, Department of Naval Architecture and Marine Engineering. University of. Glasgow
8. Barltrop N. and Adams A. (2004) 'Dynamics of Fixed Marine Structures'. MTD Limited/ Butterworth and Heinemann.
9. Benascuitti D. and Tovo R. (2006) 'Comparison of Spectral Methods for Fatigue Analysis of Broad-band Random Processes'. Probabilistic Engineering Mechanics 21 pp 287-299
10. Bendat J.S. (1964) 'Probability Functions for Random Responses'. NASA Report on contract NAS-5-4590
11. Bishop N.W.M (1988) 'The Use of Frequency Domain Parameters to Predict Structural Fatigue'. PhD Thesis, University of Warwick, UK
12. Bishop N.W.M and Sheratt F. (2000) 'Finite Element based Fatigue Calculations'. NAFEMS International Association for the Engineering Analysis Community.

13. Collins J.A. (1993) 'Failure of Materials in Mechanical Design: Analysis, Prediction and Prevention'. Second Edition, John Wiley and Sons Inc.
14. Dirlik, T. (1985): Application of Computers in Fatigue Analysis' PhD Thesis, University of Warwick, UK
15. DNV (2009) 'Offshore Standard DNV-OS-E301: Position Mooring'. Det Norske Veritas Offshore Codes.
16. DNV-CN30.7 (2003)' Fatigue Assessment of Ship Structures'. Det Norske Veritas.
17. DNV-RP-C203 (2006)' Fatigue Methodology for Offshore Ships'. Det Norske Veritas.
18. DNV-RP-C206 (2010)' Fatigue Design of Offshore Steel Structures'. Det Norske Veritas
19. Dowling N.E (2007) 'Mechanical Behaviour of Materials –Engineering Methods for Deformation, Fracture and Fatigue'. Third Edition, Prentice Hall USA.
20. Fatemi A. and Yang L. (1998) 'Cumulative Fatigue Damage and Life Prediction Theories: a Survey of the State of the Art for Homogenous Material'. International Journal of Fatigue. Volume 20 No. 1. pp 9-34
21. Gall D.S. and Hancock J.W. (1985) 'Fatigue Crack Growth under Narrow and Broad Band Stationary Loading' Report Glasgow University Marine Technology Centre, Glasgow
22. Gao. Z. and Moan T. (2006) 'Wave Induced Fatigue Damage of Mooring Chain under Combined Non-Gaussian Low and Wave Frequency Loads'. Proceedings of ASME 25th International Conference on Offshore Mechanics and Arctic Engineering. OMAE 2006-92389.
23. Halfpenny A. (1999) 'A Frequency Domain Approach for Fatigue Life Estimation from Finite Element Analysis'. Key Engineering Materials Volume 167-168 pp 401-410.
24. Heo J.H., Kang J.K., Kim K.S. and Urm H.S. (2007) 'A Study of Fatigue under Combined Tensile and Compressive Mean Stresses in Ship Structures'. 10th International Symposium on Practical Design of Ships and other Floating Structures, Texas, USA.

25. Huang W. and Moan T. (2007) 'Fatigue under Combined High and Low Frequency Loads'. Proceedings of ASME 25th International Conference on Offshore Mechanics and Arctic Engineering. OMAE 2006-92247.
26. Hwang O.J., Kwon S.M., Park G.W., Kang J.K., and Heo J.H. (2007) 'Spectral Fatigue Assessment of Agbami FPSO Hull for Onsite and Seagoing as per ABS SFA Guidance'. Proceedings of ASME 26th International Conference on Offshore Mechanics and Arctic Engineering. OMAE 2007-29392
27. ISSC (2009) 'Committee III.2 Fatigue and Fracture'. 17th International Ship and Offshore Congress. Korea.
28. Jiao G., Moan, T. (1990), Probabilistic Analysis of Fatigue due to Gaussian Load Processes'. Probabilistic Engineering Mechanics, Vol.5 No.2 pp.76-83.
29. Kam J.C.P. and Dover W.D. (1988) 'Fast Fatigue Assessment Procedure for Offshore Structures under Random Stress History' Proceedings of the Institute of Civil Engineering, Part 2 85 pp 689–700.
30. Lee Y., Lu M., Segar R.C., Welch C.D., and Rudy R.J. (1996) 'Reliability-Based Cumulative Fatigue Damage Assessment in Crack Initiation'. International Journal of Materials and Product Technology. Volume 14, No 1 pp1-16.
31. Lloyds Register (2008). 'Ship Right FOI - Design, Construction and Installation- Floating Offshore Installation of Structures Design Guidance'. Lloyds Register EMEA
32. Lotsberg I. (2005). 'Background for Revision of DNV-RP-C203 Fatigue Analysis of Offshore Steel Structure'. Proceedings of ASME 24th International Conference on Offshore Mechanics and Arctic Engineering. OMAE 2005-67549.
33. Lutes L.D., Sarkani S. (1997) 'Stochastic Analysis of Structural and Mechanical Vibrations'. Prentice-Hall.
34. Maddox S.J. (1991) 'Fatigue Strength of Welded Structures' Second Edition, Abington Publishing, England
35. Marco S.M. and Starkey W.L. (1954) 'A Concept of Fatigue Damage' Transactions of the ASME Volume 76 pp. 627–632.

36. Matsuiski M. and Endo T. (1969) ‘Fatigue of Metals Subjected to Varying Stress’. Japan Society of Mechanical Engineering
37. Petrucci G. and Zuccarello B. (2004) ‘Fatigue Life Prediction under Wide Band Random Loading’. Fatigue and Fracture of Engineering Materials and Structures, Volume 27 pp 1183-1195
38. Rice R.C. (1997) ‘SAE Fatigue Design Handbook’. Third Edition. Society for Automotive Engineers.
39. Richard F. E. and Newmark N. M. (1948) ‘A Hypothesis for the Determination of Cumulative Damage in Fatigue’ Proceedings American Society for Testing and Materials, 48, 767-800.
40. Rychlik, I. (1993): On the Narrow-and Approximation for Expected Fatigue Damage. Probabilistic Engineering Mechanics 8 pp 1-4
41. Winterstein S. (2010) ‘Fatigue of Offshore Structures: Application and Research Issues’. University of Stanford
42. Wirsching P.H. and Light M.C. (1980) ‘Fatigue under Wide Band Random Stresses’. Journal of the Structural Division ASCE 106 (1980), pp. 1593–1607.
43. Wirshing P.H., Paez T.L., and Ortiz H. (1995) ‘Random Vibration: Theory and Practice’. Wiley and Sons, New York.
44. Zhao, W.; Baker, M.J. (1992): On the Probability Density Function of Rainflow Stress Range for Stationary Gaussian Processes’. International Journal of Fatigue, vol. 14(2), pp. 121-135.

CHAPTER 6 ANALYSIS RESULTS

6.1 Low Cycle Fatigue Analysis

6.1.1 Loading /Unloading Cycles

Based on the quasi static load cases in Table 2.4, five operational scenarios are derived. The loading sequences start and end with a ballast state:

1. Sequence 1 (1-2-3-4-1): The central cargo oil tank (COT) is loaded to 50 % capacity. All the other tanks are then loaded to 50 % capacity. They are now filled to full capacity at the same time and unloading at the same time. This is the only real case operational scenario obtained from operators. It is employed by the operators of the Anasuria as one of their loading/unloading process. The remaining operational profiles are purely academic.
2. Sequence 2 (1-5a-5b-5c-4-1): The cargo oil tanks 1, 3, 5 and 7 are filled to 50 % capacity together. Then the even numbered tanks are filled to 50 % capacity. Tanks 1, 3, 5 and 7 are then filled to full capacity before finally filling the even numbered tanks to full capacity. All COT's are then unloaded.
3. Sequence 3 (1-6a-6b-6c-4-1): This is a reverse of sequence 2. The even numbered tanks are filled to 50 % capacity and then the odd numbered tanks are filled to 50 % capacity. Tanks 2, 4 and 6 are filled to full capacity and then the odd number tanks are filled fully.
4. Sequence 4 (1-7a-7b-4-1): In this loading operation, alternate cargo oil tanks are filled. 1COT port, 2COT starboard, 3COT port and so on are filled to full capacity before filling the other tanks.
5. Sequence 4 (1-8a-8b-4-1): This loading operation is a reverse of sequence 4. Here, alternate cargo oil tanks are filled. 1COT starboard, 2COT port, 3COT starboard and so on are filled to full capacity before filling the other tanks.

6.1.2 Hotspot Stress Cycles

The most critical stress cycle based on the loading and unloading sequence listed above for the details studied is presented in the following section. The stress cycles

are determined from the loading and unloading operational sequences. The stress ranges are then obtained from the stress cycles using a cycle counting procedure.

Bottom Detail Connection

The most critical stress cycles based on the sequence of loading and unloading of the cargo oil tanks listed above for the bottom detail is at BHS5 and BHS6 respectively. This is illustrated in Figure 6.1 and 6.2 respectively (see also Figure 4.14a and b).

In Figure 6.1, the stress ranges for the loading and unloading sequences considered vary between 800 and 1000 MPa, with SEQ5 causing the maximum stress range. The stresses are about three times the yield stress of the material. The maximum stress range at BHS6 of 1200 MPa is also caused by loading sequence SEQ5 as shown in Figure 6.2. The operational scenario in loading sequence SEQ1 was obtained from industry operators and shows from the analysis that it generates less critical stress range for the both hotspots than the other scenarios.

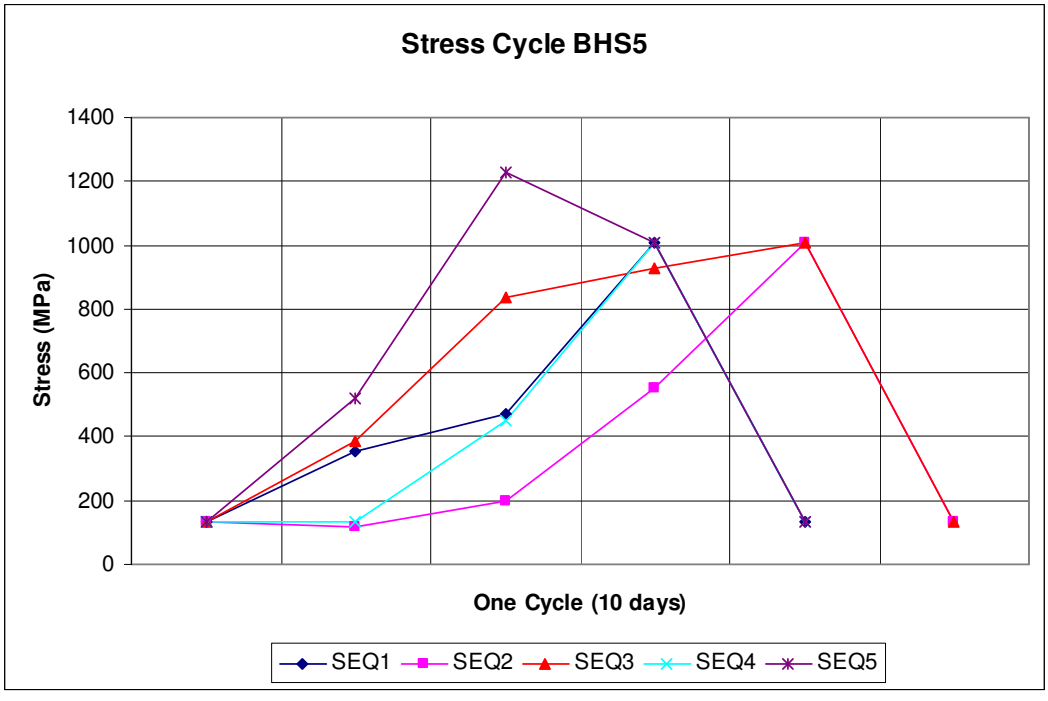

Figure 6.1: Hotspot stress cycles at BHS5

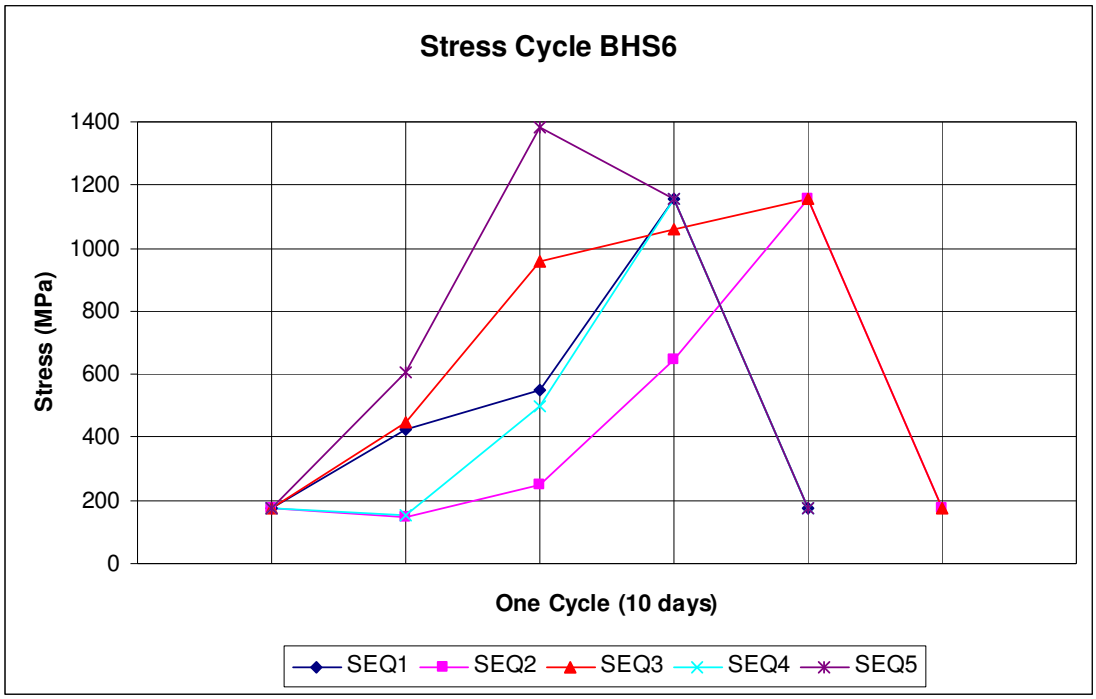

Figure 6.2: Hotspot stress cycles at BHS6

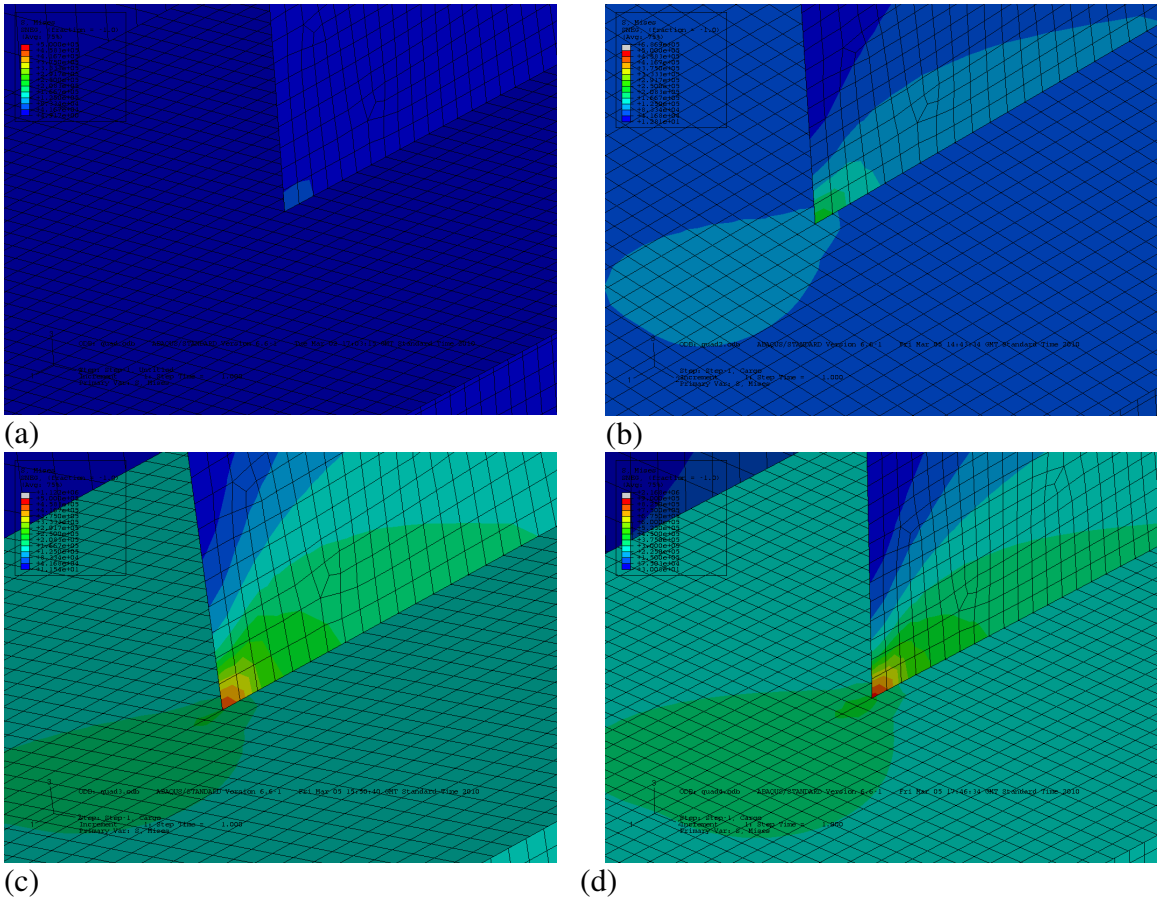

Figure 6.3: Stress contours for loading sequence, SEQ1 at BHS1

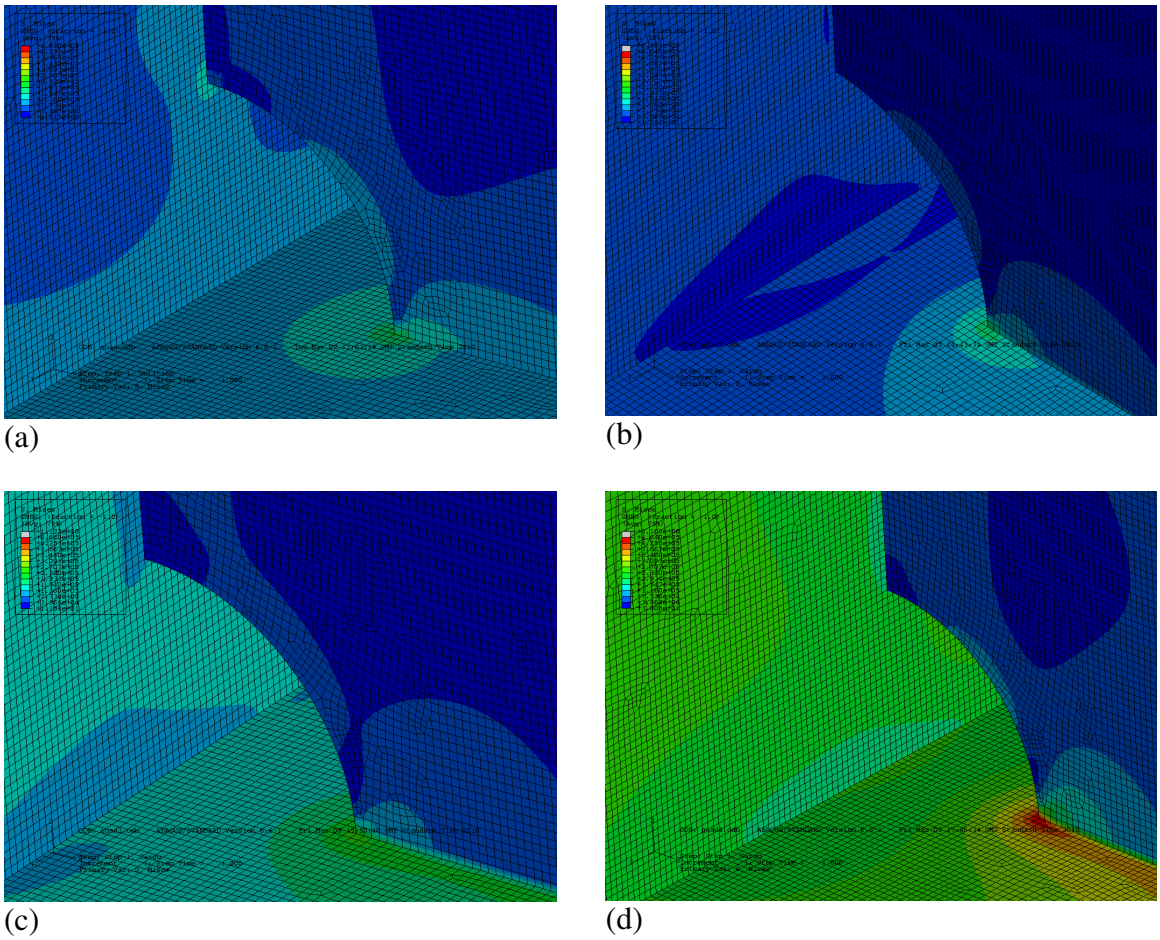

Figure 6.4: Stress contours for loading sequence, SEQ1 at BHS3 and BHS4

Figure 6.3 illustrates the stress contours for operational sequence SEQ1 at the location BHS1. Figure 6.3a shows the stress contours when the connection is subjected to ballast loading, Figure 6.3b is the stress contours at BHS1 when the central cargo oil tank is loaded halfway. Figure 6.3c and 6.3d represents the stress contours when the all the cargo oil tanks are half filled and then completely filled.

The stress contours for the same operational sequence at locations BHS3 and BHS4 is illustrated in Figure 6.4. The stress increase at the hotspot locations is obvious in the plots. In both figures, the maximum stress occurs when the FPSO is fully loaded.

Side Plating Detail Connection

The maximum hotspot stress cycle in this detail occurred at locations SHS1 and SHS5 respectively and is presented in Figure 6.5 and Figure 6.6 (see also Figure 4.21a, b and c). For SHS1, the maximum stress range at the location is 658.49 MPa. The most critical single load case is the ballast loading and in both cases loading sequence SEQ3 generates the highest range of stress. In both figures, it can be seen that the sequence of loading and unloading does not significantly affect the stresses in the side shell detail as the stress ranges varies from 604 MPa for SEQ5 to 658.4 MPa for SEQ2 at SHS1 and 474.21 MPa for SEQ1 to 514.31 MPa for SEQ3.

Figure 6.7a to 6.7d further illustrates the stress contours from the finite element model analysis at locations SHS3 and SHS5. Figure 6.7a is the stress contours due to ballast loading and Figure 6.7b is the stress contours when the central cargo oil tank loaded to 50 % capacity. Figure 6.7c represents stress contours when the all the cargo oil tanks in the FPSO are filled to 50 % capacity and Figure 6.7d shows the stress contours when all the tanks are completely filled.

The plots in Figure 6.8a to 6.8e illustrate the stress contours at locations SHS1 and SHS2 for loading operation SEQ2. Figure 6.8a shows stress contours for ballast loading and this is notably the most critical, generating the highest stresses. Figure 6.8b is the stress contours for the detail when the odd numbered cargo oil tanks are filled to 50 % capacity. Figure 6.8c is when the odd numbered tanks are fully loaded. Figure 6.8d shows the stress contours when the odd numbered tanks are at full capacity and the even numbered tanks are filled to 50 % capacity. Finally Figure 6.8e shows stress contours when all the tanks are fully loaded.

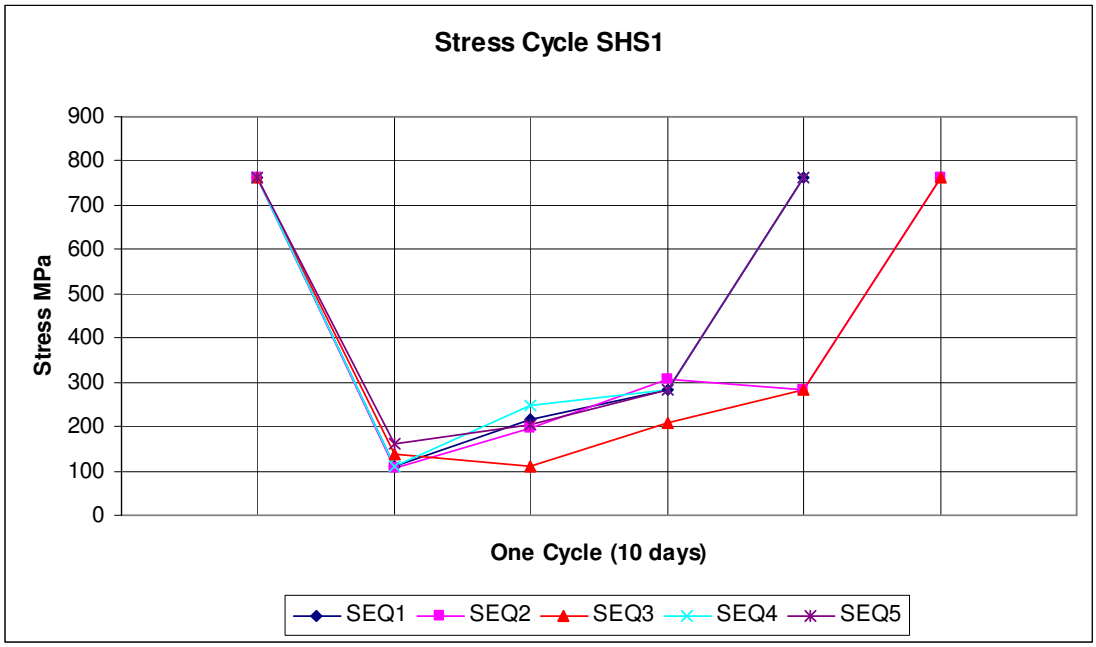

Figure 6.5: Hotspot stress cycles at SHS1

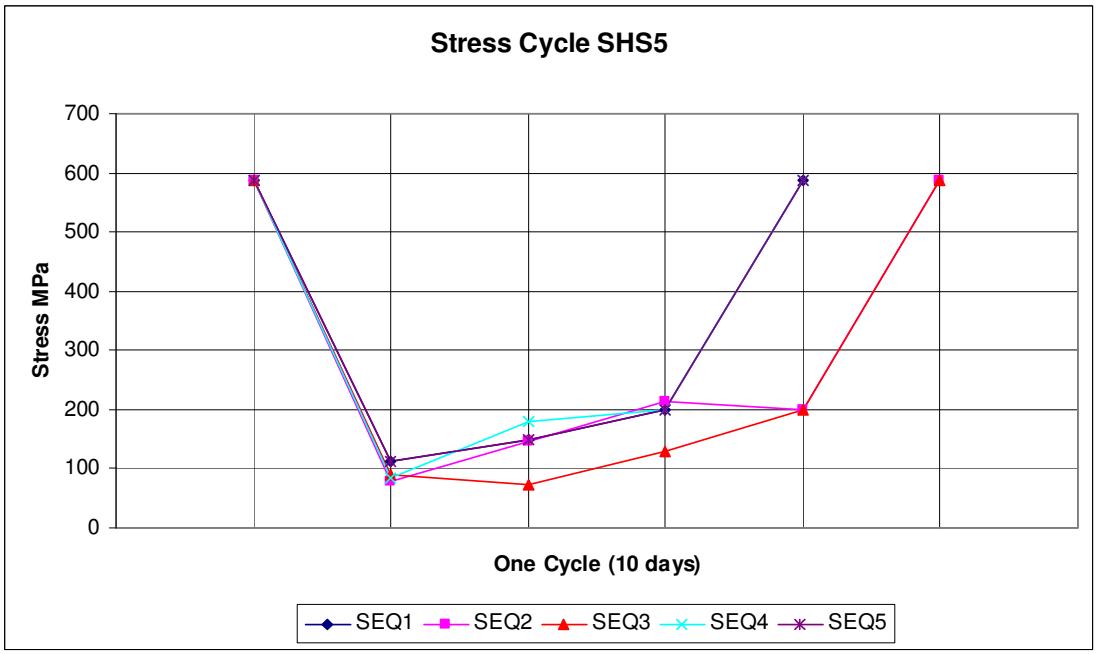

Figure 6.6: Hotspot stress cycles at SHS5

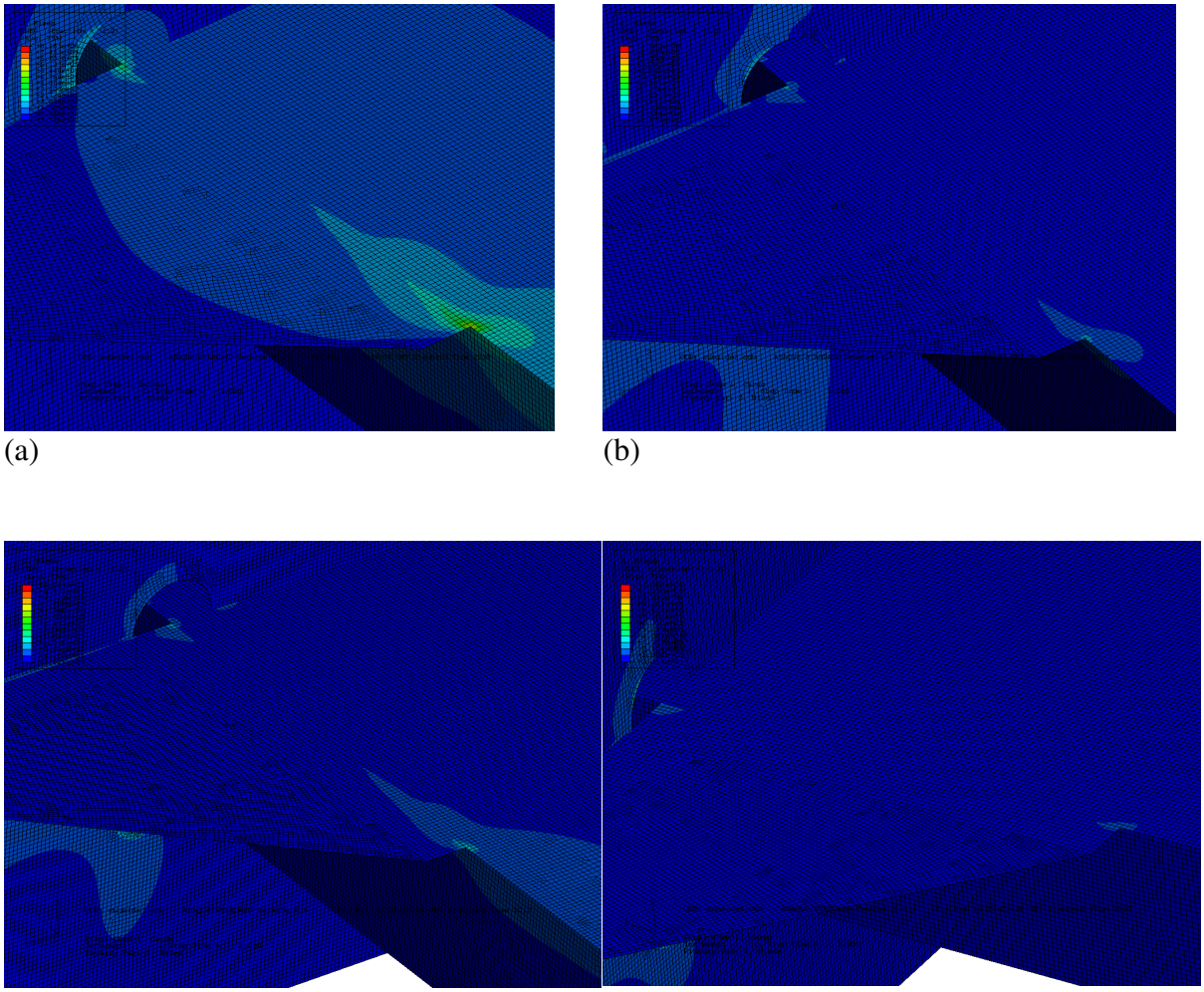

(a) (b)

(c) (d)

Figure 6.7: Stress contours at SHS3 and SHS5 for SEQ1

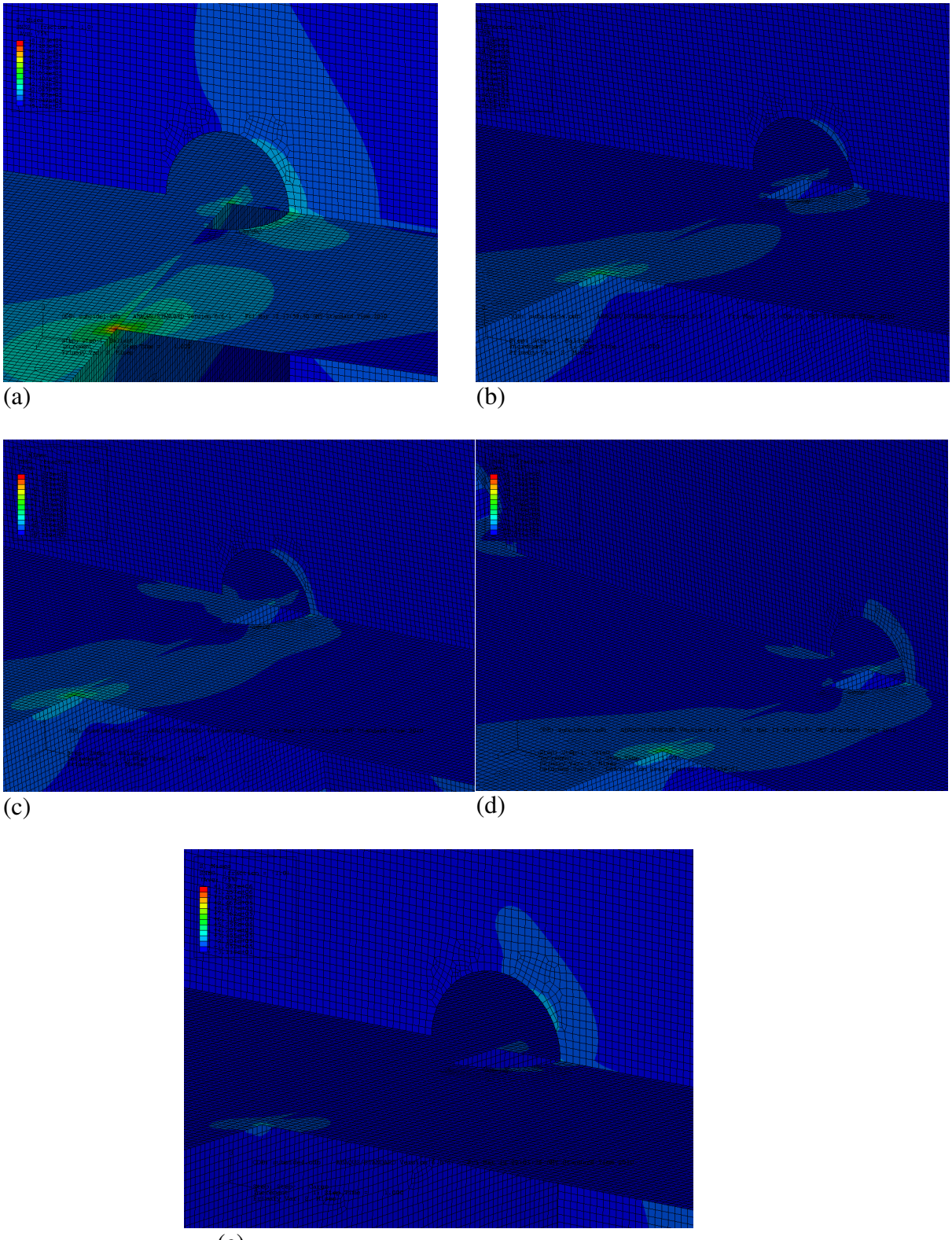

(a) (b)

(c) (d)

(e)

Figure 6.8: Stress contours at SHS1 and SHS2 for SEQ2

Inner Side Detail Connection

Figure 6.9 illustrates the most critical stress range obtained for this detail, which occurred at location IHS2 (see also Figure 5.21a, b and c). The ranges obtained – 1846.5 MPa for SEQ5 to 245.17 MPa for SEQ2 - are less than the yield stress of the material and not as significant as the ranges obtained from the other details. A maximum stress of 277 MPa is generated when the structure is subjected to a fully loaded condition. Figure 6.10 is shown to indicate that the loading sequence has very little effect on this detail.

Figure 6.11a to 6.11d illustrates the stress contours at IHS1 for loading operation 5. Figure 6.11a and 6.11d are the stress contours for ballast and fully loaded states respectively. Figure 6.11c and 6.11d shows the stress contours when alternate port and starboard tanks are at 50 % capacity and then loaded to full capacity.

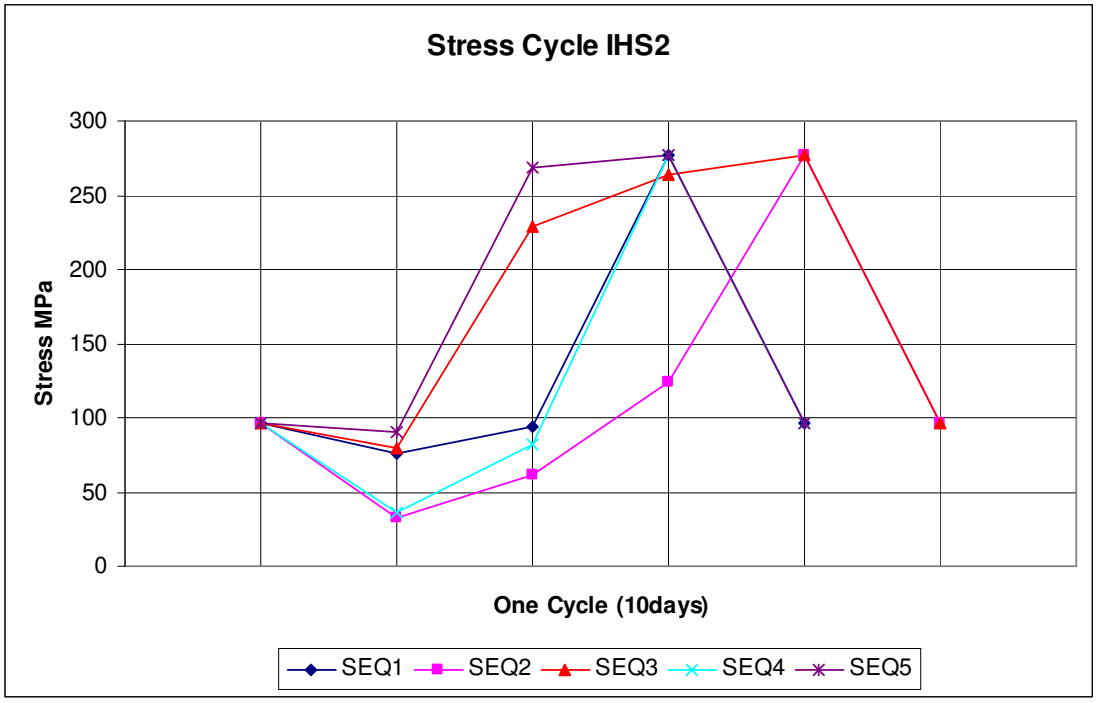

Figure 6.9: Hotspot stress cycles at IHS2

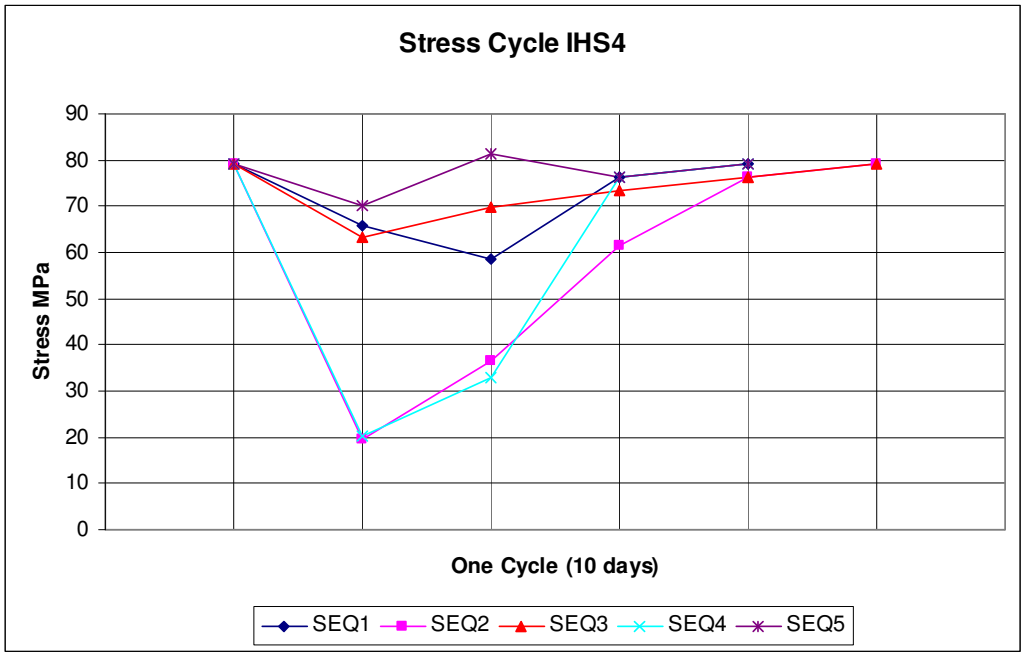

Figure 6.10: Hot spot stress range at IHS4

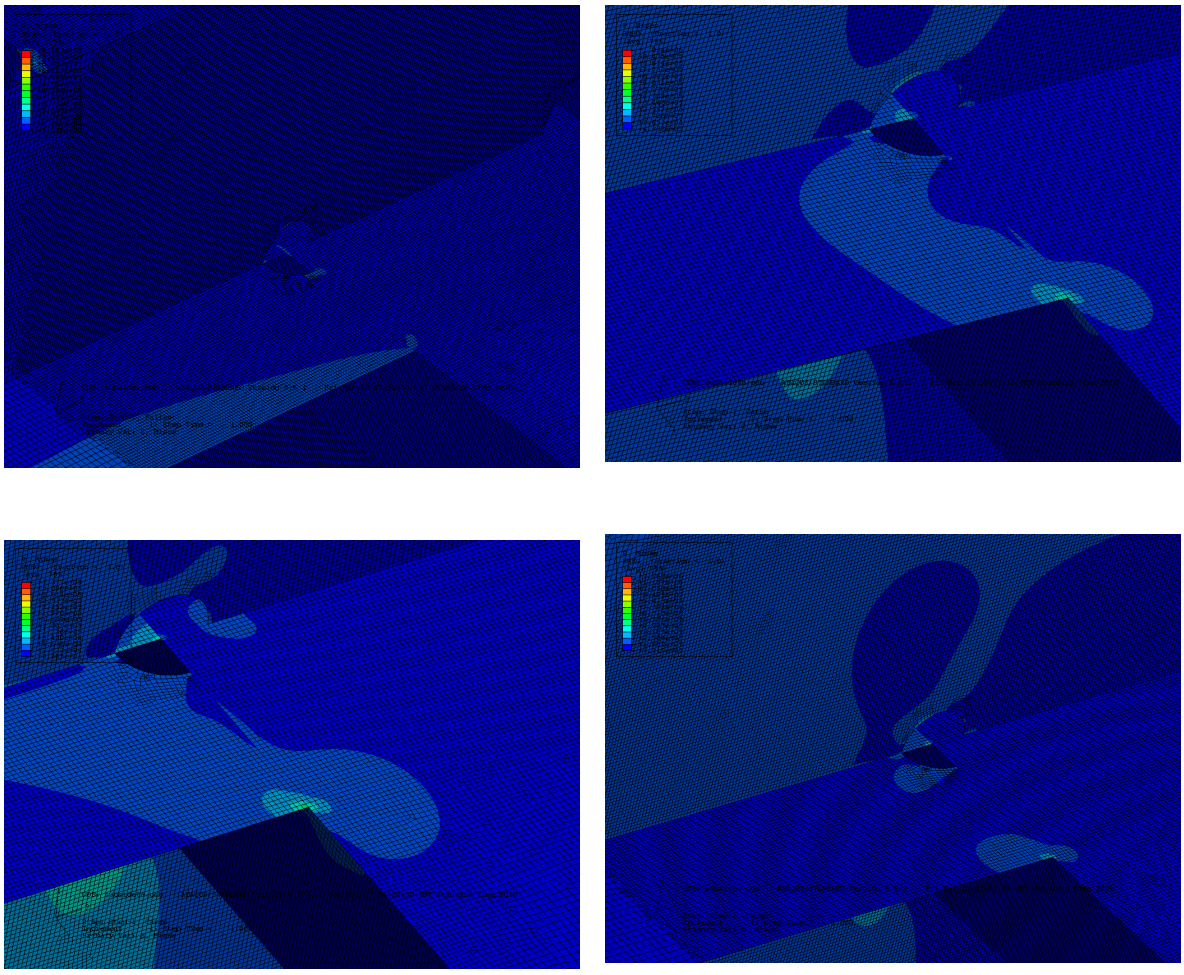

Figure 6.11: Stress contours at IHS1 SEQ5

From the results shown above, it is clear that the sequence of loading and unloading affects the potential crack locations in different parts of the structure in varying ways. SEQ5 generates the most critical stress in the bottom structural detail while SEQ3 and SEQ2 are the most critical loading sequence for the side detail connection and the inner side detail connection respectively.

Figure 6.12 illustrates the magnitudes of the maximum stress ranges - irrespective of the operational sequence - for all the critical locations. This plot shows that loading and unloading cycles can generate very high stresses and that for this FPSO; the bottom detail is more susceptible to the loading and unloading cycles than other locations.

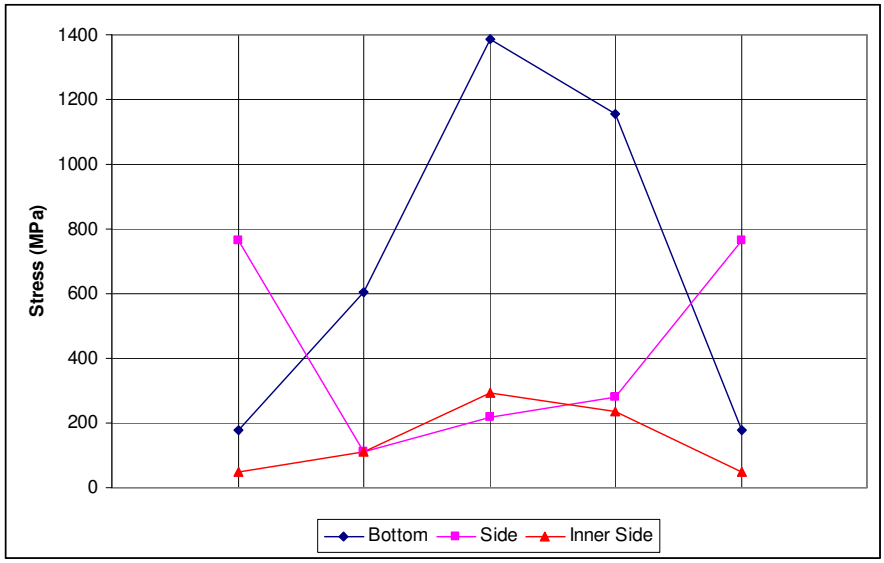

Figure 6.12: Maximum low cycle stress cycles for each detail

6.1.3 Low Cycle Damage

A typical loading and unloading cycle based on the finite element analysis data presented in section 6.1.2 is shown in Figure 6.13. The x-axis shows the cycles of loading and unloading, which is 10 days and the y-axis gives the magnitude of the stress. The stress range may be obtained from the formula:

$$\Delta\sigma = \sigma_{max} - \sigma_{min}$$

Where σ_{max} and σ_{min} are the maximum and minimum stresses respectively.

The cumulative annual damage for the each hotspot is determined based the loading and unloading cycles using the proposed rules by classification societies. The fatigue damage calculation shown here will be for the most critical locations in the details considered; Appendix D contains the low cycle fatigue damages for all the locations. Table 6.1 gives the stresses used to obtain the low cycle fatigue damage. The low cycle damage is the cumulative effect of all these loads acting on the FPSO over the design life.

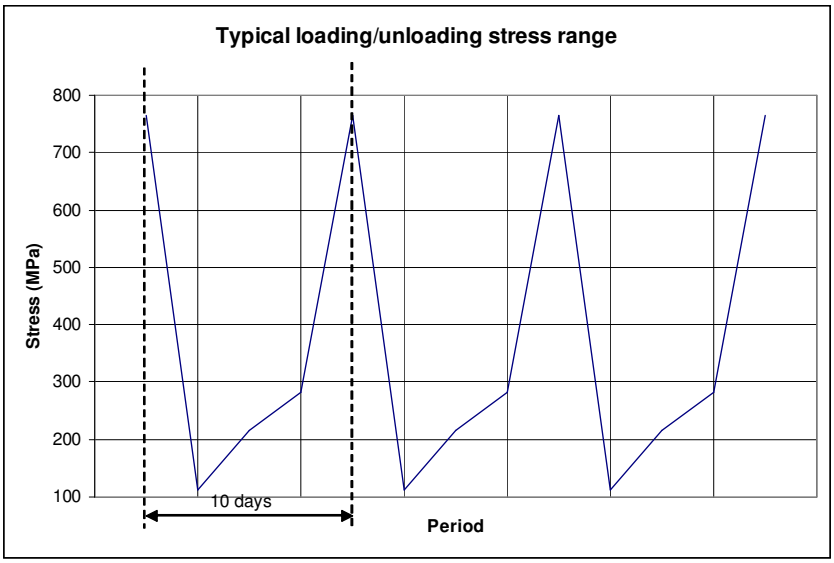

Figure 6.13: Typical loading/unloading cycle based on FE data

Table 6.1: Low Cycle Stresses

Low cycle stress (MPa)		
Bottom	Side	Inner side
176.04	764.06	96.64
605.00	138.20	32.04
1385.37	111.11	60.92
1154.36	209.1	123.49
176.04	281.64	277.21
	764.056	96.67

Figure 6.14 illustrates the low cycle fatigue damage at BHS6, which is the most critical location in the bottom detail. The low cycle fatigue damage is calculated for

the design life of the FPSO and the calculation is based on CS rules and the location of the FPSO i.e. North Sea (NS) or offshore West Africa (WA). A typical LCF estimation procedure is provided in Chapter 2. Fatigue damage is a non dimensional quantity obtained using Palmgren-Miner's hypothesis. The fatigue damage is calculated for each classification society by applying the relevant S – N curve parameters and Miner's rule. From the diagrams, it clearly shows that the ABS rule gives the highest fatigue damage for the detail while DNV and LR have similar low cycle fatigue damage results but are less than the ABS damage values by about 50 %.

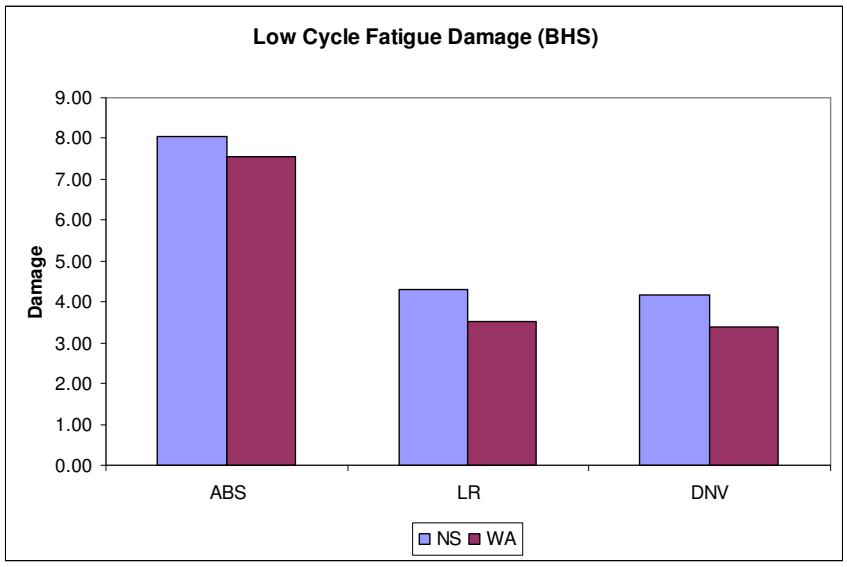

Figure 6.14: Low Cycle Fatigue Damage at BHS6

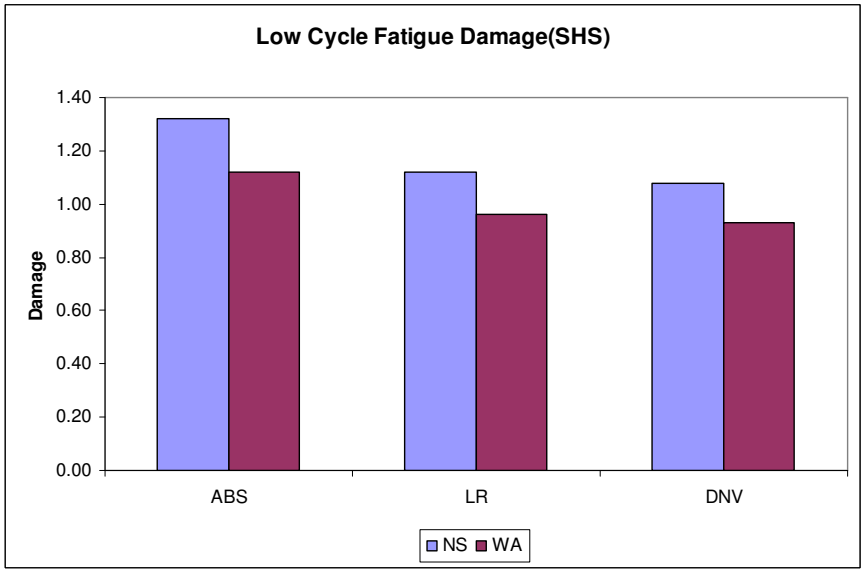

Figure 6.15: Low Cycle Fatigue Damage at SHS1

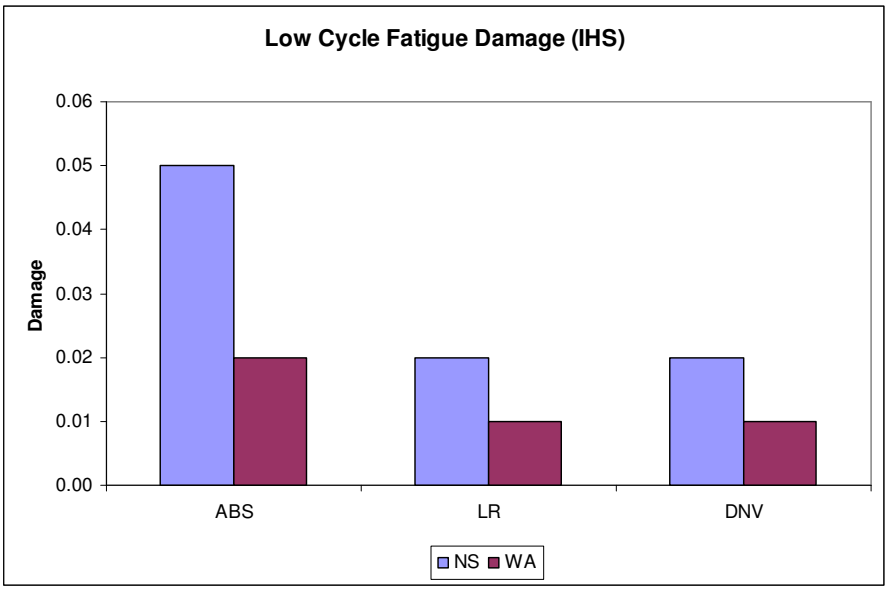

Figure 6.16: Low Cycle Fatigue Damage at IHS2

Figure 6.15 and 6.16 show the fatigue damage over the design life of the FPSO at the most critical location for the side shell longitudinal and inner side shell longitudinal connection. The S - N curve used by LR and DNV is an extension of the high cycle fatigue S-N curve with the same slope. ABS proposed a modified curve with a slope of m = 3. As there is no data to compare these results with, one cannot say whether the ABS formula overestimates the low cycle fatigue damage or the other CS underestimate the damages.

Figure 6.17 and Figure 6.18 are shown to reiterate the fact that for this particular FPSO, the bottom detail is more susceptible to low cycle fatigue damage and that for the side shell plating detail it would seem that although there is a significant damage caused by loading and unloading, the magnitude of the low cycle fatigue damage does not vary much with the loading/unloading sequence as it does in the bottom detail. Thus, the loading and unloading sequence does not affect the low cycle fatigue damage value.

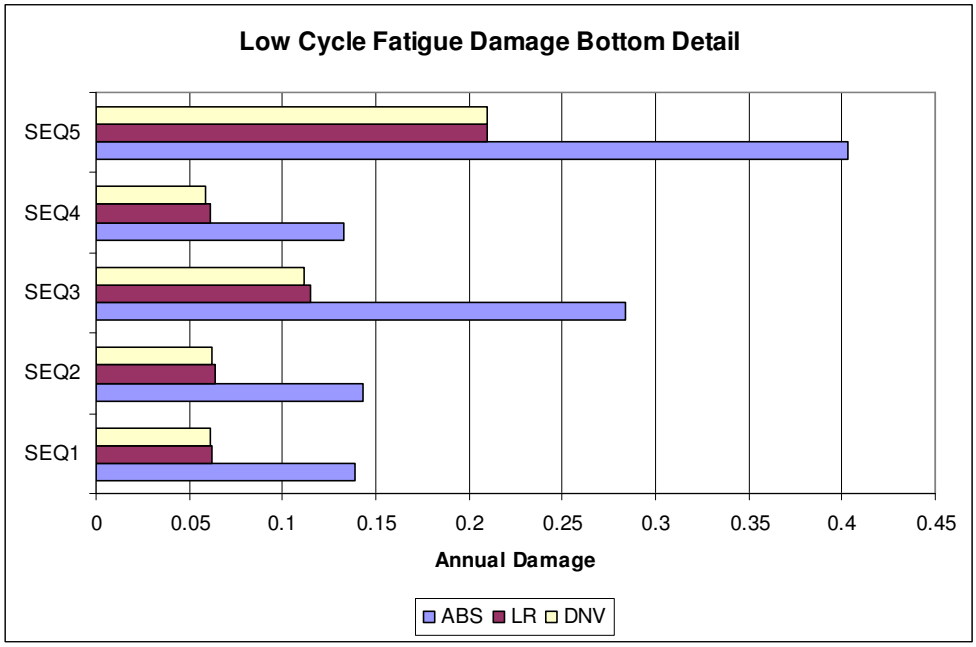

Figure 6.17: Annual low cycle fatigue damage at bottom detail

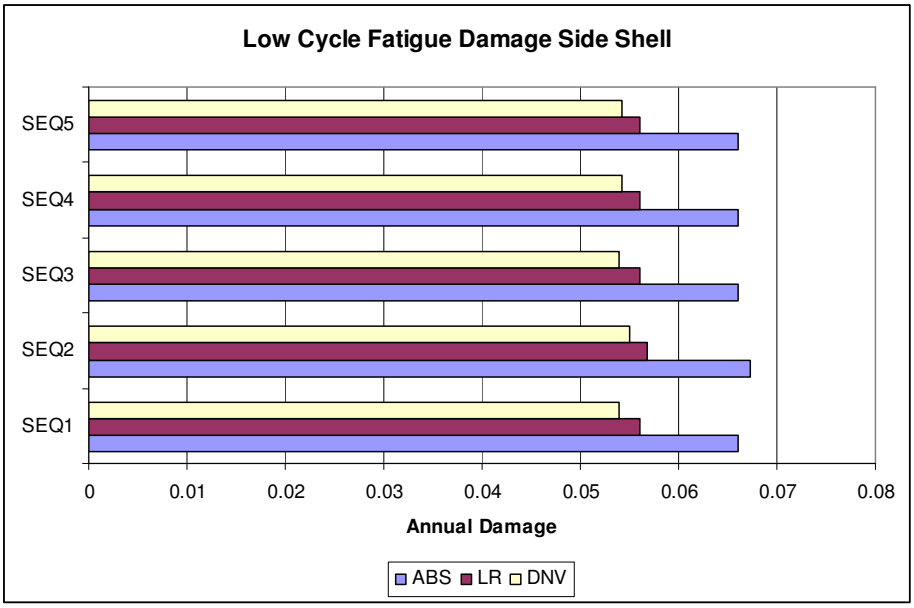

Figure 6.18: Annual low cycle fatigue damage at side detail

6.1.4 Low Cycle S - N Curves

Low cycle S-N curves based on the low cycle fatigue data is presented in Figure 6.19 through to Figure 6.21. These low cycle S-N curves are obtained by using the pseudo elastic stress to calculate the number of cycles to failure based on the S – N data from the different CS.

The S-N curve in Figure 6.19 is obtained from the pseudo stresses obtained from the 6ottom plating and stiffener connection while the S-N curves Figure 6.20 and 6.21 are obtained from the low cycle fatigue stresses at the side plating-inner plating stiffener detail respectively.

The curves show that irrespective of the large differences obtained in the low cycle fatigue damage for the different classification societies, the S-N curves produced are quite similar. The plots suggest that the higher the stresses, as seen in Figure 6.19 and 6.20, the more the curves converge at a similar value for the number of cycles to failure. Figure 6.21 shows that when the stresses are low, i.e. less than the yield stress of the material, then these curves start to diverge away from an almost uniform solution.

These curves can be applied at the design stage of an FPSO. Once the level of stress is known, the number of cycles to failure of the detail under study can be determined and the design can then be adjusted to an appropriate fatigue life.

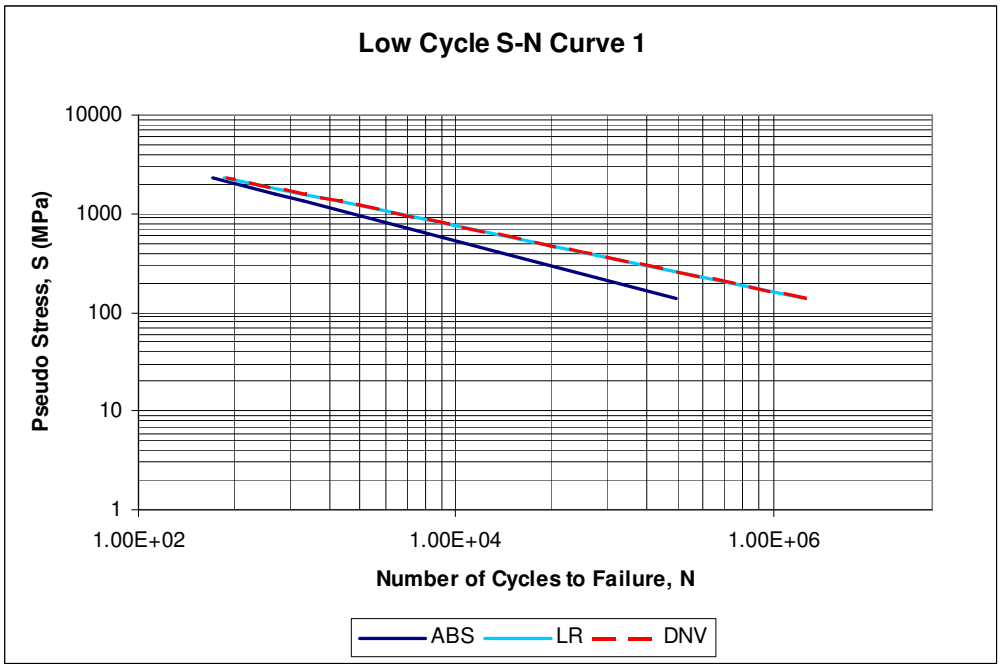

Figure 6.19: Low Cycle Fatigue S-N Curve

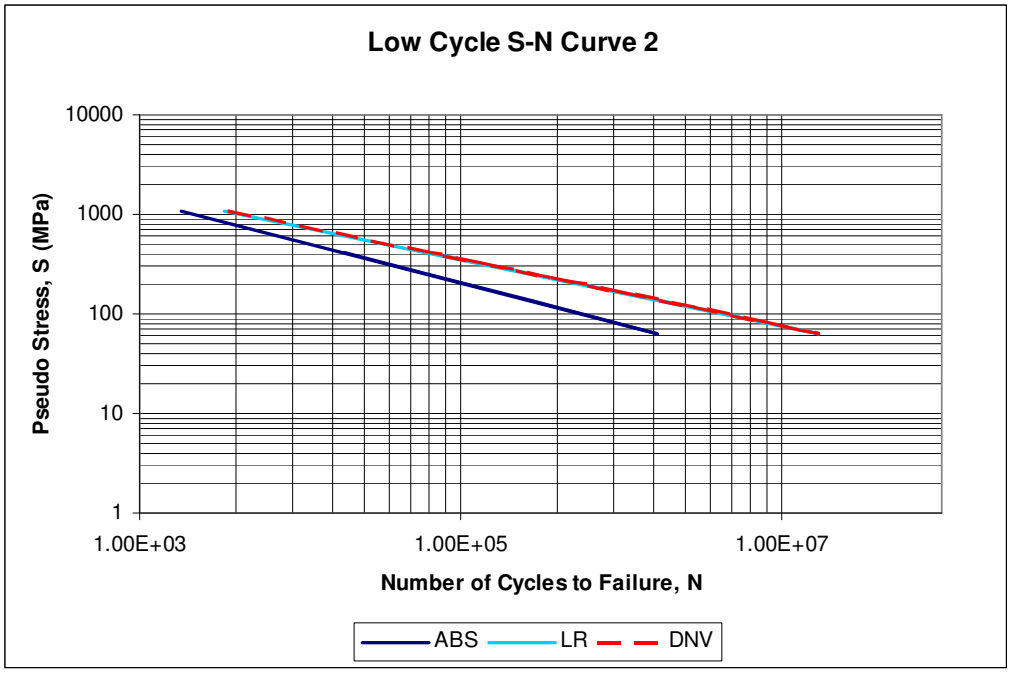

Figure 6.20: Low Cycle Fatigue S-N Curve

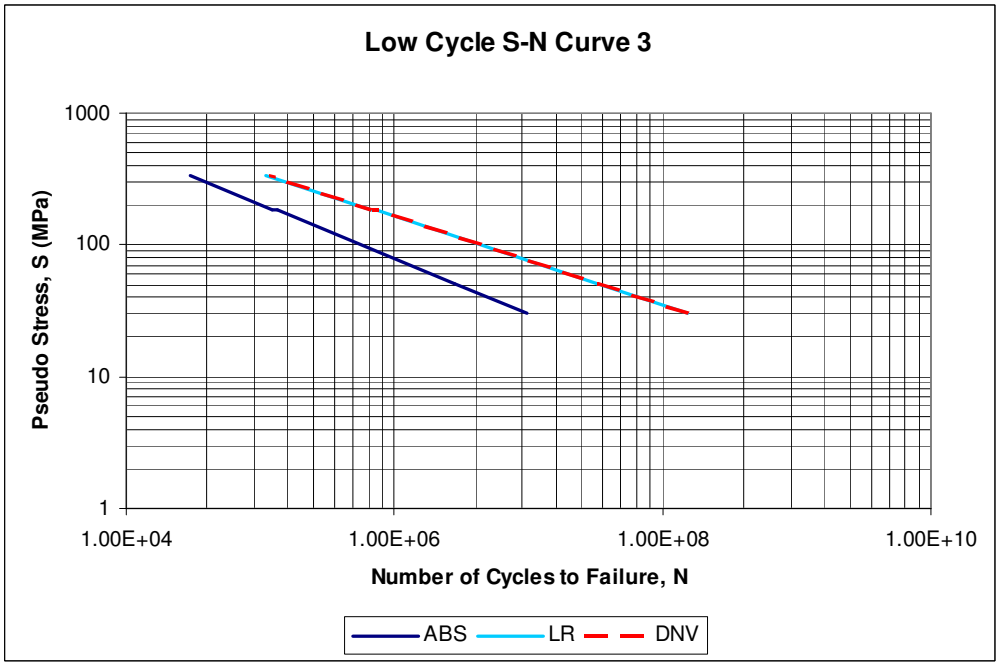

Figure 6.21: Low Cycle Fatigue S-N Curve

6.2 Wave Analysis

Spectral fatigue analysis in the frequency domain applicable to structures subjected to random loading but respond linearly with wave height at any wave period (Barltrop,

1998). It is useful in environmental loading induced fatigue damage because it can deal with the dynamic behaviour of a structure which responds at its natural frequency to part of the load spectrum. This will be difficult to do deterministically. It is easier to solve for a combination of seas and swells and direction spreading effects.

Spectral fatigue approach is based on linear theory in the frequency domain. This method is the most appropriate, albeit analytically complex and time consuming, for floating systems. In the spectral approach, various orders of spectral moments of the stress process are obtained by performing a sea keeping analysis (i.e. finding the motions and related quantities of a vessel subjected to a sea state) and subsequent mathematical manipulations. In a narrow-band spectral analysis the spectral moments, Rayleigh probability density function describing the short-term stress range distribution and the zero-up crossing frequency of the stress response is used to obtain fatigue damage. For wide band processes, a spectral bandwidth parameter for calculating the cycle counting correction factor is determined. The total fatigue damage of a structural element is calculated by adding up the short-term damages over all the applicable sea states (Wang, 2010) in a specific wave scatter diagram. Therefore, the spectral method can account for various sea states as well as their probabilities of occurrence. Frequency domain fatigue analysis has been discussed on the earlier chapter. This section will deal with spectral wave analysis on the FPSO.

Spectral fatigue analysis is a very complex task where the uncertainties and inaccuracies will tend to accumulate as one proceeds (Francois et al, 2000). This trend towards accumulated error is further enhanced by the uncertainties inherent in the data required by the procedure (environment, S-N fatigue capacity etc.) and statistical uncertainty which is fundamental to any stochastic process. Therefore, the extent to which the calculated fatigue lives represent the actual time to failure in a real structure should be considered with an appropriate amount of engineering judgement.

To achieve a spectral fatigue procedure, a full stochastic analysis is performed. A full stochastic analysis is an analysis where all load effects from global and local loads are included by use of stress concentration models and direct transfer of loads from the hydrodynamic analysis to the structural model in equilibrium. Hence, all stress components are combined using the correct phasing and without simplifications or

omissions of any stress component. This method will thus usually be the most exact for determination of fatigue damage. To achieve this, a number of specific tools are required:

- Hydrodynamic analysis from which the wave-induced loads and motions are determined.
- The mapping of the wave induced loads and motions from the hydrodynamic model to the structural model.
- Analysis of the structural model which result in stresses from the wave induced loads and motions.
- Statistical processing of the results.

There are a several ways of accomplishing the above listed steps both individually or in combination. In this thesis, the hydrodynamic analysis and the mapping of the wave induced loads and a motion from the hydrodynamic model to the structural model is carried out using AQWA SUITE. The structural analysis is carried out using ANSYS. A MathCAD programme will then be used for the statistical processing of the results. This process is illustrated in Figure 6.22.

In a spectral fatigue analysis, environmental site parameters need to be taken into account. This includes wave directions, the wave spectrum with the specification of all its parameters and relative headings of the FPSO. The hydrodynamic analysis is performed for 13 wave headings with a step of 15° from -90° to +90°. A total of 19 regular frequencies per heading ranging from 4 to 60 seconds are considered, Table 6.2 shows this information. For the two loading conditions (ballast and fully loaded state), approximately 500 load cases are analysed.

The output of the hydrodynamic analysis consists of facet pressures on the wetted surface and also accelerations due to rigid-body motions. The FPSO is assumed to operate under two loading conditions only - ballast and fully loaded conditions. Table 6.3 shows the details for the loading conditions considered. Timeshare during the 20 year design life is assumed at 50 % fully loaded and 50 % for ballast loading conditions.

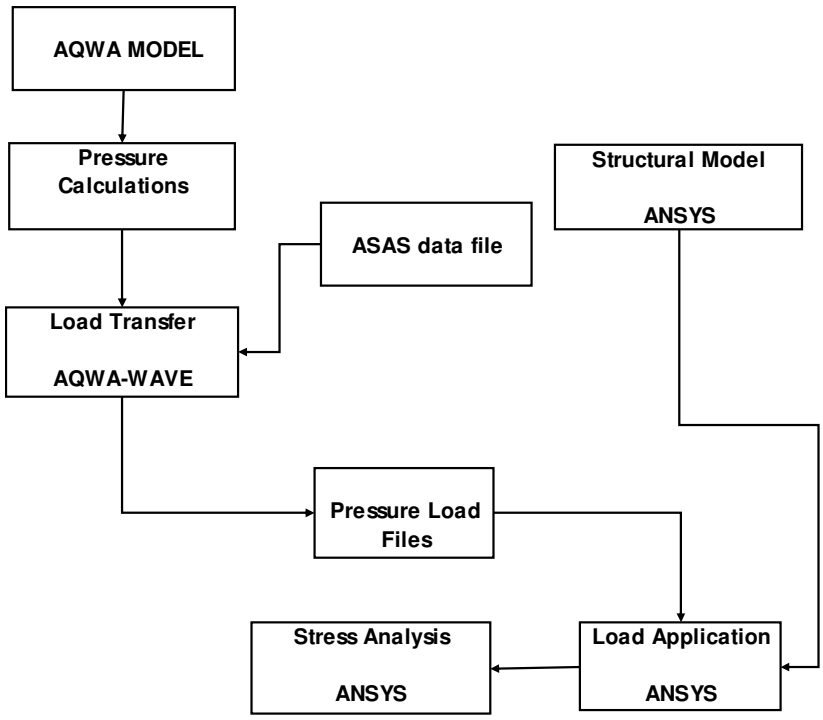

Figure 6.22: Hydrodynamic/Structural Analysis of FPSO

Table 6.2: Wave headings and periods

	Wave Headings (degrees)	Wave Freq (rads/sec)
Site Specific Analysis	-90, -75, -60, -45, -30, -15, 0, 15, 30, 45, 60, 75, 90	0.1, 0.2, 0.3, 0.4, 0.5, 0.6, 0.7, 0.8, 0.9, 1.0, 1.1, 1.2, 1.3, 1.4, 1.5, 1.6, 1.7, 1.8, 1.9

Table 6.3: Load Conditions

Load Condition	Draft (m)	Displacement (Tonnes)	% Probability
Ballast Condition	8.32	86268	50
Fully Loaded Condition	16.47	170773	50

FPSOs generally have a design life of 20 years, as such; engineers have to predict waves on the FPSO location for this period of time. The waves are described by the scatter diagrams which shows how often sea states, assumed to be stationary, will

appear on the site. A sea state is defined by the significant wave height, the mean zero wave crossing period and the shape of the spectral wave density functions. The prediction of a sea state is mainly based on historical data and assumes an unchanging climate. Two different environmental conditions will be applied -The North Atlantic (NS) sea scatter diagram and the West Africa (WA) sea state diagram. Table 6.4 shows the annual wave scatter for West Africa while Table 6.5 shows a 100 year wave scatter diagram for the North Sea. Following discussions with Professor Barltrop, who has more than 20 years of experience in fatigue design and analysis, it is decided that it is acceptable to use an annual scatter diagram for WA. The bins in the tables are probabilities of occurrence and the overall difference in fatigue results using annual scatters versus 100 year scatters are negligible. It is the hope of the author that using these two very different sea states will show variations and importance of low cycle fatigue loads.

Wave climates are normally simulated using a wave spectrum defined by the parameters H_S (wave height) and T_Z (period). The most commonly used spectra are the Pierson-Moskowitz (PM) spectrum and the JONSWAP spectrum. The PM spectrum is representative of fully developed seas and is applicable when the growth of the waves is not limited by the size of the generation area. The Pierson-Moskowitz wave spectrum is usually applied for most fatigue analyses and ultimate strength analyses and is based on significant wave height and a zero crossing period.

The JONSWAP spectrum is a peak-enhanced PM spectrum which takes into account the unbalance of energy flow in a sea state when the waves are in process of growing under strong winds, i.e. the seas are not fully developed. This is the case for extreme wave conditions in the North Sea. The JONSWAP wave spectrum is usually applied for ultimate strength analyses for vessels operating in harsh environment (e.g. North Sea). JONSWAP is based on significant wave height and the mean wave period (Figure 6.23). The PM spectrum is said to give conservative fatigue calculations (Veldkamp and van der Temple, 2004) but it is used in this analysis.

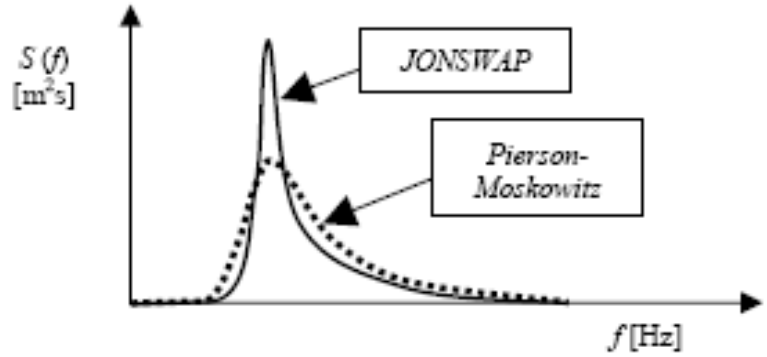

Figure 6.23: JONSWAP and Pierson-Moskowitz wave spectra (Salzmann et al, 2004)

Table 6.4: Annual wave scatter diagram for West Africa (Hogben et al, 1986)

Tz (s) / Hs (m)	3.5	4.5	5.5	6.5	7.5	8.5	9.5	10.5
0.5	23	79	83	39	11	2		
1.5	8	78	176	155	75	24	6	1
2.5	1	12	46	64	46	21	7	2
3.5		1	6	11	10	6	2	1
4.5				1	1	1		
5.5								
6.5								
7.5								
9.5								
10.5								
11.5								
12.5								
13.5								
14								

Table 6.5: 100 year wave scatter diagram for North Atlantic (DNV, 2003)

TZ(s) / Hs (m)	3.5	4.5	5.5	6.5	7.5	8.5	9.5	10.5	11.5	12.5	13.5	14.5	15.5	16.5	17.5	Sum
1.0	0	72	1416	4594	4937	2590	839	195	36	5	1	0	0	0	0	14685
2.0	0	5	356	3299	8001	8022	4393	1571	414	87	16	3	0	0	0	26167
3.0	0	0	62	1084	4428	6920	5567	2791	993	274	63	12	2	0	0	22196
4.0	0	0	12	318	1898	4126	4440	2889	1301	445	124	30	6	1	0	15590
5.0	0	0	2	89	721	2039	2772	2225	1212	494	162	45	11	2	1	9775
6.0	0	0	1	25	254	896	1482	1418	907	428	160	50	14	3	1	5639
7.0	0	0	0	7	85	363	709	791	580	311	131	46	14	4	1	3042
8.0	0	0	0	2	27	138	312	398	330	197	92	35	12	3	1	1547
9.0	0	0	0	1	8	50	128	184	171	113	58	24	9	3	1	750
10.0	0	0	0	0	3	17	50	80	82	59	33	15	6	2	1	348
11.0	0	0	0	0	1	6	18	33	37	29	17	8	3	1	0	153
12.0	0	0	0	0	0	2	7	13	15	13	8	4	2	1	0	65
13.0	0	0	0	0	0	1	2	5	6	6	4	2	1	0	0	27
14.0	0	0	0	0	0	0	1	2	2	2	2	1	1	0	0	11
15.0	0	0	0	0	0	0	0	1	1	1	1	0	0	0	0	4
16.0	0	0	0	0	0	0	0	0	0	1	0	0	0	0	0	1
Sum	0	77	1849	9419	20363	25170	20720	12596	6087	2465	872	275	81	20	6	100000

The following is the outline of wave fatigue procedure used in this work taken from Barltrop (1998):

1. For any sea state, assuming the spectrum shape remains the same, the stress is proportional to the wave height. Hence, damage may be calculated from the cubic weighted mean wave height. The number of occurrences of the mean zero crossing period band T_z is: $N(T_Z)=\sum_{i-1}^{n} n_i(H_{si},T_Z)$, where $n_i(H_{si},T_Z)$ is the number of occurrences of each significant wave height H_{si} at a period T_z as obtained from the sea scatter diagram. The cubic weighted mean stress wave height is evaluated as: $H_{CW}(T_Z)=\sqrt[3]{\dfrac{\sum_{i=1}^{n} H_i^3 n_i(H_{si},T_Z)}{N(T_Z)}}$
2. Determine the stress transfer function, $H_\sigma(\omega|\theta)$ at the structural location of interest for a particular loading condition. Structural analysis is performed for a range of wave frequencies and headings and the resulting stresses generate the stress transfer function.
3. Select a wave energy spectrum. The wave energy spectrum is used to determine the water surface elevation spectrum. In the evaluation of the spectra for each wave period band, instead of using a unity as the significant wave height, the cubic weighted mean wave height H_{CW} is used. The PM spectrum is of the form: $S_\eta(\omega|H_S,T_Z)=\dfrac{H_S^2}{4\pi}\left(\dfrac{2\pi}{T_z}\right)^4\omega^{-5}\exp\left[-\dfrac{1}{\pi}\left(\dfrac{2\pi}{T_Z}\right)^4\omega^4\right]$
4. The stress response spectra is calculated in the following manner:
   $S_\sigma(\omega|H_S,T_Z,\theta)=S_\eta(\omega|H_S,T_Z)\cdot|H_\sigma(\omega|\theta)|^2$
5. For each stress spectra, the necessary spectral moments are evaluated from which zero crossing periods and peaks may be obtained. For a narrow band process, the zero crossing period is $T_{ZCW}=(\lambda_{0\sigma}/\lambda_{2\sigma})^{1/2}$
6. For each stress response spectrum, the cubic weighted mean stress range is evaluated and the number of stress cycles per year for each zero crossing

period, j is evaluated for a narrow band process as: $n_{\sigma j} = \frac{365 \cdot 24 \cdot 60 \cdot 60}{T_{Z\sigma j}} \frac{N(T_{Zj})}{\sum_j N(T_{Zj})}$

7. From the S – N curve, the number of stress cycles to failure, $N_{\sigma j}$ for each cubic weighted stress range is evaluated. Finally the annual damage from each period band is calculated from which the annual damage from all period bands is obtained. $D_{year} = \sum_j D_j = \left(\frac{n_{\sigma j}}{N_{\sigma j}} \right)$

In this work, Dirlik's approximate rainflow counting method together with Palmgren-Miner's rule is used to obtain the fatigue damage. Professor Barltrop has written an algorithm for the entire spectral fatigue analysis procedure in a MathCAD sheet for a narrow band process. This algorithm is extended to include Dirlik's approximate rainflow fatigue damage method. This algorithm is printed with permission in Appendix E.

6.2.1 Hydrodynamic Analysis

Wave loads on an FPSO are specific to the environmental conditions prevailing at its location. In this study, 3D 1st order diffraction and radiation method is used to obtain the hydrodynamic loads and vessel motion. To this end, AQWA-LINE (2006) is used. AQWALINE is part of the AQWA suite, a hydrodynamic software. It uses 3-D radiation and diffraction theory to calculate the wave loading and response of bodies when exposed to a regular harmonic wave environment. The first order wave forces and second order mean wave drift forces are calculated in the frequency domain. The effect of mooring on the first order motions is not considered significant for this study and is ignored.

ANSYS (2007) is used to define the geometry of the dry and wet surfaces of the structure separately. A simple box shaped barge is defined with element type shell63 used for the surface mesh. AQWA-LINE uses this mesh which is composed of panels to model the structure. It assumes that there is no flow through the hull and the seabed and it also assumes a free surface condition. The wave pressures are calculated at the

panel centroid for a range of wave periods and directions. AQWA-LINE is also used to determine the shear force and bending moment along the length of the FPSO using the mass distribution of the load conditions.

6.2.2 Hydrodynamic Analysis Results

A typical sample of wave pressure contours on the ship wetted surface is shown in Figure 6.24. It illustrates the pressure contours for ballast loading state at a 0° heading and wave frequency of 0.7radians/sec (wave period of 8.98 seconds). Figure 6.25 shows the ballast loading condition for a 90° heading (beam seas).

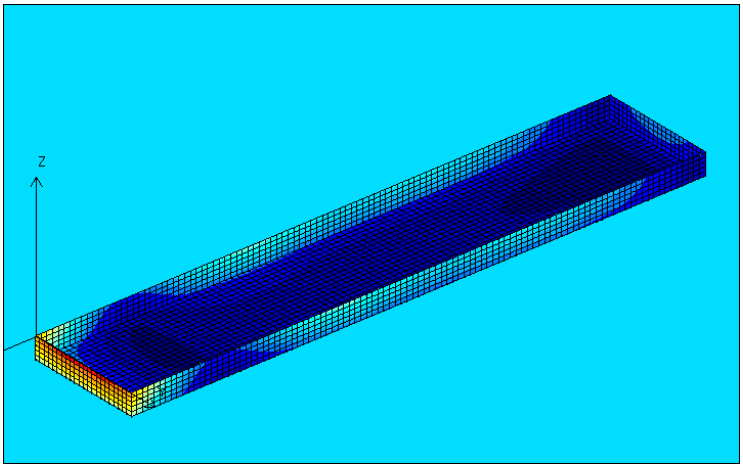

Figure 6.24: Wave pressure contour; direction = 0°, frequency = 0.7radians/sec

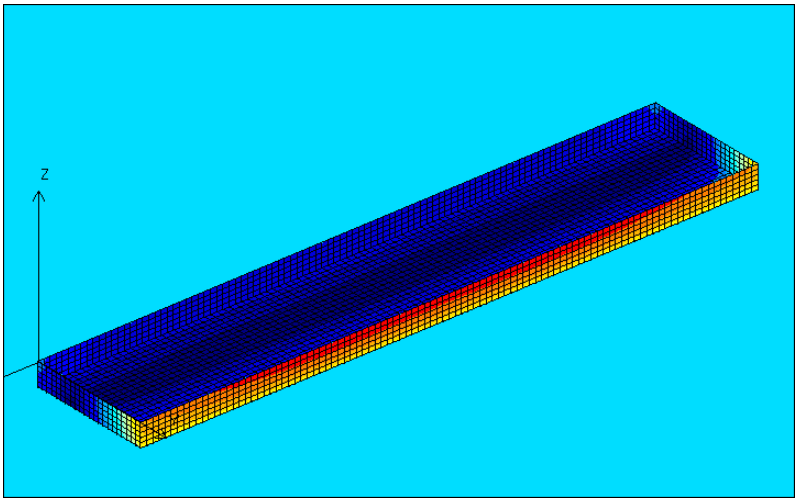

Figure 6.25: Wave pressure contour; direction = 90°, frequency = 0.7radians/sec

The hydrodynamic analysis results include Response Amplitude Operators (RAOs) and wave induced bending moments and shear force. Figures 6.26 and 6.27 illustrate the ships shear force and bending moment RAO in the ballast and fully loaded state. The force RAO for the ballast loading condition in heave and pitch is illustrated in Figure 6.28 and 6.29. Figure 6.30 and 6.31 shows the force RAO in sway and yaw for the fully loaded condition.

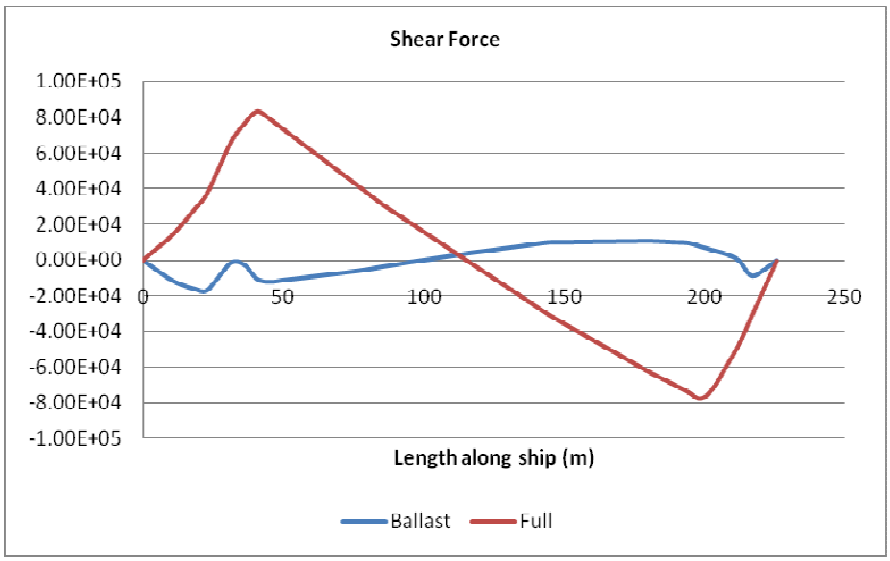

Figure 6.26: Shear force along the length of the ship

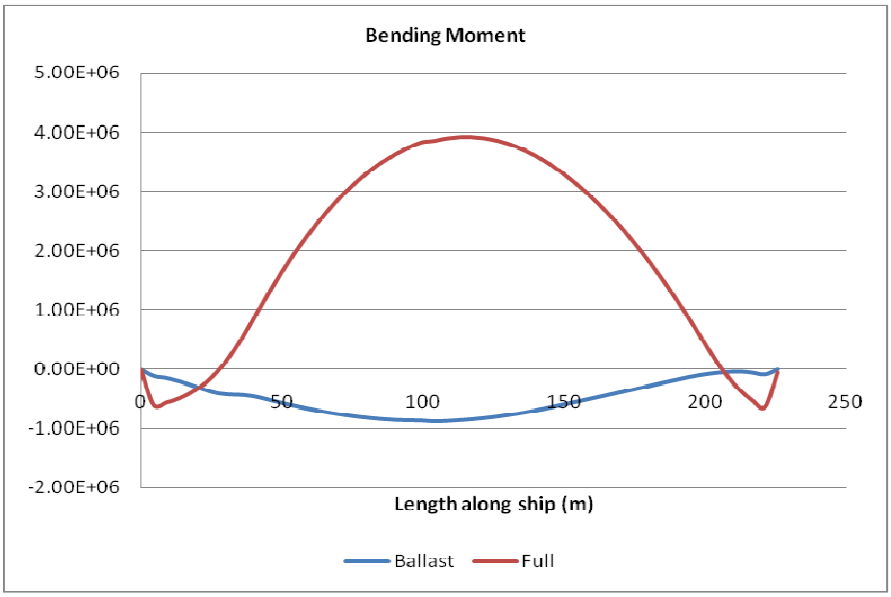

Figure 6.27: Bending moment along the length of the ship

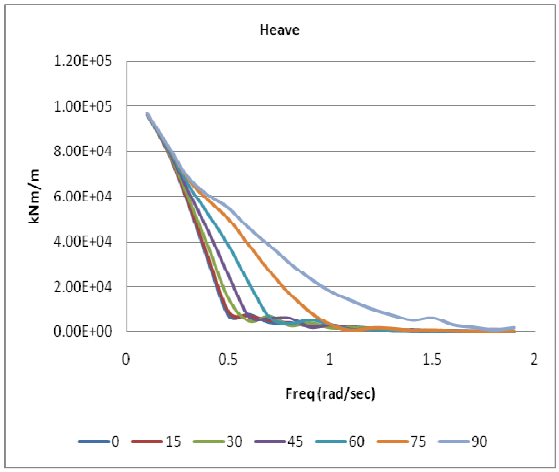

Figure 6.28: Heave RAO for ballast loading condition

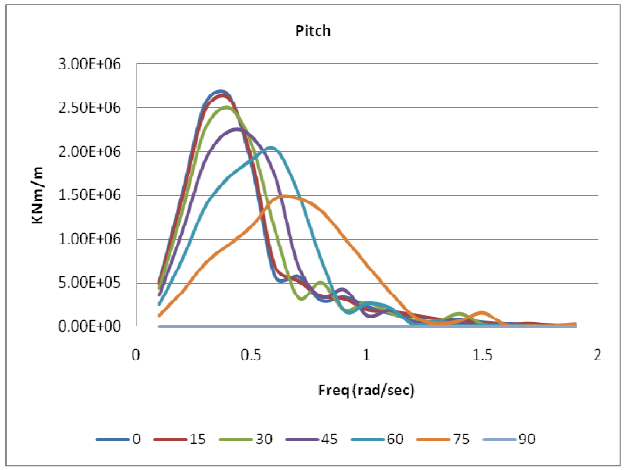

Figure 6.29: Pitch RAO for ballast loading condition

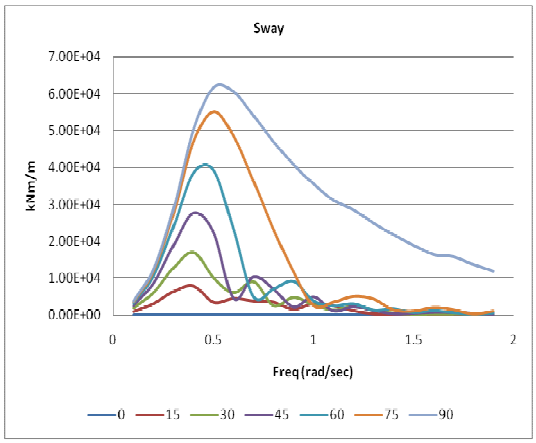

Figure 6.30: Sway RAO for full loading condition

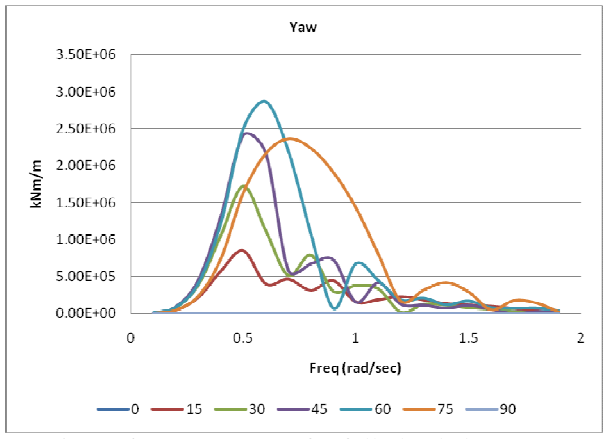

Figure 6.31: Yaw RAO for fully loaded conditiom

6.2.3 Structural Analysis

The model employed in the hydrodynamic analysis is a full 3D finite element model earlier discussed in Chapter 3. Using the finite element model, stresses are computed for each frequency with loads taken from the 3D diffraction-radiation analysis. Transfer functions for internal and external pressure and rigid body accelerations are transferred to the finite element model.

The pressure forces are directly mapped to the shell-element as surface loads and inertia forces are generated from the rigid body accelerations. AQWA-WAVE is used to map the wave pressures calculated by AQWA-LINE to the finite element model. It

generates loading for stress analysis by interpolating the loads from the AQWA forces. Figure 6.32 shows a typical mapped pressure for structural analysis.

The global/local stress patterns are affected by the mass description of the structural model so it is necessary to ensure that identical mass models are used in the hydrodynamic analysis and structural analysis. To ensure a balance of mass in the structural model, it is generally recommended that mass density is used for structural elements, pressure for external and internal hydrostatic and hydrodynamic loads and point mass for non-structural members and non-liquid cargo (this depends on type of cargo and may differ for some ship types).

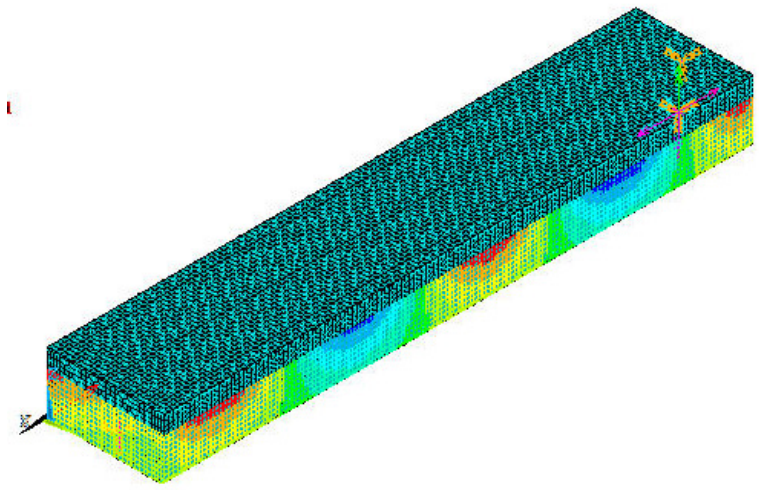

Figure 6.32: Mapped pressure for structural model (Heading: 15°, Period: 7.9 sec)

The point mass representation should be sufficiently distributed to give a correct representation of rotational mass and to avoid unintended results. Point masses should be located in structural intersections such that local response is minimised. To balance the model such that correct mass description is obtained is not a straightforward task. Even small inaccuracies in the mass description may lead to relatively large errors in global forces/moments.

Correct mass balancing is achieved by dividing the hull into several regions and adjusting the density of each region individually according to correct mass description. The internal and external hydrostatic and hydrodynamic load is

represented by pressure forces. Figure 6.33 shows the mass/load distribution for the fully loaded state. The boundary condition for the global finite element model is a 3-2-1 fixation which simulates a simply supported beam. The restraints are applied at 3 nodes at bulkhead intersections in the finite element model because of their high stiffness.

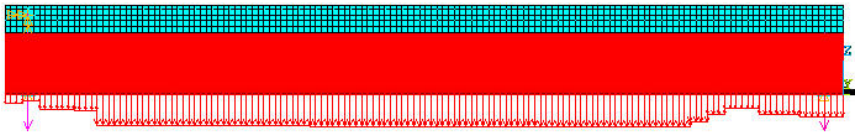

Figure 6.33: Mass distribution in fully loaded condition

Stress transfer functions obtained from the structural finite element analysis is illustrated in Figure 6.34 and Figure 6.35. These stresses are nominal stresses obtained from the global model. Structural analysis in the wave loading case is carried out only to the intermediate level. This is because the stress concentration factors at the hotspots have already been determined from the quasi-static analysis; hence it is not necessary to carry out a fine/local finite element analysis. Thus, the hotspot stresses are obtained by multiplying the nominal stresses are multiplied from the intermediate analysis by the stress concentration factors obtained from the quasi-static.

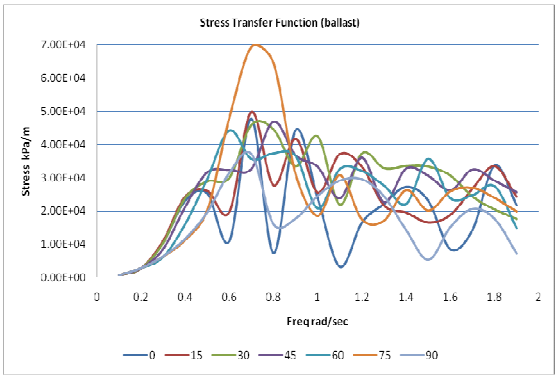

Figure 6.34: Ballast Stress transfer functions (Heading 0º to 90º)

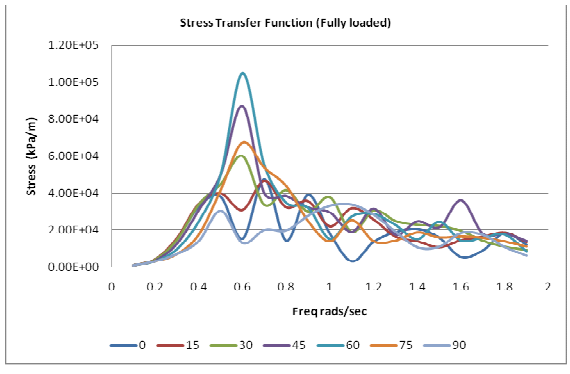

Figure 6.35: Full Stress transfer functions (Heading 0º to 90º)

6.2.4 Wave (High Cycle) Fatigue Damage

The wave scatter diagram for the NS and offshore WA are used in the wave spectral analysis. The fatigue damage for all the sea states for a design life of 20 years is computed for each hotspot. The wave hotspot stress range is obtained by multiplying the hotspot stress concentration factors obtained from the quasi-static analysis. The hotspot S – N curve parameters for the three major CS are given in Table 6.6. The fatigue damage using S – N data from three CS is computed

Table 6.6: Hotspot Stress S-N Curve Parameters

Class Society	A		m
	(MPa)	Log_{10}	
LR	4.33×10^{12}	12.636	3.0
DNV	4.467×10^{12}	12.65	3.0
ABS	3.289×10^{12}	12.5169	3.0

The annual fatigue damage using the information in Table 6.5 is obtained. Figure 6.36 illustrates a sample data from the calculated fatigue damage. It shows the fatigue damage at increasing wave periods for the hotspot location BHS3 for the same loading condition. A significant difference in the fatigue damage values is noted between the environments: North Sea and West Africa. The damage caused by the waves in the North Sea is almost five times the fatigue damage when the FPSO is situated in West Africa. This is expected because the NS is characterised by rough sea while the waves in WA are typically benign.

Fatigue damage is calculated for ballast and full loading conditions. The load conditions are taken to occur with equal probability over the design life of the FPSO. The total damage from wave loading is the taken as the mean of the damage from the ballast load case and the fully loaded case. The annual fatigue damage at the most critical hotspot location in the bottom detail and the side shell detail (BHS5 and SHS1, see Figure 4.14 and 4.21) based on classification society rules are presented in Figure 6.37 and 6.38 respectively.

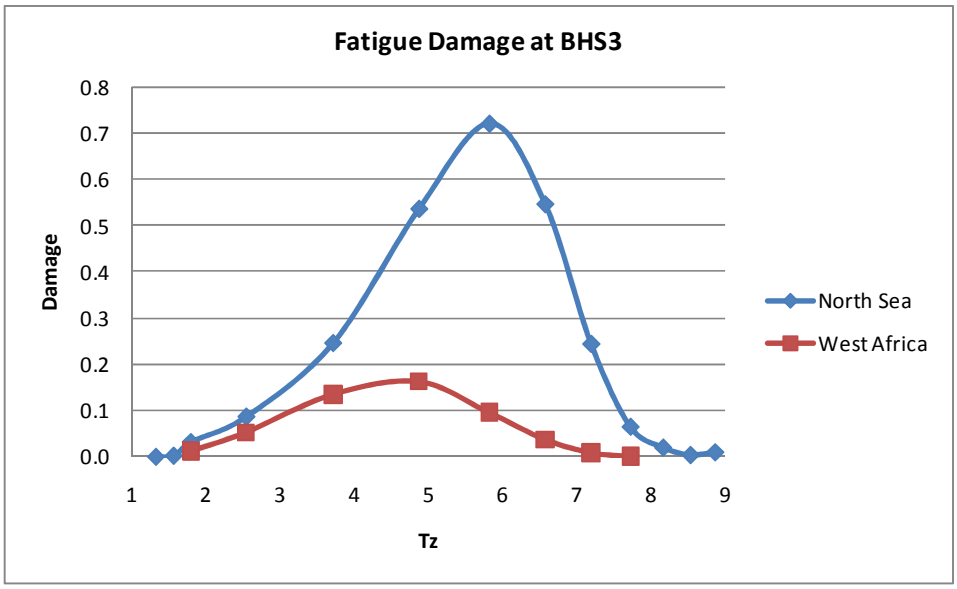

Figure 6.36: Wave fatigue damage vs. wave period at BHS3

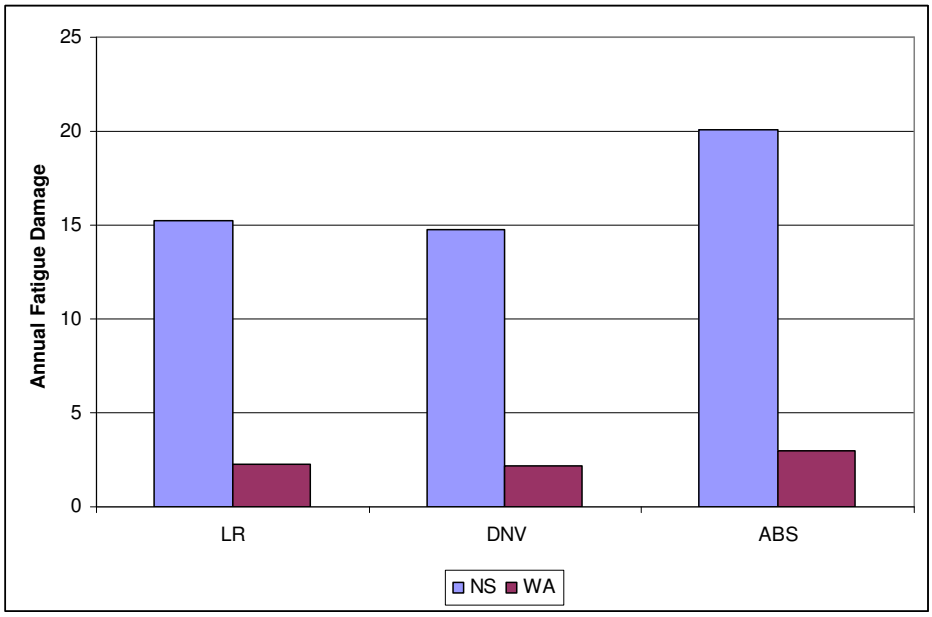

Figure 6.37: Annual Wave Fatigue damage at BHS1

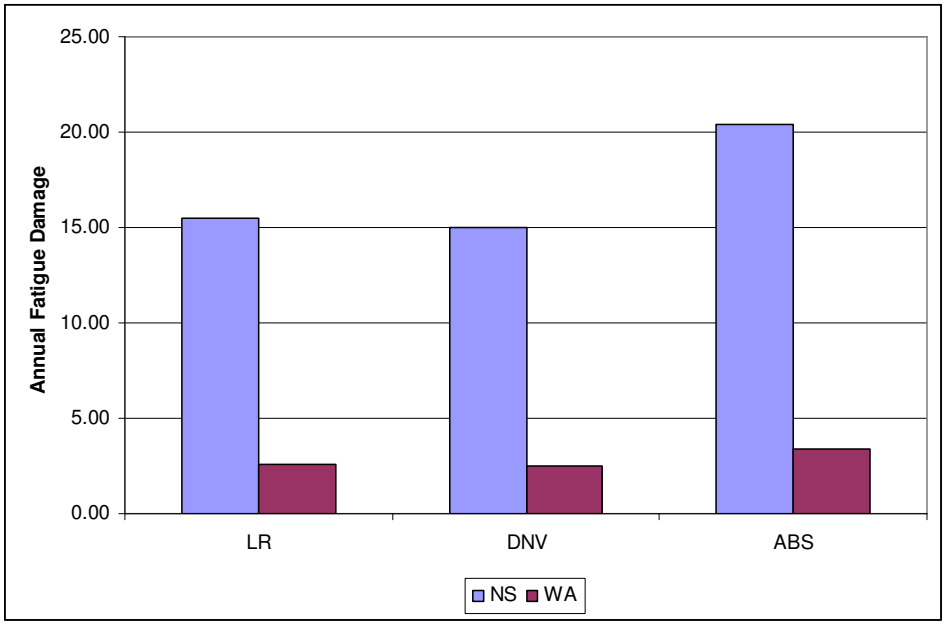

Figure 6.38: Annual Wave Fatigue damage at SHS1

From both figures, the fatigue damage from the North Sea scatter is more significant than in the West Africa, as noted earlier in Figure 6.15. The fatigue damage calculated using DNV and LR rules produce almost similar values. The fatigue damage obtained using ABS rules is about 25 % more than the fatigue damage from the other class societies. This effect is more significant in rough seas than in the benign waters of WA. Appendix C contains a summary of the annual high cycle (wave) fatigue damage for all the hotspot locations considered.

7.3 Combined Fatigue Damage

Low cycle fatigue damage is more significant when the FPSO is in benign waters than when it is located in rough seas, see Table 6.7. For example, at location BHS1, the ratio of the low cycle fatigue damage to the wave fatigue damage is 1:300 when the FPSO is in the NS and approximately 1:56 when the FPSO is located in the seas of WA. This automatically shows that low cycle fatigue damage will play a more crucial and significant role on the cumulative damage and fatigue life when the FPSO is located in the WA.

Table 6.7: Wave damage and low cycle damage for different sea scatter diagrams

	NS		WA	
	HCF Damage	LCF Damage	HCF Damage	LCF Damage
BHS1	1.44	0.0048	0.236	0.00421
BHS2	2.33	0.0754	0.349	0.0960
BHS3	3.42	0.0055	0.557	0.0045
BHS4	0.90	0.0026	0.170	0.00066
BHS5	1.52	0.1510	2.270	0.1330
BHS6	1.15	0.1880	1.660	0.1750

Damage from the wave cycle loading (high cycle) and the loading and unloading static load cases (low cycle) are combined to obtain the cumulative fatigue damage on the structural details of the FPSO. As previously discussed in Chapter 5, there are several methods of combining fatigue damage from two different processes: low cycle and high cycle. A linear summation of the fatigue damages is said to give an acceptable fatigue life estimate but would underestimate or overestimate fatigue life depending on which process is dominant. The combined spectrum method is based on the assumption that the two processes can be expressed in statistical terms i.e. spectral moments.

The following sections will apply CS rules, the linear summation approach and the SRSS method to obtain a cumulative damage from the low cycle fatigue process and the high cycle fatigue process. The methods proposed by the classification societies are compared individually with the simple linear summation method and the quadratic method. Figures 6.39 to 6.41 compares cumulative fatigue damage based on ABS, LR and DNV rules with the linear and SRSS methods for the most critical location in the bottom stiffener detail.

Figure 6.39 shows a plot of the cumulative fatigue damage obtained from ABS rules, linear summation method and the SRSS method. The plot shows that the SRSS method produces the highest fatigue damage while ABS method gives the lowest. According to API (1995), the SRSS method is always conservative and may significantly overestimate the actual fatigue damage.

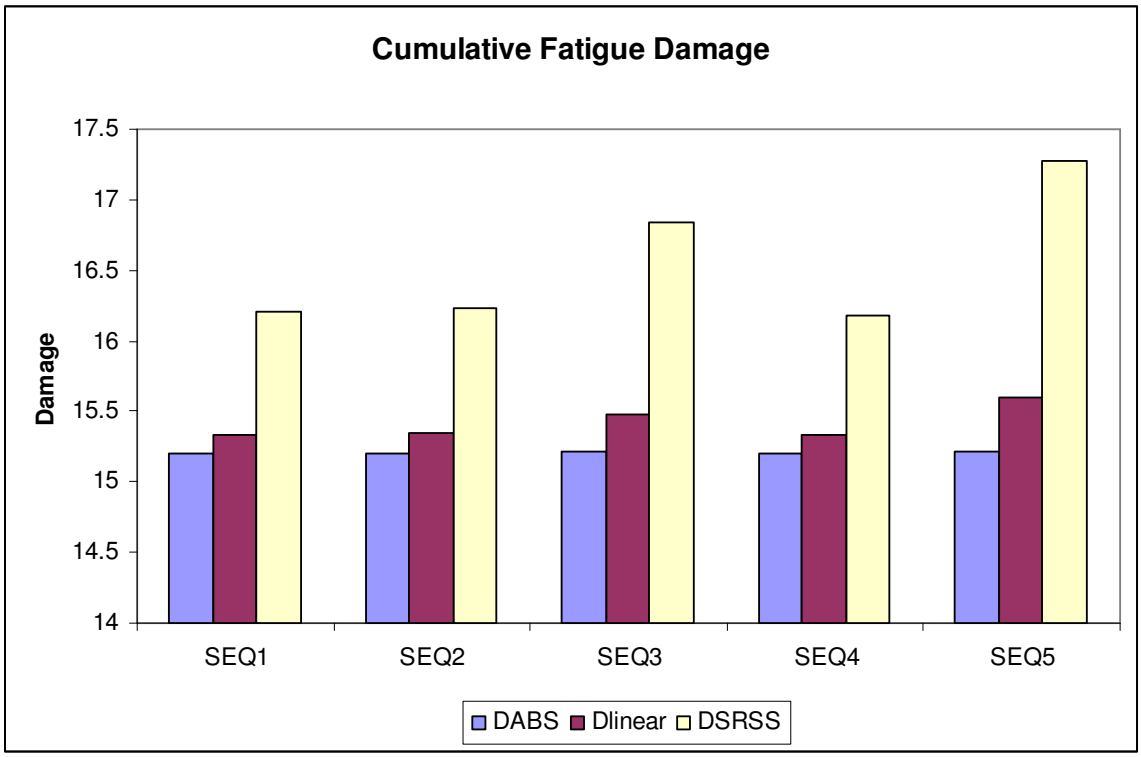

Figure 6.39: Combined fatigue damage based on ABS

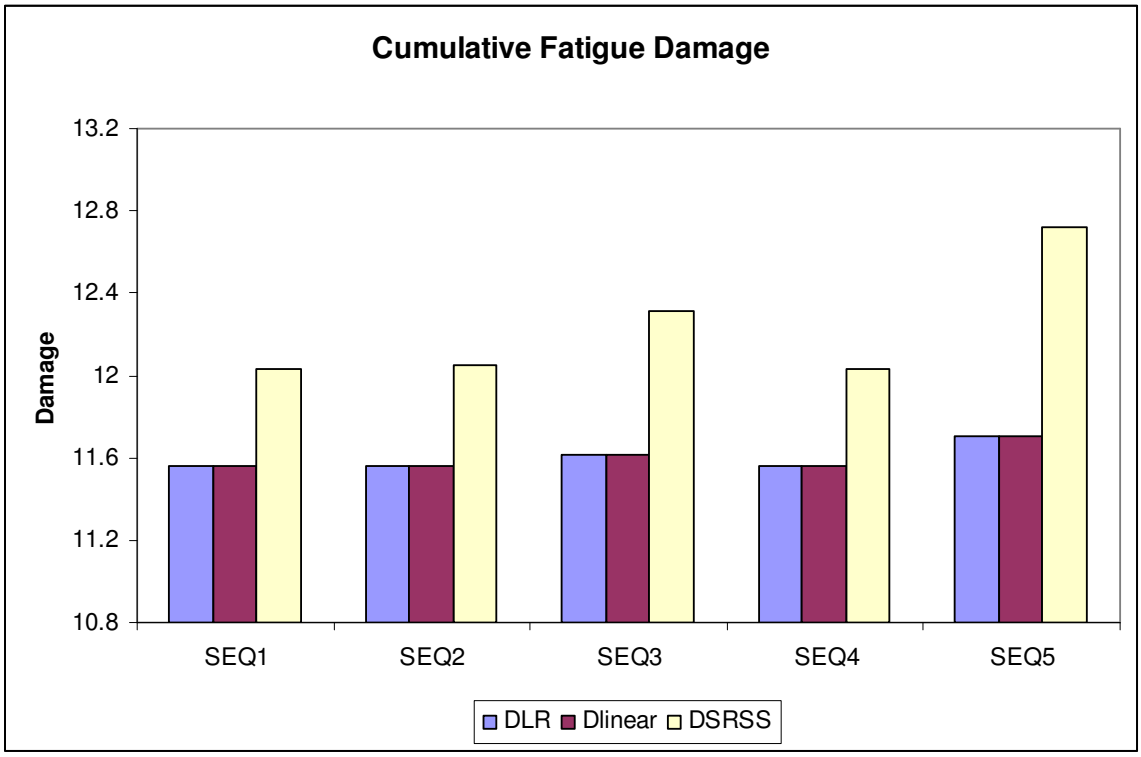

Figure 6.40: Combined fatigue damage based on LR rule

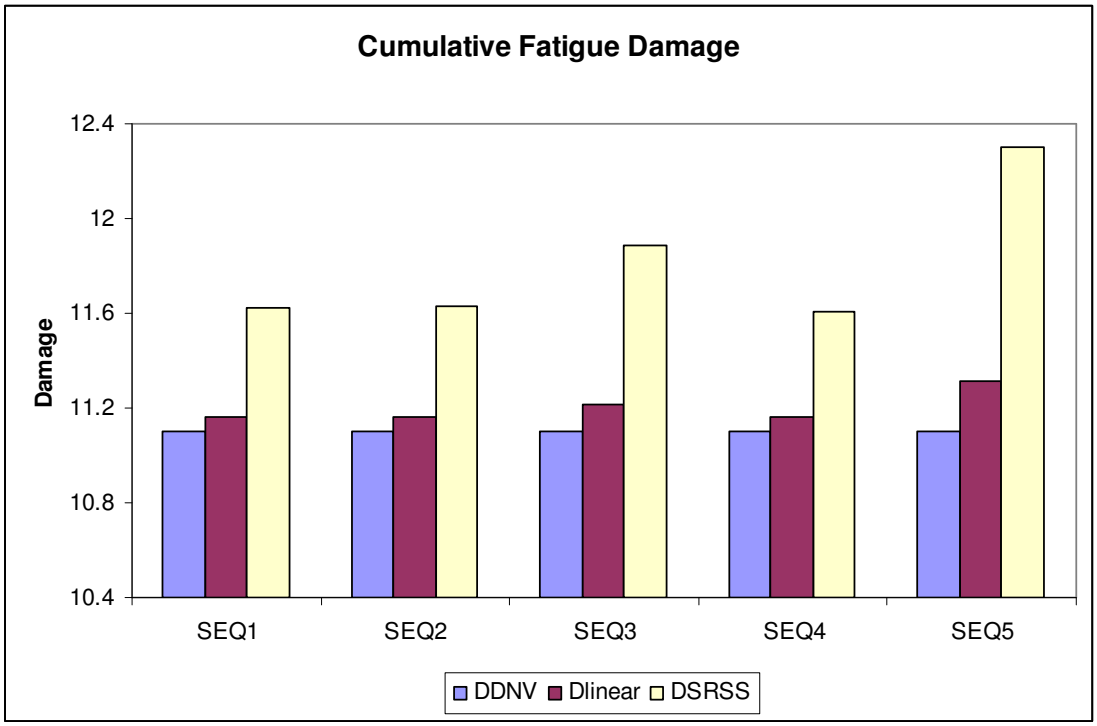

Figure 6.41: Combined fatigue damage based on DNV rule

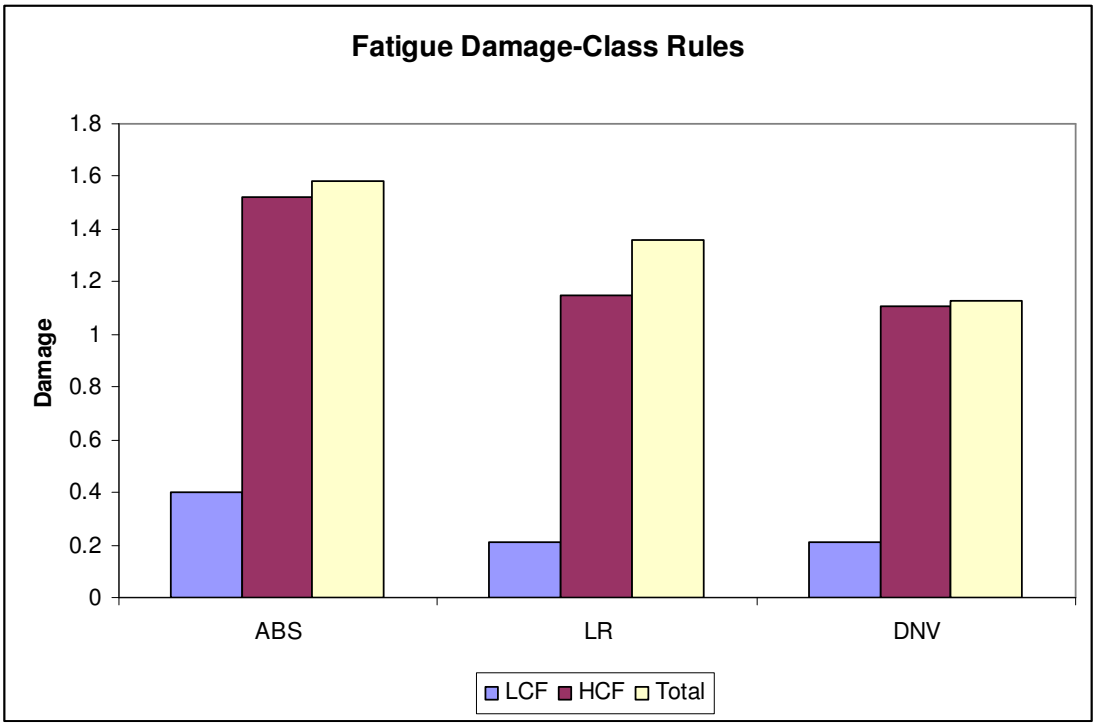

Figure 6.42: Comparison of CS rules for cumulative fatigue damage

Figure 6.40 illustrates the LR combined rule versus the linear and SRSS methods. As with Figure 6.39, the SRSS method produces the highest fatigue damage value. It is noted that the proposed LR formulation gives the same fatigue damage as the linear summation method. The D_{adj} factor in the proposed formula by LR is quite insignificant when compared to the low cycle and high cycle fatigue damages. This makes its effect on the combined damage negligible.

Figure 6.41 shows the comparison of the proposed methodology for cumulative damage by DNV with linear summation method and the SRSS method. DNV rule gives the least fatigue damage with SRSS giving the highest fatigue damage index. The cumulative damage values for all the hotspot locations studied are presented in Tables D1 to D6 in Appendix D.

Figure 6.43 compares the classification society rules for fatigue damage at the same hotspot location (BHS 5). The fatigue damages obtained from the CS rules are different-from the numerical values of the low cycle fatigue to the combined fatigue damage values. This can be attributed to two main factors. Firstly, each CS has different S – N curves for high cycle and low cycle fatigue assessment. Secondly, the proposed methodology for obtaining the cumulative damage from wave cycles effects and loading and unloading effects also differ for each CS.

6.4 Discussion

Low cycle and high cycle fatigue assessment has been carried out. A comparison of cumulative fatigue damage values using the linear summation method, the SRSS method and classification society methods has been carried out.

Fatigue damage assessment has also been carried out for two different sea environments i.e. when the FPSO is in the NS and when it is in WA. The assessment has shown that the low cycle fatigue damage has a more significant value on the total fatigue damage when the structure is located in WA than when it is located in the NS.

The magnitude of the high cycle fatigue damage is higher in the NS than in the WA because the NS is characterised by more significant wave heights than WA so when the low cycle fatigue damage is finally added to the high cycle fatigue damage, it's impact is a lot less than in WA. This is further explained in Table 7.8. The percentage of low cycle fatigue damage to the total damage ranges from 0.94 % to 2.65 % in NA but is as high as 16.85 % in WA.

Table 6.8: Combined Fatigue Damage for North Sea and West Africa

	D_{LCF}	D_{HCF}	D_{TOTAL}	% (D_{LCF}/ D_{TOTAL})
North Sea				
SEQ1	0.139	15.2	15.2062	0.91
SEQ2	0.143	15.2	15.2064	0.94
SEQ3	0.284	15.2	15.2140	1.87
SEQ4	0.133	15.2	15.2059	0.87
SEQ5	0.403	15.2	12.2215	2.65
West Africa				
SEQ1	0.129	2.19	2.1989	5.87
SEQ2	0.132	2.19	2.1993	6.00
SEQ3	0.263	2.19	2.2162	11.87
SEQ4	0.124	2.19	2.1985	5.64
SEQ5	0.377	2.19	2.2371	16.85

REFERENCES

1. ABS (2005) 'Guidance Notes on Spectral-Based Fatigue Analysis for Floating Offshore Structures'. American Bureau of Shipping. ABS Plaza, Texas.
2. ANSYS 11.1 (2007) ANSYS Inc.
3. AQWA Suite. (2006) Century Dynamics Limited, Horsham, West Sussex England.
4. Barltrop N.D.P. (1998) 'Floating Structures: A Guide for Design and Analysis'. CMPT/OPL
5. Cerda Salzmann D.J. and van der Tempel J. (2004) 'The Impact of Different Wind and Wave Data Sources on the Fatigue of Offshore Turbines'. European Wine Energy Conference and Exhibition, London UK.
6. DNV (2003) 'Classification Notes 30.7: Fatigue Assessment of Ship Structures'. Det Norske Veritas, Norway
7. Francois M., Mo O., Fricke W., Mitchell K. and Healy B. (2000) 'FPSO Integrity: Comparative Study of Fatigue Analysis Methods'. OTC 12148 Offshore Technology Conference Houston Texas.
8. Hogben N., Dacunha N.M.C., and Olivier G.F. (1986) 'Global Wave Statistics'. Complied and Edited by British Maritime Technology Limited.
9. LR (2003) 'Ship Right Level 3: Fatigue Design Assessment' Lloyds Register, London.
10. Veldkamp D. and van der Tempel J. (2004) 'Influence of Wave Modelling on the Prediction of Fatigue for Offshore Wind Turbines'. DUWIND, Delft.
11. Wang Y. (2010) 'Spectral Fatigue Analysis of a Ship Structural Detail – A Practical Study'. International Journal of Fatigue Volume 32, pp310-317

CHAPTER 7: CONCLUSIONS AND RECOMMENDATIONS

7.1 Summary

Fatigue life prediction is the most critical step of structural engineering design in many industries. It is very important in the offshore industry because the structures are often large with many complicated details. FPSOs have been growing in popularity since their debut in the 1970s and this popularity seems to be on the increase. FPSOs are subjected to combinations of loads and because of the long spells before dry docking; they are prone to fatigue cracking. The costs of failure of these structures including loss of lives and environmental damages are enormous. This cost can be significantly reduced by carrying out proper design and checks especially in fatigue.

Design rules for trading tankers have often been applied to FPSOs. Although the hull arrangements are similar, it is relevant to note that there are large differences between them. The tanker is subjected to a limited number of loading and unloading conditions, with loading occurring in sheltered locations while the FPSO has more frequent loading /offloading cycles with loading occurring with more environmental effects at play. A trading tanker is in open sea about 70 % and can avoid rough weather where necessary and also has regular dry-docking while an FPSO spends 100% of its operational life on site and undergoes continuous operations without dry-docking. Another important factor is the geometry of the structure. Tankers are generally double bottomed, but there are many FPSOs in operation that have single bottom. All these factors contribute to the fatigue strength if the structure and makes fatigue analysis and design of FPSOs a little bit more complicated than trading tanks.

Fatigue assessment of critical structural details in an FPSO, focusing on low cycle fatigue, has been carried out. Low cycle fatigue in FPSOs is attributed to continuous loading and unloading of cargo and ballast. High cycle fatigue assessment from wave loading has also been carried out to enable the calculation of cumulative fatigue

damage from the combined effect of waves and the loading and unloading of cargo and ballast.

Chapter One of this research theses presented the research motivation and an outline for the work. Chapter Two highlighted the increasing importance of FPSOs in the offshore industry and showed the structural details of the reference FPSO that was used in the study. General fatigue loads on FPSOs was discussed as well as low cycle fatigue loads. The loading and unloading load cases which were used in the remainder of the research were presented in this chapter.

A literature review of low cycle fatigue was showcased in this chapter. A summary of the milestones achieved in fatigue assessment through history was presented, and then a literature review of low cycle fatigue of metals and welded components was outlined. Investigations by the Ship Structures Committee, The Welding Institute and other researchers were reviewed.

Finite element modelling techniques were presented in Chapter Four. The most common local modelling techniques i.e. stress concentration factor, direct mesh refinement, substructure method and submodeling method were discussed in detail. The submodeling method with displacement boundary solution was employed for the accurate determination of stresses in the local details of interest.

Chapter Five covers a literature review of the hotspot stress approach. Several extrapolation procedures and finite element modelling techniques are discussed. The linear, quadratic and single point extrapolation methods were tested for the bottom stiffener connection and the quadratic extrapolation method was selected as the most applicable to this research. A critical finite element analysis of 18 possible crack locations in the FPSO was carried out using the low cycle load cases already defined and the predicted stresses at a distance from the weld toe were reported. Using the quadratic extrapolation procedure, the hotspot stresses at the selected locations were obtained.

Rainflow fatigue damage in time domain and frequency domain was discussed in Chapter Six. Several approximations to the rainflow damage in frequency domain

were discussed. Many researchers pointed out the accuracy of Dirlik's rainflow damage formula as it constantly outperforms all other available methods. After a critical review, it was decided to employ Dirlik's method to obtain fatigue damage from high cycle loads. Methods for combining low cycle fatigue damage to high cycle fatigue damage were reviewed together with classification society rules.

Chapter Seven provides analysis results. Using the hot spot stresses (for the low cycle fatigue load cases) obtained from Chapter Five, a several operational scenarios were deduced. Low cycle fatigue damage was calculated based on these scenarios and using proposed classification society rules. Spectral wave fatigue analysis result when the ship is located in the North Sea and when it is located in West Africa was also presented in this chapter. Cumulative fatigue damage was presented showing that the numerical value for the damage differs from each class society and that low cycle fatigue was more significant when the FPSO was in benign waters i.e. West Africa.

7.2 Conclusions

This thesis has investigated the effect of low cycle fatigue on typical structural details in FPSOs. The following conclusions have been reached:

1. Literature review showed that although low cycle fatigue had been identified as an important structural problem in ship structures over 30 years ago, very little research, especially when compared with the amount of research work in high cycle fatigue, has been carried out. SSC, TWI and ASTM have published information and test results on the low cycle fatigue properties of steels used in the shipping industry. The classification societies have just recently recognised that low cycle fatigue can be critical for some structural details in FPSOs and proposed guidance to address this problem. This research study is the first to compare this guidance to obtain low cycle fatigue damage of ship critical details from loading and unloading of cargo. This research has also highlighted the impact of low cycle fatigue on the total fatigue life of a structural detail.
2. This study had shown that loading and unloading of cargo and ballast can generate extremely high stresses. The stresses obtained for the bottom detail

were very high, almost four times the yield stress of the material. This clearly shows that some critical details are governed by low cycle fatigue and not high cycle fatigue. The study has also shown that the sequence of loading and unloading of the cargo has an effect on the stresses generated in a detail. In Figure 6.1, SEQ5 is the most critical loading sequence for that hotspot location. SEQ1 is a realistic loading and unloading scenario obtained from an existing FPSO operating in the North Sea. This operating scenario shows that the operators do try to minimise the stresses from loading and offloading on the structure. In most of the hotspot locations considered in the analysis, SEQ1 did not always give the worst scenario.

3. It was also discovered that for the FPSO studied, the bottom plating and stiffener connections are most susceptible to high stresses from low cycle fatigue. The FPSO employed in the analysis has a single bottom and double hull. The constant loading and unloading subjects the bottom sections to continuous bending stresses. This may explain why the stresses are very high is this case. Depending on the critical area of interest in an FPSO, care should be taken in selecting the appropriate load case that would produce the maximum stress (the worst case scenario).
4. The linear, quadratic and single point extrapolation methods were tested for the bottom stiffener connection. The quadratic extrapolation procedure has been found to yield better stress estimates than the linear extrapolation procedure and the single read out point method.
5. Low cycle fatigue damage was obtained using the procedures by three main classification societies – LR, DNV and ABS. There are notable differences in fatigue damage results and this has been attributed to the proposed low cycle fatigue assessment methods of analysis and the selection of the S- N curve. Fatigue life estimates based on LR and DNV give almost similar numerical values while ABS has a notable difference, almost 30 % higher in some cases. LR and DNV, extend the high cycle S-N curve to the low cycle region maintaining the same slope. ABS, on the other hand proposed a new S-N curve for low cycle fatigue region having a slope of 2.4.
6. The FPSO was assumed to operate in two environments – the North Sea and the coast of West Africa. Based on this assumption, high cycle fatigue damage was obtained using Dirlik's rainflow approximation method. The magnitude

high cycle fatigue damage when the structure was in the North Sea is more significant than when the structure was in West Africa. This was an expected result as the North Sea is characterised by higher waves.

7. The SRSS method for combining damage from low cycle fatigue and high cycle fatigue overestimates the fatigue damage of a structural detail. Methods of combining fatigue damage based on classification society rules were also examined. LR proposed an adjustment factor, which takes into account the stress ranges that have been included in the low cycle fatigue damage calculation. The analysis showed that this adjustment factor is very small and becomes quite negligible when compared to the overall fatigue damage. Thus, the damage using LR proposed equation becomes a simple addition of the damages from the two different processes. DNV uses the quadratic method to combine low cycle and high cycle fatigue damage and this equation gives a better result than simple linear summation as does the ABS proposed equation.

7.2 Recommendations and Future Work

This research has shown that operation is a very important factor in the fatigue life of ship structural details. Other factors that are also important include the structural configuration of the structure, the structural detail of interest and the environment in which the FPSO operates. Loading manuals are employed in ship structures and it contains cargo loading and ballasting operations. It describes design loading conditions (still water shear force and bending moment), allowable local bending and operational limits. For each step of the loading operation the loading plan should also show the amount of ballast and the tanks to be deballasted, the ship's draught and trim, and the calculated shear stress and bending moments. Exceeding the permissible limits specified in the ship's approved loading manual will lead to over-stressing of the ship's structure and may result in catastrophic failure of the hull structure. It would be worthwhile to have a unified standard for loading and unloading FPSOs. Knowing which tanks are to be loaded, how much cargo to be loaded and the maximum still water shear force and bending moment at each step will surely help reduce stresses which in turn will improve fatigue life of the structure.

The following recommendations have been made based on the results obtained:

1. This analysis has shown that low cycle fatigue is very important in FPSOs.

2. The analysis has shown that some structural details in the FPSO are governed by a low cycle fatigue limit state not high cycle fatigue. With stresses of over 1000 MPa obtained in some cases, it is clear the low cycle fatigue damage plays a more important role at some details than high cycle fatigue.

3. The analysis highlighted the fact that certain areas of FPSOs require further attention during design. In this case, because the FPSO had single bottom plating with double skin, the connections in the bottom plating detail were highly stressed from loading and unloading. It is therefore necessary to take factors like this into consideration during fatigue design.

4. This analysis has provided invaluable data showing the difference, in terms of numerical values, in fatigue life estimation based on CS rules. This is attributed to the uncertainties in the S-N curves employed for both high cycle and low cycle fatigue damages. Another factor responsible for this is the different formulations for obtaining the cumulative fatigue damage from loading and unloading cycles and wave cycles. The classification societies need to develop uniform rules for fatigue analysis and design. As it stands, no two fatigue assessment of the same detail are ever the same anyway so this would help reduce uncertainties obtained in fatigue analysis results.

5. Low cycle fatigue assessment results can be used for inspection and monitoring of structural details. A low cycle fatigue assessment of an FPSO will point out structural details that are susceptible to low cycle loads. Using this information, the owners and operators can set up a schedule for monitoring and inspection the detail and probably extend this to other similar details in the structure.

6. This research study provides a benchmark for future studies. There is very little literature available on low cycle fatigue from loading and unloading in FPSOs. This research has provided an in-depth study into low cycle fatigue

and its significance on the overall fatigue damage of the structure. Further research study into different FPSO structural configurations, different loading operational scenarios and other critical structural details in FPSOs is recommended. Also fatigue experiments and testing will be very useful in terms of validating the S-N curves.

APPENDIX A: CYCLE COUNTING METHODS

A1: Cycle Counting Methods

The process of identifying constant amplitude stress ranges and the associated number of cycles present in a stress history is known as cycle counting. The damage accumulated due to these constant amplitude blocks can be calculated individually and summed using Palmgren – Miner's rule to calculate the total accumulated damage of the structure. The two most commonly employed methods for cycle counting are the 'Reservoir method' and the 'Rainflow method'. The reservoir method extracts the largest cycles first and is used for short stress histories. The rainflow counting method extracts smallest cycles first, leaving the largest cycles as the residual cycles (1). It is employed for longer and more complex stress histories.

A2: Reservoir Counting Method

This is imagined as the cross section of a reservoir filled with water. The water is drained from each of the lowest points successively till the entire reservoir is drained. Each drainage operation represents a cycle of stress range equal in magnitude to the height of the water drained in that particular operation. The procedure is illustrated in Figure A1. The reservoir method is recommended for dealing with short term stress histories produced by individual loading events. The procedure is as described below and taken verbatim from European Steel Design Education Programme lecture notes:

The basis of the reservoir method is shown in Figure A1a. It should be assumed that a stress time history of this kind has been obtained from strain gauges attached to the structure at the detail under consideration or has been estimated by computer simulation. It is important that the results analysed should be representative of long term behaviour. To analyse these results, a representative period is chosen so that the peak stress level repeats itself and a line is drawn to join the two peaks as shown in Figure A1b. The region between these two peaks is then regarded as being filled with water to form a reservoir. The procedure is then to take the lowest trough position and imagine that one opens a tap to drain the reservoir.

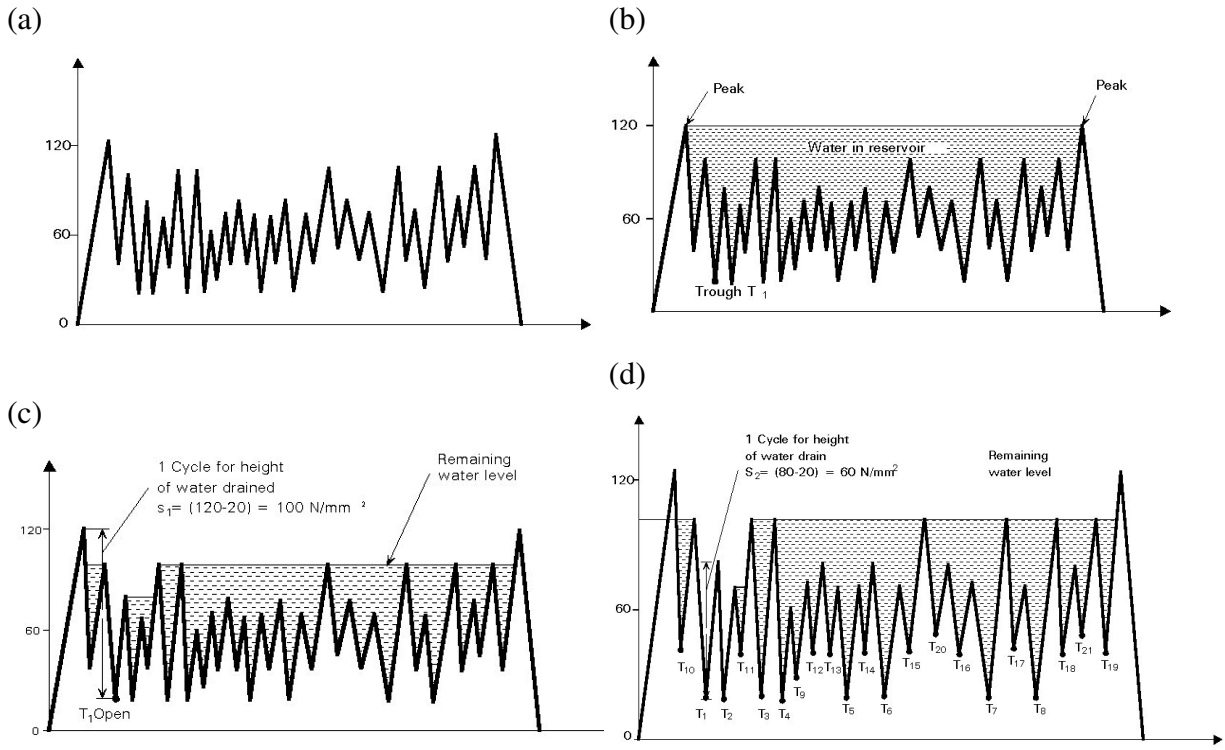

Fig A1: Reservoir Counting Method [38]

Water drains out from this trough T1 but remains tapped in adjacent troughs separated by intermediate peaks as shown in Figure A1c. The draining of the first trough T1 corresponds to one cycle of stress range S1 as shown, and the remaining level of water is now lowered to the level of the next highest peak. A tap is now opened at the next lowest trough T2 as shown in Figure A1d and the water is allowed to drain out. The height of the water released by this operation corresponds to one cycle of stress range S2. This procedure is continued sequentially through each next lowest trough, gradually building up a series of numbers of cycles of different stress ranges. It is also essential to allow for the one cycle from zero to peak stress.

A3: Rainflow Counting Method

This is a visualization of the flow of rain over a sequence of pagoda roofs. The stress or strain time history is plotted so that the time axis is pointing vertically downwards. Rainflow is assumed to begin from a peak to a trough and the distance it travels

determines the magnitude of the stress range, each flow contributing a half cycle. A practical definition of the rainflow cycle counting can be explained as follows according to ASTM standards E-1049. The procedure is illustrated in Figure A2.

Let X denotes range under consideration; Y, previous range adjacent to X; and S, starting point in the history.

1. Read next peak or valley. If out of data, go to Step 6.
2. If there are less than three points, go to Step 1. Form ranges X and Y using the three most recent peaks and valleys that have not been discarded
3. Compare the absolute values of ranges X and Y.
    a. If X<Y, go to Step 1
    b. If X≥Y, go to Step 4.
4. f range Y contains the starting point S, go to step 5; otherwise, count range Y as one cycle; discard the peak and valley of Y; and go to Step 2.
5. Count range Y as one-half cycle; discard the first point (peak or valley) in range Y; move the starting point to the second point in range Y; go to Step 2.
6. Count each range that has not been previously counted as one-half cycle.

Details of the cycle counting are as follows:

1. S=A; Y=|A-B| ; X=|B-C|; X>Y. Y contains S, that is, point A. Count |A-B| as one-half cycle and discard point A; S=B. (Figure b)
2. Y=|B-C|; X=|C-D|; X>Y. Y contains S, that is, point B. Count |B-C| as one half-cycle and discard point B; S=C. (Figure c)
3. Y=|C-D|; X=|D-E|; X<Y
4. Y=|D-E|; X=|E-F|; X<Y
5. Y=|E-F|; X=|F-G|; X>Y. Count |E-F| as one cycle and discard points E and F. (Figure d). A cycle is formed by pairing range E-F and a portion of range F-G
6. Y=|C-D|; X=|D-G|; X>Y. Y contains S, that is, point C. Count |C-D| as one-half cycle and discard point C. S=D. (Figure e)
7. Y=|D-G|; X=|G-H|; X<Y.
8. Y=|G-H|; X=|H-I|; X<Y. End of data.
9. Count |D-G| as one-half cycle, |G-H| as one-half cycle, and |H-I| as one half cycles. (Figure f)

10. End of counting. The table in Figure A2 shows a summary of the cycles counted.

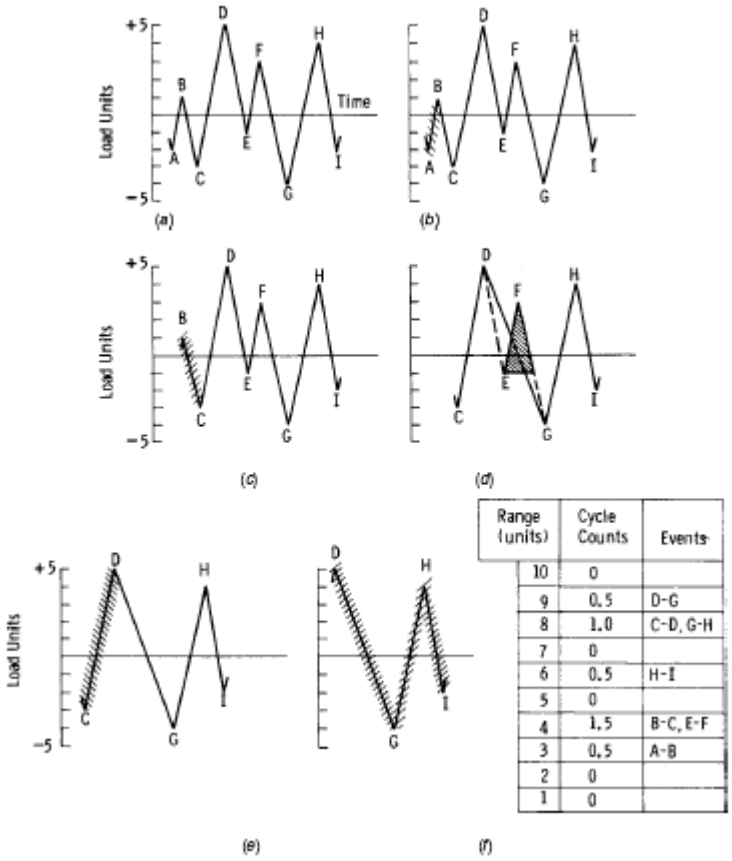

Range (units)	Cycle Counts	Events
10	0	
9	0.5	D-G
8	1.0	C-D, G-H
7	0	
6	0.5	H-I
5	0	
4	1.5	B-C, E-F
3	0.5	A-B
2	0	
1	0	

Fig A2: Example of rainflow counting method

The rainflow method is somewhat more difficult to apply correctly than the reservoir method and it is recommended that both for teaching and for design purposes the reservoir method should be used.

APPENDIX B: LOW CYCLE AND HIGH CYCLE STRESS CYCLES

Table B1: Quasi-static hotspot stress at bottom connection detail

	Low Cycle Stresses (MPa)				
BHS1					
SEQ1	SEQ2	SEQ3	SEQ4	SEQ5	
41.79	41.79	41.79	41.79	41.79	
145.79	130.70	192.06	121.37	119.86	
285.17	214.55	354.92	129.67	125.05	
533.16	367.97	441.89	533.16	533.16	
41.79	533.16	533.16	41.79	41.79	
	41.79	41.79			
BHS2					
SEQ1	SEQ2	SEQ3	SEQ4	SEQ5	
58.54	58.54	58.54	58.54	58.54	
291.30	197.82	359.46	191.27	318.03	
500.30	323.74	680.74	295.33	546.61	
948.85	624.46	813.91	948.85	948.85	
58.54	948.85	948.85	58.54	58.54	
	58.54	58.54			
BHS3					
SEQ1	SEQ2	SEQ3	SEQ4	SEQ5	
226.80	226.80	226.80	226.80	226.80	
207.27	91.64	219.90	92.30	169.55	
272.22	153.33	390.27	198.51	270.48	
496.48	328.84	441.60	496.48	496.48	
226.80	496.48	496.48	226.80	226.80	
	226.80	226.80			
BHS4					
SEQ1	SEQ2	SEQ3	SEQ4	SEQ5	
158.39	158.39	158.39	158.39	158.39	
57.75	69.74	72.07	74.74	141.07	
115.19	116.44	97.47	300.76	507.03	
194.53	159.45	145.75	194.53	194.53	
158.39	194.53	194.53	158.39	158.39	
	158.39	158.39			
BHS5					
SEQ1	SEQ2	SEQ3	SEQ4	SEQ5	
133.21	133.21	133.21	133.21	133.21	
355.86	117.95	385.14	134.05	520.38	
473.36	200.30	836.79	448.07	1228.37	
1007.59	554.94	928.97	1007.59	1007.59	
133.21	1007.59	1007.59	133.21	133.21	
	133.21	133.21			
BHS6					
SEQ1	SEQ2	SEQ3	SEQ4	SEQ5	
176.04	176.04	176.04	176.04	176.04	
422.73	145.17	449.37	154.11	605.00	
550.42	247.26	957.80	498.85	1385.37	
1154.36	648.46	1061.94	1154.36	1154.36	
176.04	1154.36	1154.36	176.04	176.04	
	176.04	176.04			

Table B2: Quasi-static hotspot stress at side plating connection detail

		Low Cycle Stresses (MPa)			
	SHS1				
	SEQ1	SEQ2	SEQ3	SEQ4	SEQ5
	764.06	764.06	764.06	764.06	764.06
	111.95	105.56	138.20	111.83	160.50
	216.79	195.16	111.11	246.04	203.69
	281.64	305.09	209.05	281.64	281.64
	764.06	281.64	281.64	764.06	764.06
		764.06	764.06		
	SHS2				
	SEQ1	SEQ2	SEQ3	SEQ4	SEQ5
	353.55	353.55	353.55	353.55	353.55
	73.26	49.08	83.85	53.02	93.91
	119.07	90.47	176.42	114.60	215.34
	250.89	160.01	218.53	250.89	250.89
	353.55	250.89	250.89	353.55	353.55
		353.55	353.55		
	SHS3				
	SEQ1	SEQ2	SEQ3	SEQ4	SEQ5
	268.39	268.39	268.39	268.39	268.39
	33.73	38.58	43.09	40.39	52.01
	70.99	70.93	40.45	86.46	65.58
	91.99	102.49	64.03	91.99	91.99
	268.39	91.99	91.99	268.39	268.39
		268.39	268.39		
	SHS4				
	SEQ1	SEQ2	SEQ3	SEQ4	SEQ5
	152.61	152.61	152.61	152.61	152.61
	23.26	18.97	37.93	21.94	30.01
	42.41	22.85	115.68	41.39	118.51
	141.75	59.58	130.77	141.75	141.75
	152.61	141.75	141.75	152.61	152.61
		152.61	152.61		
	SHS5				
	SEQ1	SEQ2	SEQ3	SEQ4	SEQ5
	586.37	586.37	586.37	586.37	586.37
	112.16	78.77	88.76	83.05	112.16
	147.90	145.00	72.05	178.98	147.90
	200.50	213.22	129.75	200.50	200.50
	586.37	200.50	200.50	586.37	586.37
		586.37	586.37		
	SHS6				
	SEQ1	SEQ2	SEQ3	SEQ4	SEQ5
	295.44	295.44	295.44	295.44	295.44
	48.33	36.11	57.14	38.69	48.33
	84.10	59.55	105.63	76.71	84.10
	157.12	106.92	113.46	157.12	157.12
	295.44	157.12	157.12	295.44	295.44
		295.44	295.44		

Table B3: Quasi-static hotspot stress at inner side plating connection detail

	Low Cycle Stresses (MPa)					
	IHS1					
	SEQ1	SEQ2	SEQ3	SEQ4	SEQ5	
	48.00	48.00	48.00	48.00	48.00	
	91.24	12.95	84.57	4.42	112.48	
	78.93	30.81	201.45	87.88	291.59	
	234.74	122.93	246.71	234.74	234.74	
	48.00	234.74	234.74	48.00	48.00	
		48.00	48.00			
	IHS2					
	SEQ1	SEQ2	SEQ3	SEQ4	SEQ5	
	96.64	96.64	96.64	96.64	96.64	
	75.61	32.04	79.80	35.66	90.69	
	94.12	60.92	228.71	81.52	268.41	
	277.21	123.49	263.78	277.21	277.21	
	96.64	277.21	277.21	96.64	96.64	
		96.64	96.64			
	IHS3					
	SEQ1	SEQ2	SEQ3	SEQ4	SEQ5	
	68.94	68.94	68.94	68.94	68.94	
	20.62	12.25	16.89	9.21	28.78	
	14.11	6.11	36.58	22.54	62.49	
	44.35	23.92	43.27	44.35	44.35	
	68.94	44.35	44.35	68.94	68.94	
		68.94	68.94			
	IHS4					
	SEQ1	SEQ2	SEQ3	SEQ4	SEQ5	
	79.00	79.00	79.00	79.00	79.00	
	65.90	19.48	63.43	20.31	70.24	
	58.56	36.57	69.63	33.03	81.50	
	76.42	61.48	73.25	76.42	76.42	
	79.00	76.42	76.42	79.00	79.00	
		79.00	79.00			
	IHS5					
	SEQ1	SEQ2	SEQ3	SEQ4	SEQ5	
	160.57	160.57	160.57	160.57	160.57	
	38.19	10.98	32.94	4.17	60.77	
	27.78	18.63	65.62	59.50	141.88	
	87.76	57.90	83.61	87.76	87.76	
	160.57	87.76	87.76	160.57	160.57	
		160.57	160.57			
	IHS6					
	SEQ1	SEQ2	SEQ3	SEQ4	SEQ5	
	36.06	36.06	36.06	36.06	36.06	
	83.72	19.14	87.82	22.73	107.95	
	101.78	41.88	247.98	66.85	289.83	
	284.65	124.49	252.82	284.65	284.65	
	36.06	284.65	284.65	36.06	36.06	
		36.06	36.06			

Table B4: Dynamic hotspot stress at bottom connection detail

Ballast	Dirlik Constant			BHS1	BHS2	BHS3	BHS4	BHS5	BHS6
NS			SCF	1.61	1.35	2.16	1.81	2.49	1.55
30.778	0.989			49.01	41.09	65.75	55.10	75.79	47.18
31.226	0.924			46.45	38.95	62.32	52.22	71.84	44.72
24.737	0.715			28.48	23.88	38.20	32.01	44.04	27.41
28.079	0.452			20.43	17.13	27.41	22.97	31.60	19.67
39.849	0.340			21.81	18.29	29.27	24.52	33.74	21.00
55.436	0.309			27.58	23.13	37.00	31.00	42.65	26.55
69.494	0.301			33.68	28.24	45.18	37.86	52.09	32.42
80.499	0.297			38.49	32.28	51.64	43.27	59.53	37.06
85.695	0.294			40.56	34.01	54.42	45.60	62.73	39.05
82.809	0.290			38.66	32.42	51.87	43.47	59.80	37.22
77.191	0.286			35.54	29.80	47.69	39.96	54.97	34.22
63.827	0.281			28.88	24.21	38.74	32.46	44.66	27.80
70.411	0.277			31.40	26.33	42.13	35.30	48.56	30.23
WA									
20.274	0.715			23.34	19.57	31.31	26.24	36.09	22.47
23.414	0.452			17.04	14.29	22.86	19.16	26.35	16.40
29.594	0.340			16.20	13.58	21.73	18.21	25.05	15.60
35.067	0.309			17.45	14.63	23.41	19.61	26.98	16.80
37.707	0.301			18.27	15.32	24.52	20.54	28.26	17.59
39.132	0.297			18.71	15.69	25.10	21.04	28.94	18.01
36.432	0.294			17.24	14.46	23.14	19.39	26.67	16.60
36.851	0.290			17.21	14.43	23.08	19.34	26.61	16.56
Full									
NS			SCF	1.72	2.22	2.27	0.96	4.16	3.91
19.459	0.987			33.03	42.64	43.60	18.44	79.90	75.10
19.892	0.981			33.56	43.32	44.30	18.73	81.18	76.30
17.271	0.629			18.69	24.12	24.66	10.43	45.19	42.48
22.661	0.399			15.55	20.07	20.52	8.68	37.61	35.35
36.587	0.339			21.33	27.53	28.15	11.91	51.60	48.50
58.471	0.345			34.70	44.78	45.79	19.37	83.92	78.87
81.545	0.384			53.86	69.52	71.08	30.06	130.26	122.43
101.094	0.425			73.90	95.38	97.53	41.25	178.73	167.99
112.127	0.457			88.14	113.76	116.32	49.19	213.17	200.36
111.049	0.479			91.49	118.09	120.75	51.06	221.28	207.98
105.064	0.492			88.91	114.76	117.34	49.62	215.04	202.11
87.665	0.500			75.39	97.31	99.50	42.08	182.34	171.39
97.244	0.503			84.13	108.59	111.03	46.96	203.48	191.25
WA									
14.155	0.629			15.31	19.77	20.21	8.55	37.04	34.81
18.896	0.399			12.97	16.74	17.11	7.24	31.36	29.48
27.172	0.339			15.84	20.45	20.91	8.84	38.32	36.02
36.987	0.345			21.95	28.33	28.97	12.25	53.08	49.89
44.246	0.384			29.22	37.72	38.57	16.31	70.68	66.43
49.144	0.425			35.92	46.37	47.41	20.05	86.89	81.67
47.669	0.457			37.47	48.36	49.45	20.91	90.62	85.18
49.418	0.479			40.71	52.55	53.73	22.72	98.47	92.55

Table B5: Dynamic hotspot stress at side plating connection detail

Ballast	Dirlik Constant			SHS1	SHS2	SHS3	SHS4	SHS5	SHS6
NS			SCF	3.68	3.60	1.93	2.62	3.09	3.49
30.778	0.989			112.02	109.58	58.75	79.75	94.06	106.23
31.226	0.924			106.18	103.87	55.69	75.59	89.16	100.70
24.737	0.715			65.09	63.67	34.14	46.34	54.65	61.73
28.079	0.452			46.71	45.69	24.49	33.25	39.22	44.29
39.849	0.340			49.86	48.78	26.15	35.50	41.87	47.28
55.436	0.309			63.04	61.67	33.06	44.88	52.93	59.78
69.494	0.301			76.98	75.30	40.37	54.80	64.64	73.00
80.499	0.297			87.98	86.07	46.14	62.64	73.88	83.44
85.695	0.294			92.72	90.70	48.63	66.01	77.85	87.93
82.809	0.290			88.37	86.45	46.35	62.92	74.21	83.81
77.191	0.286			81.24	79.48	42.61	57.84	68.22	77.05
63.827	0.281			66.00	64.57	34.62	46.99	55.42	62.59
70.411	0.277			71.77	70.21	37.64	51.10	60.27	68.07
WA									
20.274	0.715			53.34	52.19	27.98	37.98	44.79	50.59
23.414	0.452			38.95	38.10	20.43	27.73	32.70	36.94
29.594	0.340			37.03	36.22	19.42	26.36	31.09	35.12
35.067	0.309			39.88	39.01	20.91	28.39	33.48	37.82
37.707	0.301			41.77	40.86	21.91	29.74	35.07	39.61
39.132	0.297			42.77	41.84	22.43	30.45	35.91	40.56
36.432	0.294			39.42	38.56	20.67	28.06	33.10	37.38
36.851	0.290			39.33	38.47	20.63	28.00	33.02	37.30
Full									
NS			SCF	3.69	3.42	2.30	2.46	2.85	2.19
19.459	0.987			70.87	65.68	44.17	47.25	54.74	42.06
19.892	0.981			72.01	66.74	44.88	48.00	55.62	42.74
17.271	0.629			40.09	37.15	24.99	26.72	30.96	23.79
22.661	0.399			33.36	30.92	20.80	22.24	25.77	19.80
36.587	0.339			45.77	42.42	28.53	30.51	35.35	27.16
58.471	0.345			74.44	68.99	46.40	49.62	57.49	44.18
81.545	0.384			115.55	107.09	72.02	77.03	89.24	68.58
101.094	0.425			158.54	146.94	98.82	105.69	122.45	94.09
112.127	0.457			189.08	175.25	117.86	126.06	146.04	112.22
111.049	0.479			196.28	181.92	122.34	130.85	151.60	116.49
105.064	0.492			190.74	176.78	118.89	127.16	147.32	113.20
87.665	0.500			161.74	149.91	100.81	107.83	124.92	95.99
97.244	0.503			180.49	167.28	112.50	120.33	139.40	107.12
WA									
14.155	0.629			32.85	30.45	20.48	21.90	25.37	19.50
18.896	0.399			27.82	25.79	17.34	18.55	21.49	16.51
27.172	0.339			33.99	31.50	21.19	22.66	26.25	20.17
36.987	0.345			47.09	43.64	29.35	31.39	36.37	27.95
44.246	0.384			62.69	58.11	39.08	41.80	48.42	37.21
49.144	0.425			77.07	71.43	48.04	51.38	59.53	45.74
47.669	0.457			80.39	74.50	50.10	53.59	62.09	47.71
49.418	0.479			87.35	80.96	54.44	58.23	67.46	51.84

Table B6: Dynamic hotspot stress at inner side plating connection detail

Ballast	Dirlik Constant		IHS1	IHS2	IHS3	IHS4	IHS5	IHS6
NS		SCF	1.18	4.09	1.41	1.49	2.63	1.04
30.778	0.989		35.92	124.50	42.92	45.35	80.06	31.66
31.226	0.924		34.05	118.01	40.68	42.99	75.88	30.01
24.737	0.715		20.87	72.34	24.94	26.35	46.52	18.39
28.079	0.452		14.98	51.91	17.90	18.91	33.38	13.20
39.849	0.340		15.99	55.41	19.10	20.19	35.63	14.09
55.436	0.309		20.21	70.06	24.15	25.52	45.05	17.81
69.494	0.301		24.68	85.55	29.49	31.17	55.01	21.75
80.499	0.297		28.21	97.78	33.71	35.62	62.88	24.86
85.695	0.294		29.73	103.04	35.52	37.54	66.26	26.20
82.809	0.290		28.34	98.22	33.86	35.78	63.16	24.98
77.191	0.286		26.05	90.29	31.13	32.89	58.06	22.96
63.827	0.281		21.16	73.36	25.29	26.72	47.17	18.65
70.411	0.277		23.01	79.77	27.50	29.06	51.30	20.28
WA								
20.274	0.715		17.11	59.29	20.44	21.60	38.12	15.08
23.414	0.452		12.49	43.28	14.92	15.77	27.83	11.01
29.594	0.340		11.87	41.15	14.19	14.99	26.46	10.46
35.067	0.309		12.79	44.32	15.28	16.15	28.50	11.27
37.707	0.301		13.39	46.42	16.00	16.91	29.85	11.80
39.132	0.297		13.71	47.53	16.39	17.32	30.57	12.09
36.432	0.294		12.64	43.81	15.10	15.96	28.17	11.14
36.851	0.290		12.61	43.71	15.07	15.92	28.11	11.11
Full								
NS		SCF	5.76	2.58	1.09	1.06	3.15	2.41
19.459	0.987		110.63	49.55	20.93	20.36	60.50	46.29
19.892	0.981		112.40	50.35	21.27	20.68	61.47	47.03
17.271	0.629		62.57	28.03	11.84	11.52	34.22	26.18
22.661	0.399		52.08	23.33	9.86	9.58	28.48	21.79
36.587	0.339		71.44	32.00	13.52	13.15	39.07	29.89
58.471	0.345		116.19	52.05	21.99	21.38	63.54	48.62
81.545	0.384		180.36	80.79	34.13	33.19	98.64	75.47
101.094	0.425		247.48	110.85	46.83	45.54	135.34	103.55
112.127	0.457		295.15	132.20	55.85	54.32	161.41	123.49
111.049	0.479		306.39	137.24	57.98	56.38	167.56	128.19
105.064	0.492		297.74	133.36	56.34	54.79	162.83	124.58
87.665	0.500		252.48	113.09	47.78	46.46	138.07	105.64
97.244	0.503		281.74	126.20	53.32	51.85	154.08	117.88
WA								
14.155	0.629		51.28	22.97	9.70	9.44	28.05	21.46
18.896	0.399		43.43	19.45	8.22	7.99	23.75	18.17
27.172	0.339		53.06	23.77	10.04	9.76	29.02	22.20
36.987	0.345		73.50	32.92	13.91	13.53	40.20	30.75
44.246	0.384		97.87	43.84	18.52	18.01	53.52	40.95
49.144	0.425		120.30	53.89	22.77	22.14	65.79	50.34
47.669	0.457		125.48	56.20	23.75	23.09	68.62	52.50
49.418	0.479		136.35	61.07	25.80	25.09	74.56	57.05

APPENDIX C: HIGH-CYCLE (WAVE) FATIGUE DAMAGE

Table C1: Wave Fatigue Damage for North Sea and West Africa Sea at BHS1

North Sea Scatter Diagram

BALLAST						FULL									
BHS1												Damage/Year			
Hs	Tz	n/year	D_{LR}	D_{DNV}	D_{ABS}	Hs	Tz	n/year	D_{LR}	D_{DNV}	D_{ABS}		D_{LR}	D_{DNV}	D_{ABS}
0.5	1.333	507.997	1.37E-05	1.60E-05	1.86E-05	0.5	1.336	507.361	4.34E-06	4.20E-06	5.71E-06		9.01E-06	1.01E-05	1.21E-05
1.129	1.468	35560	9.35E-04	7.24E-04	1.27E-03	1.129	1.479	35470	3.02E-04	3.12E-04	3.97E-03		6.18E-04	5.18E-04	2.62E-03
1.372	1.798	1264000	1.28E-02	9.91E-03	1.70E-02	1.372	1.961	1247000	4.75E-03	0.005	6.25E-03		8.77E-03	7.26E-03	1.16E-02
1.722	2.548	3733000	3.49E-02	2.70E-02	4.70E-02	1.722	3.096	3555000	0.019	0.019	0.026		2.69E-02	2.29E-02	3.65E-02
2.315	3.715	4902000	9.85E-02	7.60E-02	1.34E-01	2.315	4.797	4376000	0.085	0.083	0.112		9.18E-02	7.94E-02	1.23E-01
3.128	4.882	4369000	2.15E-01	1.67E-01	2.92E-01	3.128	6.553	3549000	0.288	0.279	0.379		2.51E-01	2.23E-01	3.36E-01
4.028	5.827	3061000	2.89E-01	2.24E-01	3.92E-01	4.028	7.871	2263000	0.553	0.537	0.728		4.21E-01	3.80E-01	5.60E-01
4.962	6.582	1513000	2.19E-01	1.70E-01	2.98E-01	4.962	8.791	1040000	0.537	0.520	0.706		3.78E-01	3.45E-01	5.02E-01
5.717	7.203	567300	9.81E-02	7.60E-02	1.33E-01	5.717	9.47	370700	0.28	0.272	0.369		1.89E-01	1.74E-01	2.51E-01
6.035	7.725	170600	2.62E-02	2.00E-02	3.60E-02	6.035	10	107600	0.083	0.080	0.109		5.46E-02	5.02E-02	7.25E-02
6.177	8.167	64200	7.89E-03	6.12E-03	1.10E-02	6.177	10.431	39510	2.60E-02	2.57E-02	0.035		1.69E-02	1.59E-02	2.30E-02
5.621	8.543	23070	1.57E-03	1.22E-03	2.14E-03	5.621	10.791	13950	5.52E-03	5.35E-03	7.27E-03		3.55E-03	3.29E-03	4.70E-03
6.827	8.866	4354	3.93E-04	3.05E-04	5.34E-04	6.827	11.906	2600	1.41E-03	1.37E-03	1.86E-03		9.04E-04	8.37E-04	1.20E-03
												Dannual	1.44E+00	1.30E+00	1.92E+00

West Africa Scatter Diagram

1.124	1.798	757200	4.34E-03	4.21E-03	5.70E-03	1.124	1.961	746800	0.001566	0.0015176	0.002062		2.95E-03	2.87E-03	3.88E-03
1.436	2.548	3834000	2.10E-02	2.08E-02	2.80E-02	1.436	3.096	3651000	0.012	0.011196	0.015		1.65E-02	1.60E-02	2.15E-02
1.719	3.715	6512000	5.50E-02	5.36E-02	7.30E-02	1.719	4.797	5813000	0.046	0.0450333	0.061		5.05E-02	4.93E-02	6.70E-02
1.978	4.882	5184000	6.70E-02	6.45E-02	8.70E-02	1.978	6.553	4210000	0.086	0.0837178	0.114		7.65E-02	7.41E-02	1.01E-01
2.186	5.827	2537000	3.90E-02	3.82E-02	5.20E-02	2.186	7.871	1876000	0.073	0.0710813	0.096		5.60E-02	5.47E-02	7.40E-02
2.412	6.582	898300	1.50E-02	1.49E-02	2.00E-02	2.412	8.791	617700	0.037	0.0354934	0.048		2.60E-02	2.52E-02	3.40E-02
2.431	7.203	237100	3.25E-03	3.15E-03	4.27E-03	2.431	9.47	154900	0.009006	0.0087346	0.012		6.13E-03	5.94E-03	8.13E-03
2.686	7.725	60720	8.49E-04	8.23E-04	1.12E-03	2.686	10	38300	0.002599	0.0025221	0.003421		1.72E-03	1.67E-03	2.27E-03
												Dannual	2.36E-01	2.30E-01	3.11E-01

Table C2: Wave Fatigue Damage for North Sea and West Africa Sea at BHS2

BHS2						North Sea Scatter Diagram							Total Damage/Year		
Hs	Tz	n/year	D_{LR}	D_{DNV}	D_{ABS}	Hs	Tz	n/year	D_{LR}	D_{DNV}	D_{ABS}		D_{LR}	D_{DNV}	D_{ABS}
0.5	1.333	507.997	8.32E-06	8.07E-06	1.10E-05	0.5	1.336	507.361	9.33E-06	9.04E-06	1.23E-05		8.82E-06	8.55E-06	1.16E-05
1.129	1.468	35560	5.68E-04	5.51E-04	7.48E-04	1.129	1.479	35470	6.48E-04	6.71E-04	8.53E-04		6.08E-04	6.11E-04	8.00E-04
1.372	1.798	1264000	7.77E-03	7.53E-03	1.00E-02	1.372	1.961	1247000	1.00E-02	9.90E-03	1.30E-02		8.88E-03	8.72E-03	1.15E-02
1.722	2.548	3733000	2.10E-02	2.06E-02	2.80E-02	1.722	3.096	3555000	4.20E-02	4.04E-02	5.50E-02		3.15E-02	3.05E-02	4.15E-02
2.315	3.715	4902000	6.00E-02	5.81E-02	7.90E-02	2.315	4.797	4376000	1.83E-01	1.78E-01	2.41E-01		1.22E-01	1.18E-01	1.60E-01
3.128	4.882	4369000	1.31E-01	1.27E-01	1.72E-01	3.128	6.553	3549000	6.19E-01	6.00E-01	8.15E-01		3.75E-01	3.63E-01	4.94E-01
4.028	5.827	3061000	1.76E-01	1.70E-01	2.31E-01	4.028	7.871	2263000	1.19E+00	1.15E+00	1.57E+00		6.83E-01	6.62E-01	8.99E-01
4.962	6.582	1513000	1.33E-01	1.29E-01	1.76E-01	4.962	8.791	1040000	1.15E+00	1.12E+00	1.52E+00		6.44E-01	6.24E-01	8.48E-01
5.717	7.203	567300	6.00E-02	5.78E-02	7.90E-02	5.717	9.47	370700	6.03E-01	5.85E-01	7.94E-01		3.32E-01	3.21E-01	4.37E-01
6.035	7.725	170600	1.60E-02	1.55E-02	2.10E-02	6.035	10	107600	1.78E-01	1.73E-01	2.35E-01		9.70E-02	9.42E-02	1.28E-01
6.177	8.167	64200	4.79E-03	4.65E-03	6.31E-03	6.177	10.431	39510	5.70E-02	5.52E-02	7.50E-02		3.09E-02	2.99E-02	4.07E-02
5.621	8.543	23070	9.59E-04	9.28E-04	1.26E-03	5.621	10.791	13950	1.20E-02	1.15E-02	1.60E-02		6.48E-03	6.22E-03	8.63E-03
6.827	8.866	4354	2.39E-04	2.32E-04	3.15E-04	6.827	11.906	2600	3.04E-03	2.95E-03	4.00E-03		1.64E-03	1.59E-03	2.16E-03
												Dannual	2.33E+00	2.26E+00	3.07E+00
						West Africa Scatter Diagram									
1.124	1.798	757200	2.56E-03	2.48E-03	3.37E-03	1.124	1.961	746800	3.37E-03	3.26E-03	4.43E-03		2.96E-03	2.87E-03	3.90E-03
1.436	2.548	3834000	1.30E-02	1.23E-02	1.70E-02	1.436	3.096	3651000	2.50E-02	2.41E-02	3.30E-02		1.90E-02	1.82E-02	2.50E-02
1.719	3.715	6512000	3.30E-02	3.16E-02	4.30E-02	1.719	4.797	5813000	1.00E-01	9.68E-02	1.31E-01		6.65E-02	6.42E-02	8.70E-02
1.978	4.882	5184000	3.90E-02	3.80E-02	5.20E-02	1.978	6.553	4210000	1.86E-01	1.80E-01	2.45E-01		1.13E-01	1.09E-01	1.49E-01
2.186	5.827	2537000	2.30E-02	2.25E-02	3.10E-02	2.186	7.871	1876000	1.58E-01	1.53E-01	2.07E-01		9.05E-02	8.77E-02	1.19E-01
2.412	6.582	898300	9.10E-03	8.81E-03	1.20E-02	2.412	8.791	617700	7.90E-02	7.63E-02	1.04E-01		4.40E-02	4.26E-02	5.80E-02
2.431	7.203	237100	1.92E-03	1.86E-03	2.52E-03	2.431	9.47	154900	1.90E-02	1.88E-02	2.50E-02		1.05E-02	1.03E-02	1.38E-02
2.686	7.725	60720	5.01E-04	4.85E-04	6.59E-03	2.686	10	38300	5.59E-03	5.42E-03	7.36E-03		3.04E-03	2.95E-03	6.97E-03
												Dannual	3.49E-01	3.38E-01	4.62E-01

Table C3: Wave Fatigue Damage for North Sea and West Africa Sea at BHS3

BHS3						North Sea Scatter Diagram							Total Damage/Year		
Hs	Tz	n/year	D_{LR}	D_{DNV}	D_{ABS}	Hs	Tz	n/year	D_{LR}	D_{DNV}	D_{ABS}		D_{LR}	D_{DNV}	D_{ABS}
0.5	1.333	507.997	3.41E-05	3.30E-05	4.48E-05	0.5	1.336	507.361	9.96E-06	9.66E-06	1.31E-05		2.20E-05	2.14E-05	2.89E-05
1.129	1.468	35560	2.33E-03	2.26E-03	3.06E-03	1.129	1.479	35470	6.92E-04	7.17E-04	9.11E-04		1.51E-03	1.49E-03	1.98E-03
1.372	1.798	1264000	3.20E-02	3.09E-02	4.20E-02	1.372	1.961	1247000	1.10E-02	1.06E-02	1.40E-02		2.15E-02	2.07E-02	2.80E-02
1.722	2.548	3733000	8.70E-02	8.43E-02	1.14E-01	1.722	3.096	3555000	4.50E-02	4.32E-02	5.90E-02		6.60E-02	6.37E-02	8.65E-02
2.315	3.715	4902000	2.46E-01	2.38E-01	3.32E-01	2.315	4.797	4376000	1.96E-01	1.90E-01	2.58E-01		2.21E-01	2.14E-01	2.95E-01
3.128	4.882	4369000	5.36E-01	5.19E-01	7.03E-01	3.128	6.553	3549000	6.61E-01	6.41E-01	8.71E-01		5.99E-01	5.80E-01	7.87E-01
4.028	5.827	3061000	7.20E-01	6.98E-01	9.45E-01	4.028	7.871	2263000	1.27E+00	1.23E+00	1.68E+00		9.96E-01	9.66E-01	1.31E+00
4.962	6.582	1513000	5.46E-01	5.29E-01	7.17E-01	4.962	8.791	1040000	1.23E+00	1.20E+00	1.62E+00		8.90E-01	8.62E-01	1.17E+00
5.717	7.203	567300	2.44E-01	2.37E-01	3.21E-01	5.717	9.47	370700	6.45E-01	6.25E-01	8.49E-01		4.45E-01	4.31E-01	5.85E-01
6.035	7.725	170600	6.50E-02	6.34E-02	8.60E-02	6.035	10	107600	1.90E-01	1.85E-01	2.51E-01		1.28E-01	1.24E-01	1.69E-01
6.177	8.167	64200	2.00E-02	1.91E-02	2.60E-02	6.177	10.431	39510	6.10E-02	5.90E-02	8.00E-02		4.05E-02	3.90E-02	5.30E-02
5.621	8.543	23070	3.93E-03	3.80E-03	5.15E-03	5.621	10.791	13950	1.30E-02	1.23E-02	1.70E-02		8.46E-03	8.05E-03	1.11E-02
6.827	8.866	4354	9.79E-03	9.50E-04	1.29E-04	6.827	11.906	2600	3.25E-03	3.15E-03	4.28E-03		6.52E-03	2.05E-03	2.20E-03
												Dannual	3.42E+00	3.31E+00	4.50E+00
						West Africa Scatter Diagram									
1.124	1.798	757200	1.10E-02	1.02E-02	1.40E-02	1.124	1.961	746800	3.59E-03	3.49E-03	4.73E-03		7.30E-03	6.83E-03	9.37E-03
1.436	2.548	3834000	5.20E-02	5.02E-02	6.80E-02	1.436	3.096	3651000	2.70E-02	2.57E-02	3.50E-02		3.95E-02	3.80E-02	5.15E-02
1.719	3.715	6512000	1.34E-01	1.29E-01	1.76E-01	1.719	4.797	5813000	1.07E-01	1.04E-01	1.40E-01		1.21E-01	1.16E-01	1.58E-01
1.978	4.882	5184000	1.61E-01	1.56E-01	2.12E-01	1.978	6.553	4210000	1.99E-01	1.92E-01	2.62E-01		1.80E-01	1.74E-01	2.37E-01
2.186	5.827	2537000	9.50E-02	9.24E-02	1.25E-01	2.186	7.871	1876000	1.68E-01	1.63E-01	2.22E-01		1.32E-01	1.28E-01	1.74E-01
2.412	6.582	898300	3.70E-02	3.61E-02	4.90E-02	2.412	8.791	617700	8.40E-02	8.16E-02	1.11E-01		6.05E-02	5.88E-02	8.00E-02
2.431	7.203	237100	7.85E-03	7.60E-03	1.00E-02	2.431	9.47	154900	2.10E-02	2.01E-02	2.70E-02		1.44E-02	1.38E-02	1.85E-02
2.686	7.725	60720	2.05E-04	1.99E-03	2.70E-03	2.686	10	38300	5.97E-03	5.80E-03	7.87E-03		3.09E-03	3.89E-03	5.28E-03
												Dannual	5.57E-01	5.40E-01	7.33E-01

Table C4: Wave Fatigue Damage for North Sea and West Africa Sea at BHS4

BHS4						North Sea Scatter Diagram						Total Damage/Year		
Hs	Tz	n/year	D_{LR}	D_{DNV}	D_{ABS}	Hs	Tz	n/year	D_{LR}	D_{DNV}	D_{ABS}	D_{LR}	D_{DNV}	D_{ABS}
0.5	1.333	507.997	2.00E-05	1.94E-05	2.63E-05	0.5	1.336	507.361	7.54E-07	7.31E-07	9.93E-07	1.04E-05	1.01E-05	1.36E-05
1.129	1.468	35560	1.37E-03	1.33E-03	1.80E-03	1.129	1.479	35470	5.60E-05	5.42E-05	7.37E-05	7.12E-04	6.91E-04	9.35E-04
1.372	1.798	1264000	1.90E-02	1.82E-02	2.50E-02	1.372	1.961	1247000	8.26E-04	8.00E-04	1.09E-03	9.91E-03	9.48E-03	1.30E-02
1.722	2.548	3733000	5.10E-02	4.96E-02	6.70E-02	1.722	3.096	3555000	3.37E-03	3.27E-03	4.44E-03	2.72E-02	2.64E-02	3.57E-02
2.315	3.715	4902000	1.44E-01	1.40E-01	1.90E-01	2.315	4.797	4376000	1.48E-02	1.44E-02	1.95E-02	7.94E-02	7.72E-02	1.05E-01
3.128	4.882	4369000	3.15E-01	3.05E-01	4.14E-01	3.128	6.553	3549000	5.00E-02	4.85E-02	6.58E-02	1.83E-01	1.77E-01	2.40E-01
4.028	5.827	3061000	4.24E-01	4.10E-01	5.56E-01	4.028	7.871	2263000	9.63E-02	9.33E-02	1.27E-01	2.60E-01	2.52E-01	3.41E-01
4.962	6.582	1513000	3.21E-01	3.11E-01	4.22E-01	4.962	8.791	1040000	9.33E-02	9.04E-02	1.23E-01	2.07E-01	2.01E-01	2.72E-01
5.717	7.203	567300	1.44E-01	1.39E-01	1.89E-01	5.717	9.47	370700	4.88E-02	4.73E-02	6.42E-02	9.64E-02	9.33E-02	1.27E-01
6.035	7.725	170600	3.80E-02	3.73E-02	5.10E-02	6.035	10	107600	1.44E-02	1.40E-02	1.90E-02	2.62E-02	2.56E-02	3.50E-02
6.177	8.167	64200	1.20E-02	1.12E-02	1.50E-02	6.177	10.431	39510	4.61E-03	4.47E-03	6.06E-03	8.30E-03	7.84E-03	1.05E-02
5.621	8.543	23070	2.31E-03	2.24E-03	3.03E-03	5.621	10.791	13950	9.60E-04	9.31E-04	1.26E-03	1.64E-03	1.58E-03	2.15E-03
6.827	8.866	4354	5.76E-04	5.59E-04	7.56E-03	6.827	11.906	2600	2.46E-04	2.38E-04	3.24E-04	4.11E-04	3.99E-04	3.94E-03
											Dannual	9.00E-01	8.72E-01	1.19E+00
						West Africa Scatter Diagram								
1.124	1.798	757200	6.17E-03	5.99E-03	8.10E-03	1.124	1.961	746800	2.72E-04	2.64E-04	3.58E-04	3.22E-03	3.13E-03	4.23E-03
1.436	2.548	3834000	3.00E-02	2.95E-02	4.00E-02	1.436	3.096	3651000	2.01E-03	1.95E-03	2.64E-03	1.60E-02	1.57E-02	2.13E-02
1.719	3.715	6512000	7.90E-02	7.62E-02	1.03E-01	1.719	4.797	5813000	8.08E-03	7.83E-03	1.06E-02	4.35E-02	4.20E-02	5.68E-02
1.978	4.882	5184000	9.50E-02	9.17E-02	1.24E-01	1.978	6.553	4210000	1.50E-02	1.46E-02	1.98E-02	5.50E-02	5.31E-02	7.19E-02
2.186	5.827	2537000	5.60E-02	5.43E-02	7.40E-02	2.186	7.871	1876000	1.28E-02	1.24E-02	1.68E-02	3.44E-02	3.34E-02	4.54E-02
2.412	6.582	898300	2.20E-02	2.12E-02	2.90E-02	2.412	8.791	617700	6.37E-03	0.0061713	0.0083816	1.42E-02	1.37E-02	1.87E-02
2.431	7.203	237100	4.62E-03	4.47E-03	6.06E-03	2.431	9.47	154900	1.57E-03	0.0015187	0.0020627	3.09E-03	3.00E-03	4.06E-03
2.686	7.725	60720	1.21E-03	1.17E-03	1.59E-03	2.686	10	38300	4.52E-04	0.0004385	0.0005956	8.30E-04	8.04E-04	1.09E-03
											Dannual	1.70E-01	1.65E-01	2.23E-01

Table C5: Wave Fatigue Damage for North Sea and West Africa Sea at BHS5

BHS5						North Sea Scatter Diagram							Total Damage/Year		
Hs	Tz	n/year	D_{LR}	D_{DNV}	D_{ABS}	Hs	Tz	n/year	D_{LR}	D_{DNV}	D_{ABS}		D_{LR}	D_{DNV}	D_{ABS}
0.5	1.333	507.997	5.22E-05	5.06E-05	6.85E-05	0.5	1.336	507.361	6.13E-05	5.95E-05	8.07E-05		5.67E-05	5.50E-05	7.46E-05
1.129	1.468	35560	3.56E-03	3.46E-03	4.67E-03	1.129	1.479	35470	4.26E-03	4.41E-03	5.61E-03		3.91E-03	3.94E-03	5.14E-03
1.372	1.798	1264000	4.90E-02	4.73E-02	6.40E-02	1.372	1.961	1247000	6.70E-02	6.51E-02	8.80E-02		5.80E-02	5.62E-02	7.60E-02
1.722	2.548	3733000	1.33E-01	1.29E-01	1.75E-01	1.722	3.096	3555000	2.74E-01	2.66E-01	3.61E-01		2.04E-01	1.98E-01	2.68E-01
2.315	3.715	4902000	3.76E-01	3.64E-01	4.94E-01	2.315	4.797	4376000	1.21E+00	1.17E+00	1.59E+00		7.91E-01	7.68E-01	1.04E+00
3.128	4.882	4369000	8.21E-01	7.95E-01	1.08E+00	3.128	6.553	3549000	4.07E+00	3.94E+00	5.36E+00		2.45E+00	2.37E+00	3.22E+00
4.028	5.827	3061000	1.10E+00	1.07E+00	1.45E+00	4.028	7.871	2263000	7.83E+00	7.59E+00	1.03E+01		4.47E+00	4.33E+00	5.88E+00
4.962	6.582	1513000	8.37E-01	8.10E-01	1.10E+00	4.962	8.791	1040000	7.59E+00	7.36E+00	1.00E+01		4.21E+00	4.08E+00	5.55E+00
5.717	7.203	567300	3.74E-01	3.63E-01	4.91E-01	5.717	9.47	370700	3.97E+00	3.85E+00	5.23E+00		2.17E+00	2.11E+00	2.86E+00
6.035	7.725	170600	1.00E-01	9.71E-02	1.32E-01	6.035	10	107600	1.17E+00	1.14E+00	1.54E+00		6.36E-01	6.17E-01	8.38E-01
6.177	8.167	64200	3.00E-02	2.92E-02	3.90E-02	6.177	10.431	39510	3.75E-01	3.63E-01	4.93E-01		2.03E-01	1.96E-01	2.66E-01
5.621	8.543	23070	6.02E-03	5.83E-03	7.90E-03	5.621	10.791	13950	7.80E-02	7.57E-02	1.03E-01		4.20E-02	4.08E-02	5.54E-02
6.827	8.866	4354	1.50E-03	1.46E-03	1.97E-04	6.827	11.906	2600	2.00E-02	1.94E-02	2.60E-02		1.08E-02	1.04E-02	1.31E-02
												Dannual	1.52E+01	1.48E+01	2.01E+01
						West Africa Scatter Diagram									
1.124	1.798	757200	1.60E-02	1.56E-02	2.10E-02	1.124	1.961	746800	2.20E-02	2.15E-02	2.90E-02		1.90E-02	1.85E-02	2.50E-02
1.436	2.548	3834000	7.90E-02	7.69E-02	1.04E-01	1.436	3.096	3651000	1.63E-01	1.58E-01	2.15E-01		1.21E-01	1.18E-01	1.60E-01
1.719	3.715	6512000	2.05E-01	1.98E-01	2.69E-01	1.719	4.797	5813000	6.56E-01	6.37E-01	8.64E-01		4.31E-01	4.18E-01	5.67E-01
1.978	4.882	5184000	2.46E-01	2.39E-01	3.24E-01	1.978	6.553	4210000	1.22E+00	1.18E+00	1.61E+00		7.35E-01	7.12E-01	9.67E-01
2.186	5.827	2537000	1.46E-01	1.41E-01	1.92E-01	2.186	7.871	1876000	1.04E+00	1.01E+00	1.37E+00		5.92E-01	5.74E-01	7.79E-01
2.412	6.582	898300	5.70E-02	5.53E-02	7.50E-02	2.412	8.791	617700	5.18E-01	5.02E-01	6.82E-01		2.88E-01	2.79E-01	3.79E-01
2.431	7.203	237100	1.20E-02	1.16E-02	1.60E-02	2.431	9.47	154900	1.27E-01	1.24E-01	1.68E-01		6.95E-02	6.76E-02	9.20E-02
2.686	7.725	60720	3.14E-03	3.05E-03	4.13E-03	2.686	10	38300	3.70E-02	3.57E-02	4.80E-02		2.01E-02	1.94E-02	2.61E-02
												Dannual	2.27E+00	2.20E+00	2.99E+00

Table C6: Wave Fatigue Damage for North Sea and West Africa Sea at BHS6

BHS6						North Sea Scatter Diagram							Total Damage/Year		
Hs	Tz	n/year	D_{LR}	D_{DNV}	D_{ABS}	Hs	Tz	n/year	D_{LR}	D_{DNV}	D_{ABS}		D_{LR}	D_{DNV}	D_{ABS}
0.5	1.333	507.997	1.26E-05	1.22E-05	1.66E-05	0.5	1.336	507.361	5.09E-05	4.94E-05	6.70E-05		3.18E-05	3.08E-05	4.18E-05
1.129	1.468	35560	8.60E-04	7.76E-04	1.13E-03	1.129	1.479	35470	3.54E-03	3.67E-03	4.66E-03		2.20E-03	2.22E-03	2.89E-03
1.372	1.798	1264000	1.20E-02	1.06E-02	1.50E-02	1.372	1.961	1247000	5.60E-02	5.41E-02	7.30E-02		3.40E-02	3.23E-02	4.40E-02
1.722	2.548	3733000	3.20E-02	2.90E-02	4.20E-02	1.722	3.096	3555000	2.28E-01	2.21E-01	3.00E-01		1.30E-01	1.25E-01	1.71E-01
2.315	3.715	4902000	9.10E-02	8.18E-02	1.19E-01	2.315	4.797	4376000	1.00E+00	9.72E-01	1.32E+00		5.46E-01	5.27E-01	7.19E-01
3.128	4.882	4369000	1.98E-01	1.78E-01	2.61E-01	3.128	6.553	3549000	3.38E+00	3.28E+00	4.45E+00		1.79E+00	1.73E+00	2.36E+00
4.028	5.827	3061000	2.66E-01	2.40E-01	3.50E-01	4.028	7.871	2263000	6.50E+00	6.31E+00	8.56E+00		3.38E+00	3.27E+00	4.45E+00
4.962	6.582	1513000	2.02E-01	1.82E-01	2.66E-01	4.962	8.791	1040000	6.30E+00	6.11E+00	8.30E+00		3.25E+00	3.15E+00	4.28E+00
5.717	7.203	567300	9.00E-02	8.14E-02	1.19E-01	5.717	9.47	370700	3.30E+00	3.20E+00	4.34E+00		1.69E+00	1.64E+00	2.23E+00
6.035	7.725	170600	2.40E-02	2.18E-02	3.20E-02	6.035	10	107600	9.73E-01	9.45E-01	1.28E+00		4.99E-01	4.83E-01	6.57E-01
6.177	8.167	64200	7.25E-03	6.55E-03	9.55E-03	6.177	10.431	39510	3.11E-01	3.02E-01	4.10E-01		1.59E-01	1.54E-01	2.10E-01
5.621	8.543	23070	1.45E-03	1.31E-03	1.92E-03	5.621	10.791	13950	6.50E-02	6.29E-02	8.50E-02		3.32E-02	3.21E-02	4.35E-02
6.827	8.866	4354	3.62E-04	3.26E-04	1.97E-04	6.827	11.906	2600	1.70E-02	1.61E-02	2.20E-02		8.68E-03	8.21E-03	1.11E-02
												Dannual	1.15E+01	1.11E+01	1.52E+01
						West Africa Scatter Diagram									
1.124	1.798	757200	3.88E-03	3.50E-03	5.10E-03	1.124	1.961	746800	1.80E-02	1.78E-02	2.40E-02		1.09E-02	1.07E-02	1.46E-02
1.436	2.548	3834000	1.90E-02	1.72E-02	2.50E-02	1.436	3.096	3651000	1.36E-01	1.32E-01	1.79E-01		7.75E-02	7.44E-02	1.02E-01
1.719	3.715	6512000	4.90E-02	4.45E-02	6.50E-02	1.719	4.797	5813000	5.45E-01	5.29E-01	7.17E-01		2.97E-01	2.87E-01	3.91E-01
1.978	4.882	5184000	5.90E-02	5.35E-02	7.80E-02	1.978	6.553	4210000	1.02E+00	9.83E-01	1.34E+00		5.37E-01	5.19E-01	7.08E-01
2.186	5.827	2537000	3.50E-02	3.17E-02	4.60E-02	2.186	7.871	1876000	8.61E-01	8.35E-01	1.13E+00		4.48E-01	4.33E-01	5.90E-01
2.412	6.582	898300	1.40E-02	1.24E-02	1.80E-02	2.412	8.791	617700	4.30E-01	4.17E-01	5.66E-01		2.22E-01	2.15E-01	2.92E-01
2.431	7.203	237100	2.90E-03	2.61E-03	3.82E-03	2.431	9.47	154900	1.06E-01	1.03E-01	1.39E-01		5.44E-02	5.26E-02	7.14E-02
2.686	7.725	60720	7.58E-04	6.83E-04	9.98E-04	2.686	10	38300	3.10E-02	2.96E-02	4.00E-02		1.59E-02	1.52E-02	2.05E-02
												Dannual	1.66E+00	1.61E+00	2.19E+00

Table C7: Wave Fatigue Damage for North Sea and West Africa Sea at SHS1

North Sea Scatter Diagram

BALLAST SHS1						FULL						Total Damage/Year		
Hs	Tz	n/year	D_{LR}	D_{DNV}	D_{ABS}	Hs	Tz	n/year	D_{LR}	D_{DNV}	D_{ABS}	D_{LR}	D_{DNV}	D_{ABS}
0.5	1.333	507.997	1.69E-04	1.63E-04	2.22E-04	0.5	1.336	507.361	4.28E-05	4.15E-05	5.63E-05	1.06E-04	1.02E-04	1.39E-04
1.129	1.468	35560	1.20E-02	1.12E-02	1.50E-02	1.129	1.479	35470	2.97E-05	3.08E-03	3.91E-03	6.01E-03	7.12E-03	9.46E-03
1.372	1.798	1264000	1.57E-01	1.53E-01	2.07E-01	1.372	1.961	1247000	4.70E-02	4.54E-02	6.20E-02	1.02E-01	9.90E-02	1.35E-01
1.722	2.548	3733000	4.30E-01	4.17E-01	5.66E-01	1.722	3.096	3555000	1.91E-01	1.86E-01	2.52E-01	3.11E-01	3.01E-01	4.09E-01
2.315	3.715	4902000	1.21E+00	1.18E+00	1.60E+00	2.315	4.797	4376000	8.42E-01	8.17E-01	1.11E+00	1.03E+00	9.97E-01	1.35E+00
3.128	4.882	4369000	2.65E+00	2.57E+00	3.49E+00	3.128	6.553	3549000	2.84E+00	2.75E+00	3.74E+00	2.75E+00	2.66E+00	3.61E+00
4.028	5.827	3061000	3.56E+00	3.45E+00	4.69E+00	4.028	7.871	2263000	5.46E+00	5.30E+00	7.19E+00	4.51E+00	4.37E+00	5.94E+00
4.962	6.582	1513000	2.70E+00	2.62E+00	3.56E+00	4.962	8.791	1040000	5.30E+00	5.14E+00	6.98E+00	4.00E+00	3.88E+00	5.27E+00
5.717	7.203	567300	1.21E+00	1.17E+00	1.59E+00	5.717	9.47	370700	2.77E+00	2.69E+00	3.65E+00	1.99E+00	1.93E+00	2.62E+00
6.035	7.725	170600	3.23E-01	3.13E-01	4.26E-01	6.035	10	107600	8.18E-01	7.94E-01	1.08E+00	5.71E-01	5.54E-01	7.52E-01
6.177	8.167	64200	9.70E-02	9.42E-02	1.28E-01	6.177	10.431	39510	2.62E-01	2.54E-01	3.44E-01	1.80E-01	1.74E-01	2.36E-01
5.621	8.543	23070	1.90E-02	1.88E-02	2.60E-02	5.621	10.791	13950	5.40E-02	5.29E-02	7.20E-02	3.65E-02	3.58E-02	4.90E-02
6.827	8.866	4354	4.84E-03	4.70E-03	6.37E-03	6.827	11.906	2600	1.40E-02	1.35E-02	1.80E-02	9.42E-03	9.11E-03	1.22E-02
											Dannual	1.55E+01	1.50E+01	2.04E+01
West Africa Scatter Diagram														
1.124	1.798	757200	5.20E-02	5.03E-02	6.80E-02	1.124	1.961	746800	1.50E-02	1.50E-02	2.00E-02	3.35E-02	3.27E-02	4.40E-02
1.436	2.548	3834000	2.56E-01	2.48E-01	3.37E-01	1.436	3.096	3651000	1.14E-01	1.11E-01	1.50E-01	1.85E-01	1.79E-01	2.44E-01
1.719	3.715	6512000	6.61E-01	6.40E-01	8.70E-01	1.719	4.797	5813000	4.58E-01	4.45E-01	6.03E-01	5.60E-01	5.42E-01	7.37E-01
1.978	4.882	5184000	7.96E-01	7.71E-01	1.05E+00	1.978	6.553	4210000	8.53E-01	8.27E-01	1.12E+00	8.25E-01	7.99E-01	1.09E+00
2.186	5.827	2537000	4.71E-01	4.57E-01	6.20E-01	2.186	7.871	1876000	7.24E-01	7.02E-01	9.53E-01	5.98E-01	5.79E-01	7.87E-01
2.412	6.582	898300	1.84E-01	1.78E-01	2.43E-01	2.412	8.791	617700	3.61E-01	3.50E-01	4.76E-01	2.73E-01	2.64E-01	3.60E-01
2.431	7.203	237100	3.90E-02	3.76E-02	5.10E-02	2.431	9.47	154900	8.90E-02	8.62E-02	1.17E-01	6.40E-02	6.19E-02	8.40E-02
2.686	7.725	60720	1.00E-02	9.83E-03	1.30E-02	2.686	10	38300	2.60E-02	2.49E-02	3.40E-02	1.80E-02	1.74E-02	2.35E-02
											Dannual	2.55E+00	2.48E+00	3.36E+00

Table C8: Wave Fatigue Damage for North Sea and West Africa Sea at SHS2

SHS2						North Sea Scatter Diagram						Total Damage/Year		
Hs	Tz	n/year	D_{LR}	D_{DNV}	D_{ABS}	Hs	Tz	n/year	D_{LR}	D_{DNV}	D_{ABS}	D_{LR}	D_{DNV}	D_{ABS}
0.5	1.333	507.997	1.58E-04	1.53E-04	2.08E-04	0.5	1.336	507.361	3.41E-05	3.30E-05	4.49E-05	9.59E-05	9.30E-05	1.26E-04
1.129	1.468	35560	1.10E-02	1.04E-02	1.40E-02	1.129	1.479	35470	2.37E-03	2.45E-03	3.12E-03	6.68E-03	6.45E-03	8.56E-03
1.372	1.798	1264000	1.47E-01	1.43E-01	1.94E-01	1.372	1.961	1247000	3.70E-02	3.62E-02	4.90E-02	9.20E-02	8.95E-02	1.22E-01
1.722	2.548	3733000	4.02E-01	3.90E-01	5.30E-01	1.722	3.096	3555000	1.52E-01	1.48E-01	2.01E-01	2.77E-01	2.69E-01	3.66E-01
2.315	3.715	4902000	1.14E+00	1.10E+00	1.50E+00	2.315	4.797	4376000	6.70E-01	6.51E-01	8.82E-01	9.04E-01	8.76E-01	1.19E+00
3.128	4.882	4369000	2.48E+00	2.40E+00	3.27E+00	3.128	6.553	3549000	2.26E+00	2.19E+00	2.98E+00	2.37E+00	2.30E+00	3.12E+00
4.028	5.827	3061000	3.33E+00	3.23E+00	4.39E+00	4.028	7.871	2263000	4.35E+00	4.22E+00	5.73E+00	3.84E+00	3.72E+00	5.06E+00
4.962	6.582	1513000	2.53E+00	2.45E+00	3.33E+00	4.962	8.791	1040000	4.22E+00	4.09E+00	5.55E+00	3.37E+00	3.27E+00	4.44E+00
5.717	7.203	567300	1.13E+00	1.10E+00	1.49E+00	5.717	9.47	370700	2.21E+00	2.14E+00	2.90E+00	1.67E+00	1.62E+00	2.20E+00
6.035	7.725	170600	3.03E-01	2.93E-01	3.99E-01	6.035	10	107600	6.51E-01	6.32E-01	8.58E-01	4.77E-01	4.63E-01	6.29E-01
6.177	8.167	64200	9.10E-02	8.82E-02	1.20E-01	6.177	10.431	39510	2.08E-01	2.02E-01	2.74E-01	1.50E-01	1.45E-01	1.97E-01
5.621	8.543	23070	1.80E-02	1.76E-02	2.40E-02	5.621	10.791	13950	4.30E-02	4.21E-02	5.70E-02	3.05E-02	2.98E-02	4.05E-02
6.827	8.866	4354	4.53E-03	4.40E-03	5.97E-03	6.827	11.906	2600	1.10E-02	1.08E-02	1.50E-02	7.77E-03	7.58E-03	1.05E-02
											Dannual	1.32E+01	1.28E+01	1.74E+01
						West Africa Scatter Diagram								
1.124	1.798	757200	4.90E-02	4.71E-02	6.40E-02	1.124	1.961	746800	1.20E-02	1.19E-02	1.60E-02	3.05E-02	2.95E-02	4.00E-02
1.436	2.548	3834000	2.40E-01	2.32E-01	3.15E-01	1.436	3.096	3651000	9.10E-02	8.80E-02	1.19E-01	1.66E-01	1.60E-01	2.17E-01
1.719	3.715	6512000	6.18E-01	5.99E-01	8.14E-01	1.719	4.797	5813000	3.65E-01	3.54E-01	4.80E-01	4.92E-01	4.77E-01	6.47E-01
1.978	4.882	5184000	7.45E-01	7.21E-01	9.81E-01	1.978	6.553	4210000	6.79E-01	6.58E-01	8.94E-01	7.12E-01	6.90E-01	9.38E-01
2.186	5.827	2537000	4.41E-01	4.28E-01	5.81E-01	2.186	7.871	1876000	5.76E-01	5.59E-01	7.58E-01	5.09E-01	4.93E-01	6.70E-01
2.412	6.582	898300	1.73E-01	1.67E-01	2.27E-01	2.412	8.791	617700	2.88E-01	2.79E-01	3.79E-01	2.31E-01	2.23E-01	3.03E-01
2.431	7.203	237100	3.60E-02	3.52E-02	4.80E-02	2.431	9.47	154900	7.10E-02	6.87E-02	9.30E-02	5.35E-02	5.19E-02	7.05E-02
2.686	7.725	60720	9.50E-03	9.20E-03	1.30E-02	2.686	10	38300	2.00E-02	1.98E-02	2.70E-02	1.47E-02	1.45E-02	2.00E-02
											Dannual	2.21E+00	2.14E+00	2.90E+00

Table C9: Wave Fatigue Damage for North Sea and West Africa Sea at SHS3

SHS3						North Sea Scatter Diagram							Total Damage/Year		
Hs	Tz	n/year	D_{LR}	D_{DNV}	D_{ABS}	Hs	Tz	n/year	D_{LR}	D_{DNV}	D_{ABS}		D_{LR}	D_{DNV}	D_{ABS}
0.5	1.333	507.997	2.43E-05	2.36E-05	3.20E-05	0.5	1.336	507.361	1.04E-05	1.00E-05	1.36E-05		1.73E-05	1.68E-05	2.28E-05
1.129	1.468	35560	1.66E-03	1.61E-03	2.19E-03	1.129	1.479	35470	7.19E-04	7.46E-04	9.47E-04		1.19E-03	1.18E-03	1.57E-03
1.372	1.798	1264000	2.30E-02	2.20E-02	3.00E-02	1.372	1.961	1247000	1.10E-02	1.10E-02	1.50E-02		1.70E-02	1.65E-02	2.25E-02
1.722	2.548	3733000	6.20E-02	6.01E-02	8.20E-02	1.722	3.096	3555000	4.60E-02	4.50E-02	6.10E-02		5.40E-02	5.25E-02	7.15E-02
2.315	3.715	4902000	1.75E-01	1.70E-01	2.31E-01	2.315	4.797	4376000	2.04E-01	1.98E-01	2.68E-01		1.90E-01	1.84E-01	2.50E-01
3.128	4.882	4369000	3.82E-01	3.70E-01	5.03E-01	3.128	6.553	3549000	6.88E-01	6.67E-01	9.06E-01		5.35E-01	5.18E-01	7.05E-01
4.028	5.827	3061000	5.13E-01	4.98E-01	6.76E-01	4.028	7.871	2263000	1.32E+00	1.28E+00	1.74E+00		9.18E-01	8.91E-01	1.21E+00
4.962	6.582	1513000	3.90E-01	3.77E-01	5.13E-01	4.962	8.791	1040000	1.28E+00	1.24E+00	1.69E+00		8.37E-01	8.11E-01	1.10E+00
5.717	7.203	567300	1.74E-01	1.69E-01	2.29E-01	5.717	9.47	370700	6.71E-01	6.50E-01	8.83E-01		4.23E-01	4.10E-01	5.56E-01
6.035	7.725	170600	4.70E-02	4.52E-02	6.10E-02	6.035	10	107600	1.98E-01	1.92E-01	2.61E-01		1.23E-01	1.19E-01	1.61E-01
6.177	8.167	64200	1.40E-02	1.36E-02	1.80E-02	6.177	10.431	39510	6.30E-02	6.14E-02	8.30E-02		3.85E-02	3.75E-02	5.05E-02
5.621	8.543	23070	2.80E-03	2.71E-03	3.69E-02	5.621	10.791	13950	1.30E-02	1.28E-02	1.70E-02		7.90E-03	7.76E-03	2.69E-02
6.827	8.866	4354	6.98E-04	6.78E-04	9.19E-03	6.827	11.906	2600	3.38E-03	3.28E-03	4.45E-03		2.04E-03	1.98E-03	6.82E-03
												Dannual	3.14E+00	3.05E+00	4.16E+00
						West Africa Scatter Diagram									
1.124	1.798	757200	4.90E-02	7.26E-03	6.40E-02	1.124	1.961	746800	3.74E-03	3.63E-03	4.92E-03		2.64E-02	5.44E-03	3.45E-02
1.436	2.548	3834000	2.40E-01	3.58E-02	3.15E-01	1.436	3.096	3651000	2.80E-02	2.68E-02	3.60E-02		1.34E-01	3.13E-02	1.76E-01
1.719	3.715	6512000	6.18E-01	9.24E-02	8.14E-01	1.719	4.797	5813000	1.11E-01	1.08E-01	1.46E-01		3.65E-01	1.00E-01	4.80E-01
1.978	4.882	5184000	7.45E-01	1.11E-01	9.81E-01	1.978	6.553	4210000	2.07E-01	2.00E-01	2.72E-01		4.76E-01	1.56E-01	6.27E-01
2.186	5.827	2537000	4.41E-01	6.59E-02	5.81E-01	2.186	7.871	1876000	1.75E-01	1.70E-01	2.31E-01		3.08E-01	1.18E-01	4.06E-01
2.412	6.582	898300	1.73E-01	2.57E-02	2.27E-01	2.412	8.791	617700	8.80E-02	8.49E-02	1.15E-01		1.31E-01	5.53E-02	1.71E-01
2.431	7.203	237100	3.60E-02	5.42E-03	4.80E-02	2.431	9.47	154900	2.20E-02	2.09E-02	2.80E-02		2.90E-02	1.32E-02	3.80E-02
2.686	7.725	60720	9.50E-03	1.42E-03	1.30E-02	2.686	10	38300	6.21E-03	6.03E-03	8.18E-03		7.86E-03	3.72E-03	1.06E-02
												Dannual	1.48E+00	4.83E-01	1.94E+00

Table C10: Wave Fatigue Damage for North Sea and West Africa Sea at SHS4

SHS4						North Sea Scatter Diagram							Total Damage/Year		
Hs	Tz	n/year	D_{LR}	D_{DNV}	D_{ABS}	Hs	Tz	n/year	D_{LR}	D_{DNV}	D_{ABS}		D_{LR}	D_{DNV}	D_{ABS}
0.5	1.333	507.997	6.08E-05	5.90E-05	8.01E-05	0.5	1.336	507.361	1.27E-05	1.23E-05	1.67E-05		3.68E-05	3.56E-05	4.84E-05
1.129	1.468	35560	4.15E-03	4.03E-03	5.47E-03	1.129	1.479	35470	8.81E-04	9.13E-04	1.16E-03		2.52E-03	2.47E-03	3.31E-03
1.372	1.798	1264000	5.70E-02	5.51E-02	7.50E-02	1.372	1.961	1247000	1.40E-02	1.35E-02	1.80E-02		3.55E-02	3.43E-02	4.65E-02
1.722	2.548	3733000	1.55E-01	1.50E-01	2.04E-01	1.722	3.096	3555000	5.70E-02	5.50E-02	7.50E-02		1.06E-01	1.03E-01	1.40E-01
2.315	3.715	4902000	4.38E-01	4.25E-01	5.77E-01	2.315	4.797	4376000	2.49E-01	2.42E-01	3.28E-01		3.44E-01	3.33E-01	4.53E-01
3.128	4.882	4369000	9.56E-01	9.26E-01	1.26E+00	3.128	6.553	3549000	8.42E-01	8.16E-01	1.11E+00		8.99E-01	8.71E-01	1.18E+00
4.028	5.827	3061000	1.28E+00	1.24E+00	1.69E+00	4.028	7.871	2263000	1.62E+00	1.57E+00	2.13E+00		1.45E+00	1.41E+00	1.91E+00
4.962	6.582	1513000	9.75E-01	9.44E-01	1.28E+00	4.962	8.791	1040000	1.57E+00	1.52E+00	2.07E+00		1.27E+00	1.23E+00	1.68E+00
5.717	7.203	567300	4.36E-01	4.23E-01	5.74E-01	5.717	9.47	370700	8.21E-01	7.96E-01	1.08E+00		6.29E-01	6.09E-01	8.27E-01
6.035	7.725	170600	1.17E-01	1.13E-01	1.54E-01	6.035	10	107600	2.42E-01	2.35E-01	3.19E-01		1.80E-01	1.74E-01	2.37E-01
6.177	8.167	64200	3.50E-02	3.40E-02	4.60E-02	6.177	10.431	39510	7.80E-02	7.51E-02	1.02E-01		5.65E-02	5.46E-02	7.40E-02
5.621	8.543	23070	7.01E-03	6.79E-03	9.22E-03	5.621	10.791	13950	1.60E-02	1.57E-02	2.10E-02		1.15E-02	1.12E-02	1.51E-02
6.827	8.866	4354	1.75E-03	1.70E-03	2.30E-03	6.827	11.906	2600	4.14E-03	4.01E-03	5.45E-03		2.94E-03	2.85E-03	3.87E-03
												Dtotal	4.99E+00	4.84E+00	6.57E+00
						West Africa Scatter Diagram									
1.124	1.798	757200	1.90E-02	1.82E-02	2.50E-02	1.124	1.961	746800	4.58E-03	4.44E-03	6.03E-03		1.18E-02	1.13E-02	1.55E-02
1.436	2.548	3834000	9.20E-02	8.96E-02	1.22E-01	1.436	3.096	3651000	3.40E-02	3.28E-02	4.40E-02		6.30E-02	6.12E-02	8.30E-02
1.719	3.715	6512000	2.38E-01	2.31E-01	3.14E-01	1.719	4.797	5813000	1.36E-01	1.32E-01	1.79E-01		1.87E-01	1.81E-01	2.47E-01
1.978	4.882	5184000	2.87E-01	2.78E-01	3.78E-01	1.978	6.553	4210000	2.53E-01	2.45E-01	3.33E-01		2.70E-01	2.62E-01	3.56E-01
2.186	5.827	2537000	1.70E-01	1.65E-01	2.24E-01	2.186	7.871	1876000	2.14E-01	2.08E-01	2.82E-01		1.92E-01	1.86E-01	2.53E-01
2.412	6.582	898300	6.60E-02	6.44E-02	8.80E-02	2.412	8.791	617700	1.07E-01	1.04E-01	1.41E-01		8.65E-02	8.41E-02	1.15E-01
2.431	7.203	237100	1.40E-02	1.36E-02	1.80E-02	2.431	9.47	154900	2.60E-02	2.56E-02	3.50E-02		2.00E-02	1.96E-02	2.65E-02
2.686	7.725	60720	3.66E-03	3.55E-03	4.82E-03	2.686	10	38300	7.60E-03	7.38E-03	1.00E-02		5.63E-03	5.46E-03	7.41E-03
												Dtotal	8.36E-01	8.11E-01	1.10E+00

Table C11: Wave Fatigue Damage for North Sea and West Africa Sea at SHS5

SHS5						North Sea Scatter Diagram							Total Damage/Year		
Hs	Tz	n/year	D_{LR}	D_{DNV}	D_{ABS}	Hs	Tz	n/year	D_{LR}	D_{DNV}	D_{ABS}		D_{LR}	D_{DNV}	D_{ABS}
0.5	1.333	507.997	9.97E-05	9.67E-05	1.31E-04	0.5	1.336	507.361	1.97E-05	1.91E-05	2.59E-05		5.97E-05	5.79E-05	7.86E-05
1.129	1.468	35560	6.81E-03	6.61E-03	8.96E-03	1.129	1.479	35470	1.37E-04	1.42E-03	1.80E-03		3.47E-03	4.01E-03	5.38E-03
1.372	1.798	1264000	9.30E-02	9.04E-02	1.23E-01	1.372	1.961	1247000	2.20E-02	2.09E-02	2.80E-02		5.75E-02	5.56E-02	7.55E-02
1.722	2.548	3733000	2.54E-01	2.47E-01	3.35E-01	1.722	3.096	3555000	8.80E-02	8.55E-02	1.16E-01		1.71E-01	1.66E-01	2.26E-01
2.315	3.715	4902000	7.19E-01	6.97E-01	9.46E-01	2.315	4.797	4376000	3.88E-01	3.77E-01	5.10E-01		5.54E-01	5.37E-01	7.28E-01
3.128	4.882	4369000	1.57E+00	1.52E+00	2.07E+00	3.128	6.553	3549000	1.31E+00	1.27E+00	1.72E+00		1.44E+00	1.39E+00	1.89E+00
4.028	5.827	3061000	2.11E+00	2.04E+00	2.77E+00	4.028	7.871	2263000	2.52E+00	2.44E+00	3.32E+00		2.31E+00	2.24E+00	3.04E+00
4.962	6.582	1513000	1.60E+00	1.55E+00	2.11E+00	4.962	8.791	1040000	2.44E+00	2.37E+00	3.21E+00		2.02E+00	1.96E+00	2.66E+00
5.717	7.203	567300	7.15E-01	6.93E-01	9.42E-01	5.717	9.47	370700	1.28E+00	1.24E+00	1.68E+00		9.96E-01	9.65E-01	1.31E+00
6.035	7.725	170600	1.91E-01	1.86E-01	2.52E-01	6.035	10	107600	3.77E-01	3.66E-01	4.96E-01		2.84E-01	2.76E-01	3.74E-01
6.177	8.167	64200	5.70E-02	5.58E-02	7.60E-02	6.177	10.431	39510	1.21E-01	1.17E-01	1.59E-01		8.90E-02	8.63E-02	1.18E-01
5.621	8.543	23070	1.10E-02	1.11E-02	1.50E-02	5.621	10.791	13950	2.50E-02	2.44E-02	3.30E-02		1.80E-02	1.77E-02	2.40E-02
6.827	8.866	4354	2.87E-03	2.78E-03	3.77E-03	6.827	11.906	2600	6.43E-03	6.23E-03	8.47E-03		4.65E-03	4.51E-03	6.12E-03
												Dtotal	7.95E+00	7.71E+00	1.05E+01
						West Africa Scatter Diagram									
1.124	1.798	757200	3.10E-02	2.98E-02	4.00E-02	1.124	1.961	746800	7.11E-03	6.90E-03	9.35E-03		1.91E-02	1.84E-02	2.47E-02
1.436	2.548	3834000	1.10E-01	1.47E-01	1.99E-01	1.436	3.096	3651000	5.20E-02	5.09E-02	6.90E-02		8.10E-02	9.89E-02	1.34E-01
1.719	3.715	6512000	3.91E-01	3.79E-01	5.15E-01	1.719	4.797	5813000	2.11E-01	2.05E-01	2.78E-01		3.01E-01	2.92E-01	3.97E-01
1.978	4.882	5184000	4.71E-01	4.56E-01	6.20E-01	1.978	6.553	4210000	3.93E-01	3.81E-01	5.18E-01		4.32E-01	4.19E-01	5.69E-01
2.186	5.827	2537000	2.79E-01	2.70E-01	3.67E-01	2.186	7.871	1876000	3.33E-01	3.23E-01	4.39E-01		3.06E-01	2.97E-01	4.03E-01
2.412	6.582	898300	1.09E-01	1.06E-01	1.44E-01	2.412	8.791	617700	1.67E-01	1.61E-01	2.19E-01		1.38E-01	1.34E-01	1.82E-01
2.431	7.203	237100	2.30E-02	2.23E-02	3.00E-02	2.431	9.47	154900	4.10E-02	3.97E-02	5.40E-02		3.20E-02	3.10E-02	4.20E-02
2.686	7.725	60720	6.01E-03	5.82E-03	7.91E-03	2.686	10	38300	1.20E-02	1.15E-02	1.60E-02		9.00E-03	8.65E-03	1.20E-02
												Dtotal	1.32E+00	1.30E+00	1.76E+00

Table C12: Wave Fatigue Damage for North Sea and West Africa Sea at SHS6

SHS6						North Sea Scatter Diagram						Total Damage/Year		
Hs	Tz	n/year	D_{LR}	D_{DNV}	D_{ABS}	Hs	Tz	n/year	D_{LR}	D_{DNV}	D_{ABS}	D_{LR}	D_{DNV}	D_{ABS}
0.5	1.333	507.997	1.44E-04	1.39E-04	1.89E-04	0.5	1.336	507.361	8.93E-06	8.68E-06	1.18E-05	7.64E-05	7.40E-05	1.01E-04
1.129	1.468	35560	9.82E-03	9.52E-03	1.30E-02	1.129	1.479	35470	6.21E-04	6.44E-04	8.17E-04	5.22E-03	5.08E-03	6.91E-03
1.372	1.798	1264000	1.34E-01	1.30E-01	1.77E-01	1.372	1.961	1247000	9.78E-03	9.50E-03	1.30E-02	7.19E-02	6.98E-02	9.50E-02
1.722	2.548	3733000	3.67E-01	3.55E-01	4.83E-01	1.722	3.096	3555000	4.00E-02	3.88E-02	5.30E-02	2.04E-01	1.97E-01	2.68E-01
2.315	3.715	4902000	1.04E+00	1.00E+00	1.36E+00	2.315	4.797	4376000	1.76E-01	1.71E-01	2.32E-01	6.06E-01	5.87E-01	7.98E-01
3.128	4.882	4369000	2.26E+00	2.19E+00	2.98E+00	3.128	6.553	3549000	5.94E-01	5.76E-01	7.82E-01	1.43E+00	1.38E+00	1.88E+00
4.028	5.827	3061000	3.04E+00	2.94E+00	4.00E+00	4.028	7.871	2263000	1.14E+00	1.11E+00	1.50E+00	2.09E+00	2.03E+00	2.75E+00
4.962	6.582	1513000	2.31E+00	2.23E+00	3.03E+00	4.962	8.791	1040000	1.11E+00	1.07E+00	1.46E+00	1.71E+00	1.65E+00	2.25E+00
5.717	7.203	567300	1.03E+00	9.99E-01	1.36E+00	5.717	9.47	370700	5.79E-01	5.62E-01	7.62E-01	8.05E-01	7.80E-01	1.06E+00
6.035	7.725	170600	2.76E-01	2.67E-01	3.63E-01	6.035	10	107600	1.71E-01	1.66E-01	2.25E-01	2.24E-01	2.17E-01	2.94E-01
6.177	8.167	64200	8.30E-02	8.04E-02	1.09E-01	6.177	10.431	39510	5.50E-02	5.30E-02	7.20E-02	6.90E-02	6.67E-02	9.05E-02
5.621	8.543	23070	1.70E-02	1.60E-02	2.20E-02	5.621	10.791	13950	1.10E-02	1.10E-02	1.50E-02	1.40E-02	1.35E-02	1.85E-02
6.827	8.866	4354	4.13E-03	4.01E-03	5.44E-03	6.827	11.906	2600	2.92E-03	2.83E-03	3.84E-03	3.52E-03	3.42E-03	4.64E-03
											Dtotal	7.22E+00	7.00E+00	9.51E+00
						West Africa Scatter Diagram								
1.124	1.798	757200	4.40E-02	4.29E-02	5.80E-02	1.124	1.961	746800	3.23E-03	3.13E-03	4.25E-03	2.36E-02	2.30E-02	3.11E-02
1.436	2.548	3834000	2.18E-01	2.12E-01	2.87E-01	1.436	3.096	3651000	2.40E-02	2.31E-02	3.10E-02	1.21E-01	1.17E-01	1.59E-01
1.719	3.715	6512000	5.64E-01	5.46E-01	7.42E-01	1.719	4.797	5813000	9.60E-02	9.30E-02	1.26E-01	3.30E-01	3.20E-01	4.34E-01
1.978	4.882	5184000	6.79E-01	6.57E-01	8.94E-01	1.978	6.553	4210000	1.78E-01	1.73E-01	2.35E-01	4.29E-01	4.15E-01	5.65E-01
2.186	5.827	2537000	4.02E-01	3.90E-01	5.29E-01	2.186	7.871	1876000	1.51E-01	1.47E-01	1.99E-01	2.77E-01	2.68E-01	3.64E-01
2.412	6.582	898300	1.57E-01	1.52E-01	2.07E-01	2.412	8.791	617700	7.60E-02	7.33E-02	9.90E-02	1.17E-01	1.13E-01	1.53E-01
2.431	7.203	237100	3.30E-02	3.21E-02	4.40E-02	2.431	9.47	154900	1.90E-02	1.80E-02	2.40E-02	2.60E-02	2.51E-02	3.40E-02
2.686	7.725	60720	8.65E-03	8.39E-03	1.10E-02	2.686	10	38300	5.37E-03	5.21E-03	7.06E-03	7.01E-03	6.80E-03	9.03E-03
											Dtotal	1.33E+00	1.29E+00	1.75E+00

Table C13: Wave Fatigue Damage for North Sea and West Africa Sea at IHS1

North Sea Scatter Diagram

BALLAST						FULL								
IHS1												Total Damage/Year		
Hs	Tz	n/year	D_{LR}	D_{DNV}	D_{ABS}	Hs	Tz	n/year	D_{LR}	D_{DNV}	D_{ABS}	D_{LR}	D_{DNV}	D_{ABS}
0.5	1.333	507.997	5.54E-06	5.39E-06	7.29E-06	0.5	1.336	507.361	1.63E-04	1.58E-04	2.14E-04	8.42E-05	8.16E-05	1.11E-04
1.129	1.468	35560	3.78E-04	3.68E-04	4.98E-04	1.129	1.479	35470	1.10E-02	1.17E-02	1.50E-02	5.69E-03	6.04E-03	7.75E-03
1.372	1.798	1264000	5.18E-03	5.03E-03	6.81E-03	1.372	1.961	1247000	1.78E-01	1.73E-01	2.35E-01	9.16E-02	8.90E-02	1.21E-01
1.722	2.548	3733000	1.40E-02	1.37E-02	1.90E-02	1.722	3.096	3555000	7.28E-01	7.06E-01	9.59E-01	3.71E-01	3.60E-01	4.89E-01
2.315	3.715	4902000	4.00E-02	3.88E-02	5.30E-02	2.315	4.797	4376000	3.20E+00	3.11E+00	4.21E+00	1.62E+00	1.57E+00	2.13E+00
3.128	4.882	4369000	8.70E-02	8.46E-02	1.15E-01	3.128	6.553	3549000	1.08E+01	1.05E+01	1.42E+01	5.45E+00	5.28E+00	7.17E+00
4.028	5.827	3061000	1.17E-01	1.14E-01	1.54E-01	4.028	7.871	2263000	2.08E+01	2.02E+01	2.74E+01	1.05E+01	1.01E+01	1.38E+01
4.962	6.582	1513000	8.90E-02	8.62E-02	1.17E-01	4.962	8.791	1040000	2.02E+01	1.95E+01	2.65E+01	1.01E+01	9.81E+00	1.33E+01
5.717	7.203	567300	4.00E-02	3.86E-02	5.20E-02	5.717	9.47	370700	1.05E+01	1.02E+01	1.37E+01	5.29E+00	5.13E+00	6.87E+00
6.035	7.725	170600	1.10E-02	1.03E-02	1.40E-02	6.035	10	107600	3.11E+00	3.02E+00	4.10E+00	1.56E+00	1.51E+00	2.06E+00
6.177	8.167	64200	3.21E-03	3.11E-03	4.22E-03	6.177	10.431	39510	9.95E-01	9.64E-01	1.31E+00	4.99E-01	4.84E-01	6.57E-01
5.621	8.543	23070	6.40E-04	6.20E-04	8.43E-04	5.621	10.791	13950	2.07E-01	2.01E-01	2.73E-01	1.04E-01	1.01E-01	1.37E-01
6.827	8.866	4354	1.60E-04	1.55E-04	2.10E-04	6.827	11.906	2600	5.30E-02	5.14E-02	7.00E-02	2.66E-02	2.58E-02	3.51E-02
											Dannual	3.56E+01	3.45E+01	4.68E+01

West Africa Scatter Diagram

1.124	1.798	757200	1.71E-03	1.66E-03	2.25E-03	1.124	1.961	746800	5.90E-02	5.70E-02	7.70E-02	3.04E-02	2.93E-02	3.96E-02
1.436	2.548	3834000	8.42E-03	8.18E-03	1.10E-02	1.436	3.096	3651000	4.34E-01	4.20E-01	5.71E-01	2.21E-01	2.14E-01	2.91E-01
1.719	3.715	6512000	2.20E-02	2.11E-02	2.90E-02	1.719	4.797	5813000	1.74E+00	1.69E+00	2.29E+00	8.82E-01	8.56E-01	1.16E+00
1.978	4.882	5184000	2.60E-02	2.54E-02	3.50E-02	1.978	6.553	4210000	3.25E+00	3.14E+00	4.27E+00	1.64E+00	1.58E+00	2.15E+00
2.186	5.827	2537000	1.60E-02	1.51E-02	2.00E-02	2.186	7.871	1876000	2.75E+00	2.67E+00	3.62E+00	1.38E+00	1.34E+00	1.82E+00
2.412	6.582	898300	6.08E-03	5.88E-03	8.00E-03	2.412	8.791	617700	1.38E+00	1.33E+00	1.81E+00	6.91E-01	6.69E-01	9.09E-01
2.431	7.203	237100	1.28E-03	1.24E-03	1.68E-03	2.431	9.47	154900	3.38E-01	3.28E-01	4.45E-01	1.70E-01	1.65E-01	2.23E-01
2.686	7.725	60720	3.35E-04	3.24E-04	4.40E-04	2.686	10	38300	9.80E-02	9.47E-02	1.29E-01	4.92E-02	4.75E-02	6.47E-02
											Dannual	5.06E+00	4.91E+00	6.66E+00

Table C14: Wave Fatigue Damage for North Sea and West Africa Sea at IHS2

IHS2						North Sea Scatter Diagram							Total Damage/Year		
Hs	Tz	n/year	D_{LR}	D_{DNV}	D_{ABS}	Hs	Tz	n/year	D_{LR}	D_{DNV}	D_{ABS}		D_{LR}	D_{DNV}	D_{ABS}
0.5	1.333	507.997	2.32E-04	2.24E-04	3.05E-04	0.5	1.336	507.361	1.46E-05	1.42E-05	1.92E-05		1.23E-04	1.19E-04	1.62E-04
1.129	1.468	35560	1.60E-02	1.53E-02	2.10E-02	1.129	1.479	35470	1.02E-03	1.05E-03	1.34E-03		8.51E-03	8.19E-03	1.12E-02
1.372	1.798	1264000	2.16E-01	2.10E-01	2.85E-01	1.372	1.961	1247000	1.60E-02	1.55E-02	2.10E-02		1.16E-01	1.13E-01	1.53E-01
1.722	2.548	3733000	5.90E-01	5.72E-01	7.77E-01	1.722	3.096	3555000	6.50E-02	6.35E-02	8.60E-02		3.28E-01	3.18E-01	4.32E-01
2.315	3.715	4902000	1.67E+00	1.62E+00	2.20E+00	2.315	4.797	4376000	2.88E-01	2.79E-01	3.79E-01		9.78E-01	9.47E-01	1.29E+00
3.128	4.882	4369000	3.64E+00	3.52E+00	4.79E+00	3.128	6.553	3549000	9.71E-01	9.41E-01	1.28E+00		2.30E+00	2.23E+00	3.03E+00
4.028	5.827	3061000	4.89E+00	4.74E+00	6.43E+00	4.028	7.871	2263000	1.87E+00	1.81E+00	2.46E+00		3.38E+00	3.27E+00	4.45E+00
4.962	6.582	1513000	3.71E+00	3.59E+00	4.88E+00	4.962	8.791	1040000	1.81E+00	1.76E+00	2.38E+00		2.76E+00	2.67E+00	3.63E+00
5.717	7.203	567300	1.66E+00	1.61E+00	2.18E+00	5.717	9.47	370700	9.47E-01	9.18E-01	1.25E+00		1.30E+00	1.26E+00	1.72E+00
6.035	7.725	170600	4.44E-01	4.30E-01	5.85E-01	6.035	10	107600	2.80E-01	2.71E-01	3.68E-01		3.62E-01	3.51E-01	4.77E-01
6.177	8.167	64200	1.33E-01	1.29E-01	1.75E-01	6.177	10.431	39510	8.90E-02	8.67E-02	1.18E-01		1.11E-01	1.08E-01	1.47E-01
5.621	8.543	23070	2.70E-02	2.58E-02	3.50E-02	5.621	10.791	13950	1.90E-02	1.81E-02	2.50E-02		2.30E-02	2.19E-02	3.00E-02
6.827	8.866	4354	6.65E-03	6.45E-03	8.75E-03	6.827	11.906	2600	4.77E-03	4.62E-03	6.28E-03		5.71E-03	5.54E-03	7.52E-03
												Dannual	1.17E+01	1.13E+01	1.54E+01
						West Africa Scatter Diagram									
1.124	1.798	757200	7.10E-02	6.91E-02	9.40E-02	1.124	1.961	746800	5.28E-03	5.12E-03	6.94E-03		3.81E-02	3.71E-02	5.05E-02
1.436	2.548	3834000	3.51E-01	3.41E-01	4.63E-01	1.436	3.096	3651000	3.90E-02	3.78E-02	5.10E-02		1.95E-01	1.89E-01	2.57E-01
1.719	3.715	6512000	9.07E-01	8.79E-01	1.19E+00	1.719	4.797	5813000	1.57E-01	1.52E-01	2.06E-01		5.32E-01	5.15E-01	7.00E-01
1.978	4.882	5184000	1.09E+00	1.06E+00	1.44E+00	1.978	6.553	4210000	2.92E-01	2.83E-01	3.84E-01		6.92E-01	6.70E-01	9.11E-01
2.186	5.827	2537000	6.47E-01	6.27E-01	8.52E-01	2.186	7.871	1876000	2.47E-01	2.40E-01	3.26E-01		4.47E-01	4.33E-01	5.89E-01
2.412	6.582	898300	2.53E-01	2.45E-01	3.33E-01	2.412	8.791	617700	1.24E-01	1.20E-01	1.63E-01		1.89E-01	1.82E-01	2.48E-01
2.431	7.203	237100	5.30E-02	5.16E-02	7.00E-02	2.431	9.47	154900	3.00E-02	2.95E-02	4.00E-02		4.15E-02	4.06E-02	5.50E-02
2.686	7.725	60720	1.40E-02	1.35E-02	1.80E-02	2.686	10	38300	8.77E-03	8.51E-03	1.20E-02		1.14E-02	1.10E-02	1.50E-02
												Dannual	2.15E+00	2.08E+00	2.83E+00

Table C15: Wave Fatigue Damage for North Sea and West Africa Sea at IHS3

IHS3					North Sea Scatter Diagram						Total Damage/Year		
Hs	Tz	n/year	D_{LR}	D_{DNV}	D_{ABS}	Hs	Tz	n/year	D_{LR}	D_{DNV}	D_{ABS}	D_{LR}	D_{DNV}	D_{ABS}
0.5	1.333	507.997	9.47E-06	9.19E-06	1.25E-05	0.5	1.336	507.361	1.10E-06	1.07E-06	1.45E-05	5.28E-06	5.13E-06	1.35E-05
1.129	1.468	35560	6.46E-04	6.28E-04	8.51E-04	1.129	1.479	35470	7.65E-05	7.96E-05	1.01E-04	3.61E-04	3.54E-04	4.76E-04
1.372	1.798	1264000	8.84E-03	8.58E-03	1.20E-02	1.372	1.961	1247000	1.21E-03	1.17E-03	1.59E-03	5.02E-03	4.88E-03	6.79E-03
1.722	2.548	3733000	2.40E-02	2.34E-02	3.20E-02	1.722	3.096	3555000	4.93E-03	4.80E-03	6.49E-03	1.45E-02	1.41E-02	1.92E-02
2.315	3.715	4902000	6.80E-02	6.62E-02	9.00E-02	2.315	4.797	4376000	2.20E-02	2.11E-02	2.90E-02	4.50E-02	4.37E-02	5.95E-02
3.128	4.882	4369000	1.49E-01	1.44E-01	1.96E-01	3.128	6.553	3549000	7.30E-02	7.12E-02	9.60E-02	1.11E-01	1.08E-01	1.46E-01
4.028	5.827	3061000	2.00E-01	1.94E-01	2.64E-01	4.028	7.871	2263000	1.41E-01	1.37E-01	1.85E-01	1.71E-01	1.66E-01	2.25E-01
4.962	6.582	1513000	1.52E-01	1.47E-01	2.00E-01	4.962	8.791	1040000	1.37E-01	1.33E-01	1.80E-01	1.45E-01	1.40E-01	1.90E-01
5.717	7.203	567300	6.80E-02	6.59E-02	8.90E-02	5.717	9.47	370700	7.10E-02	6.94E-02	9.40E-02	6.95E-02	6.76E-02	9.15E-02
6.035	7.725	170600	1.80E-02	1.76E-02	2.40E-02	6.035	10	107600	2.10E-02	2.05E-02	2.80E-02	1.95E-02	1.91E-02	2.60E-02
6.177	8.167	64200	5.46E-03	5.30E-03	7.19E-03	6.177	10.431	39510	6.74E-03	6.55E-03	8.88E-03	6.10E-03	5.93E-03	8.03E-03
5.621	8.543	23070	1.09E-03	1.06E-03	1.44E-03	5.621	10.791	13950	1.41E-03	1.37E-03	1.85E-03	1.25E-03	1.21E-03	1.64E-03
6.827	8.866	4354	2.72E-04	2.64E-04	3.58E-04	6.827	11.906	2600	3.60E-04	3.50E-04	4.74E-04	3.16E-04	3.07E-04	4.16E-04
											Dannual	5.88E-01	5.70E-01	7.74E-01
					West Africa Scatter Diagram									
1.124	1.798	757200	2.92E-03	2.83E-03	3.84E-03	1.124	1.961	746800	3.97E-04	3.87E-04	5.23E-04	1.66E-03	1.61E-03	2.18E-03
1.436	2.548	3834000	1.40E-02	1.40E-02	1.90E-02	1.436	3.096	3651000	2.94E-03	2.86E-03	3.87E-03	8.47E-03	8.41E-03	1.14E-02
1.719	3.715	6512000	3.70E-02	3.60E-02	4.90E-02	1.719	4.797	5813000	1.20E-02	1.15E-02	1.60E-02	2.45E-02	2.38E-02	3.25E-02
1.978	4.882	5184000	4.50E-02	4.33E-02	5.90E-02	1.978	6.553	4210000	2.20E-02	2.14E-02	2.90E-02	3.35E-02	3.24E-02	4.40E-02
2.186	5.827	2537000	2.70E-02	2.57E-02	3.50E-02	2.186	7.871	1876000	1.90E-02	1.81E-02	2.50E-02	2.30E-02	2.19E-02	3.00E-02
2.412	6.582	898300	1.00E-02	1.00E-02	1.40E-02	2.412	8.791	617700	9.32E-03	9.06E-03	1.20E-02	9.66E-03	9.55E-03	1.30E-02
2.431	7.203	237100	2.18E-03	2.12E-03	2.87E-03	2.431	9.47	154900	2.29E-03	2.23E-03	3.02E-03	2.24E-03	2.17E-03	2.95E-03
2.686	7.725	60720	5.70E-04	5.53E-04	7.51E-04	2.686	10	38300	6.62E-03	6.44E-04	8.71E-04	3.59E-03	5.98E-04	8.11E-04
											Dannual	1.07E-01	1.00E-01	1.37E-01

Table C16: Wave Fatigue Damage for North Sea and West Africa Sea at IHS4

IHS4						North Sea Scatter Diagram							Total Damage/Year		
Hs	Tz	n/year	D_{LR}	D_{DNV}	D_{ABS}	Hs	Tz	n/year	D_{LR}	D_{DNV}	D_{ABS}		D_{LR}	D_{DNV}	D_{ABS}
0.5	1.333	507.997	1.12E-05	1.08E-05	1.47E-05	0.5	1.336	507.361	1.01E-06	9.84E-07	1.33E-06		6.10E-06	5.92E-06	8.03E-06
1.129	1.468	35560	7.64E-04	7.41E-04	1.01E-03	1.129	1.479	35470	7.04E-05	7.30E-05	9.27E-05		4.17E-04	4.07E-04	5.49E-04
1.372	1.798	1264000	1.00E-02	1.01E-02	1.40E-02	1.372	1.961	1247000	1.11E-03	1.08E-03	1.46E-03		5.55E-03	5.60E-03	7.73E-03
1.722	2.548	3733000	2.90E-02	2.77E-02	3.80E-02	1.722	3.096	3555000	4.54E-03	4.40E-03	5.97E-03		1.68E-02	1.60E-02	2.20E-02
2.315	3.715	4902000	8.10E-02	7.81E-02	1.06E-01	2.315	4.797	4376000	2.00E-02	1.94E-02	2.60E-02		5.05E-02	4.87E-02	6.60E-02
3.128	4.882	4369000	1.76E-01	1.70E-01	2.32E-01	3.128	6.553	3549000	6.70E-02	6.53E-02	8.90E-02		1.22E-01	1.18E-01	1.61E-01
4.028	5.827	3061000	2.36E-01	2.29E-01	3.11E-01	4.028	7.871	2263000	1.30E-01	1.26E-01	1.71E-01		1.83E-01	1.77E-01	2.41E-01
4.962	6.582	1513000	1.79E-01	1.74E-01	2.36E-01	4.962	8.791	1040000	1.26E-01	1.22E-01	1.65E-01		1.53E-01	1.48E-01	2.01E-01
5.717	7.203	567300	8.00E-02	7.77E-02	1.06E-01	5.717	9.47	370700	6.60E-02	6.37E-02	8.60E-02		7.30E-02	7.07E-02	9.60E-02
6.035	7.725	170600	2.10E-02	2.08E-02	2.80E-02	6.035	10	107600	1.90E-02	1.88E-02	2.60E-02		2.00E-02	1.98E-02	2.70E-02
6.177	8.167	64200	6.44E-03	6.25E-03	8.48E-03	6.177	10.431	39510	6.20E-03	6.01E-03	8.16E-03		6.32E-03	6.13E-03	8.32E-03
5.621	8.543	23070	1.29E-03	1.25E-03	1.70E-03	5.621	10.791	13950	1.29E-03	1.25E-03	1.70E-03		1.29E-03	1.25E-03	1.70E-03
6.827	8.866	4354	3.21E-04	3.12E-04	4.23E-04	6.827	11.906	2600	3.31E-04	3.21E-04	4.36E-04		3.26E-04	3.16E-04	4.29E-04
												Dtotal	6.31E-01	6.12E-01	8.32E-01
						West Africa Scatter Diagram									
1.124	1.798	757200	3.45E-03	3.34E-03	4.54E-03	1.124	1.961	746800	3.66E-04	3.55E-04	4.82E-04		1.91E-03	1.85E-03	2.51E-03
1.436	2.548	3834000	1.70E-02	1.65E-02	2.20E-02	1.436	3.096	3651000	2.70E-03	2.62E-03	3.56E-03		9.85E-03	9.55E-03	1.28E-02
1.719	3.715	6512000	4.40E-02	4.25E-02	5.80E-02	1.719	4.797	5813000	1.10E-02	1.05E-02	1.40E-02		2.75E-02	2.65E-02	3.60E-02
1.978	4.882	5184000	5.30E-02	5.12E-02	7.00E-02	1.978	6.553	4210000	2.00E-02	1.96E-02	2.70E-02		3.65E-02	3.54E-02	4.85E-02
2.186	5.827	2537000	3.10E-02	3.03E-02	4.10E-02	2.186	7.871	1876000	1.70E-02	1.66E-02	2.30E-02		2.40E-02	2.35E-02	3.20E-02
2.412	6.582	898300	1.20E-02	1.18E-02	1.60E-02	2.412	8.791	617700	8.57E-03	8.31E-03	1.10E-02		1.03E-02	1.01E-02	1.35E-02
2.431	7.203	237100	2.58E-03	2.50E-03	3.39E-03	2.431	9.47	154900	2.11E-03	2.04E-03	2.78E-03		2.34E-03	2.27E-03	3.08E-03
2.686	7.725	60720	6.73E-04	6.53E-04	8.86E-04	2.686	10	38300	6.08E-03	5.90E-04	8.01E-04		3.38E-03	6.21E-04	8.44E-04
												Dtotal	1.16E-01	1.10E-01	1.49E-01

Table C17: Wave Fatigue Damage for North Sea and West Africa Sea at IHS5

IHS5						North Sea Scatter Diagram							Total Damage/Year		
Hs	Tz	n/year	D_{LR}	D_{DNV}	D_{ABS}	Hs	Tz	n/year	D_{LR}	D_{DNV}	D_{ABS}		D_{LR}	D_{DNV}	D_{ABS}
0.5	1.333	507.997	6.15E-05	5.97E-05	8.09E-05	0.5	1.336	507.361	2.66E-05	2.58E-05	3.50E-05		4.40E-05	4.27E-05	5.80E-05
1.129	1.468	35560	4.20E-03	4.07E-03	5.53E-03	1.129	1.479	35470	1.85E-03	1.92E-03	2.43E-03		3.02E-03	3.00E-03	3.98E-03
1.372	1.798	1264000	5.70E-02	5.57E-02	7.60E-02	1.372	1.961	1247000	2.90E-02	2.83E-02	3.80E-02		4.30E-02	4.20E-02	5.70E-02
1.722	2.548	3733000	1.57E-01	1.52E-01	2.06E-01	1.722	3.096	3555000	1.19E-01	1.15E-01	1.57E-01		1.38E-01	1.34E-01	1.82E-01
2.315	3.715	4902000	4.43E-01	4.29E-01	5.83E-01	2.315	4.797	4376000	5.24E-01	5.08E-01	6.89E-01		4.84E-01	4.69E-01	6.36E-01
3.128	4.882	4369000	9.67E-01	9.37E-01	1.27E+00	3.128	6.553	3549000	1.77E+00	1.71E+00	2.33E+00		1.37E+00	1.32E+00	1.80E+00
4.028	5.827	3061000	1.30E+00	1.26E+00	1.71E+00	4.028	7.871	2263000	3.40E+00	3.30E+00	4.48E+00		2.35E+00	2.28E+00	3.09E+00
4.962	6.582	1513000	9.86E-01	9.55E-01	1.30E+00	4.962	8.791	1040000	3.30E+00	3.20E+00	4.34E+00		2.14E+00	2.07E+00	2.82E+00
5.717	7.203	567300	4.41E-01	4.27E-01	5.81E-01	5.717	9.47	370700	1.72E+00	1.67E+00	2.27E+00		1.08E+00	1.05E+00	1.42E+00
6.035	7.725	170600	1.18E-01	1.14E-01	1.55E-01	6.035	10	107600	5.09E-01	4.94E-01	6.70E-01		3.14E-01	3.04E-01	4.13E-01
6.177	8.167	64200	3.50E-02	3.44E-02	4.70E-02	6.177	10.431	39510	1.63E-01	1.58E-01	2.14E-01		9.90E-02	9.61E-02	1.31E-01
5.621	8.543	23070	7.09E-03	6.86E-03	9.33E-03	5.621	10.791	13950	3.40E-02	3.29E-02	4.50E-02		2.05E-02	1.99E-02	2.72E-02
6.827	8.866	4354	1.77E-03	1.71E-03	2.33E-03	6.827	11.906	2600	8.87E-03	8.41E-03	1.10E-02		5.32E-03	5.06E-03	6.66E-03
												Dtotal	8.05E+00	7.80E+00	1.06E+01
						West Africa Scatter Diagram									
1.124	1.798	757200	1.90E-02	1.84E-02	2.50E-02	1.124	1.961	746800	9.60E-03	9.32E-03	1.30E-02		1.43E-02	1.38E-02	1.90E-02
1.436	2.548	3834000	9.30E-02	9.06E-02	1.23E-01	1.436	3.096	3651000	7.10E-02	6.88E-02	9.30E-02		8.20E-02	7.97E-02	1.08E-01
1.719	3.715	6512000	2.41E-01	2.34E-01	3.17E-01	1.719	4.797	5813000	2.85E-01	2.77E-01	3.75E-01		2.63E-01	2.55E-01	3.46E-01
1.978	4.882	5184000	2.90E-01	2.81E-01	3.82E-01	1.978	6.553	4210000	5.31E-01	5.14E-01	6.99E-01		4.11E-01	3.98E-01	5.41E-01
2.186	5.827	2537000	1.72E-01	1.67E-01	2.26E-01	2.186	7.871	1876000	4.50E-01	4.37E-01	5.93E-01		3.11E-01	3.02E-01	4.10E-01
2.412	6.582	898300	6.70E-02	6.51E-02	8.90E-02	2.412	8.791	617700	2.25E-01	2.18E-01	2.96E-01		1.46E-01	1.42E-01	1.93E-01
2.431	7.203	237100	1.40E-02	1.37E-02	1.90E-02	2.431	9.47	154900	5.50E-02	5.37E-02	7.30E-02		3.45E-02	3.37E-02	4.60E-02
2.686	7.725	60720	3.70E-03	3.59E-03	4.88E-03	2.686	10	38300	1.60E-02	1.55E-02	2.10E-02		9.85E-03	9.54E-03	1.29E-02
												Dtotal	1.27E+00	1.23E+00	1.67E+00

Table C18: Wave Fatigue Damage for North Sea and West Africa Sea at IHS6

IHS6						North Sea Scatter Diagram							Total Damage/Year		
Hs	Tz	n/year	D_{LR}	D_{DNV}	D_{ABS}	Hs	Tz	n/year	D_{LR}	D_{DNV}	D_{ABS}		D_{LR}	D_{DNV}	D_{ABS}
0.5	1.333	507.997	3.80E-06	3.69E-06	5.01E-06	0.5	1.336	507.361	1.19E-05	1.16E-05	1.57E-05		7.86E-06	7.63E-06	1.03E-05
1.129	1.468	35560	2.60E-04	2.52E-04	3.42E-04	1.129	1.479	35470	8.28E-04	8.58E-04	1.09E-03		5.44E-04	5.55E-04	7.16E-04
1.372	1.798	1264000	3.55E-03	3.44E-03	4.67E-03	1.372	1.961	1247000	1.30E-02	1.27E-02	1.70E-02		8.28E-03	8.05E-03	1.08E-02
1.722	2.548	3733000	9.70E-03	9.41E-03	1.30E-02	1.722	3.096	3555000	5.30E-02	5.17E-02	7.00E-02		3.13E-02	3.06E-02	4.15E-02
2.315	3.715	4902000	2.70E-02	2.66E-02	3.60E-02	2.315	4.797	4376000	2.34E-01	2.28E-01	3.09E-01		1.31E-01	1.27E-01	1.73E-01
3.128	4.882	4369000	6.00E-02	5.79E-02	7.90E-02	3.128	6.553	3549000	7.92E-01	7.67E-01	1.04E+00		4.26E-01	4.12E-01	5.61E-01
4.028	5.827	3061000	8.00E-02	7.79E-02	1.06E-01	4.028	7.871	2263000	1.52E+00	1.48E+00	2.00E+00		8.01E-01	7.77E-01	1.06E+00
4.962	6.582	1513000	6.10E-02	5.90E-02	8.00E-02	4.962	8.791	1040000	1.48E+00	1.43E+00	1.94E+00		7.69E-01	7.45E-01	1.01E+00
5.717	7.203	567300	2.70E-02	2.64E-02	3.60E-02	5.717	9.47	370700	7.72E-01	7.48E-01	1.02E+00		4.00E-01	3.87E-01	5.26E-01
6.035	7.725	170600	7.30E-03	7.07E-03	9.61E-03	6.035	10	107600	2.28E-01	2.21E-01	3.00E-01		1.18E-01	1.14E-01	1.55E-01
6.177	8.167	64200	2.19E-03	2.13E-03	2.89E-03	6.177	10.431	39510	7.30E-02	7.06E-02	9.60E-02		3.76E-02	3.64E-02	4.94E-02
5.621	8.543	23070	4.38E-04	4.24E-04	5.77E-04	5.621	10.791	13950	1.50E-02	1.47E-02	2.00E-02		7.72E-03	7.57E-03	1.03E-02
6.827	8.866	4354	1.09E-04	1.06E-04	1.44E-04	6.827	11.906	2600	3.89E-03	3.77E-03	5.12E-03		2.00E-03	1.94E-03	2.63E-03
												Dtotal	2.73E+00	2.65E+00	3.60E+00
						West Africa Scatter Diagram									
1.124	1.798	757200	1.17E-03	1.14E-03	1.54E-03	1.124	1.961	746800	4.30E-03	4.17E-03	5.66E-03		2.74E-03	2.66E-03	3.60E-03
1.436	2.548	3834000	5.77E-03	5.60E-03	7.60E-03	1.436	3.096	3651000	3.20E-02	3.08E-02	4.20E-02		1.89E-02	1.82E-02	2.48E-02
1.719	3.715	6512000	1.50E-02	1.45E-02	2.00E-02	1.719	4.797	5813000	1.28E-01	1.24E-01	1.68E-01		7.15E-02	6.92E-02	9.40E-02
1.978	4.882	5184000	1.80E-02	1.74E-02	2.40E-02	1.978	6.553	4210000	2.38E-01	2.30E-01	3.13E-01		1.28E-01	1.24E-01	1.69E-01
2.186	5.827	2537000	1.10E-02	1.03E-02	1.40E-02	2.186	7.871	1876000	2.02E-01	1.96E-01	2.65E-01		1.07E-01	1.03E-01	1.40E-01
2.412	6.582	898300	4.16E-03	4.03E-03	5.48E-03	2.412	8.791	617700	1.01E-01	9.76E-02	1.33E-01		5.26E-02	5.08E-02	6.92E-02
2.431	7.203	237100	8.76E-04	8.49E-04	1.15E-03	2.431	9.47	154900	2.50E-02	2.40E-02	3.30E-02		1.29E-02	1.24E-02	1.71E-02
2.686	7.725	60720	2.29E-04	2.22E-04	3.01E-04	2.686	10	38300	7.02E-03	6.94E-03	9.41E-03		3.62E-03	3.58E-03	4.86E-03
												Dtotal	3.97E-01	3.84E-01	5.22E-01

APPENDIX D: COMBINED FATIGUE DAMAGE

Table D1: Cumulative Fatigue Damage at Bottom Detail

	North Sea	ABS					LR						DNV					
	Load Seq	D_{lcf}	D_{hcf}	D_{ABS}	D_{linear}	$D_{quadratic}$	D_{lcf}	D_{hcf}	D_{adj}	D_{LR}	D_{linear}	$D_{quadratic}$	D_{lcf}	D_{hcf}	D_{factor}	D_{DNV}	D_{linear}	$D_{quadratic}$
	SEQ1	0.0084	1.92	1.920186	1.9284	1.920018	0.003	1.44	2.7E-08	1.443	1.443	1.440003	0.002876	1.3	2.61E-08	1.302876	1.302876	1.300003
	SEQ2	0.009941	1.92	1.920225	1.929941	1.920026	0.0036	1.44	3.23E-08	1.4436	1.4436	1.440004	0.00348	1.3	3.14E-08	1.30348	1.30348	1.300005
BHS1	SEQ3	0.0133	1.92	1.920312	1.9333	1.920046	0.00484	1.44	3.23E-08	1.44484	1.44484	1.440008	0.0047	1.3	3.14E-08	1.3047	1.3047	1.300008
	SEQ4	0.00749	1.92	1.920164	1.92749	1.920015	0.00257	1.44	2.7E-08	1.44257	1.44257	1.440002	0.0025	1.3	2.61E-08	1.3025	1.3025	1.300002
	SEQ5	0.00748	1.92	1.920164	1.92748	1.920015	0.00256	1.44	2.7E-08	1.44256	1.44256	1.440002	0.0025	1.3	2.61E-08	1.3025	1.3025	1.300002
	SEQ1	0.0665	3.07	3.07205	3.1365	3.07072	0.0155	2.33	2.92E-08	2.3455	2.3455	2.330052	0.071	2.26	2.83E-08	2.331	2.331	2.261115
	SEQ2	0.0741	3.07	3.072376	3.1441	3.070894	0.0754	2.33	3.51E-08	2.4054	2.4054	2.33122	0.073	2.26	3.4E-08	2.333	2.333	2.261179
BHS2	SEQ3	0.0112	3.07	3.074281	3.0812	3.07002	0.012	2.33	3.51E-08	2.342	2.342	2.330031	0.107	2.26	3.4E-08	2.367	2.367	2.262532
	SEQ4	0.061	3.07	3.071826	3.131	3.070606	0.0714	2.33	3.51E-08	2.4014	2.4014	2.331094	0.069	2.26	2.83E-08	2.329	2.329	2.261053
	SEQ5	0.0689	3.07	3.072151	3.1389	3.070773	0.074	2.33	2.92E-08	2.404	2.404	2.331175	0.072	2.26	2.83E-08	2.332	2.332	2.261147
	SEQ1	0.00857	4.5	4.50018	4.50857	4.500008	0.0033	3.42	6.51E-08	3.4233	3.4233	3.420002	0.00316	3.31	6.31E-08	3.31316	3.31316	3.310002
	SEQ2	0.0091	4.5	4.500191	4.5091	4.500009	0.0035	3.42	7.81E-08	3.4235	3.4235	3.420002	0.00335	3.31	7.57E-08	3.31335	3.31335	3.310002
BHS3	SEQ3	0.0146	4.5	4.500316	4.5146	4.500024	0.0055	3.42	7.81E-08	3.4255	3.4255	3.420004	0.0053	3.31	7.57E-08	3.3153	3.3153	3.310004
	SEQ4	0.00765	4.5	4.50016	4.50765	4.500007	0.00285	3.42	6.51E-08	3.42285	3.42285	3.420001	0.00285	3.31	6.31E-08	3.31285	3.31285	3.310001
	SEQ5	0.00873	4.5	4.500183	4.50873	4.500008	0.00327	3.42	6.51E-08	3.42327	3.42327	3.420002	0.00317	3.31	6.31E-08	3.31317	3.31317	3.310002
	SEQ1	0.000858	1.19	1.190017	1.190858	1.19	0.00041	0.9	3.83E-08	0.90041	0.90041	0.9	0.00039	0.871	3.71E-08	0.87139	0.87139	0.871
	SEQ2	0.00108	1.19	1.190022	1.19108	1.19	0.00051	0.9	4.59E-08	0.90051	0.90051	0.9	0.0005	0.871	4.45E-08	0.8715	0.8715	0.871
BHS4	SEQ3	0.001	1.19	1.19002	1.191	1.19	0.00048	0.9	4.59E-08	0.90048	0.90048	0.9	0.00046	0.871	4.45E-08	0.87146	0.87146	0.871
	SEQ4	0.00195	1.19	1.190041	1.19195	1.190002	0.00088	0.9	3.83E-08	0.90088	0.90088	0.9	0.00085	0.871	3.71E-08	0.87185	0.87185	0.871
	SEQ5	0.00714	1.19	1.190164	1.19714	1.190021	0.0026	0.9	3.83E-08	0.9026	0.9026	0.900004	0.0025	0.871	3.71E-08	0.8735	0.8735	0.871004
	SEQ1	0.0874	2.01	2.013646	2.0974	2.011899	0.0712	1.52	9.96E-08	1.5912	1.5912	1.521667	0.069	1.48	9.66E-08	1.549	1.549	1.481608
	SEQ2	0.0895	2.01	2.01378	2.0995	2.011992	0.072	1.52	1.2E-07	1.592	1.592	1.521704	0.07	1.48	1.16E-07	1.55	1.55	1.481654
BHS5	SEQ3	0.18	2.01	2.021629	2.19	2.018044	0.092	1.52	1.2E-07	1.612	1.612	1.522782	0.089	1.48	1.16E-07	1.569	1.569	1.482674
	SEQ4	0.0845	2.01	2.013464	2.0945	2.011775	0.071	1.52	9.96E-08	1.591	1.591	1.521657	0.068	1.48	9.66E-08	1.548	1.548	1.481561
	SEQ5	0.259	2.01	2.031756	2.269	2.026618	0.151	1.52	9.96E-08	1.671	1.671	1.527482	0.147	1.48	9.66E-08	1.627	1.627	1.487282
	SEQ1	0.139	1.52	1.529111	1.659	1.526342	0.062	1.15	2.4E-08	1.212	1.212	1.15167	0.061	1.11	2.33E-08	1.171	1.171	1.111675
	SEQ2	0.143	1.52	1.529559	1.663	1.526712	0.064	1.15	2.88E-08	1.214	1.214	1.151779	0.062	1.11	2.8E-08	1.172	1.172	1.11173
BHS6	SEQ3	0.284	1.52	1.551887	1.804	1.546304	0.115	1.15	2.4E-08	1.265	1.265	1.155736	0.112	1.11	2.8E-08	1.222	1.222	1.115636
	SEQ4	0.133	1.52	1.528458	1.653	1.525808	0.061	1.15	2.4E-08	1.211	1.211	1.151617	0.059	1.11	2.33E-08	1.169	1.169	1.111567
	SEQ5	0.403	1.52	1.580308	1.923	1.572517	0.188	1.15	2.4E-08	1.338	1.338	1.165266	0.182	1.11	2.33E-08	1.292	1.292	1.124822

Table D2: Cumulative Fatigue Damage at Bottom Detail

West Africa

		ABS					LR						DNV					
	Load Seq	D_{lcf}	D_{hcf}	D_{ABS}	D_{linear}	$D_{quadratic}$	D_{lcf}	D_{hcf}	D_{adj}	D_{LR}	D_{linear}	$D_{quadratic}$	D_{lcf}	D_{hcf}	D_{factor}	D_{DNV}	D_{linear}	$D_{quadratic}$
	SEQ1	0.00717	0.311	0.311226	0.31817	0.311083	0.00258	0.236	3.96E-10	0.23858	0.23858	0.236014	0.000251	0.23	3.84E-10	0.230251	0.230251	0.23
	SEQ2	0.00845	0.311	0.311284	0.31945	0.311115	0.0031	0.236	4.75E-10	0.2391	0.2391	0.23602	0.0003	0.23	4.61E-10	0.2303	0.2303	0.23
BHS1	SEQ3	0.0113	0.311	0.311431	0.3223	0.311205	0.00421	0.236	4.75E-10	0.24021	0.24021	0.236038	0.00041	0.23	4.61E-10	0.23041	0.23041	0.23
	SEQ4	0.00644	0.311	0.311195	0.31744	0.311067	0.00225	0.236	3.96E-10	0.23825	0.23825	0.236011	0.00022	0.23	3.84E-10	0.23022	0.23022	0.23
	SEQ5	0.00643	0.311	0.311195	0.31743	0.311066	0.00225	0.236	3.96E-10	0.23825	0.23825	0.236011	0.00022	0.23	3.84E-10	0.23022	0.23022	0.23
	SEQ1	0.006	0.402	0.402165	0.408	0.402045	0.0648	0.349	2.49E-10	0.4138	0.4138	0.354965	0.0063	0.338	2.42E-10	0.3443	0.3443	0.338059
	SEQ2	0.00666	0.402	0.402188	0.40866	0.402055	0.067	0.349	2.99E-10	0.416	0.416	0.355373	0.0065	0.338	2.9E-10	0.3445	0.3445	0.338062
BHS2	SEQ3	0.0101	0.402	0.402329	0.4121	0.402127	0.096	0.349	2.99E-10	0.445	0.445	0.361963	0.0093	0.338	2.9E-10	0.3473	0.3473	0.338128
	SEQ4	0.00552	0.402	0.402148	0.40752	0.402038	0.062	0.349	2.49E-10	0.411	0.411	0.354464	0.006	0.338	2.42E-10	0.344	0.344	0.338053
	SEQ5	0.00621	0.402	0.402172	0.40821	0.402048	0.065	0.349	2.49E-10	0.414	0.414	0.355001	0.0063	0.338	2.42E-10	0.3443	0.3443	0.338059
	SEQ1	0.00676	0.733	0.733166	0.73976	0.733031	0.00262	0.557	1.15E-09	0.55962	0.55962	0.557006	0.0025	0.54	1.12E-09	0.5425	0.5425	0.540006
	SEQ2	0.00679	0.733	0.733167	0.73979	0.733031	0.00278	0.557	1.39E-09	0.55978	0.55978	0.557007	0.0027	0.54	1.34E-09	0.5427	0.5427	0.540007
BHS3	SEQ3	0.0113	0.733	0.733313	0.7443	0.733087	0.0045	0.557	1.39E-09	0.5615	0.5615	0.557018	0.0044	0.54	1.34E-09	0.5444	0.5444	0.540018
	SEQ4	0.00607	0.733	0.733147	0.73907	0.733025	0.0023	0.557	1.15E-09	0.5593	0.5593	0.557005	0.00223	0.54	1.12E-09	0.54223	0.54223	0.540005
	SEQ5	0.00662	0.733	0.733162	0.73962	0.73303	0.00255	0.557	1.15E-09	0.55955	0.55955	0.557006	0.0025	0.54	1.12E-09	0.5425	0.5425	0.540006
	SEQ1	0.000573	0.223	0.223012	0.223573	0.223001	0.000273	0.17	5.91E-10	0.170273	0.170273	0.17	0.00026	0.165	5.73E-10	0.16526	0.16526	0.165
	SEQ2	0.000583	0.223	0.223012	0.223583	0.223001	0.00034	0.17	7.09E-10	0.17034	0.17034	0.17	0.00033	0.165	6.88E-10	0.16533	0.16533	0.165
BHS4	SEQ3	0.000533	0.223	0.223011	0.223533	0.223001	0.000317	0.17	7.09E-10	0.170317	0.170317	0.17	0.00031	0.165	6.88E-10	0.16531	0.16531	0.165
	SEQ4	0.00144	0.223	0.223033	0.22444	0.223005	0.000658	0.17	5.91E-10	0.170658	0.170658	0.170001	0.000638	0.165	5.73E-10	0.165638	0.165638	0.165001
	SEQ5	0.00591	0.223	0.223196	0.22891	0.223078	0.00218	0.17	5.91E-10	0.17218	0.17218	0.170014	0.00211	0.165	5.73E-10	0.16711	0.16711	0.165013
	SEQ1	0.076	2.94	2.942502	3.016	2.940982	0.063	2.27	1.54E-09	2.333	2.333	2.270874	0.061	2.2	1.49E-09	2.261	2.261	2.200846
	SEQ2	0.0778	2.94	2.942585	3.0178	2.941029	0.0633	2.27	1.84E-09	2.3333	2.3333	2.270882	0.0614	2.2	1.79E-09	2.2614	2.2614	2.200857
BHS5	SEQ3	0.157	2.94	2.947325	3.097	2.944189	0.113	2.27	1.84E-09	2.383	2.383	2.272811	0.11	2.2	1.79E-09	2.31	2.31	2.202748
	SEQ4	0.0737	2.94	2.942397	3.0137	2.940924	0.0615	2.27	1.54E-09	2.3315	2.3315	2.270833	0.06	2.2	1.49E-09	2.26	2.26	2.200818
	SEQ5	0.23	2.94	2.953569	3.17	2.948983	0.133	2.27	1.54E-09	2.403	2.403	2.273893	0.129	2.2	1.49E-09	2.329	2.329	2.203779
	SEQ1	0.129	2.19	2.196372	2.319	2.193796	0.0582	1.66	3.96E-10	1.7182	1.7182	1.66102	0.056	1.61	3.84E-10	1.666	1.666	1.610974
	SEQ2	0.132	2.19	2.19661	2.322	2.193974	0.0589	1.66	4.75E-10	1.7189	1.7189	1.661045	0.057	1.61	4.61E-10	1.667	1.667	1.611009
BHS6	SEQ3	0.263	2.19	2.210958	2.453	2.205735	0.106	1.66	4.75E-10	1.766	1.766	1.663381	0.103	1.61	4.61E-10	1.713	1.713	1.613291
	SEQ4	0.124	2.19	2.195984	2.314	2.193508	0.0562	1.66	3.96E-10	1.7162	1.7162	1.660951	0.0545	1.61	3.84E-10	1.6645	1.6645	1.610922
	SEQ5	0.377	2.19	2.229643	2.567	2.222213	0.175	1.66	3.96E-10	1.835	1.835	1.669199	0.169	1.61	3.84E-10	1.779	1.779	1.618846

Table D3: Cumulative Fatigue Damage at Side Plating Detail

North Sea

		ABS					LR						DNV					
	Load Seq	D_{lcf}	D_{hcf}	D_{ABS}	D_{linear}	$D_{quadratic}$	D_{lcf}	D_{hcf}	D_{adj}	D_{LR}	D_{linear}	$D_{quadratic}$	D_{lcf}	D_{hcf}	D_{factor}	D_{DNV}	D_{linear}	$D_{quadratic}$
	SEQ1	6.60E-02	20.4	20.401427	20.466	20.4001068	0.056	15.5	1.11587E-06	15.556	15.556	15.5001	0.054	15	1.08164E-06	15.054	15.054	15.0001
	SEQ2	6.73E-02	20.4	20.401457	20.4673	20.400111	0.0568	15.5	1.11587E-06	15.5568	15.5568	15.5001	0.055	15	1.08164E-06	15.055	15.055	15.0001
SHS1	SEQ3	6.60E-02	20.4	20.401427	20.466	20.4001068	0.056	15.5	1.11587E-06	15.556	15.556	15.5001	0.054	15	1.08164E-06	15.054	15.054	15.0001
	SEQ4	6.61E-02	20.4	20.401429	20.4661	20.4001071	0.056	15.5	1.11587E-06	15.556	15.556	15.5001	0.0543	15	1.08164E-06	15.0543	15.0543	15.0001
	SEQ5	6.60E-02	20.4	20.401427	20.466	20.4001068	0.056	15.5	1.11587E-06	15.556	15.556	15.5001	0.0543	15	1.08164E-06	15.0543	15.0543	15.0001
	SEQ1	7.35E-03	17.4	17.400149	17.40735	17.4000016	0.0029	13.2	9.15598E-07	13.2029	13.2029	13.2	0.00285	12.8	8.87517E-07	12.80285	12.80285	12.8
	SEQ2	7.43E-03	17.4	17.400150	17.40743	17.4000016	0.003	13.2	9.15598E-07	13.203	13.203	13.2	0.0029	12.8	8.87517E-07	12.8029	12.8029	12.8
SHS2	SEQ3	7.77E-03	17.4	17.400157	17.40777	17.4000017	0.0031	13.2	9.15598E-07	13.2031	13.2031	13.2	0.003	12.8	8.87517E-07	12.803	12.803	12.8
	SEQ4	7.34E-03	17.4	17.400148	17.40734	17.4000015	0.0029	13.2	9.15598E-07	13.2029	13.2029	13.2	0.0028	12.8	8.87517E-07	12.8028	12.8028	12.8
	SEQ5	7.61E-03	17.4	17.400154	17.40761	17.4000017	0.0031	13.2	9.15598E-07	13.2031	13.2031	13.2	0.00297	12.8	8.87517E-07	12.80297	12.80297	12.8
	SEQ1	1.95E-03	4.16	4.160039	4.16195	4.16000046	0.00088	3.14	2.60411E-07	3.14088	3.14088	3.14	0.00085	3.05	2.52424E-07	3.05085	3.05085	3.05
	SEQ2	1.99E-03	4.16	4.160040	4.16199	4.16000048	0.0009	3.14	2.60411E-07	3.1409	3.1409	3.14	0.00087	3.05	2.52424E-07	3.05087	3.05087	3.05
SHS3	SEQ3	1.96E-03	4.16	4.160040	4.16196	4.16000046	0.00088	3.14	2.60411E-07	3.14088	3.14088	3.14	0.00085	3.05	2.52424E-07	3.05085	3.05085	3.05
	SEQ4	1.96E-03	4.16	4.160040	4.16196	4.16000046	0.00088	3.14	2.60411E-07	3.14088	3.14088	3.14	0.00086	3.05	2.52424E-07	3.05086	3.05086	3.05
	SEQ5	1.96E-03	4.16	4.160040	4.16196	4.16000046	0.00088	3.14	2.60411E-07	3.14088	3.14088	3.14	0.00085	3.05	2.52424E-07	3.05085	3.05085	3.05
	SEQ1	0.000928	6.57	6.570019	6.570928	6.57000007	0.000437	4.99	3.42325E-07	4.990437	4.990437	4.99	0.000424	4.84	3.31826E-07	4.840424	4.840424	4.84
	SEQ2	0.000933	6.57	6.570019	6.570933	6.57000007	0.00044	4.99	3.42325E-07	4.99044	4.99044	4.99	0.000428	4.84	3.31826E-07	4.840428	4.840428	4.84
SHS4	SEQ3	0.00104	6.57	6.570021	6.57104	6.57000008	0.00049	4.99	3.42325E-07	4.99049	4.99049	4.99	0.000474	4.84	3.31826E-07	4.840474	4.840474	4.84
	SEQ4	0.000928	6.57	6.570019	6.570928	6.57000007	0.000437	4.99	3.42325E-07	4.990437	4.990437	4.99	0.000424	4.84	3.31826E-07	4.840424	4.840424	4.84
	SEQ5	0.000975	6.57	6.570020	6.570975	6.57000007	0.00046	4.99	3.42325E-07	4.99046	4.99046	4.99	0.00045	4.84	3.31826E-07	4.84045	4.84045	4.84
	SEQ1	0.0241	10.5	10.500510	10.5241	10.5000277	0.00754	7.95	8.1794E-08	7.95754	7.95754	7.950004	0.0073	7.71	7.92854E-08	7.7173	7.7173	7.710003
	SEQ2	0.0243	10.5	10.500514	10.5243	10.5000281	0.0077	7.95	8.1794E-08	7.9577	7.9577	7.950004	0.0075	7.71	7.92854E-08	7.7175	7.7175	7.710004
SHS5	SEQ3	0.024	10.5	10.500507	10.524	10.5000274	0.00752	7.95	8.1794E-08	7.95752	7.95752	7.950004	0.0073	7.71	7.92854E-08	7.7173	7.7173	7.710003
	SEQ4	0.0241	10.5	10.500510	10.5241	10.5000277	0.00756	7.95	8.1794E-08	7.95756	7.95756	7.950004	0.0073	7.71	7.92854E-08	7.7173	7.7173	7.710003
	SEQ5	0.0241	10.5	10.500510	10.5241	10.5000277	0.00754	7.95	8.1794E-08	7.95754	7.95754	7.950004	0.0073	7.71	7.92854E-08	7.7173	7.7173	7.710003
	SEQ1	0.00402	9.51	9.510081	9.51402	9.51000085	0.00169	7.22	3.18527E-07	7.22169	7.22169	7.22	0.00164	7	3.08758E-07	7.00164	7.00164	7
	SEQ2	0.00352	9.51	9.510071	9.51352	9.51000065	0.001522	7.22	3.18527E-07	7.221522	7.221522	7.22	0.00148	7	3.08758E-07	7.00148	7.00148	7
SHS6	SEQ3	0.00306	9.51	9.510062	9.51306	9.51000049	0.00132	7.22	3.18527E-07	7.22132	7.22132	7.22	0.00128	7	3.08758E-07	7.00128	7.00128	7
	SEQ4	0.00401	9.51	9.510081	9.51401	9.51000085	0.00169	7.22	3.18527E-07	7.22169	7.22169	7.22	0.00164	7	3.08758E-07	7.00164	7.00164	7
	SEQ5	0.00402	9.51	9.510081	9.51402	9.51000085	0.00169	7.22	3.18527E-07	7.22169	7.22169	7.22	0.00164	7	3.08758E-07	7.00164	7.00164	7

Table D4: Cumulative Fatigue Damage at Side Plating Detail

	West Africa	ABS					LR						DNV					
	Load Seq	D_{lcf}	D_{hcf}	D_{ABS}	D_{linear}	$D_{quadratic}$	D_{lcf}	D_{hcf}	D_{adj}	D_{LR}	D_{linear}	$D_{quadratic}$	D_{lcf}	D_{hcf}	D_{factor}	D_{DNV}	D_{linear}	$D_{quadratic}$
	SEQ1	0.0511	4.36	4.361321	4.4111	4.36029944	0.0438	2.55	5.07291E-08	2.5938	2.5938	2.550376	0.0425	2.48	4.91733E-08	2.5225	2.5225	2.480364
	SEQ2	0.0272	4.36	4.360629	4.3872	4.36008484	0.0445	2.55	5.07291E-08	2.5945	2.5945	2.550388	0.0431	2.48	4.91733E-08	2.5231	2.5231	2.480374
SHS1	SEQ3	0.0248	4.36	4.360567	4.3848	4.36007053	0.0434	2.55	5.07291E-08	2.5934	2.5934	2.550369	0.0421	2.48	4.91733E-08	2.5221	2.5221	2.480357
	SEQ4	0.0512	4.36	4.361325	4.4112	4.36030061	0.043	2.55	5.07291E-08	2.593	2.593	2.550363	0.0418	2.48	4.91733E-08	2.5218	2.5218	2.480352
	SEQ5	5.11E-02	4.36	4.361321	4.4111	4.36029944	0.043	2.55	5.07291E-08	2.593	2.593	2.550363	0.0417	2.48	4.91733E-08	2.5217	2.5217	2.480351
	SEQ1	0.00735	2.9	2.900156	2.90735	2.90000931	0.0018	2.21	4.06589E-08	2.2118	2.2118	2.210001	0.00177	2.14	3.9412E-08	2.14177	2.14177	2.140001
	SEQ2	0.0049	2.9	2.900102	2.9049	2.90000414	0.0019	2.21	4.06589E-08	2.2119	2.2119	2.210001	0.0018	2.14	3.9412E-08	2.1418	2.1418	2.140001
SHS2	SEQ3	0.00524	2.9	2.900110	2.90524	2.90000473	0.002	2.21	4.06589E-08	2.212	2.212	2.210001	0.00197	2.14	3.9412E-08	2.14197	2.14197	2.140001
	SEQ4	0.00734	2.9	2.900156	2.90734	2.90000929	0.0018	2.21	4.06589E-08	2.2118	2.2118	2.210001	0.00176	2.14	3.9412E-08	2.14176	2.14176	2.140001
	SEQ5	0.00761	2.9	2.900162	2.90761	2.90000998	0.00195	2.21	4.06589E-08	2.21195	2.21195	2.210001	0.00189	2.14	3.9412E-08	2.14189	2.14189	2.140001
	SEQ1	0.00137	1.94	1.940028	1.94137	1.94000048	0.00062	1.48	1.2083E-08	1.48062	1.48062	1.48	0.0006	0.483	1.17124E-08	0.4836	0.4836	0.483
	SEQ2	0.00755	1.94	1.940166	1.94755	1.94001469	0.00064	1.48	1.2083E-08	1.48064	1.48064	1.48	0.00062	0.483	1.17124E-08	0.48362	0.48362	0.483
SHS3	SEQ3	0.000723	1.94	1.940015	1.940723	1.94000013	0.00063	1.48	1.2083E-08	1.48063	1.48063	1.48	0.00061	0.483	1.17124E-08	0.48361	0.48361	0.483
	SEQ4	0.00138	1.94	1.940028	1.94138	1.94000049	0.00063	1.48	1.2083E-08	1.48063	1.48063	1.48	0.00061	0.483	1.17124E-08	0.48361	0.48361	0.483
	SEQ5	0.00137	1.94	1.940028	1.94137	1.94000048	0.00062	1.48	1.2083E-08	1.48062	1.48062	1.48	0.000605	0.483	1.17124E-08	0.483605	0.483605	0.483
	SEQ1	0.000433	1.1	1.100009	1.100433	1.10000009	0.000206	0.836	1.51534E-08	0.836206	0.836206	0.836	0.0002	0.811	1.46887E-08	0.8112	0.8112	0.811
	SEQ2	0.00031	1.1	1.100006	1.10031	1.10000004	0.00021	0.836	1.51534E-08	0.83621	0.83621	0.836	0.0002	0.811	1.46887E-08	0.8112	0.8112	0.811
SHS4	SEQ3	0.000416	1.1	1.100008	1.100416	1.10000008	0.00026	0.836	1.51534E-08	0.83626	0.83626	0.836	0.00025	0.811	1.46887E-08	0.81125	0.81125	0.811
	SEQ4	0.000433	1.1	1.100009	1.100433	1.10000009	0.00021	0.836	1.51534E-08	0.83621	0.83621	0.836	0.0002	0.811	1.46887E-08	0.8112	0.8112	0.811
	SEQ5	0.00048	1.1	1.100010	1.10048	1.1000001	0.00023	0.836	1.51534E-08	0.83623	0.83623	0.836	0.00022	0.811	1.46887E-08	0.81122	0.81122	0.811
	SEQ1	0.019	1.76	1.760483	1.779	1.76010255	0.00626	1.32	2.36378E-08	1.32626	1.32626	1.320015	0.0061	1.3	2.29129E-08	1.3061	1.3061	1.300014
	SEQ2	0.0099	1.76	1.760226	1.7699	1.76002784	0.0069	1.32	2.36378E-08	1.3269	1.3269	1.320018	0.0067	1.3	2.29129E-08	1.3067	1.3067	1.300017
SHS5	SEQ3	0.00962	1.76	1.760219	1.76962	1.76002629	0.0067	1.32	2.36378E-08	1.3267	1.3267	1.320017	0.0065	1.3	2.29129E-08	1.3065	1.3065	1.300016
	SEQ4	0.0191	1.76	1.760486	1.7791	1.76010364	0.00628	1.32	2.36378E-08	1.32628	1.32628	1.320015	0.006	1.3	2.29129E-08	1.306	1.306	1.300014
	SEQ5	0.019	1.76	1.760483	1.779	1.76010255	0.00626	1.32	2.36378E-08	1.32626	1.32626	1.320015	0.006	1.3	2.29129E-08	1.306	1.306	1.300014
	SEQ1	0.00211	1.75	1.750043	1.75211	1.75000127	0.000941	1.33	1.18946E-08	1.330941	1.330941	1.33	0.00091	1.29	1.15298E-08	1.29091	1.29091	1.29
	SEQ2	0.00119	1.75	1.750024	1.75119	1.7500004	0.00096	1.33	1.18946E-08	1.33096	1.33096	1.33	0.00093	1.29	1.15298E-08	1.29093	1.29093	1.29
SHS6	SEQ3	0.00123	1.75	1.750025	1.75123	1.75000043	0.00098	1.33	1.18946E-08	1.33098	1.33098	1.33	0.00095	1.29	1.15298E-08	1.29095	1.29095	1.29
	SEQ4	0.0021	1.75	1.750043	1.7521	1.75000126	0.00094	1.33	1.18946E-08	1.33094	1.33094	1.33	0.00091	1.29	1.15298E-08	1.29091	1.29091	1.29
	SEQ5	0.00211	1.75	1.750043	1.75211	1.75000127	0.00094	1.33	1.18946E-08	1.33094	1.33094	1.33	0.00092	1.29	1.15298E-08	1.29092	1.29092	1.29

Table D5: Cumulative Fatigue Damage at Inner Side Plating Detail

	North Sea																	
		ABS					LR						DNV					
	Load Seq	D_{lcf}	D_{hcf}	D_{ABS}	D_{linear}	$D_{quadratic}$	D_{lcf}	D_{hcf}	D_{adj}	D_{LR}	D_{linear}	$D_{quadratic}$	D_{lcf}	D_{hcf}	D_{factor}	D_{DNV}	D_{linear}	$D_{quadratic}$
	SEQ1	4.70E-03	46.8	46.80009	46.8047	46.8	0.00165	35.6	3.80266E-06	35.60165	35.60165	35.6	0.0016	34.5	3.68603E-06	34.5016	34.5016	34.5
1HS1	SEQ2	4.47E-03	46.8	46.80009	46.80447	46.8	0.00166	35.6	3.80266E-06	35.60166	35.60166	35.6	0.00161	34.5	3.68603E-06	34.50161	34.50161	34.5
	SEQ3	5.13E-03	46.8	46.80010	46.80513	46.8	0.00196	35.6	3.80266E-06	35.60196	35.60196	35.6	0.0019	34.5	3.68603E-06	34.5019	34.5019	34.5
	SEQ4	4.45E-03	46.8	46.80009	46.80445	46.8	0.00164	35.6	3.80266E-06	35.60164	35.60164	35.6	0.00159	34.5	3.68603E-06	34.50159	34.50159	34.5
	SEQ5	5.24E-03	46.8	46.80011	46.80524	46.8	0.002	35.6	3.80266E-06	35.602	35.602	35.6	0.00193	34.5	3.68603E-06	34.50193	34.50193	34.5
	SEQ1	2.35E-03	15.4	15.40005	15.40235	15.4	0.00098	11.7	7.45535E-07	11.70098	11.70098	11.7	0.00095	11.3	5.02135E-07	11.30095	11.30095	11.3
IHS2	SEQ2	2.37E-03	15.4	15.40005	15.40237	15.4	0.001	11.7	7.45535E-07	11.701	11.701	11.7	0.00096	11.3	5.02135E-07	11.30096	11.30096	11.3
	SEQ3	3.22E-03	15.4	15.40006	15.40322	15.4	0.0014	11.7	7.45535E-07	11.7014	11.7014	11.7	0.00135	11.3	5.02135E-07	11.30135	11.30135	11.3
	SEQ4	2.32E-03	15.4	15.40005	15.40232	15.4	0.00097	11.7	7.45535E-07	11.70097	11.70097	11.7	0.00094	11.3	5.02135E-07	11.30094	11.30094	11.3
	SEQ5	2.91E-03	15.4	15.40006	15.40291	15.4	0.00124	11.7	7.45535E-07	11.70124	11.70124	11.7	0.0012	11.3	5.02135E-07	11.3012	11.3012	11.3
	SEQ1	7.75767E-05	0.774	0.77400	0.7740776	0.774	3.4102E-05	0.588	3.29673E-08	0.588034	0.588034	0.588	3.30561E-05	0.57	3.19563E-08	0.570033	0.570033	0.57
IHS3	SEQ2	7.77714E-05	0.774	0.77400	0.7740778	0.774	3.41599E-05	0.588	3.29673E-08	0.588034	0.588034	0.588	3.31122E-05	0.57	3.19563E-08	0.570033	0.570033	0.57
	SEQ3	8.26278E-05	0.774	0.77400	0.7740826	0.774	3.58091E-05	0.588	3.29673E-08	0.588036	0.588036	0.588	3.47109E-05	0.57	3.19563E-08	0.570035	0.570035	0.57
	SEQ4	7.75739E-05	0.774	0.77400	0.7740776	0.774	3.4111E-05	0.588	3.29673E-08	0.588034	0.588034	0.588	3.30648E-05	0.57	3.19563E-08	0.570033	0.570033	0.57
	SEQ5	8.66701E-05	0.774	0.77400	0.7740867	0.774	3.76528E-05	0.588	3.29673E-08	0.588038	0.588038	0.588	3.6498E-05	0.57	3.19563E-08	0.570036	0.570036	0.57
	SEQ1	0.00014444	0.832	0.83200	0.8321444	0.832	6.5152E-05	0.631	8.60411E-09	0.631065	0.631065	0.631	6.31539E-05	0.612	8.34023E-09	0.612063	0.612063	0.612
IHS4	SEQ2	0.000138081	0.832	0.83200	0.8321381	0.832	6.24043E-05	0.631	8.60411E-09	0.631062	0.631062	0.631	6.04904E-05	0.612	8.34023E-09	0.61206	0.61206	0.612
	SEQ3	0.00016092	0.832	0.83200	0.8321609	0.832	7.20636E-05	0.631	8.60411E-09	0.631072	0.631072	0.631	6.98535E-05	0.612	8.34023E-09	0.61207	0.61207	0.612
	SEQ4	0.000129374	0.832	0.83200	0.8321294	0.832	5.90201E-05	0.631	8.60411E-09	0.631059	0.631059	0.631	5.721E-05	0.612	8.34023E-09	0.612057	0.612057	0.612
	SEQ5	0.00015663	0.832	0.83200	0.8321566	0.832	7.07082E-05	0.631	8.60411E-09	0.631071	0.631071	0.631	6.85397E-05	0.612	8.34023E-09	0.612069	0.612069	0.612
	SEQ1	0.000864707	10.6	10.60002	10.600865	10.6	0.000410199	8.05	4.79549E-08	8.05041	8.05041	8.05	0.000397618	7.8	4.64842E-08	7.800398	7.800398	7.8
IHS5	SEQ2	0.000868799	10.6	10.60002	10.600869	10.6	0.000411927	8.05	4.79549E-08	8.050412	8.050412	8.05	0.000399294	7.8	4.64842E-08	7.800399	7.800399	7.8
	SEQ3	0.000891593	10.6	10.60002	10.600892	10.6	0.000421639	8.05	4.79549E-08	8.050422	8.050422	8.05	0.000408708	7.8	4.64842E-08	7.800409	7.800409	7.8
	SEQ4	0.000868835	10.6	10.60002	10.600869	10.6	0.00041205	8.05	4.79549E-08	8.050412	8.050412	8.05	0.000399412	7.8	4.64842E-08	7.800399	7.800399	7.8
	SEQ5	0.000952709	10.6	10.60002	10.600953	10.6	0.000451814	8.05	4.79549E-08	8.050452	8.050452	8.05	0.000437957	7.8	4.64842E-08	7.800438	7.800438	7.8
	SEQ1	0.002087196	3.6	3.60004	3.6020872	3.6000006	3.4102E-05	2.73	2.92824E-09	2.730034	2.730034	2.73	3.30561E-05	2.65	2.83843E-09	2.650033	2.650033	2.65
IHS6	SEQ2	0.00209652	3.6	3.60004	3.6020965	3.6000006	3.41599E-05	2.73	2.92824E-09	2.730034	2.730034	2.73	3.31122E-05	2.65	2.83843E-09	2.650033	2.650033	2.65
	SEQ3	0.002991445	3.6	3.60006	3.6029914	3.6000012	3.58091E-05	2.73	2.92824E-09	2.730036	2.730036	2.73	3.47109E-05	2.65	2.83843E-09	2.650035	2.650035	2.65
	SEQ4	0.002046776	3.6	3.60004	3.6020468	3.6000006	3.4111E-05	2.73	2.92824E-09	2.730034	2.730034	2.73	3.30648E-05	2.65	2.83843E-09	2.650033	2.650033	2.65
	SEQ5	0.002820258	3.6	3.60006	3.6028203	3.6000011	3.76528E-05	2.73	2.92824E-09	2.730038	2.730038	2.73	3.6498E-05	2.65	2.83843E-09	2.650036	2.650036	2.65

Table D6: Cumulative Fatigue Damage at Inner Side Plating Detail

West Africa

		ABS					LR						DNV					
	Load Seq	D_{lcf}	D_{hcf}	D_{ABS}	D_{linear}	$D_{quadratic}$	D_{lcf}	D_{hcf}	D_{adj}	D_{LR}	D_{linear}	$D_{quadratic}$	D_{lcf}	D_{hcf}	D_{factor}	D_{DNV}	D_{linear}	$D_{quadratic}$
	SEQ1	0.00117	6.66	6.660024	6.66117	6.6600001	0.00051	5.06	1.85351E-07	5.06051	5.06051	5.06	0.00049	4.91	1.80463E-07	4.91049	4.91049	4.91
	SEQ2	0.00118	6.66	6.660024	6.66118	6.6600001	0.00052	5.06	1.85351E-07	5.06052	5.06052	5.06	0.0005	4.91	1.80463E-07	4.9105	4.9105	4.91
1HS1	SEQ3	0.00182	6.66	6.660037	6.66182	6.6600002	0.00082	5.06	1.85351E-07	5.06082	5.06082	5.06	0.0008	4.91	1.80463E-07	4.9108	4.9108	4.91
	SEQ4	0.00115	6.66	6.660023	6.66115	6.6600001	0.0005	5.06	1.85351E-07	5.0605	5.0605	5.06	0.00049	4.91	1.80463E-07	4.91049	4.91049	4.91
	SEQ5	1.93E-03	6.66	6.660039	6.66193	6.6600003	0.00086	5.06	1.85351E-07	5.06086	5.06086	5.06	0.00083	4.91	1.80463E-07	4.91083	4.91083	4.91
	SEQ1	0.00115	2.83	2.830023	2.83115	2.8300002	0.00051	2.15	1.94027E-08	2.15051	2.15051	2.15	0.00049	2.08	1.88076E-08	2.08049	2.08049	2.08
	SEQ2	0.00113	2.83	2.830023	2.83113	2.8300002	0.00052	2.15	1.94027E-08	2.15052	2.15052	2.15	0.00051	2.08	1.88076E-08	2.08051	2.08051	2.08
IHS2	SEQ3	0.00198	2.83	2.830040	2.83198	2.8300007	0.00092	2.15	1.94027E-08	2.15092	2.15092	2.15	0.00089	2.08	1.88076E-08	2.08089	2.08089	2.08
	SEQ4	0.00113	2.83	2.830023	2.83113	2.8300002	0.0005	2.15	1.94027E-08	2.1505	2.1505	2.15	0.00048	2.08	1.88076E-08	2.08048	2.08048	2.08
	SEQ5	0.00172	2.83	2.830035	2.83172	2.8300005	0.00077	2.15	1.94027E-08	2.15077	2.15077	2.15	0.00075	2.08	1.88076E-08	2.08075	2.08075	2.08
	SEQ1	3.74412E-05	0.137	0.137001	0.1370374	0.137	0.000508526	0.107	1.36755E-09	0.107509	0.107509	0.107001	0.00049293	0.1	1.32561E-09	0.100493	0.100493	0.100001
	SEQ2	2.34807E-05	0.137	0.137000	0.1370235	0.137	0.000521018	0.107	1.36755E-09	0.107521	0.107521	0.107001	0.000505039	0.1	1.32561E-09	0.100505	0.100505	0.100001
IHS3	SEQ3	2.83371E-05	0.137	0.137001	0.1370283	0.137	0.00091846	0.107	1.36755E-09	0.107918	0.107918	0.107004	0.000890291	0.1	1.32561E-09	0.10089	0.10089	0.100004
	SEQ4	3.74385E-05	0.137	0.137001	0.1370374	0.137	0.000499118	0.107	1.36755E-09	0.107499	0.107499	0.107001	0.00048381	0.1	1.32561E-09	0.100484	0.100484	0.100001
	SEQ5	4.65347E-05	0.137	0.137001	0.1370465	0.137	0.000769281	0.107	1.36755E-09	0.107769	0.107769	0.107003	0.000745688	0.1	1.32561E-09	0.100746	0.100746	0.100003
	SEQ1	8.28183E-05	0.149	0.149002	0.1490828	0.149	3.53143E-05	0.116	4.85004E-09	0.116035	0.116035	0.116	3.42313E-05	0.11	4.70129E-08	0.110034	0.110034	0.11
	SEQ2	5.6326E-05	0.149	0.149001	0.1490563	0.149	3.25576E-05	0.116	4.85004E-09	0.116033	0.116033	0.116	3.15591E-05	0.11	4.70129E-08	0.110032	0.110032	0.11
IHS4	SEQ3	7.91651E-05	0.149	0.149002	0.1490792	0.149	4.22168E-05	0.116	4.85004E-09	0.116042	0.116042	0.116	4.09221E-05	0.11	4.70129E-08	0.110041	0.110041	0.11
	SEQ4	6.77522E-05	0.149	0.149001	0.1490678	0.149	2.91825E-05	0.116	4.85004E-09	0.116029	0.116029	0.116	2.82875E-05	0.11	4.70129E-08	0.110028	0.110028	0.11
	SEQ5	9.50087E-05	0.149	0.149002	0.149095	0.149	4.08706E-05	0.116	4.85004E-09	0.116041	0.116041	0.116	3.96171E-05	0.11	4.70129E-08	0.11004	0.11004	0.11
	SEQ1	0.000376794	1.67	1.670008	1.6703768	1.67	0.00017952	1.27	1.27264E-07	1.270179	1.27018	1.27	0.000174014	1.23	1.23361E-06	1.230173	1.230174	1.23
	SEQ2	0.000233182	1.67	1.670005	1.6702332	1.67	0.000182428	1.27	1.27264E-07	1.270182	1.270182	1.27	0.000176833	1.23	1.23361E-06	1.230176	1.230177	1.23
IHS5	SEQ3	0.000255976	1.67	1.670005	1.670256	1.67	0.00019214	1.27	1.27264E-07	1.270192	1.270192	1.27	0.000186247	1.23	1.23361E-06	1.230185	1.230186	1.23
	SEQ4	0.000380923	1.67	1.670008	1.6703809	1.67	0.000181371	1.27	1.27264E-07	1.270181	1.270181	1.27	0.000175808	1.23	1.23361E-06	1.230175	1.230176	1.23
	SEQ5	0.000464796	1.67	1.670009	1.6704648	1.6700001	0.000221135	1.27	1.27264E-07	1.270221	1.270221	1.27	0.000214353	1.23	1.23361E-06	1.230213	1.230214	1.23
	SEQ1	0.001127096	0.522	0.522024	0.5231271	0.5220012	0.000493862	0.397	5.69948E-08	0.397494	0.397494	0.397	0.000478716	0.384	5.52468E-07	0.384478	0.384479	0.384
	SEQ2	0.001133604	0.522	0.522024	0.5231336	0.5220012	0.000498987	0.397	5.69948E-08	0.397499	0.397499	0.397	0.000483683	0.384	5.52468E-07	0.384483	0.384484	0.384
IHS6	SEQ3	0.002028529	0.522	0.522045	0.5240285	0.5220039	0.000915755	0.397	5.69948E-08	0.397916	0.397916	0.397001	0.00088767	0.384	5.52468E-07	0.384887	0.384888	0.384001
	SEQ4	0.001086676	0.522	0.522023	0.5230867	0.5220011	0.000475426	0.397	5.69948E-08	0.397475	0.397475	0.397	0.000460845	0.384	5.52468E-07	0.38446	0.384461	0.384
	SEQ5	0.001860157	0.522	0.522041	0.5238602	0.5220033	0.000825908	0.397	5.69948E-08	0.397826	0.397826	0.397001	0.000800578	0.384	5.52468E-07	0.3848	0.384801	0.384001

APPENDIX E: MATHCAD SHEETS FOR WAVE ANALYSIS

WAVE FATIGUE ANALYSIS

SEA STATE

ORIGIN ≡ 1

M ≡ 1

Tz

Hs

$$SD := \begin{pmatrix} 0 & 1.5 & 2.5 & 3.5 & 4.5 & 5.5 & 6.5 & 7.5 & 8.5 & 9.5 & 10.5 & 11.5 & 12.5 & 13.5 \\ 13.5 & 0 & 0 & 0 & 0 & 0 & 0 & 0 & 0 & 0 & 0 & 1 & 0 & 0 \\ 12.5 & 0 & 0 & 0 & 0 & 0 & 0 & 0 & 0 & 0 & 1 & 4 & 0 & 0 \\ 11.5 & 0 & 0 & 0 & 0 & 0 & 0 & 0 & 0 & 2 & 9 & 7 & 1 & 0 \\ 10.5 & 0 & 0 & 0 & 0 & 0 & 0 & 0 & 1 & 6 & 36 & 12 & 2 & 1 \\ 9.5 & 0 & 0 & 0 & 0 & 0 & 0 & 0 & 6 & 88 & 50 & 11 & 3 & 1 \\ 8.5 & 0 & 0 & 0 & 0 & 0 & 0 & 2 & 47 & 279 & 54 & 23 & 12 & 4 \\ 7.5 & 0 & 0 & 0 & 0 & 0 & 0 & 25 & 486 & 365 & 93 & 42 & 13 & 4 \\ 6.5 & 0 & 0 & 0 & 0 & 0 & 8 & 310 & 1408 & 394 & 149 & 42 & 13 & 7 \\ 5.5 & 0 & 0 & 0 & 0 & 12 & 165 & 2431 & 1550 & 500 & 112 & 44 & 16 & 8 \\ 4.5 & 0 & 0 & 0 & 2 & 147 & 2372 & 4357 & 1570 & 507 & 76 & 57 & 23 & 4 \\ 3.5 & 0 & 0 & 3 & 151 & 2059 & 7426 & 3866 & 1390 & 364 & 115 & 50 & 16 & 2 \\ 2.5 & 0 & 4 & 165 & 2788 & 9877 & 7438 & 3642 & 1346 & 338 & 161 & 23 & 11 & 0 \\ 1.5 & 0 & 40 & 3218 & 10066 & 9638 & 4847 & 2253 & 1067 & 640 & 244 & 101 & 41 & 0 \\ 0.5 & 2 & 102 & 1962 & 3562 & 1703 & 522 & 382 & 233 & 110 & 25 & 20 & 10 & 0 \end{pmatrix}$$

CUBIC WEIGHTED MEAN SEA STATE HEIGHT

$jc := 2 .. cols(SD)$ $jr := 2 .. rows(SD)$ $rows(SD) = 15$

$Hs_{jr} := SD_{jr,1} \cdot m$ $T_{z_{jc}} := SD_{1,jc} \cdot sec$

$$\sum_{jc}\left[\sum_{jr}\left(SD_{jr,jc}\right)\right] = 10 \times 10^4$$

$$Hs3_{jc} := \sqrt[3]{\frac{\sum_{jr}\left[\left(Hs_{jr}\right)^3 \cdot SD_{jr,jc}\right]}{\sum_{jr}\left(SD_{jr,jc}\right)}}$$

$Hs3^T = (0 \quad 0.5 \quad 1.129 \quad 1.372 \quad 1.722 \quad 2.315 \quad 3.128 \quad 4.028 \quad 4.962 \quad 5.717 \quad 6.035 \quad 6.177 \quad 5.621 \quad 6.827)$

PIERSON MOSKOWITZ SPECTRUM

$$S_{\eta\eta}(f, H_s, T_z) := \frac{H_s^{\,2}}{4\cdot\pi\cdot T_z^{\,4}\cdot f^{5}}\cdot\exp\left(\frac{-1}{\pi\cdot f^{4}\cdot T_z^{\,4}}\right)$$

$$Nf := 100 \qquad jf := 1..Nf \qquad fmax := 1\cdot Hz \qquad f_{jf} := \frac{jf}{Nf}\cdot fmax \qquad \delta f := \frac{fmax}{Nf}$$

$$Sv_{\eta\eta_{jf,jc}} := S_{\eta\eta}\left(f_{jf}, H_{s3_{jc}}, T_{z_{jc}}\right)$$

CHECKS

$$m0_{jc} := \sum_{jf}\left(Sv_{\eta\eta_{jf,jc}}\cdot\delta f\right) \qquad m2_{jc} := \sum_{jf}\left[Sv_{\eta\eta_{jf,jc}}\cdot\left(f_{jf}\right)^2\cdot\delta f\right]$$

$$H_{sc_{jc}} := 4\cdot\sqrt{m0_{jc}} \qquad T_{zc_{jc}} := \sqrt{\frac{m0_{jc}}{m2_{jc}}}$$

STRESS TRANSFER FUNCTION FROM FEA

$$freq := \begin{pmatrix} 0.016 \\ 0.032 \\ 0.048 \\ 0.064 \\ 0.08 \\ 0.095 \\ 0.111 \\ 0.127 \\ 0.143 \\ 0.159 \\ 0.175 \\ 0.191 \\ 0.207 \\ 0.223 \\ 0.239 \\ 0.255 \\ 0.271 \\ 0.286 \\ 0.302 \end{pmatrix}\cdot Hz \qquad tf := \begin{pmatrix} 2.51 \\ 9.92 \\ 29.75 \\ 66.32 \\ 93.54 \\ 117.13 \\ 163.28 \\ 133.66 \\ 122.23 \\ 98.23 \\ 98.25 \\ 107.58 \\ 87.32 \\ 89.90 \\ 85.09 \\ 80.38 \\ 93.25 \\ 93.77 \\ 66.59 \end{pmatrix}\cdot\frac{M\cdot Pa}{m}$$

$$TF_{jf} := linterp(freq, tf, f_{jf})$$

RESPONSE SPECTRUM

$$S_{\sigma\sigma_{jf,jc}} := \left(TF_{jf}\right)^2 \cdot Sv\eta\eta_{jf,jc} \qquad m0\sigma_{jc} := \sum_{jf}\left(S_{\sigma\sigma_{jf,jc}} \cdot \delta f\right)$$

$$m1\sigma_{jc} := \sum_{jf}\left[S_{\sigma\sigma_{jf,jc}} \cdot \left(f_{jf}\right) \cdot \delta f\right]$$

$$m2\sigma_{jc} := \sum_{jf}\left[S_{\sigma\sigma_{jf,jc}} \cdot \left(f_{jf}\right)^2 \cdot \delta f\right]$$

$$m4\sigma_{jc} := \sum_{jf}\left[S_{\sigma\sigma_{jf,jc}} \cdot \left(f_{jf}\right)^4 \cdot \delta f\right] \qquad T_{zc\sigma_{jc}} := \sqrt{\frac{m0\sigma_{jc}}{m2\sigma_{jc}}}$$

CUBIC WEIGHTED MEAN STRESS RANGE (RAYLEIGH DISTRIBUTION)

$$S3_{jc} := 3.108 \cdot \sqrt{m0\sigma_{jc}}$$

$$yr = 3.156 \times 10^7 \, s$$

$$n_{jc} := \frac{1}{T_{zc\sigma_{jc}}} \cdot \left[\frac{\sum_{jr}\left(SD_{jr,jc}\right)}{\sum_{jc}\left[\sum_{jr}\left(SD_{jr,jc}\right)\right]}\right] \cdot yr$$

$$A := 4.33 \cdot 10^{12}$$

$$N_{jc} := A \cdot \left[(S3)_{jc}\right]^{-3}$$

Damage per year by each sea state

$$D_{jc} := \frac{n_{jc}}{N_{jc}}$$

DIRLIKS METHOD

$$\beta_{jc} := \frac{m2\sigma_{jc}}{\sqrt{m0\sigma_{jc} \cdot m4\sigma_{jc}}} \qquad x_{jc} := \frac{m1\sigma_{jc}}{m0\sigma_{jc}} \cdot \sqrt{\frac{m2\sigma_{jc}}{m4\sigma_{jc}}}$$

$$T_{xc\sigma_{jc}} := \sqrt{\frac{m2\sigma_{jc}}{m4\sigma_{jc}}} \qquad Ni := 1000$$

$$i := 50, 100 .. Ni \qquad y_i := i \cdot Pa$$

INPUT VARIABLES

$$Z_{jc} := \frac{S3_{jc}}{2 \cdot \sqrt{m0\sigma_{jc}}} \qquad D1_{jc} := \frac{2 \cdot \left[x_{jc} - \left(\beta_{jc} \right)^2 \right]}{1 + \left(\beta_{jc} \right)^2}$$

$$R_{jc} := \frac{\left[\beta_{jc} - x_{jc} - \left(D1_{jc} \right)^2 \right]}{1 - \beta_{jc} - D1_{jc} + \left(D1_{jc} \right)^2} \qquad yr = 3.156 \times 10^7 \, s$$

$$D2_{jc} := \frac{1 - \beta_{jc} - D1_{jc} + \left(D1_{jc} \right)^2}{1 - R_{jc}}$$

$$D3_{jc} := 1 - D1_{jc} - D2_{jc}$$

$$Q_{jc} := \frac{1.25 \cdot \left[\beta_{jc} - D3_{jc} - \left(D2_{jc} \cdot R_{jc} \right) \right]}{D1_{jc}}$$

PROBABILITY DENSITY OF STRESS RANGE (DIRLIK)

$$PRF_{jc} := \frac{\frac{D1_{jc}}{Q_{jc}} \exp\left[\frac{(-Z)_{jc}}{Q_{jc}} \right] + \frac{D2_{jc} \cdot Z_{jc}}{\left(R_{jc} \right)^2} \exp\left[\frac{-\left(Z_{jc} \right)^2}{2 \left(R_{jc} \right)^2} \right] + D3_{jc} \, Z_{jc} \cdot \exp\left[\frac{-\left(Z_{jc} \right)^2}{2} \right]}{2 \cdot \sqrt{m0\sigma_{jc}}}$$

$$x_{jc} := \frac{1}{T_{xc\sigma_{jc}}} \cdot \left[\frac{\sum_{jr} \left(SD_{jr,jc} \right)}{\sum_{jc} \left[\sum_{jr} \left(SD_{jr,jc} \right) \right]} \right] \cdot yr$$

DAMAGE BASED ON DIRLIKS METHOD

$$M3_{jc} := \left[\sqrt{(4 \cdot m0\sigma)_{jc}} \right]^3 \cdot \left[6 \cdot D1_{jc} \cdot \left(Q_{jc} \right)^3 + \left[\left[3.7618 \cdot D2_{jc} \cdot \left(\left| R_{jc} \right| \right)^3 \right] + D3_{jc} \right] \right] \cdot x_{jc} \cdot \frac{1}{A}$$

$$b_{jc} := \left[\frac{\sum_{jr} \left(SD_{jr,jc} \right)}{\sum_{jc} \left[\sum_{jr} \left(SD_{jr,jc} \right) \right]} \right] \cdot yr$$